

**ANALYSIS OF STATIC CONTACT IN LAMINATED  
COMPOSITE PLATES USING DAMAGE MECHANICS**

FINAL  
IN-24-1-  
50149  
p. 190

Final Technical Report

submitted by

David H. Allen

Center for Mechanics of Composites  
Texas A&M University  
College Station, TX 77843-3141

to

NASA Langley Research Center  
Hampton, VA 23665

NASA-CR-198656) ANALYSIS OF  
TATIC CONTACT IN LAMINATED  
OMPOSITE PLATES USING DAMAGE  
ECHANICS Final Technical Report  
Texas A&M Univ.) 190 p

N95-28809

Unclass

G3/24 0050149

Contract No. NAG-1-1407  
May 1995

## **INTRODUCTION**

This report details results of research performed during the period April 1, 1992 through September 30, 1994 under NASA contract no. NAG-1-1407.

The general objective of this research has been to construct a model capable of predicting the damage development caused by out-of-plane static loading in laminated graphite/epoxy composite plates.

## **SUMMARY OF COMPLETED RESEARCH**

The following is a summary of research completed during the contract period:

- 1) a cohesive zone model has been developed for predicting delamination growth in thermoset composites;
- 2) the cohesive zone model has been shown to be thermodynamically acceptable and consistent with the continuum mechanics approach to fracture prediction;
- 3) the cohesive zone model has been implemented to a finite element computer algorithm developed specifically for use under this contract;
- 4) preliminary predictions have been made with the model;
- 5) preliminary experiments have been performed as a means of model verification; and
- 6) the model predictions have been compared favorably to experimental results.

The results reported above are documented in Appendix A.

## PUBLICATIONS

The following papers have been completed under the terms of this contract:

1. Lo, D.C., Allen, D.H. and Harris, C.E., "Modeling the Progressive Failure of Laminated Composites with Continuum Damage Mechanics," Fracture Mechanics: Twenty-third Symposium, ASTM STP 1189, Ravinder Chona, Ed., American Society for Testing and Materials, Philadelphia, 1993, pp. 680-695.
2. Costanzo, F. and Allen, D.H., "A Continuum Mechanics Approach to Some Problems in Subcritical Crack Propagation," International Journal of Fracture, Vol. 63, No. 1, pp. 27-57, 1993 (also CMC Report No. 92-19, October 1992).
3. Lo, D.C., and Allen, D.H., "Modeling of Delamination Damage Evolution in Laminated Composites Subjected to Low Velocity Impact," International Journal of Damage Mechanics, Vol. 3, No. 4, pp. 378-407, October 1994.
4. Costanzo, F., and Allen, D.H., "A Continuum Thermodynamic Analysis of Cohesive Zone Models," accepted for publication in the International Journal of Engineering Science, 1995.
5. Lo, D.C., Costanzo, F., Zocher, M.A., and Allen, D.H., "Modeling of Damage Evolution in Thick Laminates Subjected to Low Velocity Impact," in Mechanics of Thick Composites, AMD-Vol. 162, Y.D.S. Rajapakse, ed., American Society of Mechanical Engineers, New York, pp. 137-150, 1993.
6. Lo, D. and Allen, D.H., "Modeling the Damage Evolution in Laminated Composites with Delaminations Containing a Damage Zone," Damage Mechanics in Composites 1994, AMD-Vol. 185, D.H. Allen and J.W. Ju, eds., American Society of Mechanical Engineers, pp. 57-72, 1994.
7. Harris, C.E., Coats, T.W., Allen, D.H. and Lo, D.C., "Progressive Damage Analysis of Laminated Composites due to Tension Fatigue," submitted for publication in the proceedings of the 2nd Pacific International Conference on Aerospace Science and Technology -- 6th Australian Aeronautical Conference, Melbourne, Australia, March 20-23, 1995.
8. Lo, D.C., Costanzo, F., and Allen, D.H., "Delamination Evolution in Composites Using a Cohesive Zone Model," submitted for publication in the proceedings of the International Conference on Computational Engineering Science (ICES '95), Honolulu, Hawaii, July 30-August 3, 1995.
9. Lo, D.C. and Allen, D.H., "Damage Evolution in Viscoelastic Composites with Delaminations Containing a Process Zone," submitted for publication in the proceedings of the *Symposium on Dynamic Behavior and Response of Composites* to be held at the 1995 ASME Winter Annual Meeting (International Mechanical Engineering Congress and Exposition), San Francisco, California, November 12-17, 1995.

## **PRESENTATIONS**

The following presentations have been given under the terms of this contract:

1. Costanzo, F. and Allen, D.H., "A Thermodynamic Analysis of Propagating Subcritical Cracks with Cohesive Zones," NASA Langley Workshop on Computational Methods for Failure Analysis and Life Prediction, Hampton, Virginia, October 1992.
2. Lo, D.C., Costanzo, F., Zocher, M.A., and Allen, D.H., "Modeling of Damage Evolution in Thick Laminates Subjected to Low Velocity Impact," The 1<sup>st</sup> Joint Mechanics Meeting of ASME/ASCE/SES—MEET'N'93, Charlottesville, Virginia, June 1993.
3. Costanzo, F., and Allen, D.H., "A Continuum Thermodynamic Analysis of Cohesive Zone Models," 31st Society of Engineering Science Conference, Texas A&M University, October, 1994.
4. Lo, D. and Allen, D.H., "Modeling the Damage Evolution in Laminated Composites with Delaminations Containing a Damage Zone," ASME Winter Annual Meeting, Chicago, 1994.
5. Allen, D.H., "Delamination Evolution in Composites Using a Cohesive Zone Model," NASA Langley Research Center, Hampton VA, December 1994.
6. Lo, D.C., and Allen, D.H., "Damage Evolution in Laminated Polymer Matrix Composites," ASME Summer Annual Meeting, UCLA, June, 1995.
7. Lo, D.C., Costanzo, F., and Allen, D.H., "Delamination Evolution in Composites Using a Cohesive Zone Model," International Conference on Computational Engineering Science (ICES '95), Honolulu, Hawaii, July 30-August 3, 1995.
8. Lo, D.C. and Allen, D.H., "Damage Evolution in Viscoelastic Composites with Delaminations Containing a Process Zone," ASME Winter Annual Meeting (International Mechanical Engineering Congress and Exposition), San Francisco, California, November 12-17, 1995.

## **DISCLOSURES**

The computer code entitled **DANCOM** has been written as a part of this contract. A hard copy of this code is included in Appendix B.

## **DISSERTATIONS**

The following Ph.D. dissertations have been completed under funding provided by this contract:

1. Costanzo, F., *A Continuum Thermodynamic Model of Crack Growth with a Cohesive Zone*, Texas A&M University, December, 1993.
2. Lo, D.C., *Damage Evolution in Laminated Composites with Delaminations Containing a Cohesive Zone*, Texas A&M University, August, 1995.

## **APPENDIX A**

## Modeling the Progressive Failure of Laminated Composites with Continuum Damage Mechanics

REFERENCE: Lo, D. C., Allen, D. H., and Harris, C. E., "Modeling the Progressive Failure of Laminated Composites with Continuum Damage Mechanics," *Fracture Mechanics: Twenty-Third Symposium, ASTM STP 1189*, Ravinder Chona, Ed., American Society for Testing and Materials, Philadelphia, 1993, pp. 680-695.

**ABSTRACT:** A continuum-damage-mechanics-based model is proposed for the analysis of the progressive failure process in laminated composite structures. The laminate's response is determined by nonlinear constitutive equations that account for each type of matrix-dominated damage through strain-like internal state variables. Evolution of these internal state variables is governed by the damage-dependent ply-level stresses. The updated damage state and the ply-level stresses are then employed in the local-global evaluation of component failure. This model is incorporated into a finite-element analysis code to facilitate the examination of structures with spatially varying stress fields. The stress and damage distribution obtained from the analysis at various points in the loading history provide information about the progression of events leading to the failure of the component. The progressive failure of fatigue-loaded rectangular crossply-laminated plates containing a centered circular cutout has been examined with the model. Most of the predicted damage is localized in a region near the cutout. Rather than propagating outward, the damage intensifies in this region until failure occurs. The feasibility of modeling the evolution of each type of subcritical damage is demonstrated with the current framework. This ability to simulate the progressive failure process at this level of detail will assist in the design of safer and more efficient composite structures.

**KEY WORDS:** laminated composites, progressive failure, matrix damage, continuum damage mechanics, finite-element analysis, damage accumulation, fracture mechanics, fatigue (materials)

The accumulation of subcritical damage in laminated composites is of major concern especially in light of the increased use of these advanced material systems in critical engineering applications. Although in some instances distributed damage can retard the failure process in a component by redistributing load away from the high stress region, it is still the primary contributing factor to the eventual catastrophic failure. While efforts can be made to delay the development of damage by modifying the laminate stacking sequence or the component design, distributed damage is present throughout the life of the component. Even before entering service, damage is inflicted on the component by the manufacturing process.

To produce safe and reliable laminated composite components, it is essential to know how such damage affects the performance and failure of these components. Experimental approaches are not economical due to the large numbers of parameters that can be varied by the designer. Thus, much effort has been placed on the development of analytical methods to

<sup>1</sup> Graduate research assistant and director, respectively, Center for Mechanics of Composites, Aerospace Engineering Department, Texas A&M University, College Station, TX 77843-3141.

<sup>2</sup> Head, Mechanics of Materials Branch, NASA Langley Research Center, Hampton, VA 23665-5225.

supplement the designer's database. To accomplish this task requires a thorough knowledge of the failure characteristics of laminated composites as well as the ability to analytically model this failure process.

The progressive nature of the failure process in laminated composites has been well documented in the published literature [1-4]. This process involves the accumulation of several types of damage. Generally, the first type of damage to appear is matrix cracking in regions of high stress gradients. Along the free edges and at the intersection of matrix cracks from adjacent plies, delaminations are propagated by large intralaminar stresses. The stress redistribution resulting from these two types of damage in turn assist in the development of damage in the surrounding areas. As matrix-dominated damage accumulates, the loads are transferred to the plies with fiber orientation aligned closest to the direction of the applied loads. The bonds between the fibers and matrix are fractured in these plies. This is accompanied by the fracture of the fibers. Since the reinforcing fibers are the primary load-carrying component of the laminate, their fracture signifies the imminent failure of the structure itself. This failure process is in contrast to that observed in conventional homogeneous materials where failure can be traced to the propagation of a single flaw. In composites, each flaw in the laminate will not greatly affect the overall response of the structure; instead, it influences the development of other flaws. It is the cumulative effect of the subcritical damage that results in the failure of the structure. Thus, any attempt to predict the residual strength and life of laminated composite structures must address the damage accumulation process as well as its effect on the response of the material.

Most analyses have not adequately accounted for this history-dependent subcritical damage accumulation process. Some linear elastic fracture mechanics based approaches replace the distributed damage with a single equivalent macrocrack [5,6]. When the stress intensity factor or the strain energy release rate is equal to the fracture toughness, failure occurs. Other approaches calculate the stress field with the assumption of no accumulated damage. To compensate for the stress redistribution, the failure criteria are either evaluated at a distance away from the stress concentrator or are evaluated using the stresses that are averaged within this region [7-9]. A limitation of these approaches lies in the determination of the equivalent macrocrack size or the evaluation zone. Analytical expressions are not provided to relate the distributed damage to the equivalent geometric properties. Instead, these values are selected to correlate with experimental data and thus are restricted to similar geometries and loading histories [10]. Often these values that are supposed to describe the evolving damage state are assumed to be constant throughout the failure process. Furthermore, in light of the increasing inhomogeneity with damage accumulation, these indirect approaches to the accounting of subcritical damage do not provide sufficient information to predict accurately the evolution of the damaged region and the eventual failure of the component.

Ply discount methods have also been used in conjunction with the aforementioned approaches to model the stress redistribution process, but the abrupt loss of stiffness does not reflect the gradual degradation that occurs with subcritical damage accumulation. Recent efforts have explicitly modeled each flaw in the damaged region to capture the conditions leading to failure. Elasticity solutions are available for idealized component geometries and sparse damage states. However, numerical computational approaches such as the finite-element method have to be employed for typical damage configurations [11-16]. To obtain accurate stress fields, each flaw is modeled by a large number of elements. The stress fields are then used in the failure criteria to determine the initiation and propagation of each flaw. It is necessary to update the finite-element model as the damage state evolves. This type of analysis, unfortunately, can rapidly become computationally untenable since a component may accumulate many interacting flaws before failure occurs.

The requirement for information concerning the subcritical damage accumulation and the



desire for a tractable analysis scheme have prompted the use of the continuum-damage-mechanics approach in the analysis of progressive failure in laminated composite structures [17–20]. The size and distribution of the subcritical damage found in laminated composites enable the selection of a representative volume element (RVE) of material that is small in scale relative to the structure, but is of sufficient size to characterize the damage contained within by statistically averaged quantities. These averaged quantities, known as internal state variables, describe the physical attributes of each mode of damage. The resulting effects of the distributed damage are then reflected in the constitutive relationship through the internal state variables. Therefore, a medium containing a multitude of small internal cracks can be analyzed as a continuum without internal boundaries. Due to the nonlinear nature of the constitutive equations, this type of analysis is approached numerically by methods such as finite elements. This homogenization of the subcritical damage eliminates the task of modeling individual flaws; but since the homogenization is performed at a scale that is small with respect to the structure, the results are of sufficient resolution to provide an indication of the damage accumulation and stress redistribution.

A progressive failure model incorporating the continuum-damage-mechanics approach to model-matrix-dominated damage has been under development by the authors [21–26]. The model's capability to predict the development of matrix cracks under tension-tension fatigue loading conditions is used to examine the development of damage in composite laminates. The information obtained is then used to predict the failure of the component.

### Progressive Failure Model

The proposed progressive failure model consists of three components. The first is the nonlinear constitutive relationships derived using continuum damage mechanics. Next is the structural analysis algorithm incorporating the aforementioned constitutive relationships, and, finally, failure criteria to indicate the catastrophic failure of the structure. Due to the progressive nature of the failure process, these components are employed in a time-stepping manner to evaluate the stress state and damage evolution throughout the loading history. The results obtained at each step are then used to update the model for the next step in the loading history. The following sections will first present the essential aspects of each component of the progressive failure model. These components will then be assembled in an analysis scheme to form the progressive failure model. More in-depth discussions on these components can be found in the published literature [21–26].

### *Damage-Dependent Constitutive Relationships*

The damage-dependent constitutive relationships form the foundation of this progressive failure model. These relationships determine the stress-strain response in the presence of internal damage as represented by the internal state variables. Within the framework of continuum damage mechanics, the rate of change of these internal state variables is calculated from history-dependent damage-evolution laws. Thus, in the course of the analysis, both the changes in the stress state as well as in the damage state are determined. The probable location and mode of failure can then be inferred from these results calculated at sequential points in the loading history. The principles of continuum damage mechanics further require the selection of local volume elements in which homogenization is performed. For matrix cracking, this volume can be specified at the ply level. This selection of the local volume serves as the logical building block in this analysis. The model of a composite laminate can then be formed by assembling these building blocks together. By also developing damage evolution laws and failure functions to be applicable at the ply level, the formulation becomes independent of the

lamination geometry. The relative scale and location of occurrence of delamination damage preclude its specification at the ply level; it is instead introduced at the laminate level. To maintain the geometric independence of the model, a set of damage-dependent lamination equations with modifications to accommodate the effects of the delamination damage is employed.

The kinematic effects of the matrix cracks and delaminations are quantified by the internal state variables used in this model. Matrix cracking is measured by the volume averaged dyadic product of the crack face displacement,  $u_r$ , and the crack face normal,  $n_r$ , as proposed by Vukobratovic and Kachanov [27]

$$\alpha_{ij}^M = \frac{1}{V_L} \int_S u_r n_r dS \quad (1)$$

where  $\alpha_{ij}^M$  is the second-order tensor internal state variable,  $V_L$  is the local representative volume in the deformed state, and  $S$  is the crack surface area. This product represents the averaged kinematics of the crack faces and can be interpreted as additional strains incurred by the material as a result of the internal damage. Since the internal state variable is a second-order tensor, it is capable of modeling all three kinematic modes of crack face displacement. From micromechanics, it has been found that the effects of the matrix cracks can be introduced into the ply-level constitutive equations as follows [28]

$$\{\sigma_L\} = [Q]\{\epsilon_L - \alpha_L^M\} \quad (2)$$

where  $\sigma_L$  are the locally averaged components of stress,  $[Q]$  is the ply-level transformed stiffness matrix,  $\epsilon_L$  are the locally averaged components of strain, and  $\alpha_L^M$  are the components of the internal state variable for matrix cracking. Since interlaminar delaminations are not statistically homogeneous through the laminate thickness, their effects cannot be homogenized at the ply level like the matrix cracks. The effects of the delamination are modeled instead using an RVE at the laminate level. The presence of interply delaminations in a laminate introduces jump discontinuities in the displacement and rotation of the normal line to the midplane of the plate. The Kirchhoff-Love hypothesis is thus modified to account for these discontinuities at the damage interfaces as shown here [29]

$$u(x, y, z) = u''(x, y) - z[\beta'' + H(z - z_i)\beta_i^p] + H(z - z_i)u_i^p \quad (3)$$

$$v(x, y, z) = v''(x, y) - z[\eta'' + H(z - z_i)\eta_i^p] + H(z - z_i)v_i^p \quad (4)$$

$$w(x, y, z) = w''(x, y) + H(z - z_i)w_i^p \quad (5)$$

where  $u''$ ,  $v''$ , and  $w''$  are the midplane displacements;  $\beta''$  and  $\eta''$  are the ply rotations;  $u_i^p$ ,  $v_i^p$ , and  $w_i^p$  are the ply jump displacement due to delamination;  $\beta_i^p$  and  $\eta_i^p$  are the ply jump rotations due to delaminations; and  $H(z - z_i)$  is the Heavyside step function. These displacement equations are averaged over a local area to produce locally averaged displacements. The results are then used in the calculation of the average strains via the ply level constitutive relationship shown in Eq 2. Integrating these ply stresses through the thickness of the laminate will produce the following damage-dependent lamination equations

$$\begin{aligned} \{N\} = & \sum_{k=1}^n [Q]_k (z_k - z_{k-1}) \{\epsilon_k''\} - \frac{1}{2} \sum_{k=1}^n [Q]_k (z_k^2 - z_{k-1}^2) \{\kappa_k''\} + \sum_{i=1}^d [\bar{Q}]_i \{\alpha_i^M\} \\ & + \sum_{i=1}^d [\bar{Q}]_i (z_i - z_{i-1}) \{\alpha_i^D\} - \sum_{i=1}^d [Q]_i (z_i - z_{i-1}) \{\alpha_i^M\} \quad (6) \end{aligned}$$

$$\{M\} = \frac{1}{2} \sum_{k=1}^n [Q]_k (\bar{z}_k^2 - z_k^2) \{\epsilon_k^m\} + \frac{1}{2} \sum_{k=1}^n [Q]_k (\bar{z}_k^2 - z_k^2) \{\kappa_k^m\} + \sum_{i=1}^d [\bar{Q}]_i \{\alpha^D\}_i + \sum_{i=1}^d [\bar{Q}]_i (\bar{z}_i^2 - z_i^2) \{\alpha^D\}_i - \frac{1}{2} \sum_{k=1}^n [Q]_k (\bar{z}_k^2 - z_k^2) \{\alpha^m\}_k \quad (7)$$

where  $N$  is the component of the resultant force per unit length;  $M$  is the component of the resultant moments per unit length;  $\bar{n}$  is the number of plies in the laminate;  $\epsilon_k^m$  and  $\kappa_k^m$  are components of the midplane strains and curvatures;  $[Q]_k$  is the elastic modulus matrix for the  $k^{\text{th}}$  ply in laminate coordinates;  $\{\alpha^m\}_k$  contains the matrix cracking internal state variables for the  $k^{\text{th}}$  ply;  $d$  is the number of delaminated interfaces; and  $[\bar{Q}]_i$  are the weight-averaged stiffness matrices of the sublaminates associated with the  $i^{\text{th}}$  delaminated interface [26]. This sublaminates is composed of the ply directly above and below the delaminated interface.  $t_i$  is the thickness of this sublaminates.  $\{\alpha^D\}_i$  are components of the delamination damage internal state variable, which includes components for crack face displacements and rotations, for the  $i^{\text{th}}$  delaminated interface. These delamination internal state variables are defined in a similar manner as for matrix cracking. However, the local volume is now specified at the sublaminates level. The effects of the internal damage are accounted for by the last three terms on the right-hand side of Eqs 6 and 7, the first two representing the contribution from delamination and the last term from matrix cracking. These terms can be viewed as "damage induced" forces and moments whose application to the undamaged material will produce midplane strain and curvature contributions equivalent to those resulting from the damage-induced compliance increase. If no damage were present, these equations would reduce to the elastic lamination equations.

The internal state variables for the matrix cracks and delaminations can be determined either from experimental data [22,28] or damage evolution equations [30]. The former method requires prior knowledge of the damage state in the structure. Since the objective of this research effort is to predict the accumulation of damage and its effect on the structure, damage evolution equations are used in this model. These relationships describe the rate at which the internal state variables are changing in the RVE and are functions of only the current state at each locally averaged material point. The damage state at any point in the loading history is then found by integrating the damage evolutionary laws. For symmetric crossply laminates subjected to uniaxial loading conditions, the predominant type of damage is the Mode I opening intraply matrix crack. It is assumed that all the crack surfaces are oriented perpendicular to the plane formed by the ply. Thus, matrix damage in each ply can be characterized by only one component of the damage tensor. This component,  $\alpha_{22}^M$ , is associated with the displacement of the crack face in a direction parallel to the crack face normal. Based on the observation that the accumulation of matrix crack is related to the strain energy release rate,  $G$ , in a power law manner [31], the authors have proposed the following evolutionary relationship for this component of the damage tensor when the load is applied cyclically [30]

$$d\alpha_{22}^M = \frac{d\alpha_{22}^M}{dS} \bar{k} G^{\bar{n}} dN \quad (8)$$

where the term  $d\alpha_{22}^M/dS$  reflects the changes in the internal state variable with respect to changes in the crack surfaces. This term is calculated analytically from a relationship describing the average crack surface displacements in the pure opening mode (Mode I) for a medium containing alternating  $0^\circ$  and  $90^\circ$  plies [28]. It has been found that for typical brittle graphite/epoxy material systems  $d\alpha_{22}^M/dS$  varied little with damage when subjected to fatigue at constant

load levels. Therefore,  $d\epsilon_{ij}^M/dS$  is assumed to be independent of the number of matrix cracks in the ply. This approximation leaves the component of the far-field load normal to the crack surface and the layer thickness as the determining factor for the value of  $d\epsilon_{ij}^M/dS$ .  $G$  is the strain energy release rate calculated from the ply-level damage-dependent stresses. The material parameters,  $\bar{k}$  and  $\bar{n}$ , are phenomenological in nature and must be determined from experimental data. For the present model,  $\bar{k}$  and  $\bar{n}$  are determined from the damage history of a [O<sub>2</sub>/90<sub>2</sub>], AS4/3502-6 graphite/epoxy laminate fatigue loaded at a maximum stress amplitude of 296.5 MPa and a cycle ratio of 0.1 as reported by Chou et al. [31]. The parameters have been found to be

$$\bar{k} = 4.42, \quad \bar{n} = 6.39 \quad (9)$$

for this material system. Because  $\bar{k}$  and  $\bar{n}$  are assumed to be material parameters, the values determined from one laminate stacking sequence should be valid for other laminates as well. This has been found to be accurate for crossply laminates with varying numbers of transverse plies and stress amplitudes [32]. Further investigation of other laminate stacking sequences will be required to determine whether this assumption is valid for noncrossply layups. Since the interactions with the adjacent plies and damage sites are implicitly reflected in the calculation of the ply-level response through the laminate-averaging process, Eq 8 is not restricted to a particular laminate stacking sequence. Thus, both the transverse matrix cracking and axial splits in a crossply laminate subjected to tensile cyclic loading conditions can be modeled with the same equation.

### Structural Analysis Algorithm

To incorporate the damage-dependent laminate constitutive relationship into a finite-element formulation, the damage-dependent force and moment resultants, Eqs 6 and 7, are substituted into the plate equilibrium equations. The restriction to symmetric laminate stacking sequence is taken to simplify the formulation. This assumption produces a zero coupling stiffness matrix and results in uncoupled governing differential equations. These governing differential equations are integrated against variations in the displacement components to produce a weak formulation of the damage-dependent laminated plate equilibrium equations. The current algorithm uses a three-node triangular element with five degrees of freedom at each node; this consists of two in-plane displacements, one out-of-plane displacement, and two out-of-plane rotations. This element is formed by combining a constant strain triangular element and a nonconforming plate bending element. Corresponding displacement interpolation functions are substituted into the weak formulation of the plate equilibrium equations to produce the following equilibrium equations in matrix form [33]

$$\begin{bmatrix} K^{11} & K^{12} & 0 \\ K^{21} & K^{22} & 0 \\ 0 & 0 & K^{33} \end{bmatrix} \begin{Bmatrix} u \\ v \\ \delta \end{Bmatrix} = \begin{Bmatrix} F_A^1 \\ F_A^2 \\ F_A^3 \end{Bmatrix} + \begin{Bmatrix} F_M^1 \\ F_M^2 \\ F_M^3 \end{Bmatrix} + \begin{Bmatrix} F_D^1 \\ F_D^2 \\ F_D^3 \end{Bmatrix} \quad (10)$$

where  $[K]$  is the element stiffness matrix,  $\{\delta\}$  contains the out-of-plane displacement and rotations,  $\{F_A\}$  is the applied force vector, and  $\{F_M\}$  and  $\{F_D\}$  are the "damage-induced" force vectors resulting from matrix cracking and delamination, respectively. The effects of the internal damage now appear on the right-hand side of the equilibrium equations as damage-induced force vectors. This representation eliminates the need to recalculate the elemental stiffness matrices each time the damage state evolves, thus saving much computational time.

### *Failure Criteria*

The objective of the failure criteria is to evaluate the structural integrity of the component using the current stress and damage states calculated by the model. This entails the examination of the failure process at both the local material level and the global structural level because the failure at one material point may create stress redistributions that can cause simultaneous failure in the surrounding regions. Typical failure during tensile conditions is signaled by fiber fracture in the principal load carrying plies of a multidirectional laminate. This is evaluated by the following criterion

$$\epsilon_{11} \geq \epsilon_{11f} \quad (11)$$

where  $\epsilon_{11}$  is the average ply level strain in the fiber direction and  $\epsilon_{11f}$  is the tensile failure strain measured from a unidirectional laminate. After failure has been declared, the ply no longer can support additional load. The current analysis considers this condition as the failure of component. In situations where the failure process is permitted to progress beyond the first fiber failure, the stability of the failure process is evaluated at the global level. The stress state for the entire structure with the updated damage is recalculated using the current loading condition. Local laminate failure is evaluated once again in the structure. If it has been determined that additional laminate failure has not occurred, then the failure process is stable and the analysis is continued to the next increment of loads. On the other hand, new local laminate failure would indicate an unstable fracture process and signals the initiation of global failure. This local-global procedure forms the failure evaluation of the progress failure model. Other modes of failure can be included in the evaluation by the application of the appropriate criteria at the local level of the analysis.

### *Progressive Analysis Scheme*

The aforementioned components are assembled together as shown in Fig. 1 to form the progressive failure model. In a typical analysis, the applied loads and initial damage state are entered into the damage dependent constitutive relationships to determine the effective damage-induced forces. These resultant damage forces along with the applied forces are used in the structural analysis algorithm to calculate the global structural response. The results are once again sent to the constitutive relationships where the local stress/strain response is obtained. The changes in the damage state are also determined at this stage by the damage evolutionary relationships using the local ply stresses. The failure criteria are evaluated locally with the updated damage state; if failure has occurred, global failure is examined. Next, the entire process is repeated for the next load step. This model is coded into a computational program to facilitate the analysis of engineering structures.

### **Numerical Results and Discussion**

The proposed progressive failure model is employed to examine the residual life of a crossply laminated plate subjected to fatigue loading conditions. A circular cutout is placed at the center of the plate to produce stress gradients that are conducive to the growth of subcritical damage. This configuration is similar to those used to model fastener holes found in many composite structures. Thus, by examining how the stresses are redistributed and damage accumulates near the fastener hole, information can be gathered to determine the merits of a particular design. The dimensions of the rectangular plate used in this study are 25.4 by 50.8 mm. The circular cutout has a diameter of 6.4 mm. A cyclic tensile load is applied at the nar-

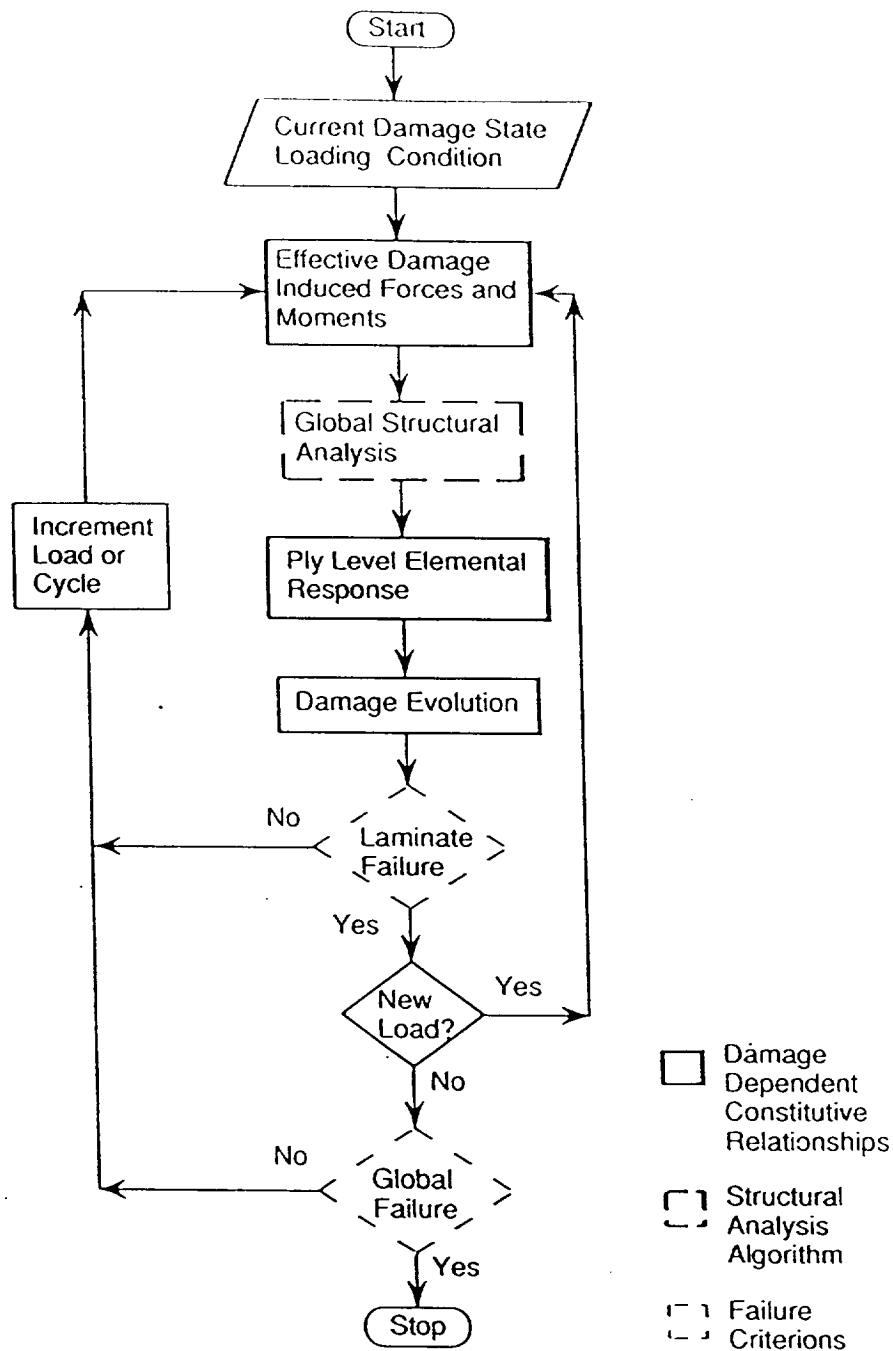


FIG. 1—Progressive failure analysis methodology.

row end of the plate. Due to symmetry about the length and width of the plate, the finite-element mesh represents a quarter of the plate. It is discretized into 90 three-node triangular elements, as shown in Fig. 2. The plate has a  $[0/90_2]_s$  laminate stacking sequence. The material properties, shown in Table I, for AS4/3501-6 graphite/epoxy have been used in the calculation. The fatigue load is applied at a cycle ratio of 0.1 and follows the maximum stress history shown in Fig. 3. The first 50 cycles consist of the ramp up to the test load. This is done in part

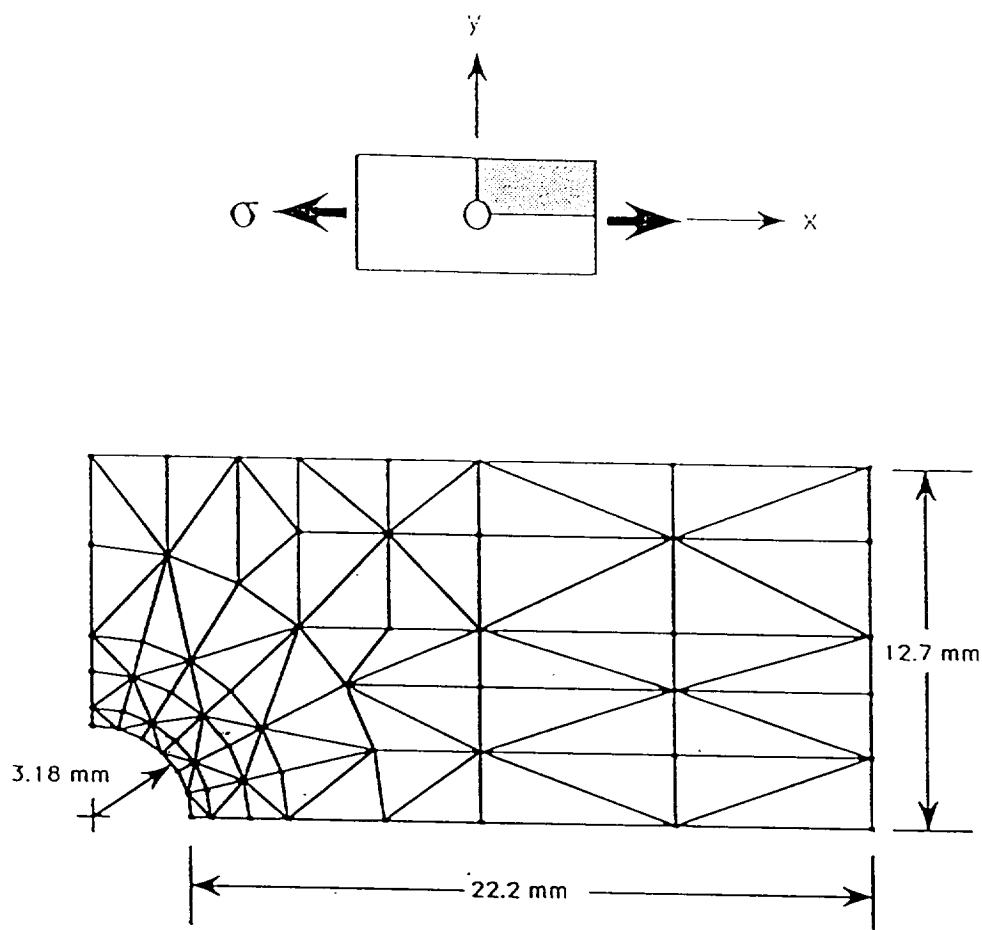


FIG. 2—Finite-element mesh of plate with circular cutout.

to control the incremental changes to the damage state during the initial portion of the loading history. In this simulation, matrix cracking is assumed to be the only form of damage mode and because of the crossply stacking sequence, component failure is assumed to occur at the first fiber fracture in the  $0^\circ$  plies.

The predicted accumulation of matrix crack damage in the  $90^\circ$  plies of a panel loaded at a maximum stress of 184.0 MPa is shown in Fig. 4. The amount of damage is expressed in terms

TABLE 1—Ply-level material properties for AS4/3501-6 used in simulation.

$E_{11}$	146.9 GPa
$E_{22}$	10.4 GPa
$G_{12}$	4.3 GPa
$\nu_{12}$	0.26
$\nu_{21}$	0.42
$t_{ply}$	0.128 mm
$\epsilon'_{f1crit}$	15 000 $\mu$ strain
GROWTH LAW PARAMETERS	
$\bar{k}$	4.42
$\bar{n}$	6.39

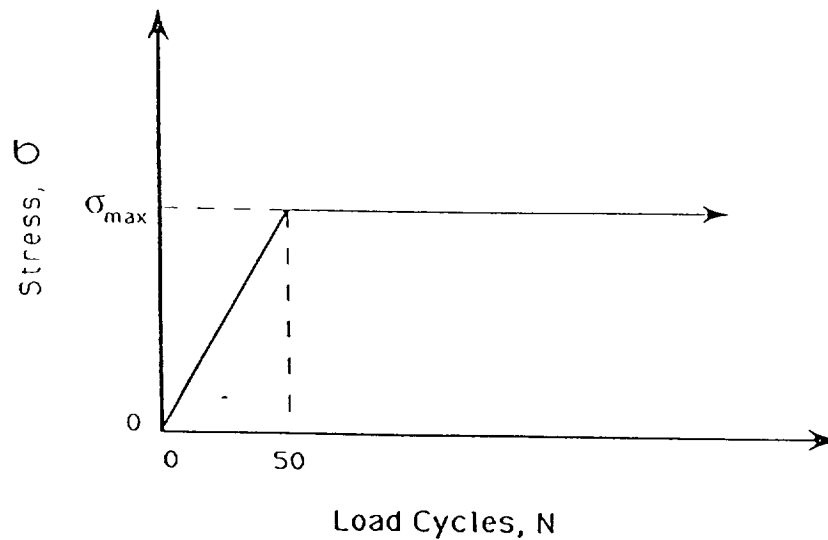
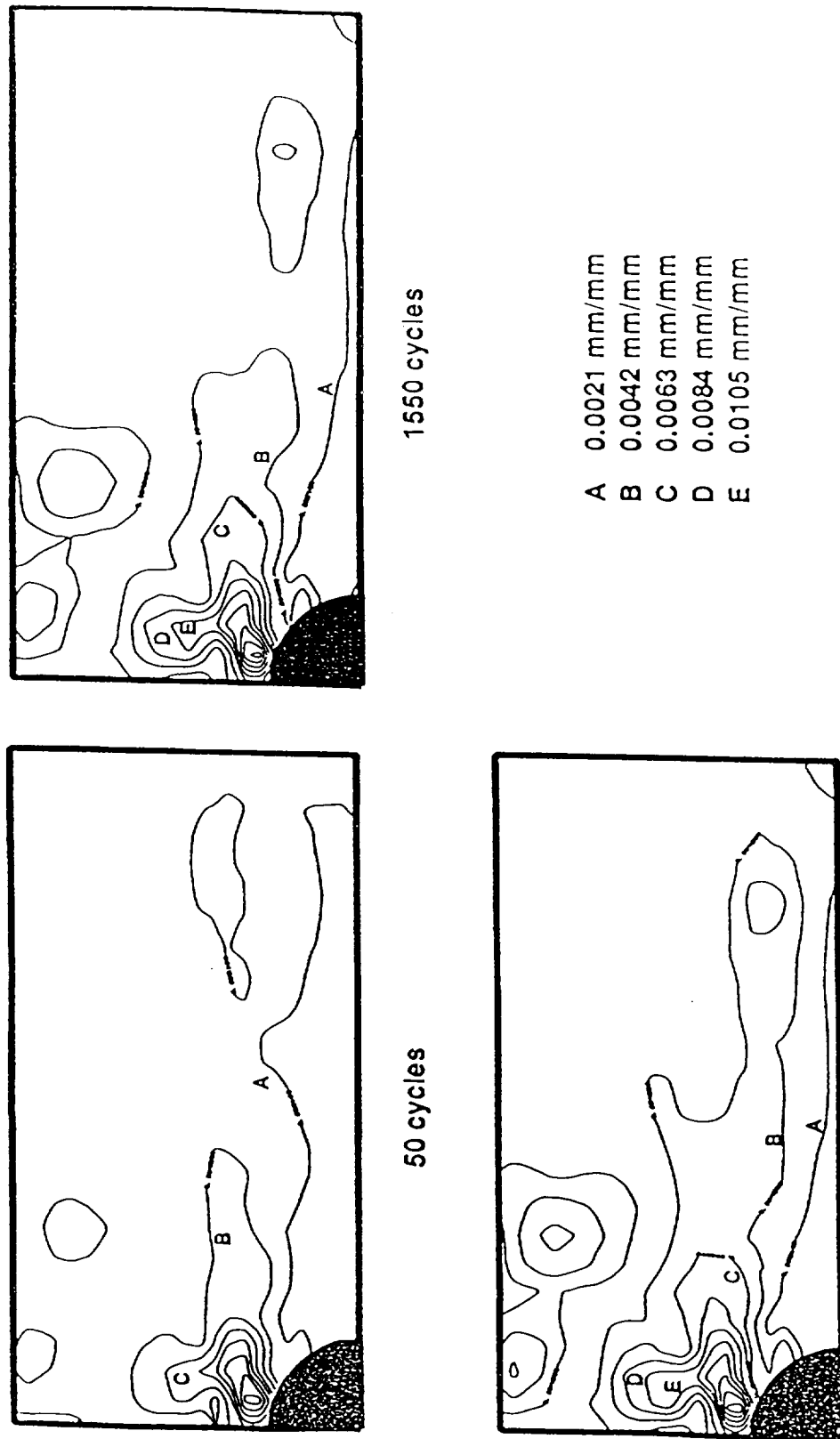


FIG. 3—Maximum fatigue stress history used in simulation ( $R = 0.1$ ).

of the volume-averaged crack face displacement as defined by Eq 1. At the end of the load ramp up, matrix damage has developed throughout the plate. The greatest damage being located near the notch. This region of high damage gradient expands outward after 1550 cycles. The amount of damage also increases in the rest of the plate. However, after 7550 cycles, much of the damage evolution emanates from the region adjacent to the notch. This shift in the damage evolution reflects the load redistribution occurring inside the laminate. The corresponding axial stress history for the  $0^\circ$  plies is shown in Fig. 5. The effects of the damage growth that occurs between 50 and 1550 cycles can be seen by the increase in stress near the notch. The interesting changes in the stress distribution beyond this point in the loading history are not discernible from the stress contour plots; but examination of the numerical data indicates load transfer taking place in a confined area adjacent to the notch. This decelerated change in the stress distribution is in part due to the small fraction of the total load initially carried by the  $90^\circ$  plies. Any loss in the load carrying capability in the  $90^\circ$  plies will translate to small changes in the stress state in the  $0^\circ$  plies. The accumulation of damage further reduces the load available for transfer. However, a sufficient amount of load is transferred to the  $0^\circ$  plies to cause fiber fracture and component failure after 7634 cycles. During the life of the plate, the greatest accumulation of matrix damage is located at a region adjacent to the notch. Rather than expanding outward, the damage intensifies in this region until first fiber failure in the  $0^\circ$  plies. This behavior has also been predicted by Chang et al. [34] in crossply laminates subjected to monotonically increasing tensile loading conditions.

The predicted cycles to first fiber failure at various maximum fatigue stress levels are shown in Fig. 6. At the higher stresses, the load redistribution progresses rapidly from the formation of the high-damage gradient zone to the failure of the first fiber. This indicates a sufficient amount of energy was available after the formation of this zone to produce this result. At lower applied stresses, a large portion of the available energy is expended during the formation of the damage zone. Therefore, the intensification stage spans over a relatively high number of fatigue cycles. The increase in the number of cycles to failure from decreasing the applied stress at the lower stress levels is large. Decreasing the applied stress from 185.7 to 183.4 MPa increases the cycles to failure by more than 100 000 cycles. A possible cause for this response is related to the amount of load redistribution taking place inside the laminate. Recall that these predictions are based on the assumption that matrix cracking is the only type of matrix-





7550 cycles

FIG. 4—Matrix crack damage accumulation in the 90° ply of a plate fatigue loaded at a maximum stress of 184.0 MPa

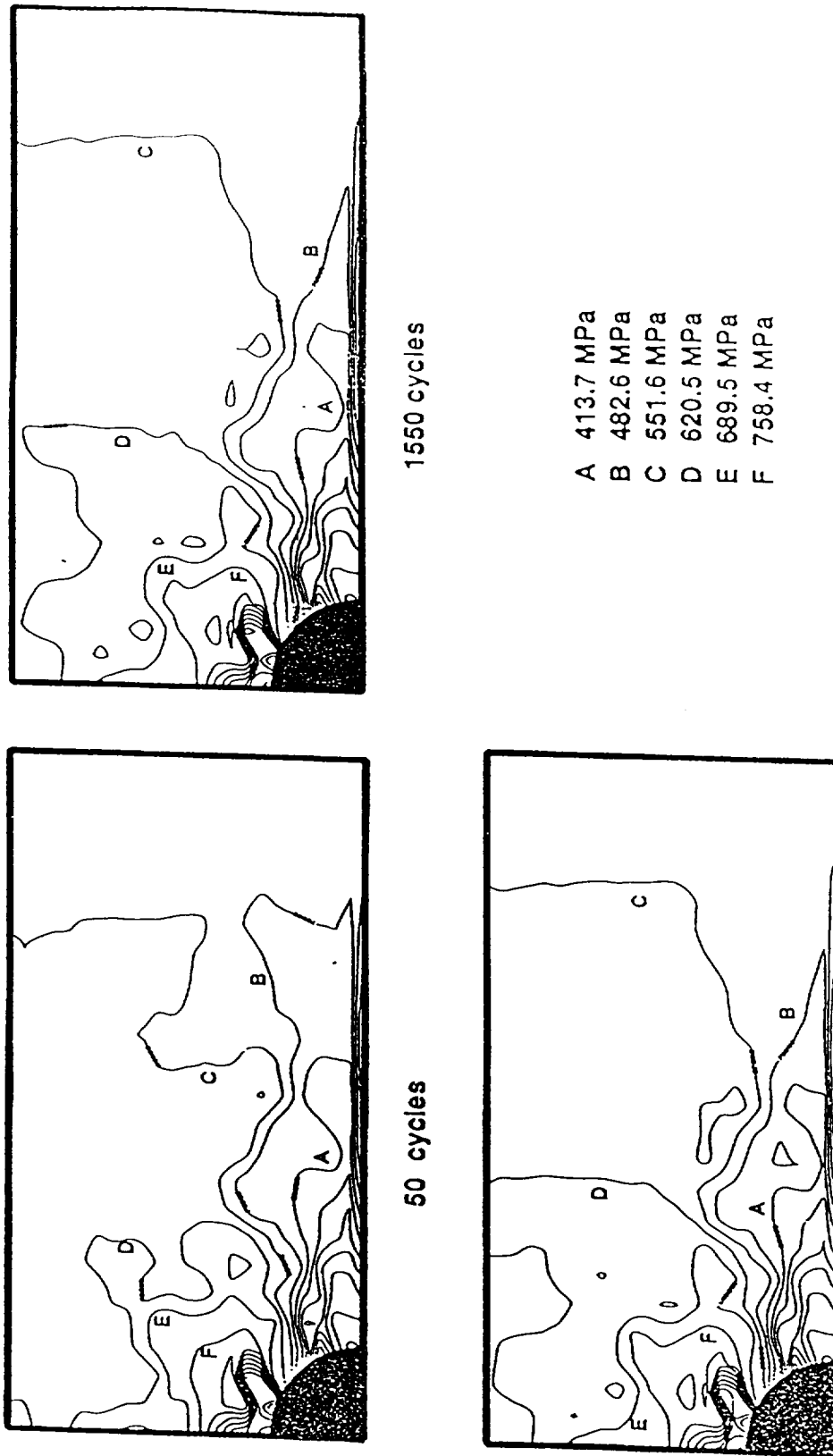


FIG. 5—Axial stress distribution in the  $0^\circ$  plies of a plate fatigue loaded at a maximum stress of 184.0 MPa

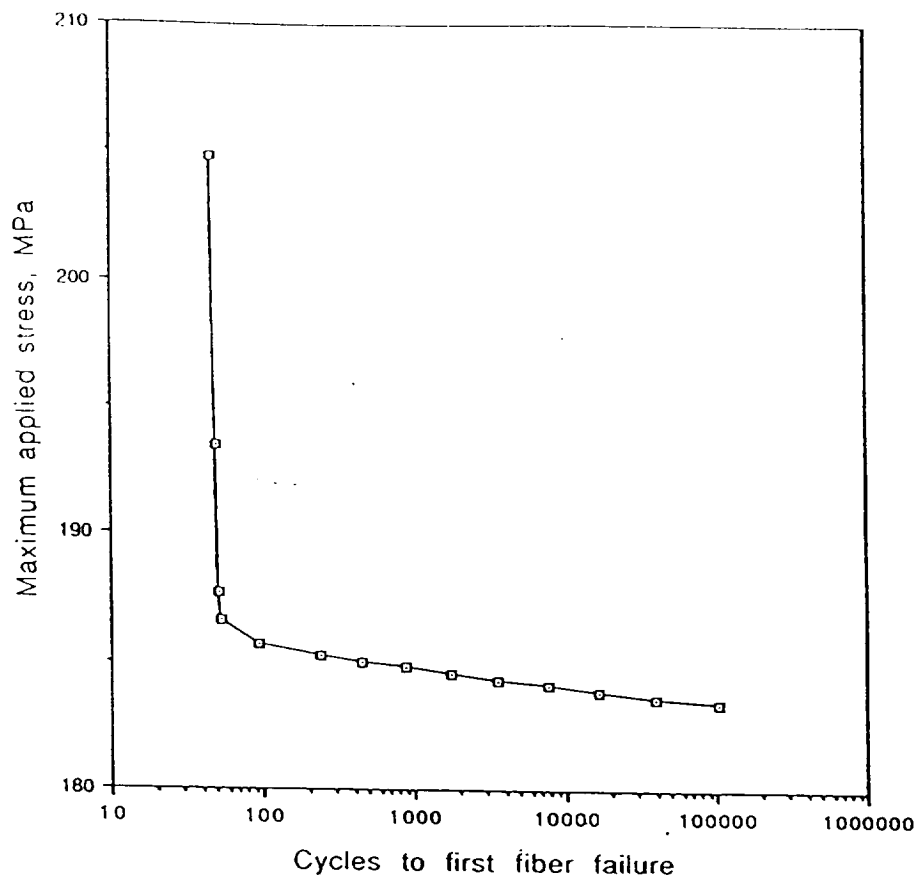


FIG. 6—Predicted cycles to first fiber failure of fatigue-loaded plate with a circular cutout.

dominated damage present. The inclusion of delamination damage into the analysis will alter the stress redistribution and damage accumulation. Its effects will be most apparent at the lower stress levels where the delamination damage can initiate and accumulate before fiber failure occurs. The number of fatigue cycles required for first fiber failure at these stress levels will decrease due to the additional source of load redistribution. Since the stress redistribution and damage formation are coupled, additional analysis and experimental verification would be required before any quantitative conclusions can be drawn about effects of including delamination damage. However, it would enable the current progressive failure analysis framework to capture a more complete picture of the complex interactive process and enhance the model predictions.

The type of information obtained from the simulation could be potentially very useful to the designer or analyst. The ability to locate critical regions and to track the evolution of damage in these regions would allow designers to create safer and more efficient components. Alternately, a damaged region detected in a component can be characterized and then entered into the model to determine its effect on the residual responses so that it can be removed from service at the appropriate time. The proposed model demonstrates the feasibility of the continuum-damage-mechanics approach. Further developments are in progress to achieve the capabilities for analyzing more complex damage states.

The current analysis assumes component failure to occur at the first fracture of fibers in the principal load carrying plies. This assumption is valid in narrow specimens where there is not sufficient area to redistribute the tensile loads within these plies. In wider specimens, global

fracture can be stable; thus, the progressive failure process extends beyond the first fiber failure. Therefore, the full implementation of the matrix-dominated damage evolution laws and the introduction of fiber fracture internal state variables and growth laws are future objectives of the research effort. This will be followed by the modeling of compressive failure modes.

### Conclusion

The use of continuum damage mechanics in the progressive failure model provides an efficient means of modeling distributed damage found in laminated composites. Each type of damage is represented by a set of strain-like internal state variables. The internal state variables evolve with the accumulation of damage at each material point. These values are predicted by damage evolution relationships that are functions of the current state of the material including all the damage present. Since the formulation permits the gradual accumulation of damage and the concurrent growth of different damage types, the analysis reflects the events occurring inside the laminate. The current framework operates in a time-stepping manner where the stress distribution and damage accumulation predicted at each step are employed in the local-global structural integrity evaluation. This ability to simulate the progressive failure process will enhance the design and maintenance of laminated composite structures by reducing the dependence on experimental support.

Even though continuum damage mechanics is suited for the examination of damages that are distributed in nature and fracture mechanics is applicable for the evaluation of well-defined macrocracks, there are situations that require the incorporation of the two approaches. One such case is the existence of a sharp notch in a composite laminate. In this instance, a damage zone containing many distributed microcracks will develop ahead of this notch when load is applied. To account for the stress redistribution in this zone, continuum mechanics can be used to determine the state of the material. These results can then be evaluated on the global scale using fracture mechanics. Thus, rather than choosing one method over the other, they should be viewed as integral units in the failure analysis of laminated composite structures.

### Acknowledgment

The support from NASA Langley Research Center under Contracts NGT-50262 and NAG-1-1120 is gratefully appreciated by Mr. Lo and Mr. Allen.

### References

- [1] Stinchcomb, W. W. and Reifsnider, K. L., "Fatigue Damage Mechanisms in Composite Materials: A Review," *Fatigue Mechanisms, ASTM STP 675*, J. J. Fong, Ed., American Society for Testing and Materials, Philadelphia, 1979, pp. 762-787.
- [2] Stinchcomb, W. W., Reifsnider, K. L., Yeung, P., and Masters, J., "Effect of Ply Constraint on Fatigue Damage Development in Composite Material Laminates," *Fatigue of Fibrous Composite Materials, ASTM STP 723*, K. N. Lauraitis, Ed., American Society for Testing and Materials, Philadelphia, 1981, pp. 65-84.
- [3] Reifsnider, K. L. and Jamison, R., "Fracture of Fatigue-Loaded Composite Laminates," *International Journal of Fatigue*, Vol. 4, No. 4, Oct. 1982, pp. 187-197.
- [4] Jamison, R. D., Schulte, K., Reifsnider, K. L., and Stinchcomb, W. W., "Characterization and Analysis of Damage Mechanisms in Tension-Tension Fatigue of Graphite/Epoxy Laminates," *Effects of Defects in Composite Materials, ASTM STP 836*, K. L. Reifsnider, Ed., American Society for Testing and Materials, Philadelphia, 1984, pp. 21-55.
- [5] Cruse, T. A., "Tensile Strength of Notched Composites," *Journal of Composite Materials*, Vol. 7, April 1973, pp. 218-228.
- [6] Tirosh, J., "On the Tensile and Compressive Strength of Solids Weakened (Strengthened) by an Inhomogeneity," *Journal of Applied Mechanics*, Vol. 44, No. 3, Sept. 1977, pp. 449-454.

- [7] Whitney, J. M. and Nuismer, R. J., "Stress Fracture Criteria for Laminated Composites Containing Stress Concentrations," *Journal of Composite Materials*, Vol. 8, July 1974, pp. 253-265.
- [8] Nuismer, R. J. and Labor, J. D., "Application of the Average Stress Failure Criterion: Part I—Tension," *Journal of Composite Materials*, Vol. 12, July 1978, pp. 238-249.
- [9] Chang, F. K., Scott, R. A., and Springer, G. S., "Failure Strength of Nonlinearly Elastic Composite Laminates Containing a Pin-Loaded Hole," *Journal of Composite Materials*, Vol. 18, Sept. 1984, pp. 464-477.
- [10] Awerbuch, J. and Madhukar, M. S., "Notched Strength of Composite Laminates: Predictions and Experiments—A Review," *Journal of Reinforced Plastics and Composites*, Vol. 4, No. 1, 1985, pp. 3-159.
- [11] O'Brien, F. K. and Raju, I. S., "Strain-Energy-Release Rate Analysis of Delamination Around an Open Hole in Composite Laminates," AIAA Paper 84-0961, American Institute of Aeronautics and Astronautics, New York, 1984.
- [12] Whitcomb, J. D. and Raju, I. S., "Analysis of Interlaminar Stresses in Thick Composite Laminates With and Without Edge Delamination," *Delamination and Debonding of Materials*, ASTM STP 876, W. S. Johnson, Ed., American Society for Testing and Materials, Philadelphia, 1985, pp. 69-94.
- [13] Mahishi, J. M. and Adams, D. F., "Energy Release Rate During Delamination Crack Growth in Notched Composite Laminates," *Delamination and Debonding of Materials*, ASTM STP 876, W. S. Johnson, Ed., American Society for Testing and Materials, Philadelphia, 1985, pp. 95-111.
- [14] Whitcomb, J. D., "Instability-Related Delamination Growth of Embedded and Edge Delaminations," NASA TM 100655, National Aeronautics and Space Administration, Hampton, VA, Aug. 1988.
- [15] Reddy, E. S., Wang, A. S. D., and Zhong, Y., "Simulation of Matrix Cracks in Composite Laminates Containing a Small Hole," *Journal of Reinforced Plastics and Composites*, Vol. 9, March 1990, pp. 104-117.
- [16] Wang, A. S. D., Reddy, E. S., and Zhong, Y., "Three-Dimensional Simulation of Crack Growth in Notched Laminates," *Journal of Reinforced Plastics and Composites*, Vol. 9, March 1990, pp. 134-150.
- [17] Harris, C. E., Allen, D. H., and Lo, D. C., "A Mechanics Framework for a Progressive Failure Methodology for Laminated Composites," *Proceedings*, Fourth ASC Conference on Composites, Blacksburg, VA, Oct. 1989.
- [18] de Rouvray, A. and Haug, E., "Failure of Brittle and Composite Materials by Numerical Methods," *Structural Failure*, T. Wierzbicki and N. Jones, Eds., Wiley, New York, 1989, pp. 193-254.
- [19] Ladeveze, P., Allix, O., and Daudeville, L., "Mesomodeling of Damage for Laminate Composites Application to Delamination," *Proceedings*, IUTAM Symposium on Inelastic Deformation of Composite Materials, Troy, NY, 29 May-1 June 1990.
- [20] Allix, O., Daudeville, L., and Ladeveze, P., "Delamination and Damage Mechanics," *International Journal of Fatigue and Fracture of Engineering Materials and Structures*, to be published.
- [21] Allen, D. H., Harris, C. E., and Groves, S. E., "A Thermomechanical Constitutive Theory for Elastic Composites with Distributed Damage—Part I: Theoretical Development," *International Journal of Solids and Structures*, Vol. 23, No. 9, 1987, pp. 1301-1318.
- [22] Allen, D. H., Harris, C. E., and Groves, S. E., "A Thermomechanical Constitutive Theory for Elastic Composites with Distributed Damage—Part II: Application to Matrix Cracking in Laminated Composites," *International Journal of Solids and Structures*, Vol. 23, No. 9, 1987, pp. 1319-1338.
- [23] Allen, D. H., Harris, C. E., Groves, S. E., and Norvell, R. G., "Characterization of Stiffness Loss in Crossply Laminates with Curved Matrix Cracks," *Journal of Composite Materials*, Vol. 22, No. 1, 1988, pp. 71-80.
- [24] Harris, C. E., Allen, D. H., and Nottorf, E. W., "Damage Induced Changes in the Poisson's Ratio of Cross-Ply Laminates: An Application of a Continuum Damage Mechanics Model for Laminated Composites," *Damage Mechanics in Composites*, AD-Vol. 12, A. S. D. Wang and G. K. Haritos, Eds., The American Society of Mechanical Engineers, New York, 1987, pp. 17-23.
- [25] Harris, C. E., Allen, D. H., and Nottorf, E. W., "Modeling Stiffness Loss in Quasi-Isotropic Laminates Due to Microstructural Damage," *Journal of Engineering Materials and Technology*, Vol. 110, 1988, pp. 128-133.
- [26] Allen, D. H., Nottorf, E. W., and Harris, C. E., "Effect of Microstructural Damage on Ply Stresses in Laminated Composites," *Recent Advances in the Macro and Micro-Mechanics of Composite Materials Structures*, AD-Vol. 13, D. Hui and J. R. Vinson, Eds., The American Society of Mechanical Engineers, New York, 1988, pp. 135-145.
- [27] Vakulenko, A. A. and Kachanov, M. L., "Continuum Theory of Cracked Media," *Izvestia AN SSR, Mekhanika Tverdogo Tela*, Vol. 6, 1971, p. 159.

- [28] Lee, J. W., Allen, D. H., and Harris, C. E., "Internal State Variable Approach for Predicting Stiffness Reductions in Fibrous Laminated Composites with Matrix Cracks," *Journal of Composite Materials*, Vol. 23, 1989, pp. 1273-1291.
- [29] Allen, D. H., Groves, S. E., and Harris, C. E., "A Cumulative Damage Model for Continuous Fiber Composite Laminates with Matrix Cracking and Interply Delaminations," *Composite Materials Testing and Design (Eighth Conference)*, ASTM STP 972, J. D. Whitcomb, Ed., American Society for Testing and Materials, Philadelphia, 1988, pp. 57-80.
- [30] Lo, D. C., Allen, D. H., and Harris, C. E., "A Continuum Model for Damage Evolution in Laminated Composites," *Proceedings, IUTAM Symposium on Inelastic Deformation of Composite Materials*, Troy, NY, 29 May-1 June 1990.
- [31] Chou, P. C., Wang, A. S. D., and Miller, H., "Cumulative Damage Model for Advanced Composite Materials," AFWAL-TR-82-4083, Air Force Wright Aeronautical Laboratories, OH, 1982.
- [32] Lo, D. C., "A Matrix Damage Accumulation Model for Laminated Composites," Master's thesis, Texas A&M University, College Station, TX, May 1990.
- [33] Buie, K. D., "A Finite Element Model for Laminated Composite Plates with Matrix Cracks and Delaminations," Master's thesis, Texas A&M University, College Station, TX, Dec. 1988.
- [34] Chang, K. Y., Liu, S., and Chang, F. K., "Damage Tolerance of Laminated Composites Containing an Open Hole and Subjected to Tensile Loadings," *Journal of Composite Materials*, Vol. 25, 1991, pp. 274-301.

## A continuum mechanics approach to some problems in subcritical crack propagation

FRANCESCO COSTANZO and DAVID H. ALLEN

Center for Mechanics of Composites, Texas Engineering Experiment Station,  
The Texas A&M University System, College Station, Texas 77843-3141, USA

Received 24 November 1992; accepted in revised form 20 July 1993

**Abstract.** The results of the so-called energetic approach to fracture for the cases of a sharp crack without and with a cohesive zone are briefly reviewed with particular attention to the crack tip singularity analysis and to the issue of energy dissipation due to crack propagation. The case of a crack with a cohesive zone removing all thermomechanical singularities is then further analyzed, focusing the attention on the question of the thermodynamic admissibility of subcritical crack growth, and on some of the hypotheses that lead to the derivation of subcritical crack growth laws. A two-phase cohesive zone model for discontinuous crack growth is presented and its thermodynamics analyzed, followed by an example of its possible application.

### 1. Introduction

Subcritical crack growth (SCG), under both general and cyclic loading conditions, is a phenomenon that has been receiving more and more attention during the last forty years. Starting with early investigations mainly on fatigue in metals [1–9], current research covers a wide variety of materials, especially those such as polymers [9–13] and ceramics [14] that are becoming important in the fabrication of composites. The phenomena of interest also include phase transformation toughening and discontinuous crack propagation in polymers, *R*-toughening by crack bridging in ceramics and interface evolution and degradation both at fiber-matrix interfaces in fiber reinforced composites and at the lamina-lamina interface in laminated composites. In all these phenomena experimental research has shown the existence of a zone, often referred to as a *cohesive zone* or *damage zone* located at the crack tip, whose special behavior relieves the stress and/or strain singularity that otherwise would be predicted at the crack tip of a sharp crack and allows for some inelastic behavior to occur.

From the theoretical standpoint, the problem is that of relating crack growth to the load history. In this sense, fundamental understanding has been provided by the energetic approach to fracture [15–32] that showed [15–19] how subcritical crack propagation is strictly related to the rate of energy dissipation in the vicinity of the crack front, although the distinction between the surroundings of the crack, generically referred to as a *process zone*, and the rest of the body is often unclear. Such an ambiguity leads also to inconsistencies in the development of a thermodynamic theory of fracture. In fact, several theoretical studies in the continuum thermodynamics of fracture, especially those by Cherepanov [15, 21] and Rice [22–23] and, more recently, Gurtin [24–25] and Nguyen [27–32] have shown that, independently of the global or local (around the tip) constitutive assumptions, a sharp crack with no cohesive zone (i.e. a system of cohesive forces acting on the crack surface) is constrained to evolve according to the Griffith criterion [20], the latter being a direct consequence of the second law of thermodynamics. This result is in open contrast with many of the results obtained in fatigue,

### 2.1. Basic equations

The first two laws of thermodynamics, in the pointwise form, read [37]

$$\rho \dot{u} = \sigma_{ij} \dot{\varepsilon}_{ij} - q_{i,i} + \rho r, \quad (1)$$

$$\rho \dot{s} + \left( \frac{q_i}{T} \right)_{,i} - \rho \frac{r}{T} \geq 0, \quad (2)$$

where  $u = u(x_k, t)$  is the specific internal energy;  $\rho = \rho(x_k, t)$  is the density;  $s = s(x_k, t)$  is the (total) specific entropy;  $T = T(x_k, t)$  is the absolute temperature;  $\sigma_{ij} = \sigma_{ij}(x_k, t)$  is the Cauchy stress tensor;  $\varepsilon_{ij} = \varepsilon_{ij}(x_k, t)$  is the small strain tensor;  $q_i = q_i(x_k, t)$  is the heat flux;  $r = r(x_k, t)$  is the heat source.

The dot over a generic variable represents the material time derivative  $d/dt$  and  $x_k$  is the position vector. In addition to (1) and (2) we also have

$$\sigma_{ji,j} + \rho f_i = 0, \quad (3)$$

$$\varepsilon_{ij} = \frac{1}{2}(u_{i,j} + u_{j,i}), \quad (4)$$

where  $f_i = f_i(x_k, t)$  and  $u_i = u_i(x_k, t)$  are the body force and the displacement vector fields, respectively. As for the pointwise material behavior, we assume that it is described by the following set of equations [33]:

$$\begin{aligned} \sigma_{ij} &= \sigma_{ij}(\varepsilon_{kl}, T, \alpha^n), \\ q_i &= q_i(\varepsilon_{kl}, T, T_{,k}, \alpha^n), \\ u &= u(\varepsilon_{kl}, T, \alpha^n), \\ s &= s(\varepsilon_{kl}, T, \alpha^n), \end{aligned} \quad (5)$$

such that

$$\sigma_{ij} = \rho \frac{\partial h}{\partial \varepsilon_{ij}}; \quad s = - \frac{\partial h}{\partial T}, \quad (6)$$

where  $h = h(x_k, t)$  is the Helmholtz free energy

$$h \equiv u - Ts, \quad (7)$$

and  $\alpha^n = \alpha^n(x_k, t)$  is a set of  $N$  internal state variables ( $n = 1, \dots, N$ ) whose evolution is governed by  $N$  rate laws of the type

$$\dot{\alpha}^n = \Omega^n(\varepsilon_{kl}, T, \alpha^m); \quad n, m = 1, \dots, N. \quad (8)$$



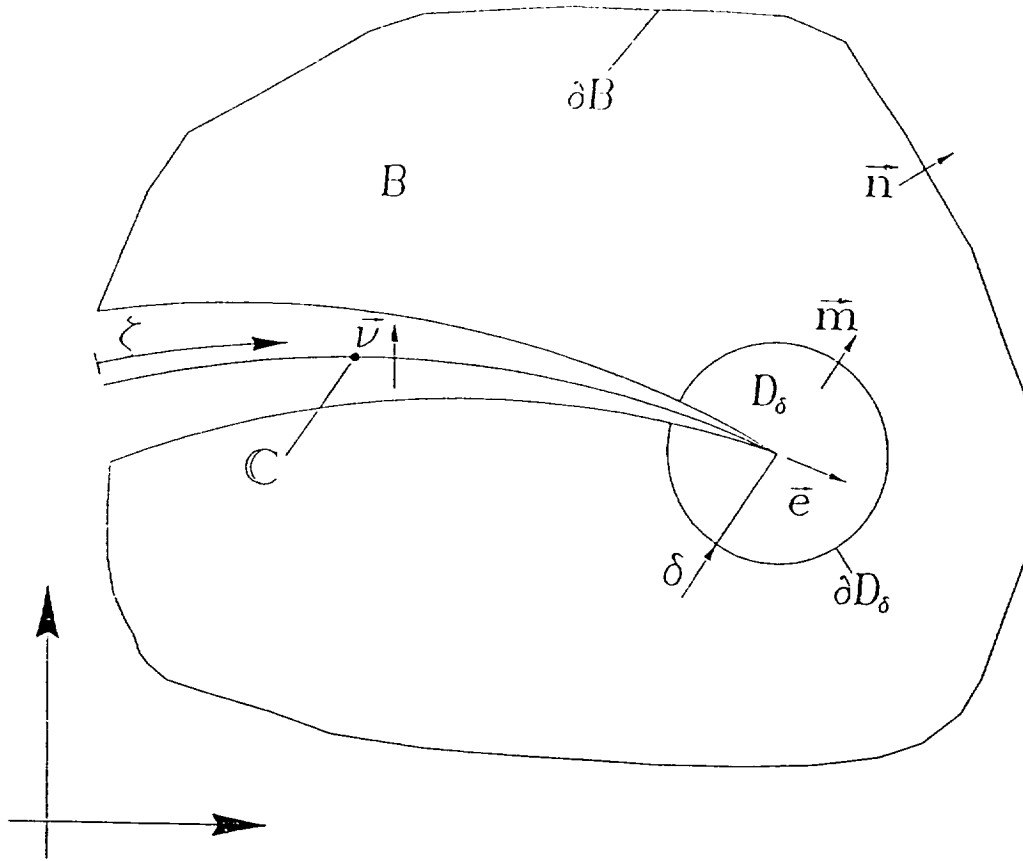


Fig. 1. Crack without a cohesive zone.

generic field variable  $\phi$ , let

$$\phi^\pm = \lim_{\xi \rightarrow 0} \phi(x_k \pm \xi v_k, t); \quad \xi \in \mathbb{R}^+, \quad x_k \in \mathbb{C}(t) - l(t),$$

$$\phi^+ - \phi^- = [\phi]. \quad (16)$$

By the above definition, each field variable is allowed to suffer at most a jump discontinuity across the interior of the crack surface. The behavior of such variables in the neighborhood of the crack tip will be discussed separately for each variable if and when the problem is encountered. Following Gurtin [24–25] we define a circle  $D_\delta$  of radius  $\delta$ , with center at the crack tip and translating with the crack tip itself. Thus, all points on the boundary  $\partial D_\delta$  of  $D_\delta$  are characterized by the same velocity vector as that of the crack tip. The unit normal vector to  $\partial D_\delta$ , outward with respect to  $D_\delta$ , will be called  $m_i$ , as shown in Fig. 1.

## 2.2. Thermodynamics of a crack without a cohesive zone

In this section the key results of the continuum thermodynamics analysis of a moving sharp crack without a cohesive zone are stated. For a complete derivation of the relationships reported here see the works by Gurtin [24–25] and those by Nguyen [28–29].

The second law of thermodynamics for the body B and the crack tip alone, respectively, can be proved to take on the form:

$$\int_{\Pi} \rho \eta_{\text{mic}} T \, dA \geq 0; \quad (G - 2\gamma_0)\dot{l} \geq 0. \quad (21)$$

*Remark 2.1.* The second of (21) is nothing but the Griffith criterion:

$$\dot{l} > 0 \quad \text{if} \quad G \geq 2\gamma_0.$$

Subcritical crack growth, i.e.  $\dot{l} > 0$  and  $0 < G < 2\gamma_0$ , violates the second of (21) and as such is not thermodynamically admissible for the conditions described above (i.e. no cohesive zone). It is important to realize that relationships (21) are independent of the chosen constitutive equations as long as the resulting thermomechanical fields satisfy assumptions A1 and A2, and that they are a direct consequence of having assumed that the crack tip is sharp, i.e. represented by a single geometrical point. Thus, theories that introduce a damaged zone around the crack (with special constitutive behavior) but that still consider the crack tip as a single point in general will not result in thermodynamical admissibility of SCG.

*Remark 2.2.* The temperature behavior at the crack tip is essentially determined by assumptions A1 and A2 rather than the heat conduction law assumed. In fact, for the right hand side of (19) not to vanish it is necessary that the heat flux be singular of order  $1/r$ . Thus, if we have a heat conduction law in which the heat flux is proportional to the temperature gradient, then the temperature field is singular at the crack tip, and the singularity must be weaker than  $1/r$ . In particular, if the Fourier law of heat conduction is assumed, then  $T$  is singular of order  $\log(r)$  [29, 42–43]

$$T = \frac{(G - 2\gamma_0)\dot{l}}{2k\pi} \log r + \text{more regular terms.} \quad (22)$$

The above equation shows that  $T$  has the sign of  $(G - 2\gamma_0)\dot{l}$ . This result reinforces the significance of (21) and what was discussed in Remark 2.1 since subcritical crack growth would imply that the absolute temperature becomes infinite and negative at the crack tip. This is clearly thermodynamically and physically incorrect. Note that relationships (21) and (22) suggest the interesting interpretation of a moving crack tip as a moving heat source, and this is consistent with numerous observations of intense heating ahead of a propagating crack [42–43].

*Remark 2.3.* Through singularity analysis various authors, such as Rice [35], Kfoury and Rice [36] and Nguyen [28–29], have shown that the quantity  $G$  is automatically null for the running crack problem, for almost every type of material behavior except the thermoelastic one. In other words, the quantity  $G$ , as a fracture parameter, is meaningless in most cases, such as in viscoplasticity. Nguyen has also shown that this is due to the fact that  $G$  (as given in (20)) is determined under the erroneous assumption that the field equations remain everywhere elliptic. In [44], for a nonlinear elastic material, the governing equations of the crack propagation problem have been shown to change their nature, becoming locally hyperbolic and therefore

Surface energy is in fact an essential component of the driving force in sintering [50]. Note that, assuming that the second law holds in the form given in (24) but not in (21), SCG appears to be possible only when some volumetric dissipation is present, in order to compensate for the negative contribution due to the crack advancement [18]. Thus, even under the assumption that inequality (24) holds, the present thermodynamic analysis is unable to cope with the problem of SCG in ceramic materials that behave in a virtually perfectly brittle fashion.

In Section 3 it will be shown that SCG can occur even under the restrictions of (21) when a dissipative cohesive zone is present ahead of the crack tip or, in other words, when the crack tip is no longer considered to be a single geometrical point but a finite length crack line segment that can display a special characteristic behavior of its own. The dissipation analysis for a crack with a cohesive zone will show that, in such a case, no problems arise concerning the temperature field and that a continuum thermodynamic theory consistent with SCG in brittle materials can be provided.

### 2.3. Thermodynamics of a crack with a cohesive zone

As mentioned above, the analysis of the running crack problem (without a cohesive zone) presents major difficulties in that the parameter  $G$  becomes meaningless except for materials that behave, at least asymptotically, as if they were thermoelastic. Moreover, the dissipation analysis leads to uncertain results especially as far as the temperature field is concerned. A way to overcome some of these difficulties, while remaining in the framework of continuum thermodynamics, is to postulate the existence of a cohesive zone (c.z.) ahead of the crack tip.

With reference to Fig. 2, a cohesive zone is defined as a portion of the crack line  $C(t): \{\zeta: 0 \leq \zeta \leq \beta(t)\}$  (a more formal definition is given later) such that along  $\alpha(t) \leq \zeta \leq \beta(t)$ , a system of cohesive forces is acting. At this moment it is not necessary to specify the nature of the cohesive force system. From its definition it appears clear that a cohesive zone, even when characterized by a certain opening displacement, has no volume associated with it. Thus, a c.z. appears to be more a 'mathematical' entity rather than a 'physical' one, but, as it will be shown later, its introduction into the model allows one to overcome most of the aforementioned problems in the context of continuum thermodynamics, without using nonlocal theories. A c.z. is not to be confused with a so-called process zone. The latter is usually defined as a region of finite volume around the crack tip and possibly all around the crack faces with special constitutive equations that translate the behavior of the damaged material ahead of the crack tip and in the crack wake. Note that in principle the existence of a process zone does not necessarily overcome both the problem concerning  $G$  and that concerning the singularity in the temperature field since the crack tip is still considered a single geometrical point and since the process zone constitutive equations are not, in general, those of a thermoelastic material.

The crack is now defined as follows

$$\begin{aligned} C(t) &= \{x_k(\zeta): 0 \leq \zeta \leq \beta(t)\}, \\ \text{c.z.} &= \{x_k(\zeta): \alpha(t) \leq \zeta \leq \beta(t)\}. \end{aligned} \tag{25}$$

After Gurtin [26], we define the crack internal energy per unit length (surface),  $\varepsilon$  such that

$$\varepsilon = \begin{cases} 2\gamma_0 = \text{const}, & 0 \leq \zeta \leq \alpha(t), \\ \varepsilon(\zeta, t), & \alpha(t) < \zeta < \beta(t), \\ 0, & \zeta = \beta(t). \end{cases} \quad (27)$$

An analogous definition can be given to the crack entropy  $\varphi$

$$\varphi = \begin{cases} \varphi_0 = \text{const}, & 0 \leq \zeta \leq \alpha(t), \\ \varphi(\zeta, t), & \alpha(t) < \zeta < \beta(t), \\ 0, & \zeta = \beta(t). \end{cases} \quad (28)$$

Let  $\vartheta = \vartheta(\zeta, t) \geq 0$  be the crack absolute temperature, such that

$$\begin{aligned} \vartheta &= T^+ = T^- \\ \forall \zeta: \zeta \in \text{c.z.} \end{aligned} \quad (29)$$

The above definition implies that the temperature field is continuous across the c.z. From (27)–(29) the crack Helmholtz free energy  $\psi$  is defined in the traditional way

$$\psi = \varepsilon - \varphi \vartheta. \quad (30)$$

Given the above definitions, the first law of thermodynamics for the cohesive zone alone can be proven to take on the form

$$\frac{d}{dt} \int_{\alpha(t)}^{\beta(t)} \varepsilon d\zeta + 2\gamma_0 \dot{\alpha} = \int_{\alpha(t)}^{\beta(t)} (\sigma_i \dot{\delta}_i - [q_i] v_i) d\zeta, \quad (31)$$

Eqn. (31) can also be given the following local form

$$\dot{\varepsilon} = \sigma_i \dot{\delta}_i - [q_i] v_i. \quad (32)$$

A statement of the second law for the c.z. cannot be deduced using the same arguments employed to derive (21), but rather it must be postulated. Thus, the second law for the c.z. alone will be given the following global and local forms respectively, after Gurtin [26]

$$\int_{\alpha(t)}^{\beta(t)} \left( \dot{\varphi} + \frac{[q_i] v_i}{\vartheta} \right) d\zeta \geq 0, \quad (33)$$

$$\dot{\lambda} = \dot{\varphi} + \frac{[q_i] v_i}{\vartheta} \geq 0, \quad (34)$$

where  $\lambda = \lambda(\zeta, t)$  for  $\alpha < \zeta < \beta$  and  $\lambda = 0$  for  $\zeta = \beta$ , is the intrinsic entropy production per unit length in the cohesive zone. It can be proven that relationships (33) and (34) are consistent with

analyze the energetics of a few significant cases of cohesive zone evolution. The analysis begins with the characterization of the thermodynamic force or work conjugate to the kinematic variable  $\alpha$ , since, as a consequence of definitions (27) and (28) that set  $\dot{\alpha}(f, t) = 0$  and  $\varphi(f, t) = 0$ ,  $\alpha$  is the only independent state variable at the global level that characterizes the c.z. growth process.

### 3.1. Model development

In order to properly characterize the thermodynamic force conjugate to the rate of  $\alpha$ , the rate of change of all the thermodynamic quantities of interest must be decomposed into a part due solely to the change of  $\alpha$  and a part due to the change of the other global independent state variables, e.g. the boundary conditions. Since  $\alpha$  is a global independent state variable [34], any generic dependent variable  $\phi$  can be written as explicitly dependent on  $\alpha$  [34]

$$\phi(x_k, t) = \phi(\alpha, t). \quad (38)$$

Hence, the material time derivative of  $\phi$  can be more conveniently rewritten as follows

$$\dot{\phi} = \frac{\partial \phi}{\partial \alpha} \dot{\alpha} + \frac{\partial \phi}{\partial t} \quad \left| \alpha = \text{const} \right. \quad (39)$$

In order to proceed further into the analysis, we now need to specify a set of c.z. constitutive equations. For the sake of simplicity and completeness (i.e. to study a c.z. with internal dissipative mechanisms) we will use the set of constitutive equations introduced below, inspired by an elementary theory of plasticity.

Consider the following decomposition of the c.z. opening displacement

$$\delta_i = \delta_i^e + \delta_i^p, \quad (40)$$

where  $\delta_i^e$  is the recoverable part of the opening displacement, i.e.  $\sigma_i = 0 \Rightarrow \delta_i^e = 0$ , and  $\delta_i^p$  is the permanent, unrecoverable one. Also let

$$\psi = \psi(\delta_i^e, g), \quad (41)$$

such that

$$\frac{\partial \psi}{\partial \delta_i^e} = \sigma_i; \quad - \frac{\partial \psi}{\partial g} = \varphi. \quad (42)$$

Thus, from (37) we obtain

$$g \dot{\gamma} = \sigma_i \dot{\delta}_i^p \geq 0. \quad (43)$$

The associated flow rule is assumed to be given by the traditional form

$$\dot{\delta}_i^p = \frac{\partial \sigma_i}{\partial g}, \quad (44)$$

Thus, rewriting (48) as follows

$$(R - G)z = \int_{x_0}^{x_1} ([q_1]v_1 - [q_2]v_2) dz, \quad (50)$$

and from definition (47), we see that subcritical crack growth, when it occurs, can be viewed as a heat absorption mechanism, where the primary heat source is represented by inelastic mechanisms such as plasticity that are active within the cohesive zone. Note that the result presented here is absolutely general and independent of the chosen constitutive equations. This can be seen from the fact that the term  $[q_1]v_1$  in (47) can be defined also by the expression on the right hand side of the equality sign, which is independent of the c.z. constitution. From inequality (49) it can also be inferred that in order for SCG to happen there is need of some kind of dissipative mechanism reflected in the first term of (49) that is able to drive the crack propagation. This consideration is important for a better understanding of SCG in nearly perfectly brittle systems where it appears to be consistent with experimental findings that reveal the presence of phase transformation phenomena and bridging force systems ahead of an advancing crack [53-54]. In other words, even in materials whose bulk behavior is mainly elastic, SCG and/or R-curve behavior are possible due to the presence of a small dissipative c.z. and thus with a behavior very different in nature from that of the bulk. Note also that a stricter interpretation of (49) leads to the conclusion that SCG can only happen in the presence of a cohesive zone. This latter interpretation, which is of course limited by the assumptions used to derive (49), can be considered more properly an invitation to check for the presence of a cohesive zone when subcritical propagation is observed rather than a necessary requirement for SCG to occur.

*Remark 3.1.* As mentioned earlier,  $\alpha$  can be treated as a global internal state variable [34] whose presence into the problem formulation should be accompanied by a corresponding evolution equation [33-34]. In other words, the evolution equation for  $\alpha$  cannot be simply derived using the conservation laws already used in the formulation of the problem, such as (50), because this would make it impossible to construct a corresponding well posed boundary value problem. On the other hand, a crack evolution law and a well posed problem can be derived using a thermodynamic analysis such as the one presented here if some additional and ad hoc assumptions are made. Clearly, the validity of such assumptions must be evaluated depending on the specific problem at hand. This matter will be more extensively considered in cases 2 and 3 presented below.

### 3.2. Simplified examples

We will now apply the analysis presented so far to three important cases of crack propagation:

CASE 1: self similar crack propagation

CASE 2: slow crack growth under general deformation of the c.z.

CASE 3: slow crack growth under cyclic loading

Case 1. Let  $\Delta$  be the length of the cohesive zone of a rectilinear crack

$$\Delta = \beta(t) - x(t).$$

(51)

consider a case in which  $\varphi$  is constant along the c.z. Thus, from (34), (42) and (52) we have

$$\varphi = -\frac{c_{\varphi}^2}{c_{\varphi}^2} z = 0, \quad (57)$$

and

$$\dot{\gamma} \beta = \sigma' \delta \beta' = [q_i] v_i. \quad (58)$$

Equation (58) illustrates the point. Note that (57) implies that the transformation is isentropic for the c.z.

**Case 2.** During rapid crack propagation a significant temperature concentration is observed at the crack tip and its vicinities. During slow crack growth, instead, the heating in the vicinity of the crack tip is much more contained. Up to the point that, in some instances it is reasonable to assume that the heat flux out of the crack tip is null. This assumption can be given the following mathematical form:

$$\int_{\beta(t)}^{x(t)} [q_i] v_i d\zeta = 0. \quad (59)$$

Note that (59) does not imply that there is no heating around the crack tip, it only implies that there is no contribution to that heating from the movement of the cohesive zone, or, in other words, that the cohesive zone is not behaving like a line heat source. Heating around the cohesive zone can still occur due to the presence of dissipation mechanisms within the bulk of the material.

Substituting (59) into (48) we obtain

$$\int_{\beta(t)}^{x(t)} [q_i] v_i d\zeta + (G - R) \dot{z} = 0. \quad (60)$$

Recalling that the first term on the left hand side represents the heat flux due to c.z. inelastic dissipation computed at constant  $\alpha$  and that therefore it cannot be negative, in order for (60) to be satisfied the crack extension process ( $\dot{\alpha} > 0$ ) must necessarily be subcritical, i.e.  $(G - R) < 0$ . Moreover, under assumption (59) it is possible to derive the crack evolution law directly from the first law of thermodynamics for the c.z., i.e. (60). In fact, since both the first term on the left hand side of (60) and the generalized thermodynamic force  $(G - R)$  are independent of the crack propagation rate, it is possible, under the circumstance, to solve (60) with respect to the crack propagation rate to obtain

$$\dot{z} = \frac{\int_{\beta(t)}^{x(t)} [q_i] v_i d\zeta}{(R - G)}. \quad (61)$$

*Remark 3.3.* Note that (59) also implies that, in this case, the c.z. evolution takes place with no net dissipation, which means that all of the energy dissipated by inelastic mechanisms in the c.z.

In practical applications, (62) is often used in a much simplified form. For example, it is often assumed that

$$G_M = G_{max}; \quad R_M = 2\gamma_0, \quad \frac{d\varphi}{dt} = 0, \quad (65)$$

where  $G_{max}$  is the maximum value of  $G$  in a given cycle. Thus, (62) is simplified to

$$\Delta x = \frac{2\gamma_0 - G_{max}}{\Delta V}, \quad (66)$$

where

$$\Delta V = \int_{t+\Delta t}^t \left[ \int_{f(t)}^{x(t)} \sigma_t \frac{\partial \delta_f^t}{\partial t} dz \right] dt. \quad (67)$$

As can be seen from (67),  $\Delta V$  is the part of the plastic work per cycle done independently of an advancement of  $x$ . In studies in metal fatigue with small scale yielding, it is usually considered acceptable to approximate  $G_{max}$  and  $\Delta V$  as follows [15-16, 19]

$$G_{max} = aK_{max}^2; \quad \Delta V = b\Delta K^4, \quad (68)$$

where  $K_{max}$  is the maximum value of the stress intensity factor and  $\Delta K$  is the stress intensity factor range during a cycle;  $a$  and  $b$  are constants. Thus, (66) is then rewritten in the well known form

$$\Delta x = A \frac{K_{cr}^2 - K_{max}^2}{\Delta K^4} \quad (69)$$

where  $A$  is a constant that accounts for the geometry of the body and  $K_{cr}$  is the critical value of the stress intensity factor.

Note that when the denominator of (69) is constant the advancement per cycle appears to be proportional to the fourth power of the stress intensity factor range, which has been experimentally verified by Paris [2-3]. The derivation of (69) has been presented here not only to show that, after a great deal of simplifying assumptions a law of the Paris type can be derived, but also to explicitly show the number and type of the mentioned assumptions. In particular, the three main simplifying hypotheses behind (69) consist of:

- (1) assuming that the process is globally non-dissipative, as discussed in Remark 3.3;
- (2) that the resistance to crack growth reduces to a constant value, as shown in (65); and
- (3) that the process is independent of the temperature field around the crack as can be seen by the comparison of (63) and (67).

For these reasons the authors feel that there is still a strong need for theoretical research in the field of fatigue and evolution laws for crack propagation in general, and that the application of



craze zone itself. Thus, a complete study of DCP requires the development of time dependent constitutive equations for the craze zone together with the adoption of time dependent material properties. It also requires a stability analysis capable of predicting when the unstable fracture takes the place of the craze subcritical propagation and when DCP will turn into FCG. Very few models for DCP have been presented in the open literature [12, 66], at least to the authors' knowledge, and the thermodynamics of the process certainly needs further study. In what follows, a two-phase cohesive zone model for DCP together with its thermodynamic analysis will be presented. From a conceptual viewpoint, the model presented here is based on a generalization of definitions (27) and (28). The focus of the discussion will be on the analysis of subcritical craze propagation during DCP, leaving a more detailed and complete analysis to future studies.

#### 4.1. A two-phase cohesive zone model for DCP

With reference to Fig. 3, consider a cohesive zone of length  $\beta - \alpha$  that presents two phases (zones) with distinct structure and behavior. It is assumed that the structure of phase 2 can be changed into that of phase 1 when the c.z. is under load. Such a structure change will be referred to as a phase change. Clearly, in order for this phase change to occur it is necessary to expend a certain amount of energy. It is assumed that a phase change energy per unit length  $\chi = \chi(x_i, t)$  can be defined.  $\chi$  is a material property, generally a function of time and temperature and it is to be experimentally determined. Let  $\xi(t)$  be the position of the phase boundary along the c.z. The c.z. opening displacement  $\delta_i$  must be a continuous function, whereas a discontinuity for the cohesive force  $\sigma_i$  will be allowed at  $\xi = \xi$  in order to differentiate between the constitutive behavior of the two phases. Such a difference in behavior also justifies the assumption that both the c.z. internal energy and the c.z. entropy may have discontinuities at the phase boundary.

$$\lim_{p \rightarrow 0} e(\xi(t) - d, t) = e_1; \quad \lim_{p \rightarrow 0} e(\xi(t) + d, t) = e_2, \\ \lim_{p \rightarrow 0} \phi(\xi(t) - d, t) = \phi_1; \quad \lim_{p \rightarrow 0} \phi(\xi(t) + d, t) = \phi_2, \quad (70)$$

where  $d \in \mathbb{R}^+$ , and, in general,  $e_1 \neq e_2$  and  $\phi_1 \neq \phi_2$ . Recall that (31) is valid independently of the number of phases within the c.z. Using relationships (70) and the transport theorem, the first and second laws for the c.z. can be rewritten as follows

$$\frac{d}{dt} \int_{\beta(t)}^{\alpha(t)} e \, d\xi + 2\gamma\alpha + (e_2 - e_1)\xi = \int_{\beta(t)}^{\alpha(t)} (\sigma_i \delta_i - [q_i]v_i) \, d\xi, \quad (71)$$

$$\frac{d}{dt} \int_{\beta(t)}^{\alpha(t)} \phi \, d\xi + \phi(\xi) \dot{\xi} = \alpha_i \dot{\xi} + (\phi_2 - \phi_1)\dot{\xi} + \int_{\beta(t)}^{\alpha(t)} \frac{\theta}{[q_i]v_i} \, d\xi \geq 0, \quad (72)$$

where the more general  $\gamma = \gamma(t)$  has been used instead of the (constant)  $\gamma_0$ . Note that  $(e_2 - e_1)d\xi$  and  $(\phi_2 - \phi_1)d\xi$  are, respectively, the energy and the entropy necessary to transform an amount  $d\xi$  of phase 2 into phase 1. Thus, we have

$$\chi \equiv e_2 - e_1, \\ \Phi \equiv \phi_2 - \phi_1, \quad (73)$$

where the phase change entropy per unit length  $\Phi$  is also a material property.

Thus, (75) can be simplified to

$$[G^* - (2\gamma + \chi)]\dot{z} = \int_{\beta(z)}^{\alpha(z)} [q_1] v_1 dz \quad (80)$$

where

$$G^* = \int_{\beta(z)}^{\alpha(z)} \sigma_1 d\delta_1 \quad (81)$$

From (80), when  $\chi > 0$ , we see that the material is toughened by the presence of a two-phase system since it behaves with an apparent surface energy  $2\gamma^*$  which is greater than the surface energy  $2\gamma$  in the crack tip wake

$$2\gamma^* = 2\gamma + \chi \quad (82)$$

Note that in order for such an evolution to be thermodynamically admissible the following condition must be satisfied

$$G^* \geq 2\gamma^* \quad (83)$$

The result in (82) is of a certain importance because it offers a stronger justification for the study of a two-phase cohesive zone. In fact the study of such a c.z. could be of great interest not only for DCP but also for the understanding of phase transformation toughening phenomena both in polymers and in ceramics [53-54, 67].

*Remark 4.1.* The two-phase model presented can be simplified in such a way that only one phase is present in the cohesive zone and that it is still possible to describe DCP. Such a simplification is achieved by postulating the existence of a single phase and by changing (27) and (28) as follows

$$\varepsilon = \begin{cases} 2\gamma, & 0 \leq \zeta \leq \alpha(t) \\ \alpha(\zeta, t), & \alpha(t) \leq \zeta \leq \beta(t) \\ \chi, & \zeta = \beta(t) \end{cases} \quad (84)$$

$$\phi = \begin{cases} \phi', & 0 \leq \eta \leq \alpha(t) \\ \phi(\zeta, t), & \alpha(t) \leq \zeta \leq \beta(t) \\ \Phi, & \zeta = \beta(t) \end{cases} \quad (85)$$

where  $\phi'$  is the crack surface entropy outside the c.z. The c.z. evolution is then analyzed using the same procedure outlined above.

of geometry and material properties both for the body and the cohesive zone is not intended to represent any real material system but rather is made in such a way that the resulting boundary value problem can be solved in closed form. In particular, as shown in Fig. 4, the body is assumed to be infinitely extended and linear elastic. Figure 4 also shows the loading conditions, represented by a uniform traction distribution in the direction perpendicular to the crack plane. The cohesive zone has been assumed to behave, in each of the phases, like a Dugdale model. Each phase is therefore characterized by a uniform cohesive force distribution of known value, as shown in Fig. 5. Such an approach is rather common in the study of crazing in polymers [12, 58-59, 63]. The problem outlined was solved, in closed form, with the use of Muskhelishvili complex potentials [68], under the assumption of plane stress deformation, using the material constants for Polystyrene given in [56-57] and summarized in Table I. The following empirical instability condition has been chosen: an advancement of  $\alpha$  to the position occupied by  $\beta$  occurs when  $(\tilde{\epsilon} - \epsilon) \geq 0.95(\beta - \alpha)$ . Such a criterion is based on the observations by Hertzberg et al. [65] that, for different polymers, the craze zone ahead of a crack tip seems to become unstable during the last 10 percent of its life cycle, which corresponds roughly to a craze development between 90 and 100 percent of the length of the entire cohesive zone.

Figures 6a-6e show the trend of two cases of DCP, obtained with the use of (126) together with the following approximations

$$G_{iM}^* = G_{iM}^{*max}; \quad R_{iM}^* = \gamma. \quad (92)$$

The results shown in Fig. 6a and Fig. 6b have been computed using 0.1 MPa as the value for the maximum applied load  $T_0$  and  $5.0 \times 10^{-3}$  m as the value of the initial crack length. The results

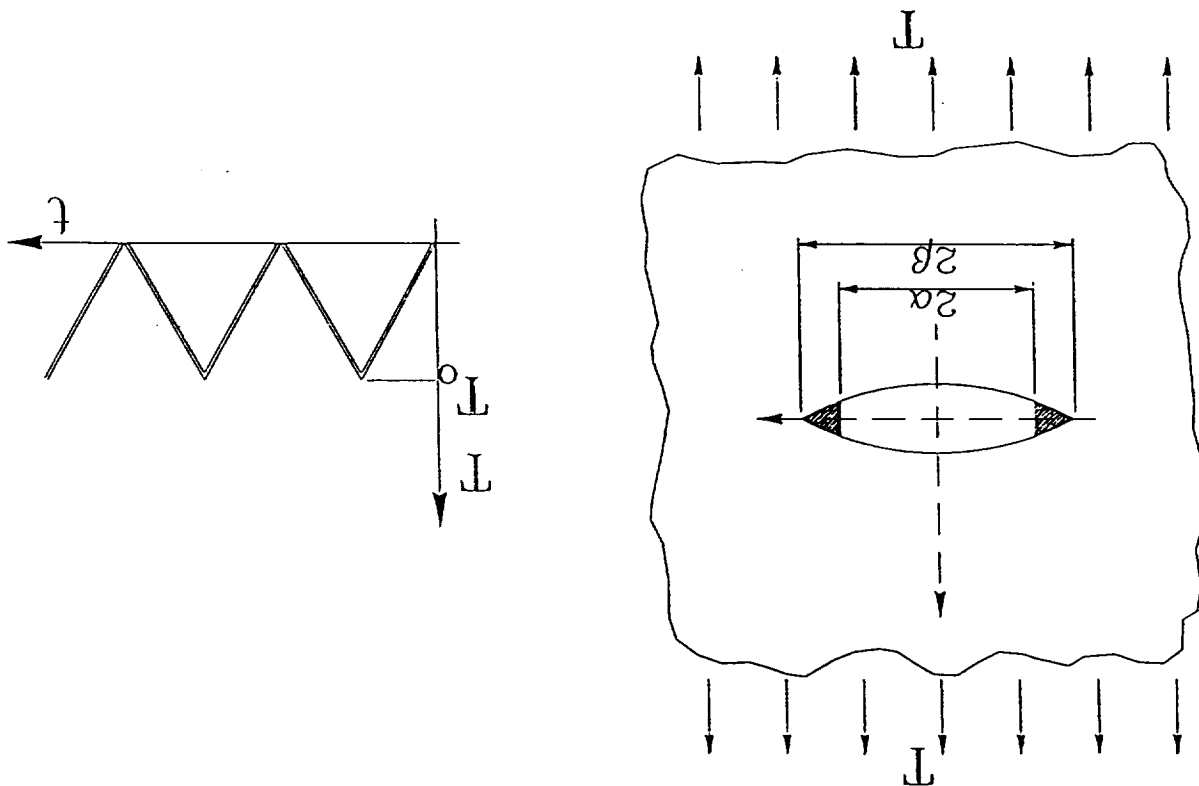


Fig. 4. Example geometry and load conditions.

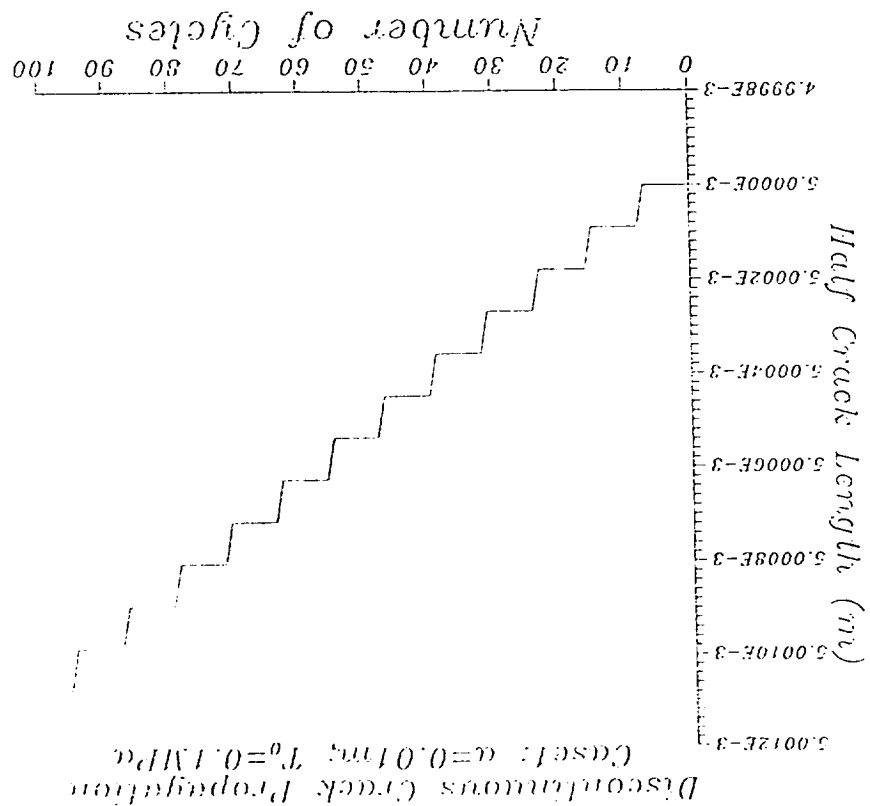


Fig. 6a. Discontinuous crack propagation.

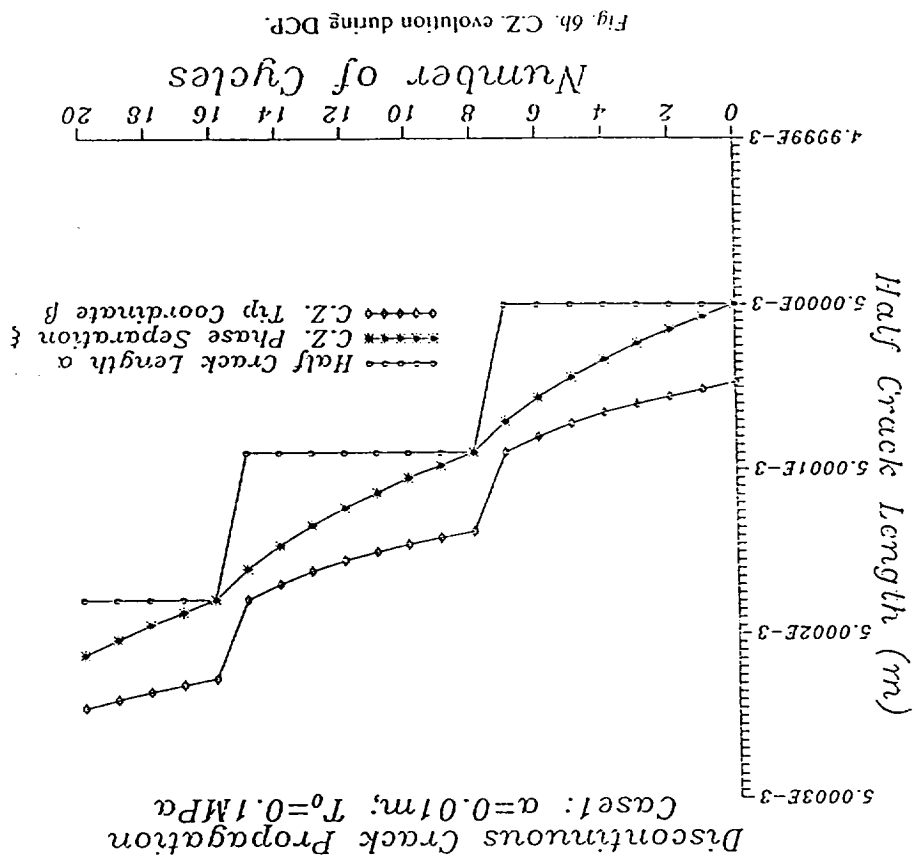


Fig. 6b. CZ evolution during DCP.

# Discontinuous Crack Propagation

$$a = 0.01 \text{ m}$$

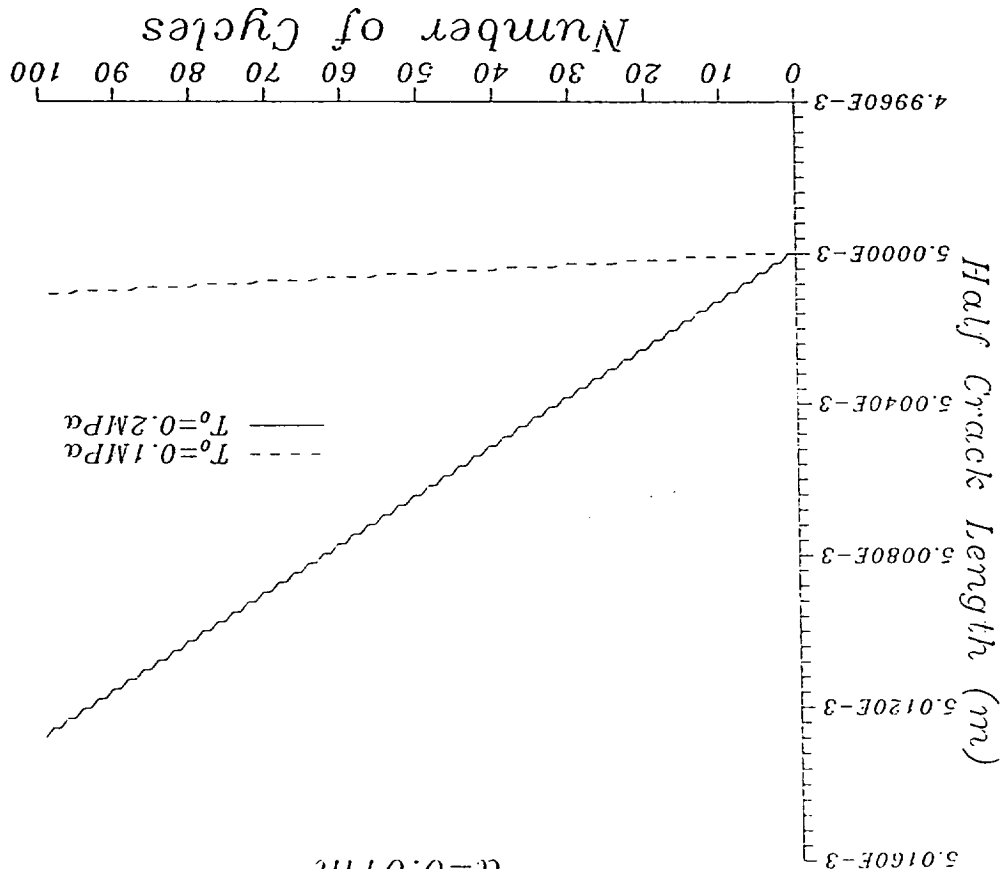


Fig. 6e. Comparison of the two DCP cases.

As far as discontinuous crack propagation is concerned, it is felt that a detailed accurate thermodynamic analysis is necessary, especially regarding the stability of the cohesive zone evolution and the transition from a DCP mode to a SCG mode, during which crack propagation occurs at every load cycle. Possible applications of the theory include the study of delamination in laminated composites, R-toughening in ceramics and problems of matrix-fiber interface degradation in fiber reinforced composites.

## Acknowledgments

The authors are grateful to Dr. J.G. Boyd for valuable discussions and gratefully acknowledge partial funding for this research, which was supplied by NASA Langley Research Center, under Grant NAG 1-1120.

## References

1. P.C. Paris, in *Fatigue Thresholds*, J. Backlund, A.F. Blom and C.J. Bevers (eds.), Chanclem, London, 1 (1982) 3-10.
2. P.C. Paris, *The Growth of Cracks Due to the Variations in Loads*, Ph.D. thesis, Lehigh University, Bethlehem, Pa. (1962).

53. T. Fett and D. Munz, *Journal of the American Ceramic Society* 75 (1992) 958-963.
54. K. Jakus, J.E. Ritter and R.H. Schwilinski, *Journal of the American Ceramic Society* 76 (1993) 33-38.
55. J.R. Rice, *Journal of Applied Mechanics* 35 (1968) 379-386.
56. J. Boissis, A. Chudnovsky and A. Moer, *International Journal of Fracture* 33 (1987) 263-276.
57. *Ibid.* 33 (1987) 277-284.
58. N. Verheulpen-Heymans and J.C. Baauwens, *Journal of Materials Science* 11 (1976) 1-6.
59. *Ibid.* 11 (1976) 7-16.
60. B.D. Lauterwasser and E.J. Kramer, *Philosophical Magazine*, A 39 (1979) 469-493.
61. R. Schirrer, J. LeMasson, B. Tomatis and R. Lang, *Polymer Engineering and Science* 24 (1984) 820-824.
62. E.J. Kramer, *Polymer Engineering and Science* 24 (1984) 761-769.
63. S.S. Chern and C.C. Hiao, *Journal of Applied Physics* 53 (1982) 6541-6551.
64. B. Budiansky and J.W. Hutchinson, *Journal of Applied Mechanics* 45 (1978) 267-276.
65. R.W. Herzberg, M.D. Skibo and J.A. Manson, in *Fatigue Mechanisms*, ASTM STP 675, (1979) 471-500.
66. K. Kadota and A. Chudnovsky, in *Recent Advances in Damage Mechanics and Plasticity*, AMD-Vol. 132/Md-Vol. 30, J.W. Ju (ed.), ASME (1992) 115-130.
67. J. Kim and R.E. Robertson, *Journal of Material Science* 27 (1992) 3000-3009.
68. N.I. Muskhelishvili, *Some Basic Problems of the Mathematical Theory of Elasticity*, Noordhoff, Groningen, The Netherlands (1963).

PHOTOCOPIED FROM A MICROFILM OF THE ORIGINAL

# Modeling of Delamination Damage Evolution in Laminated Composites Subjected to Low Velocity Impact

DAVID C. LO\* AND DAVID H. ALLEN\*\*

*Center for Mechanics of Composites  
Texas A&M University  
College Station, TX 77843*

**ABSTRACT:** This study examines the delamination evolution, under quasi-static conditions, of laminated polymeric composites with mechanically nonlinear resin rich interfaces. The constitutive behavior of the interface is represented by two models developed by Needleman [1] and Tvergaard [2]. These models assumed that the interfacial tractions, a function of only the interfacial displacement, will behave similarly to the interlaminar forces generated during the interlaminar separation. The interface material's parameters control the load at which the delamination growth initiates and the final delamination size. A wide range of damage accumulation responses have been obtained by varying the model parameters. These results show that Tvergaard's model has been found to be better suited of the two models in predicting damage evolution for the configurations examined.

**KEY WORDS:** delamination damage, low velocity impact, laminated composites, finite element modeling.

## INTRODUCTION

LAMINATED COMPOSITES IMPACTED at low velocity by blunt objects are susceptible to the development of interply delaminations. While this subsurface damage is not readily visible at the surface, it is capable of substantially reducing the residual strength and stiffness of the laminate. The resultant damage induced stress redistribution can lead to the failure of the component. Therefore, it is essential to be able to predict the damage evolution that occurs during the impact event so that the serviceability of the laminate can be determined.

Much effort has been directed in recent years toward gaining a better understanding of the damage that results when laminated composites are subjected to low velocity impact (LVI). This is evident from the numerous studies,

both experimental and analytical, that have appeared in the literature. A brief overview of the literature is presented here.

Greszczuk [3] provides an excellent treatment of the fundamentals involved in the analysis of LVI. He has divided the problem into three logical steps: "(1) determination of impactor-induced surface pressure and its distribution," (the contact problem), "(2) determination of internal stresses in the composite target caused by the surface pressure, and (3) determination of failure modes in the target caused by the internal stresses."

Although most LVI events are three-dimensional in nature, a great deal can be learned from a two-dimensional simplification of the problem (as in the current work). Choi et al. [4,5] have conducted an extensive experimental and analytical study of LVI that is two-dimensional. They have used a line-nosed impactor so as to produce a uniformly distributed transient dynamic load across the specimen width, thereby reducing the complexity of the problem from 3-D to 2-D. Tests were conducted on specimens of several different stacking sequences constructed from T300/976. Different values of mass and impact velocity were used as test parameters. A phenomenon observed to be common to all of the specimen types tested was that damage initiation took the form of what the authors called critical matrix cracks. These critical matrix cracks were located in the 90° plies, near the specimen midplane and were inclined at an angle of about 45°. Delaminations and concomitant secondary matrix cracks were observed to form and propagate after the formation of critical matrix cracks. The authors conducted a two-dimensional transient dynamic finite element analysis in an attempt to model the impact event. They assumed Hertzian contact and used plane strain constitutive relations. They were able to predict the location of damage initiation reasonably well using a matrix failure theory. Once the critical matrix crack had been predicted by the model, a "post-failure" analysis was conducted to predict damage growth. This analysis was executed by setting to zero certain members of the material modulus matrix for elements where the critical matrix crack occurred. Bogdanovich and Larve [6,7] have conducted a two-dimensional analysis of the LVI problem. They investigated the impact of a rigid body of revolution on several different laminates, some of which possessed energy absorbing interleaves. The analysis used in this work employs polynomial spline interpolation functions. A maximum stress failure criterion is used to predict failure initiation. Their results show that interleaves can provide significant benefits. Sun and Rechkak [8] have also conducted a two-dimensional analysis of the problem. They reported the presence of matrix cracks inclined at 45°. In addition, they addressed the optimal location of interleaf layers so as to reduce damage. Jih and Sun [9] and Sankar et al. [10] have shown that when the impact event is characterized by a heavy impactor traveling at low velocities the impact event can be modeled as a quasi-static process. In addition, Sankar found that for large contact areas, the contact stress deviates from the often used Hertzian solution [11].

\*Graduate Research Assistant.

\*\*Director and author to whom correspondence should be addressed.

While few papers have appeared which attempt to address the three-dimensional problem of LVI, noteworthy are those of Wu and Springer [12, 13] and of Wu and Chang [14]. In these works a three-dimensional transient dynamic finite element analysis is presented for the study of LVI. With the exception of the research by Liu et al. [15], the authors have found no papers in the literature which model internal delaminations due to impact as traction free surfaces.

Although many aspects of the LVI problem have been investigated, the current understanding of the process is still incomplete. This is due to the complexity of the mechanisms involved in LVI damage. One area that has not received much attention is the constitutive modeling of the resin rich ply interface region in which delaminations are located. Fractiographs of delamination surfaces from polymeric matrix composites show the presence of fibrils and hackles [16-23]. The former is associated with the formation of crazes ahead of the delamination and is normally found in thermoplastic resins. The latter is associated with the formation of micro shear cracks in front of the delamination. These micro cracks are oriented along the plane of principal tensile stress and is found predominantly in thermosets. In the regions that transform into crazes and shear cracks, the material can be subjected to large strains and may not behave in a linear elastic manner as assumed in the rest of the laminate. While the mechanical response of the interface region may only have a small effect on the overall mechanical behavior of a laminate with a fixed damage state, it can significantly influence the evolution of damage and in turn the laminate's response. Such behavior indicates a need to account for the different material response found in the resin rich interface region. Unfortunately, this region is not explicitly modeled in most LVI damage analyses and of those analyses that do take this resin rich region into account most are for modeling linear elastic interleaves [6-8]. An exception is Ladevez's damage model in which the interface is explicitly modeled [24]. In his model, the mechanical properties of the interface are governed by internal state damage variables. Since the internal state variables are volume averaged representations of the damage state, the stresses and strains obtained from this analysis are also averaged quantities. To the knowledge of the authors, none of the delamination damage models found in the published literature accounts for the development of the process zone ahead of the delamination front and the resulting nonlinearity in the interfacial mechanical response. The current paper will attempt to address this issue by presenting an LVI damage analysis that employs nonlinear constitutive relationships in the modeling of the interfacial response caused by some of the available deformation mechanisms ahead of the delamination. The effects of the interfacial parameters on the evolution of LVI damage in laminated composites will then be examined in detail.

## PROBLEM APPROACH

At the present time, the LVI damage analysis is modeled as a two-dimensional

three-point bending problem. In this paper, LVI is simulated by monotonically increasing loads applied under quasi-static conditions. As previously stated, experimental evidence supports this simplification [9]. The stress states in the individual plies and resin rich interfaces are obtained from finite element analysis. However, due to the nonlinear response of the interface, incremental and iterative solution techniques are employed with the finite element algorithm. Delamination propagation is evaluated using a critical interfacial separation criterion at each load step. If conditions are sufficient for propagation, the amount of growth is calculated and the corresponding change in the interfacial constitutive properties is updated accordingly for the next load step. This procedure is repeated until the maximum impact load is reached. The details of this analysis are presented in the following sections.

## Interface Model

The interface region in which the matrix cracks and delaminations initiate and propagate is composed of resin rich matrix material. Depending on the polymer classification of the resin, the deformation process can be attributed to many mechanisms at the molecular level. These mechanisms include uncoiling and straightening of molecular chains, dislocation movement, reorientation of molecular chain segments, void formation, and chain breakage [25]. Whether one or more of these dissipative mechanisms is activated will depend on such factors as loading rate, temperature, and processing history. Moreover, the mechanical response of the resin in the interface region may be different from that of the response measured in bulk resin specimens. The addition of reinforcing fibers, especially when the resin is sandwiched between two plies with different fiber orientations, will impose constraints that will alter the stress state in the resin rich region, thus suppressing some deformation mechanisms while enabling other deformation mechanisms to occur. Therefore an understanding of the molecular behavior is helpful in order to accurately predict the response of the resin under these conditions.

Since this process is quite complex, phenomenological models for approximating the interfacial response will be used as a first approximation. In the current analysis, two interface models, originally applied to interfacial debonding between the fibers and matrix in metal matrix composites, are considered. Both models assume that the normal traction exerted on the interface during purely normal separation behaves similarly to the interatomic forces during interatomic separation.

The first model, proposed by Needleman, describes the interface surface tractions in two dimensions as follows [1]:

$$T_n = \frac{27}{4} \sigma_{max} \left( \left( \frac{u_n}{\delta} \right) \left[ 1 - 2 \left( \frac{u_n}{\delta} \right) + \left( \frac{u_n}{\delta} \right)^2 \right] + \alpha \left( \frac{u_t}{\delta} \right)^2 \left[ \left( \frac{u_n}{\delta} \right) - 1 \right] \right) \quad (1)$$



$$T_r = \frac{27}{4} \sigma_{max} \left\{ \alpha \left( \frac{u_r}{\delta} \right) \left[ 1 - 2 \left( \frac{u_n}{\delta} \right) + \left( \frac{u_r}{\delta} \right)^2 \right] \right\} \quad (2)$$

for  $u_n \leq \delta$ . Where  $T$  is the interfacial traction and  $u$  is the interfacial displacement. The subscripts  $n$  and  $r$  signify the normal and tangential components of the specific quantity, respectively.  $\sigma_{max}$  is the maximum traction acting on the interface during a purely normal separation.  $\delta$  is the characteristic length and  $\alpha$  is the ratio of the interfacial shear stiffness to the normal stiffness. When  $u_n/\delta$  is equal to one, complete separation has taken place and the tractions are equal to zero. If we consider the expression for the normal component of the interfacial traction, Equation (1), the work done by this traction going from  $u_n/\delta = 0$  to  $u_n/\delta = 1$  in a pure opening mode ( $u_r/\delta = 0$ ) is

$$W_{n,n} = \frac{9}{16} \sigma_{max} \delta \quad (3)$$

Needleman refers to this as the work of separation. Thus, a larger  $\sigma_{max}$  or  $\delta$  will result in a greater amount of energy required to fail an interface.

The second model was proposed by Tvergaard [2] and is a modification of Needleman's model. The modification was undertaken to give the constitutive equations a higher order dependence on the interfacial shear separation and also to include the shear separation into the determination of interfacial failure. A parameter,  $\lambda$ , representing the norm of the interfacial displacement vector, defined by

$$\lambda = \sqrt{\left( \frac{u_n}{\delta_n} \right)^2 + \left( \frac{u_r}{\delta_r} \right)^2} \quad (4)$$

is introduced into the polynomial function. The interfacial tractions are defined in this model by

$$T_n = \frac{27}{4} \sigma_{max} \frac{u_n}{\delta_n} (1 - 2\lambda + \lambda^2) \quad (5)$$

$$T_r = \alpha \frac{27}{4} \sigma_{max} \frac{u_r}{\delta_r} (1 - 2\lambda + \lambda^2) \quad (6)$$

for  $0 \leq \lambda \leq 1$ . Complete separation occurs when  $\lambda \geq 1$ . The parameters for this model are similar to Needleman's except for the individual characteristic length assigned to each component of the interfacial displacement vector. When

the interface is undergoing a pure normal separation, both models are identical and the work of separation, as shown in Equation (3), is applicable to Tvergaard's model as well. Under this interfacial opening condition, the normal component of traction increases to a value of  $\sigma_{max}$  at  $u_n/\delta = u_n/\delta_n = 1/3$  then decreases to zero at  $u_n/\delta = u_n/\delta_n = 1$  as shown in Figure 1.

### Analytic Formulation

Due to the nonlinearity introduced by the interface failure criterion, the virtual work equation is solved in incremental form, resulting in [26]:

$$\int_V C_{ijkl} \Delta \epsilon_k \delta \Delta \epsilon_l dV \cong \int_{\partial V} T_i^{n,r} \delta \Delta u_i dS - \int_V \sigma_{ij} \delta \Delta \epsilon_{ij} dV \quad (7)$$

where  $C_{ijkl}$  is the material tangent modulus tensor,  $\epsilon_{ij}$  is the infinitesimal strain tensor,  $T_i$  is the traction vector,  $\Delta u_i$  is the displacement increment vector, and  $\sigma_{ij}$  is the stress tensor. Also, the domain of interest has interior  $V$  and boundary  $\partial V$ . The superscripts  $i$  and  $r$  denote quantities at time  $t$  (which are assumed to be known) and quantities at time  $t + \Delta t$ , respectively. In the current paper the modulus tensor  $C_{ijkl}$  is everywhere constant and linear elastic except at the interface, where it changes with the interfacial separation. The approximate nature of Equation (1) is due to the fact that higher order terms in  $\Delta u_i$  are neglected in the incrementalization process. However, this approximation is accounted for in a

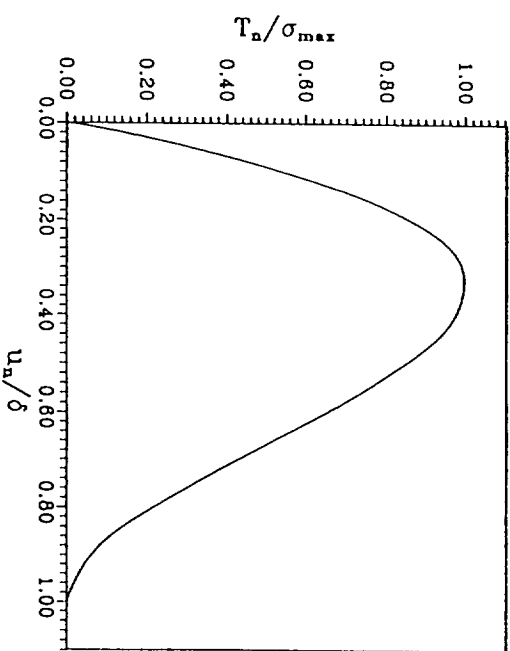


Figure 1. Normal traction—normal displacement response of Needleman's model.

rather standard way by incorporating a Newton-Raphson iteration scheme for each increment of boundary tractions. Thus, the displacement increment is successively updated as follows for the  $j$ th iteration:

$$\{\Delta u\}_j = \{\Delta u\}_{j-1} + \{\Delta \Delta u\}_j \quad (8)$$

where  $\{\Delta \Delta u\}_j$  is obtained by solving the following on the  $j$ th iteration:

$$[K]\{\Delta \Delta u\}_j = \{F^{*av}\}_j - \{R^{*av}\}_{j-1} \quad (9)$$

where  $[K]$  is the global stiffness matrix,  $\{F\}$  is the global force matrix, and  $\{R\}$  is the global reaction matrix.

Equations (2) and (3) are solved recursively until the following convergence criterion is satisfied:

$$\frac{|\Delta u|_j - |\Delta u|_{j-1}}{|\Delta u|_j} \leq r_{tol} \quad (10)$$

where  $r_{tol}$  is a user specified convergence tolerance and  $|\cdot|$  signifies the Euclidean norm.

This algorithm has been implemented into a FORTRAN finite element code developed by the authors. The code utilizes constant strain triangles except at the interfaces, wherein both shearing and normal bar elements are incorporated at each node. Their mechanical response follows that of the aforementioned interfacial models.

## COMPUTATIONAL RESULTS

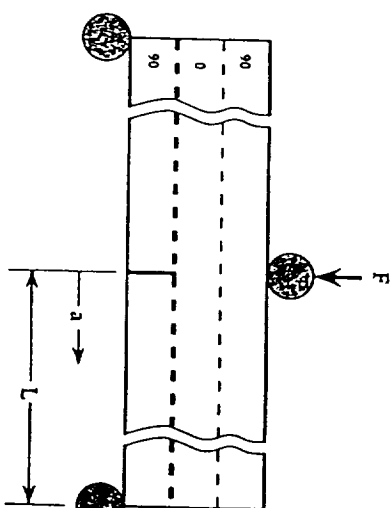
### Parametric Study

The first part of this section examines the effects of the interfacial parameters on the evolution of delamination damage. By knowing how each parameter influences the damage process, it might be possible to tailor the properties of a laminate to respond in a beneficial manner. This may be to resist LVI induced damage or it may be to accumulate damage in a controlled manner so as to dissipate energy. Recall from the previous section that Needleman's and Tvergaard's models share similar model parameters, the only exception being Tvergaard's specification of separate characteristic lengths associated with the normal and shear displacement components. For the purpose of this study, these two characteristic lengths,  $\delta_n$  and  $\delta_s$ , will be set to identical values and thus the parameters to be examined will be the maximum interfacial stress,  $\sigma_{max}$ ; the ratio of the interfacial shear stiffness to the normal stiffness,  $\alpha$ ; and the characteristic length,  $\delta$ . The range of parameters used in this study is listed in Table 1.

Table 1. Range of model parameters examined in parametric study.

Parameter Examined	$\sigma_{max}'$ MPa (ksi)	$\delta$ , mm (in)	$\alpha$
$\sigma_{max}$	13.8 to 68.9 (2.0 to 10.0)	$1.0 \times 10^{-1}$ (3.9 $\times 10^{-1}$ )	0.3
$\delta$	34.5 (5.0)	$2.5 \times 10^{-1}$ to $2.5 \times 10^{-1}$ (1.0 $\times 10^{-1}$ to 1.0 $\times 10^{-1}$ )	0.3
$\alpha$	34.5 (5.0)	$1.0 \times 10^{-1}$ (3.9 $\times 10^{-1}$ )	0.2 to 1.4

The three-point load configuration shown in Figure 2 is utilized for the study. This laminate has a  $[90_2/0_2/90_2]$  stacking sequence and possesses the ply level mechanical properties shown in Table 2. Due to the low transverse strength of the lamina, a transverse matrix crack will often appear in the mid-span of the lower  $90^\circ$  layer upon application of load. This transverse matrix crack then serves as the initiation point for the delamination at the lower  $0^\circ/90^\circ$  interface. In order to focus on the evolution of this delamination, the transverse matrix crack is assumed to exist prior to load application and interfacial elements are therefore



$[90_2/0_2/90_2]$   
 $F^* = 178 \text{ N (40 lbs)}$   
 $L = 25.4 \text{ mm (1.0 in.)}$   
 $a = 0.128 \text{ mm (0.00505 in.)}$

--- Interfacial Element  
 --- Locations

Figure 2. Schematic showing the geometry of the three-point loaded  $[90_2/0_2/90_2]$  laminate used in the parametric study.

**Table 2. Ply level mechanical properties for laminates tested.**

$E_x$	120.0 GPa	(17.4 Msi)
$E_y$	9.8 GPa	(1.4 Msi)
$E_z$	9.8 GPa	(1.4 Msi)
$G_{xy}$	5.2 GPa	(0.8 Msi)
$G_{yz}$	3.5 GPa	(0.5 Msi)
$\nu_{xy}$	0.3	0.3
$\nu_{yz}$	0.3	0.3

placed only at this 0°/90° interface. Furthermore, the damage state is assumed to be symmetric about the mid-span, so that only the right half of the span has been modeled by the finite element algorithm. Finally, the impact force is applied as a point load that increases monotonically and at constant loading rate.

The first set of results illustrates the effect of the maximum interfacial stress,  $\sigma_{max}$ , on the delamination evolution. The range of maximum interfacial stress values has been chosen to reflect the tensile strengths of typical polymers used in fiber reinforced polymer laminates. Figure 3 shows the delamination evolution with respect to the applied load as predicted by Needleman's model. Delamination evolution was found to proceed in distinct stages. Initially, the growth is relatively slow until a critical load has been reached. This critical load level ap-

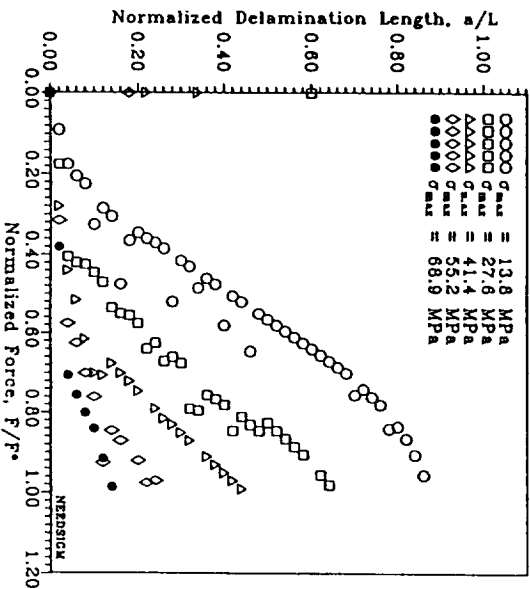


**Figure 3. The effects of the maximum interfacial stress,  $\sigma_{max}$ , on delamination growth for Needleman's model.**

pears to be related to  $\sigma_{max}$ . The next stage is characterized by rapid growth with the rate of growth decreasing with increasing  $\sigma_{max}$ . For the lowest value of the maximum interfacial stress,  $\sigma_{max} = 13.8$  MPa, a third stage appears and is characterized by a slower rate of growth. This slower rate of growth is believed to be related to the advanced state of delamination damage in the laminate.

This set of results is characterized by the initiation of multiple delaminations along the same ply interface. As shown in Figure 4, secondary delaminations are formed ahead of the main delamination; then at a higher load, the delaminations link up into a single unit. A convergence tolerance study has been performed to investigate possible numerical causes of this behavior. However, it is not possible

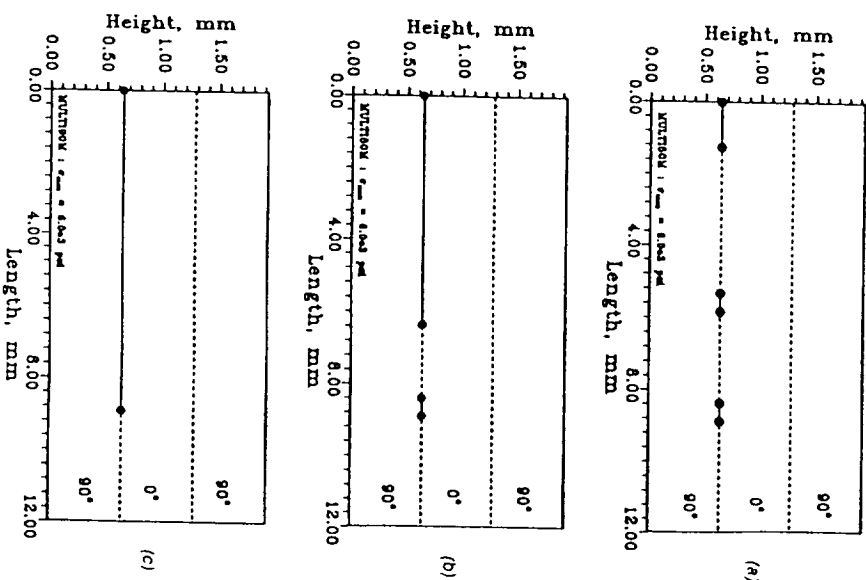


**Figure 4. Delamination development for a three-point loaded  $[90^\circ/0^\circ/90^\circ]$  laminate at a) 50%, b) 80%, and c) 90% of maximum load as predicted by Needleman's model using the following model parameter values:  $\sigma_{max} = 41.4$  MPa,  $\delta = 1.0 \times 10^{-3}$  mm, and  $\alpha = 0.3$ .**

completely eliminate this effect. Thus, there might be other causes for the multiple initiations.

The delamination evolution predicted by Tvergaard's model is shown in Figure 5. This model also exhibits the three stage growth behavior predicted by Needleman's model. However, Tvergaard's model is not as sensitive to the maximum interfacial stress as is Needleman's model. An interesting result predicted by Tvergaard's model is the delamination evolution for  $\sigma_{max} = 68.9$  MPa. In this case, the delamination has the tendency to arrest momentarily before resuming at a higher applied load, perhaps due to an energy dissipating mechanism. Then, when sufficient energy has been supplied to overcome this barrier, the delamination propagation resumes.

Figures 6 and 7 illustrate the typical force-displacement response predicted by Needleman's and Tvergaard's models, respectively. For Tvergaard's model, the reduction in the transverse stiffness corresponds to the onset of rapid delamination growth. While rapid delamination growth occurs after the reduction in the transverse stiffness has taken place for Needleman's model. This delay in the onset of rapid damage growth is most likely attributed to the use of only the normal component of the interfacial displacement in the determination of interfacial failure in Needleman's model.

Results from both interface models indicate that increasing the value of  $\sigma_{max}$  will produce intermittent crack arrest of the delamination and a shorter delamination length. This behavior is related to the energy required to fail the interfaces,

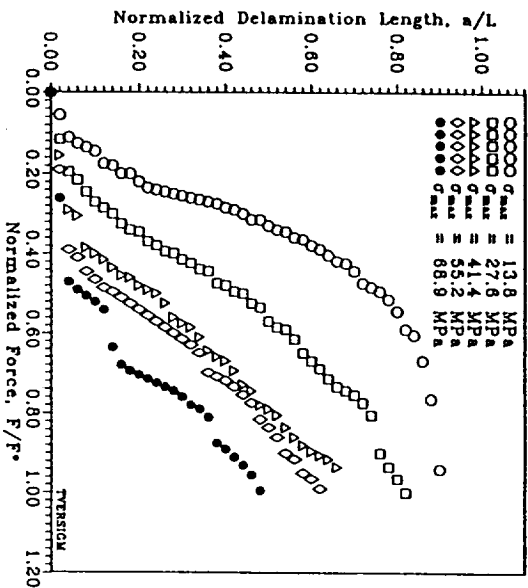


Figure 5. The effects of the maximum interfacial stress,  $\sigma_{max}$ , on delamination growth for Tvergaard's model.

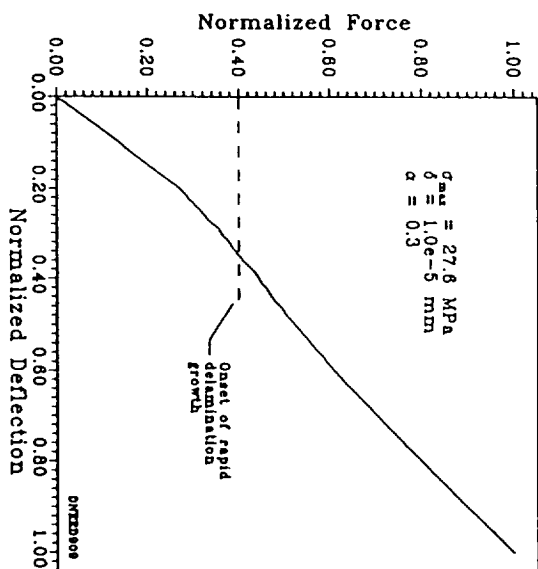


Figure 6. Deflection at the point of load application for the  $[90_2/0_2/90_2]$  laminate as predicted by Needleman's model.

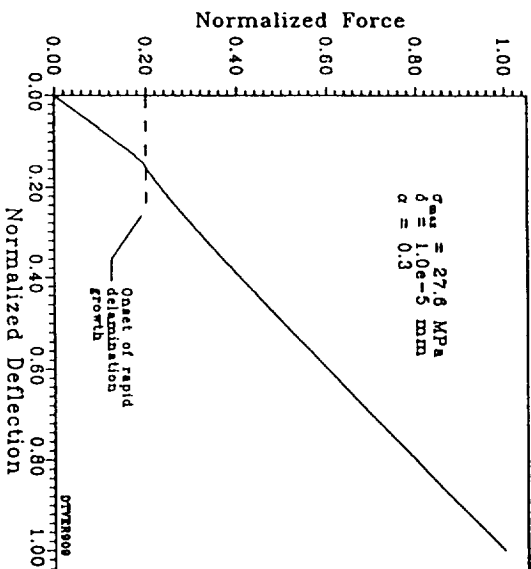


Figure 7. Deflection at the point of load application for the  $[90_2/0_2/90_2]$  laminate as predicted by Tvergaard's model.

as described in Equation (3). Clearly, the required energy increased as  $\sigma_{max}$  increased, thus increasing the fracture toughness of a material.

The next parameter examined is the characteristic length,  $\delta$ . Values of  $\delta$  ranging from  $2.5 \times 10^{-4}$  mm to  $2.5 \times 10^{-3}$  mm are considered, the largest  $\delta$  being on the same order of magnitude as the thickness of the resin rich interfacial layer in laminated composites which is generally observed to be of several fiber diameters in thickness. The delamination evolution predicted by Needleman's model for these values of  $\delta$  is shown in Figure 8. It appears that the characteristic length has only a minor effect on the rate of damage growth and the critical load at which the growth accelerates. The final length of the delamination is shorter for smaller values of  $\delta$ , while larger values of  $\delta$  cause local regions of unstable growth. Once again, multiple delamination initiations are predicted in a single interface by Needleman's model.

With the exception of  $\delta = 2.5 \times 10^{-3}$  mm, the results, shown in Figure 9, from Tvergaard's model are almost identical for the different values of the characteristic length.  $\delta$  has little effect on the critical load, rate of damage growth, and final delamination length; but for  $\delta = 2.5 \times 10^{-3}$  mm, the delamination grows unstably across the entire interface after reaching the critical load. This growth is halted only briefly mid-way along the interface and no multiple delaminations are observed. The corresponding force-displacement response is shown in Figure 10. Distinct changes in the transverse stiffness are apparent for this case. Such behavior has also been observed by Jackson and Poe [27].

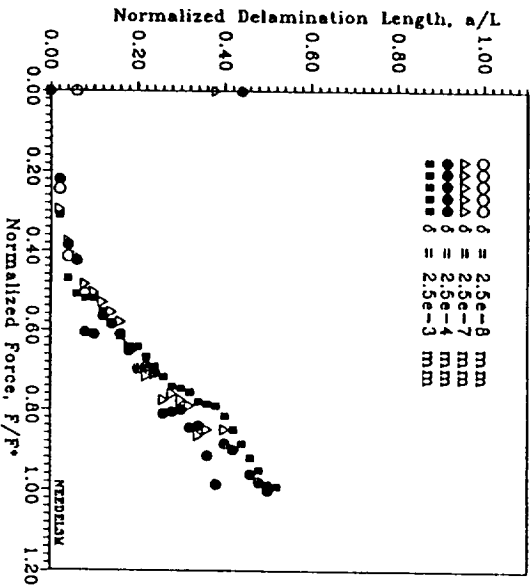


Figure 8. The effects of the characteristic length,  $\delta$ , on delamination evolution for Needleman's model.

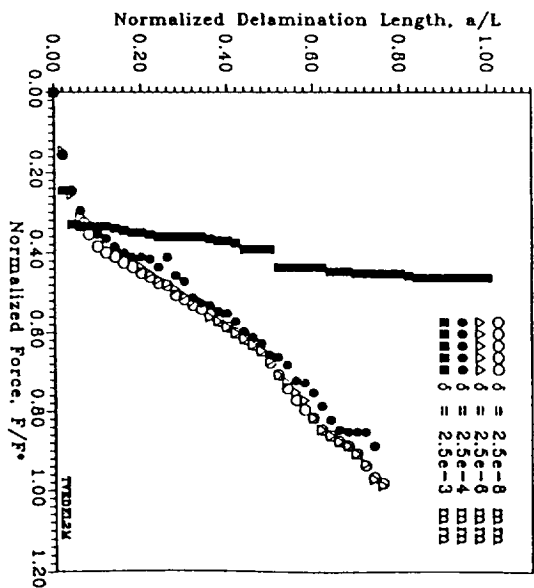


Figure 9. The effects of the characteristic length,  $\delta$ , on delamination evolution for Tvergaard's model.

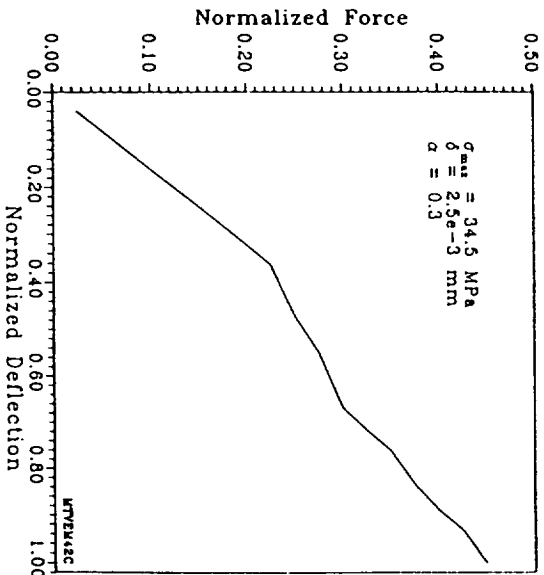


Figure 10. Deflection at the point of load application for the  $[90_2/0_2/90_2]$  laminate as predicted by Tvergaard's model using the following model parameter values:  $\sigma_{max} = 34.5$  MPa,  $\delta = 2.5 \times 10^{-3}$  mm, and  $\alpha = 0.3$ .

For both models it appears that the characteristic length does not affect the damage accumulation to a large degree for certain ranges of  $\delta$ . When it does, the results are dramatic as illustrated by Tvergaard's model for  $\delta = 2.5 \times 10^{-3}$  mm. This response obtained by Tvergaard's model is related to the relative stiffness between the interface and the surrounding region. A relatively compliant interface produces an interfacial displacement distribution that decreases gradually as one moves away from the tip of the delamination. Increasing the relative stiffness of the interface causes sharper decreases in this displacement distribution. Therefore, a compliant interface will have a larger region that is close to the critical displacement for failure than a stiffer interface. Thus, when the interface experiences an increase in displacement, a larger increment of the delamination growth occurs in the compliant interface. Consider Needleman's expression for the normal tractions as an example once again. The initial stiffness in a pure mode I opening case is,

$$\left. \frac{\partial T_n}{\partial u_n} \right|_{u_n=0} = \frac{27}{4} \frac{\sigma_{max}}{\delta} \quad (11)$$

Note that Equation (11) is also valid for Tvergaard's model. Using  $\sigma_{max} = 34.5$  MPa, the initial stiffness corresponding to the  $\delta$ s used in this parametric study range in order of magnitude from  $10^4$  MPa/mm to  $10^9$  MPa/mm. It is postulated that in the case of  $\delta = 2.5 \times 10^{-3}$  mm, the stiffness is low enough as to cause the unstable delamination growth.

Since the insensitivity of the damage evolution to the characteristic length,  $\delta$ , appears to contradict the trends set by the expression for the work of separation, Equation (3), further investigation is required. Studies where  $\sigma_{max}$  and  $\delta$  are varied in a way that keeps the work of separation or the initial stiffness constant could provide insight into this problem.

The final parameter to be examined is the shear stiffness to normal stiffness ratio,  $\alpha$ . Since the ratio of the shear modulus to Young's modulus for typical polymers used in laminated composites is less than 1.0, values of  $\alpha$  between 0.2 and 1.4 are examined. Figure 11 illustrates the delamination evolution predicted by Needleman's model. In general, the critical load increases with  $\alpha$  while the final delamination length and damage growth rate decreases with  $\alpha$ . However, these changes are very minute. Only for the case where  $\alpha = 0.2$  does there seem to be a notable variation in behavior. This case produces unexpected fluctuations in the rate of delamination damage growth. This response is possibly attributed to the fact that only the normal displacement is considered in Needleman's interfacial failure criterion. In the current damage configuration, the delamination propagation is initially Mode I opening dominated. As the delamination grows, Mode I dominance decreases until its contribution is almost the same as the Mode II contribution [28]. Decreasing  $\alpha$  would have the effect of reducing the

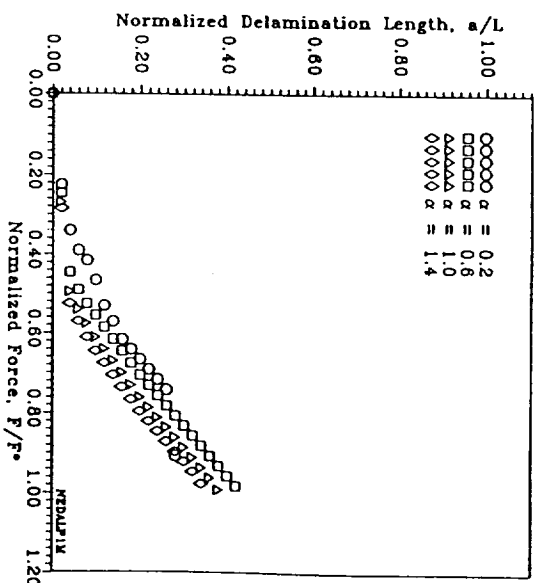


Figure 11. The effects of the interfacial shear to normal stiffness ratio,  $\alpha$ , on delamination growth as predicted by Needleman's model.

shear stiffness of the interfaces and thus increasing the interfacial shear displacements and Mode II contribution. This increase in the shear displacement may reduce the normal displacements to such a degree as to postpone failure under Needleman's criterion to a higher load, thus explaining the many changes in the rate of growth and the abrupt cessation of the delamination evolution.

When Tvergaard's model is used, the effect of  $\alpha$  on the damage evolution, shown in Figure 12, is similar to that for Needleman's model. In this case, the effects are more apparent than in Needleman's model. For both interfacial models in general, the shear stiffness to normal stiffness ratio,  $\alpha$ , affects the damage evolution in a similar way as the maximum interfacial stress,  $\sigma_{max}$ . This is due to the fact that for the current interfacial models, the expression for the work of separation in a mixed mode opening case will have the following form,

$$W_{up} = W_n + \alpha W_s \quad (12)$$

where  $W_n$  and  $W_s$  are components of the work of separation in the normal and shearing directions, respectively. As  $\alpha$  is increased, the work of separation is also effectively increased. However, the increase will not be linear as  $u_n$  and  $u_s$  used in calculating  $W_n$  and  $W_s$  are dependent on  $\alpha$ .

### Multiple Interface Examples

The second part of this section illustrates situations in which more than one in-

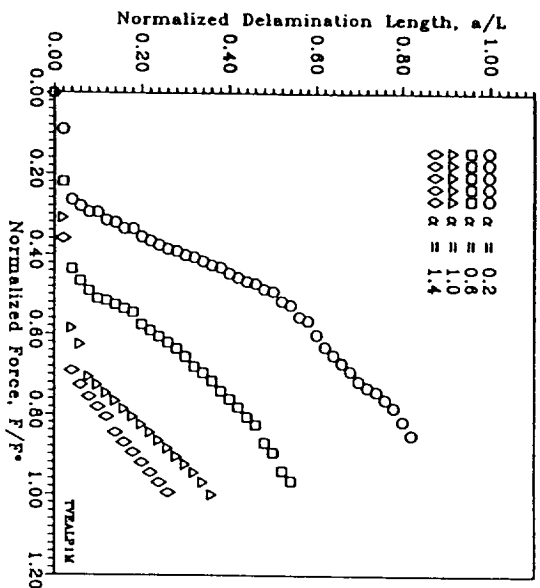


Figure 12. The effects of the interfacial shear to normal stiffness ratio,  $\alpha$ , on delamination growth as predicted by Tvergaard's model.

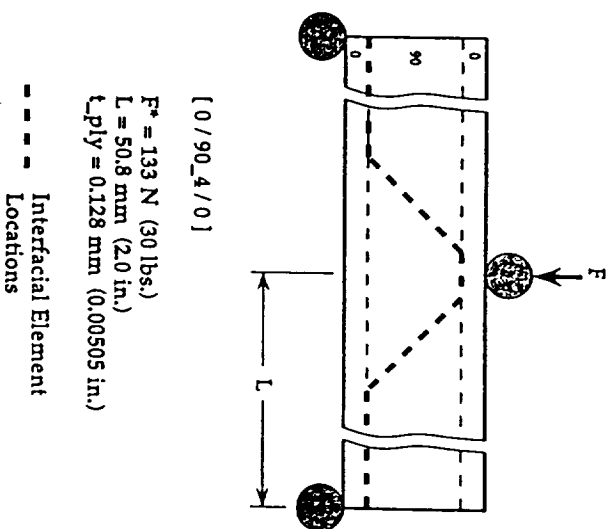


Figure 13. Schematic showing the geometry of the three-point loaded [0/90<sub>4</sub>/0] laminate used in the three interface damage evolution configuration.

terface is undergoing damage development. This process occurs when load is redistributed from a damaged region to an adjacent region. The additional load in turn initiates and propagates damage in the adjacent region. Sometimes the load transfer removes sufficient energy from the initially damaged area to prevent further damage growth, while in other situations damage in both regions can propagate simultaneously. The first example to be considered is shown in Figure 13. This laminate has a [0/90<sub>4</sub>] stacking sequence and the finite element mesh of this configuration contains three interfaces. One interface is located at each 90° interface, as shown in Figure 13. The remaining interface is located in the 90° layer and inclined at a 45° angle. Based on experimental observations of other cross-ply laminates [4], it is positioned close to the point of load application, as shown in Figure 14. This interface models the "critical" matrix crack that initiates the delaminations at both 0/90 interfaces. The ply level mechanical properties used

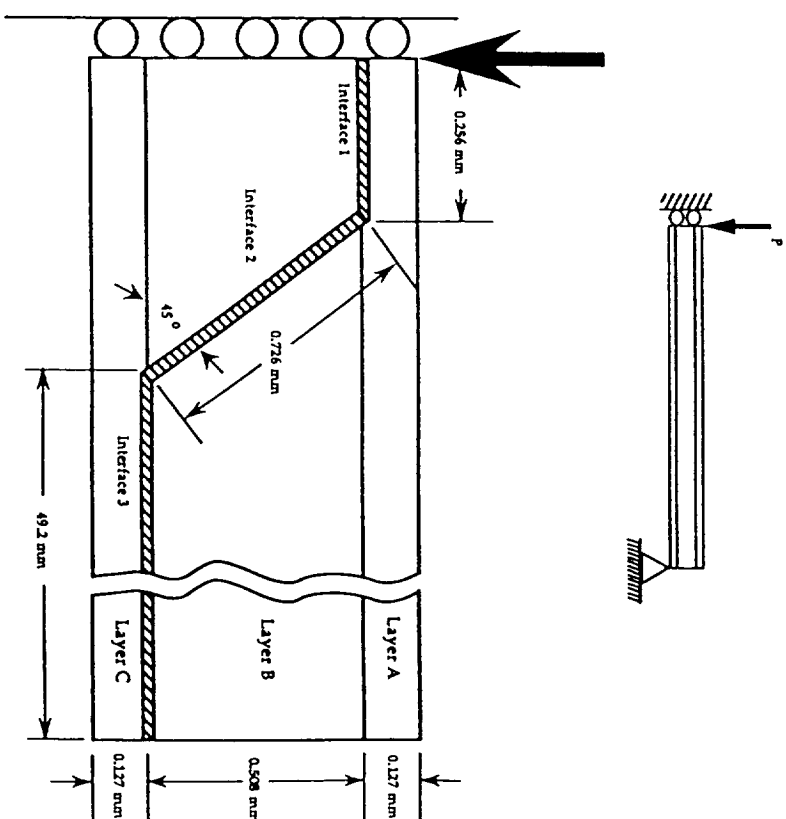


Figure 14. Schematic showing the location of the interfaces in the [0/90<sub>4</sub>/0] laminate.

in this problem are the same as those used in the parametric study. Listed in Table 3 are the properties for the interfaces. For simplicity, the delaminations and the "critical" matrix crack have identical interfacial properties. In addition, the impact load is applied in the finite element model as a monotonically increasing statically applied point load.

Figures 15 and 16 show the damage state near the point of load application during various stages of the loading history for Needleman's and Tvergaard's models, respectively. The results from Needleman's model indicate that the "critical" matrix crack initiates at the lower 0°/90° interface and then propagates in a stable manner towards the upper 0°/90° interface. The matrix crack advances approximately three fourths of the thickness of the 90° layer before being arrested. In the mean time the delamination at the lower 0°/90° interface initiates and starts to propagate. This delamination continues to grow for the remainder of the loading history. The upper interface, however, remains intact. Delamination growth at and near the upper interface is most likely suppressed by the compressive stresses around the point of load application. Recall that in Needleman's model, interfacial failure occurs when the normal component of the interfacial displacement is greater than the characteristic length. In other words, the tangential displacement does not play a role in the determination of failure.

The initiation of the "critical" matrix crack is predicted to occur at a higher load by Tvergaard's model than the load predicted by Needleman's model. The matrix crack appears to propagate continuously across the ply. At 87% of maximum load, the matrix crack has completely propagated across the 90° layer, a delamination forms at the lower 0°/90° interface and another one has initiated at the upper interface. The delamination at the lower interface does not experience further growth as the load increases, but the delamination at the upper interface proceeds along the interface toward a region directly under the point of load application. The prediction by Tvergaard's model of a delamination in the region around the point of load application, which is consistent with experimental observations for cross-ply laminates [4], is due to the use of both interfacial displacement components in the form of a displacement norm to determine failure. Thus, even though the normal displacement may be much smaller than the characteristic length, the tangential displacement is sufficient to initiate the failure. It should be noted that this analysis omits Tvergaard's friction force term. Had this

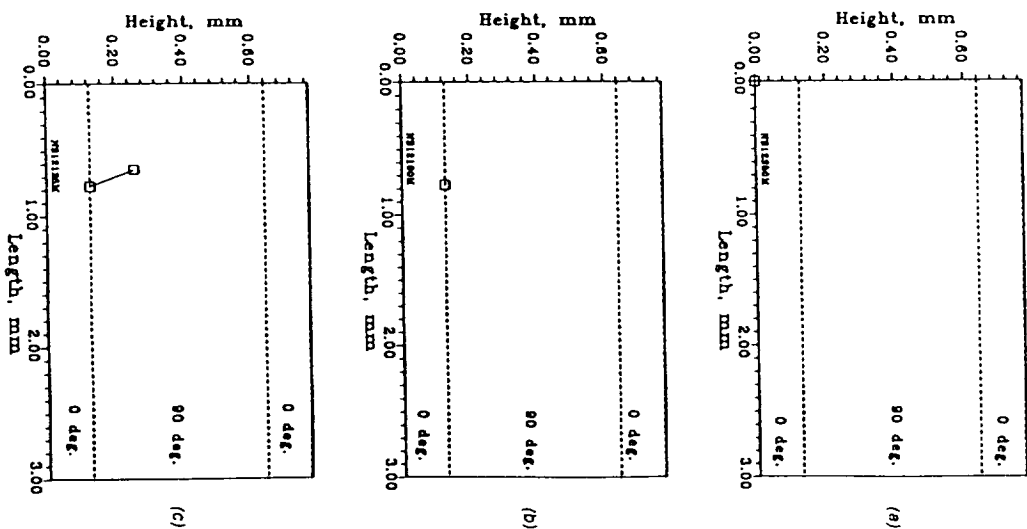


Figure 15. Damage evolution in the three-point loaded (0/90/0) laminate as predicted by Needleman's model at a) 25%, b) 50%, c) 62%, d) 75%, e) 87%, and f) 100% of maximum load.

Table 3. Interfacial parameters for three interfaces test case.

$\sigma_{max}$	68.9 MPa	(10.0 ksi)
$\delta$	$1.0 \times 10^{-4}$ mm	( $3.9 \times 10^{-4}$ in)
$\alpha$	1.0	1.0



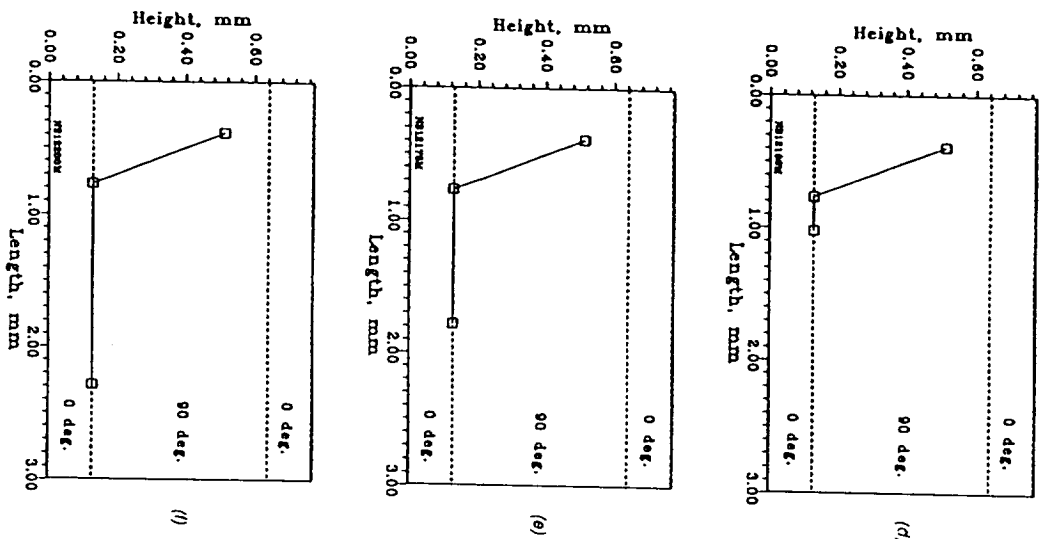


Figure 15 (continued). Damage evolution in the three-point loaded  $[0/90/0]$  laminate as predicted by Needelman's model at a) 25%, b) 50%, c) 62%, d) 75%, e) 87%, and f) 100% maximum load.

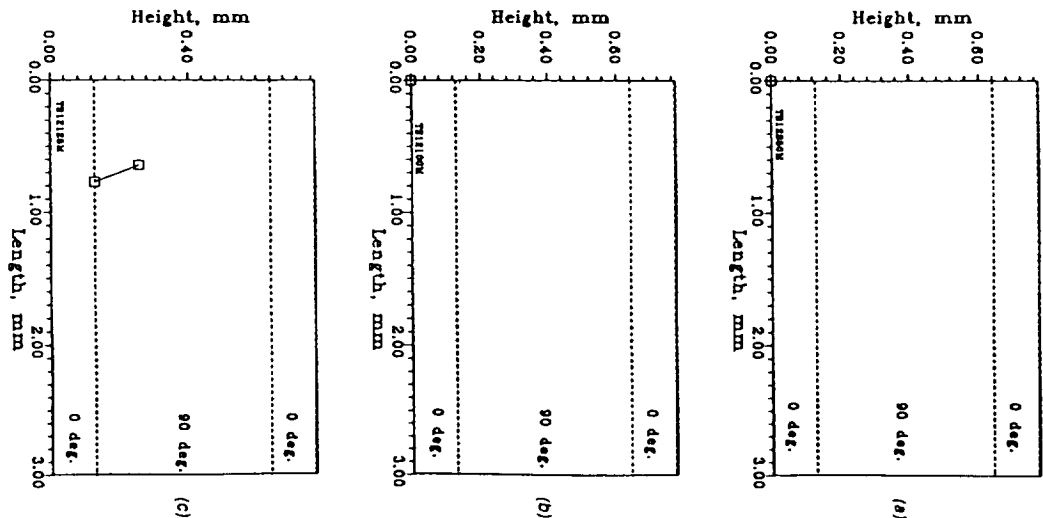


Figure 16. Damage evolution in the three-point loaded  $[0/90/0]$  laminate as predicted by Tvergaard's model at a) 25%, b) 50%, c) 62%, d) 75%, e) 87%, and f) 100% of maximum load.

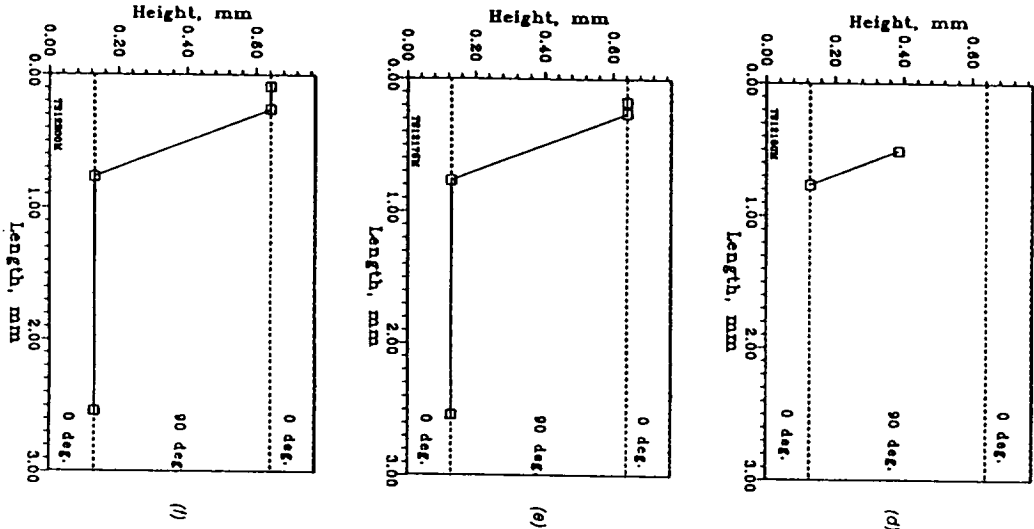


Figure 16 (continued). Damage evolution in the three-point loaded  $[0/90_2/0]$  laminate as predicted by Tvergaard's model at a) 25%, b) 50%, c) 62%, d) 75%, e) 87%, and f) 100% of maximum load.

been activated when the normal displacement is compressive, it would have reduced the amount of tangential displacement and the delamination length.

The next multiple interface example is shown in Figure 17. This example contains eight interfaces; each interface located in between the  $0^\circ$  and  $90^\circ$  ply groups of the  $[(0_2/90_2)_2/0_2]$  laminate. The ply level mechanical properties used in this case are identical to those used in the previous example. Listed in Table 4 are the interfacial properties used in the current example. Once again, simplifying assumptions are made in this analysis. Presumption of a symmetric damage state about the mid span of the laminate enables the finite element modeling of only half the length of the laminate. Also, the impact load is modeled as a monotonically increasing quasi-statically applied point load. The delamination damage state predicted by Needleman's model for this eight interface example is shown in Figure 18. Only a small amount of damage is predicted and it is located at the bot-

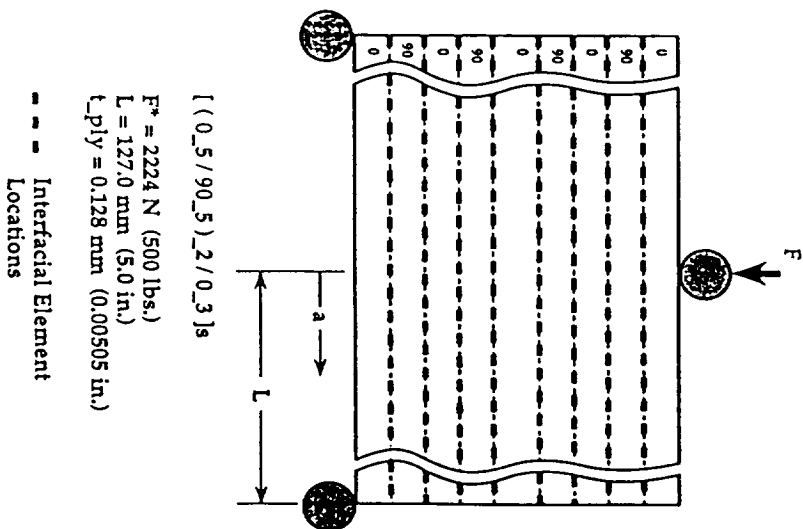
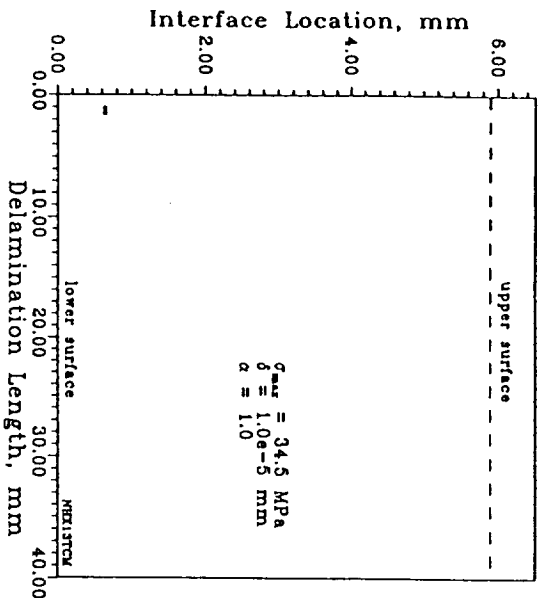


Figure 17. Schematic showing the geometry of the three-point loaded  $[(0_2/90_2)/0_2]$  laminate used in the eight interface damage evolution configuration.

**Table 4. Interfacial parameters for eight interfaces test case.**

$\sigma_{max}$	34.5 MPa	(5.0 ksi)
$\delta$	$1.0 \times 10^{-4}$ mm	( $3.9 \times 10^{-7}$ in)
$\alpha$	1.0	1.0

tom most interface. This delamination initiates at 85% of the maximum applied load but it does not propagate any further as the load is increased. The results from Tvergaard's model are shown in Figure 19. Delaminations are predicted in three of the eight interfaces. The largest delamination and also the first to initiate is located at the bottom interface. This delamination will be referred to as the "main" delamination. At the interface immediately above the bottom interface, a delamination about half the size of the main delamination is predicted. The final delamination is located two interfaces down from the upper surface. Its size is also about half that of the main delamination. Since the failed interfaces are not connected to each other by matrix cracks, initiation and propagation of subsequent delaminations in the other interfaces are due to the redistribution of load among the plies and are not due to the high stresses ahead of the crack front. Damage evolves from the bottom interface and moves toward the upper surface in a sequential manner. A new delamination initiates in another interface shortly



**Figure 18. Delamination damage state for the three-point loaded  $(0_g/90_g)_2/0_g$  laminate as predicted by Needleman's model.**

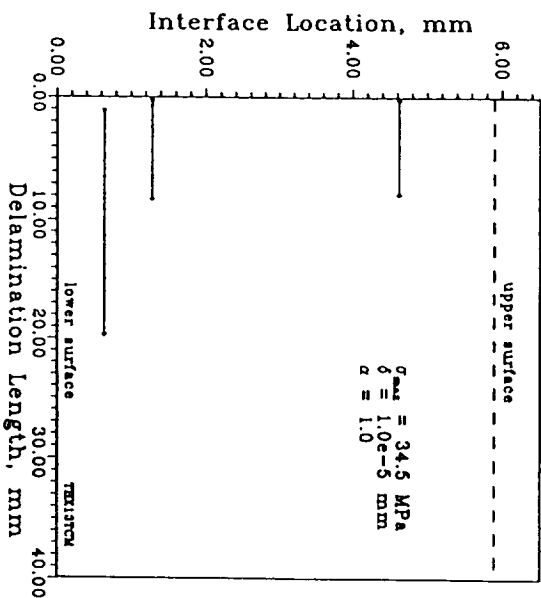


**Figure 19. Delamination damage state for the three-point loaded  $(0_g/90_g)_2/0_g$  laminate as predicted by Tvergaard's model.**

before the current delamination arrests. The delamination pattern predicted by Tvergaard's model appears to more closely follow the triangular profile observed experimentally in LVI damaged specimens [29] than Needleman's model. Inclusion of transverse matrix cracks into the finite element model will probably enhance the damage development in the interfaces located in the middle of the laminate.

## CONCLUSION

This study illustrates the range of damage accumulation that can be obtained with Needleman's and Tvergaard's interface models. The parameters found in these models control the stiffness of the interface, work of separation, and interfacial separation at failure. This in turn affects the load at which the delamination growth accelerates, the rate of delamination growth, and the amount of damage accumulated. Influence of the interfacial properties on the damage evolution is most apparent in cases associated with parametric values that are at the extremes of the range of values tested in this study. These parametric values cause a particular factor that controls the damage growth to become dominant and produced responses that differ from the trend established by the other parametric values in the range examined. It is thus possible to obtain a wide range of damage response from brittle to ductile by varying these model parameters. This behavior, unfortunately, means that in order to study the damage response of a specific material,

precise values of the associated model parameters must be determined. On the other hand, if the physical characteristics of a material can be related to these parameters, it would aid in the design of materials to meet interfacial damage design requirements.

For the cases considered, Tvergaard's model predicts a greater amount of damage than Needleman's model. This can be traced to the mode in which the delamination is propagating. In the current examples, both the normal and shear components of interfacial displacement contribute to the failure of the interface. Needleman's model, however, only considers the normal displacement component in the failure criterion. This results in the delayed detection or omission of interfacial failure and may contribute to the numerical irregularities experienced by some of the test cases using Needleman's model. Tvergaard uses both components of interfacial displacement in the form of a displacement norm and therefore predicts a greater amount of damage. This approach weighs both displacement components equally. It should be noted that the displacement component may need to be weighed differently in order to reflect the deformation or failure mechanisms at the interface. One way this can be accomplished is to use different values of the characteristic length for the two displacement components as proposed by Tvergaard. The different responses predicted by the two interface models are also attributed to how the interfacial displacement terms are introduced into the expressions for the interfacial tractions, Equations (1), (2), (4), and (5). For example, the expressions for the tangential traction, Equations (2) and (5), are identical for the two models except for the use of the displacement norm for Tvergaard's model in place of the normal interfacial displacement found in Needleman's model. Since the norm of the displacement will be greater than or equal to the absolute value of each individual component for a given interfacial displacement, Tvergaard's model will be further along the tangential traction versus displacement curve than Needleman's model and thus closer to failure.

The difference in response between the two interface models is greatest for the test case with eight interfaces. In this case, the ability of the interface to transfer load from one ply group to the adjacent group affects the damage evolution in the other interfaces. The development of the interface models is based on the assumption that the interfacial traction behaves similarly to the force generated during interatomic separation. This means that the traction force initially increases with interfacial separation. Once the maximum force has been reached, the traction force decreases with separation until the interface fails. During this period of decreasing traction force, the load is transferred from this portion of the interface to other parts of the laminate. Since the use of the displacement norm in Tvergaard's model places the response further along the traction versus displacement curve than Needleman's model, an interface modeled by Tvergaard's model will undergo the unloading process sooner, thus hastening the conditions for failure in the adjacent interfaces. Overall, Tvergaard's model appears to be

better suited for predicting the mixed mode damage evolution found in the three-point bend configurations tested.

The discussion now turns to the accuracy of these two models in the prediction of damage in laminated fiber reinforced polymeric composites. As mentioned in a previous section, there are numerous mechanisms at the molecular level that cause the deformation and failure in the resin rich interface. The activity of the deformation mechanisms is dependent on the molecular structure of the polymer, loading conditions, temperature, and processing history. These mechanisms may occur sequentially or concurrently. The objective is to relate these molecular mechanisms to the response of the interface at the continuum level. Because the interface models are functions of only the interfacial displacements, they will not have the capability to capture the effects of rate and temperature dependent mechanisms. Fortunately, models have been developed for the viscoelastic response of polymers and can be incorporated into the present study [30,31]. Likewise, there are models available to represent the fibril dominated structures found in craze zones ahead of a crack tip [32]. Due to the wide ranging nature and unique response of each mechanism a model developed based on the behavior of a single mechanism would not be sufficient to predict the entire deformation response up to failure. The ideal model should contain components for representing each deformation mechanism. Criteria should be established to govern the activities of these components. Thus, the models examined in this study would serve as a starting point in the development of a comprehensive procedure for modeling the polymeric interface.

#### ACKNOWLEDGEMENT

The authors are grateful for the support provided by NASA Contract no. 32531-40960 to Texas A&M University.

#### REFERENCES

1. Needleman, A. 1987. "A Continuum Model for Void Nucleation by Inclusion Debonding," *Journal of Applied Mechanics*, 54:525-531.
2. Tvergaard, V. 1990. "Effects of Fibre Debonding in a Whisker-Reinforced Metal," *Materials Science & Engineering A: Structural Materials: Properties, Microstructure, and Processing*, A125(2):203-213.
3. Greszczuk, L. B. 1982. "Damage in Composite Materials Due to Low Velocity Impact," *Impact Dynamics*. New York: John Wiley & Sons, Chap. 3.
4. Choi, H. Y., R. J. Downs and F. K. Chang. 1991. "A New Approach toward Understanding Damage Mechanisms and Mechanics of Laminated Composites Due to Low Velocity Impact: Part I—Experiments," *Journal of Composite Materials*, 25:992-1011.
5. Choi, H. Y., H. T. Wu and F. K. Chang. 1991. "A New Approach toward Understanding Damage Mechanisms and Mechanics of Laminated Composites Due to Low Velocity Impact: Part II—Analysis," *Journal of Composite Materials*, 25:1012-1038.
6. Bogdanovich, A. E., E. V. Jarve and S. P. Joshi. 1990. "Impact Deformation and Failure Analysis of Laminated Composite Plates," *Impact and Buckling of Structures*, ASME AMD, 114:1-5.

7. Bogdanovich, A. E. and E. V. Larve, 1992, "Numerical Analysis of Impact Deformation and Failure in Composite Plates," *Journal of Composite Materials*, 26:520-545.
8. Sun, C. T. and S. Rechk, 1988, "Effect of Adhesive Layers on Impact Damage in Composite Laminates," *Composite Materials Testing and Design (ASTM STP 972)*, pp. 97-123.
9. Jih, C. J. and C. T. Sun, 1993, "Prediction of Delamination in Composite Laminates Subjected to Low Velocity Impact," *Journal of Composite Materials*, 27(7):684-701.
10. Sankar, B. V., P. T. Nguyen and C. Ku, 1990, "Nondimensional Impact Models for Composite Laminates," *Proceedings of the American Society for Composites, Fifth Technical Conference*, pp. 600-610.
11. Sankar, B. V, 1985, "Contact Law for Transversely Isotropic Materials," *Proceedings of the 26th AIAA/ASME/ASCE/ASHS Structures, Structural Dynamics and Materials Conference*, Orlando, FL, pp. 516-521.
12. Wu, H. T. and G. S. Springer, 1988, "Measurements of Matrix Cracking and Delamination Caused by Impact on Composite Plates," *Journal of Composite Materials*, 22:518-532.
13. Wu, H. T. and G. S. Springer, 1988, "Impact Induced Stresses, Strains, and Delaminations in Composite Materials," *Journal of Composite Materials*, 22:533-560.
14. Wu, H. T. and F. K. Chang, 1989, "Transient Dynamic Analysis of Laminated Composite Plates Subjected to Transverse Impact," *Computers and Structures*, 31:453-466.
15. Liu, S., Z. Kuitu and F. Chang, 1993, "Matrix Cracking and Delamination in Laminated Composite Beams Subjected to a Transverse Concentrated Line Load," *Journal of Composite Materials*, 27(5).
16. Gilbert, D. G., P. W. R. Beaumont and W. C. Nixon, 1983, "Direct Observations of the Micromechanisms of Fracture in Polymeric Solids Using the Scanning Electron Microscope," *Mechanical Behaviors of Materials-IV, ICM4*, 2:705-710.
17. Purslow, D, 1987, "Matrix Fractography of Fibre-Reinforced Thermoplastics, Part 1. Peel Failures," *Composites*, 18(5):365-374.
18. Purslow, D, 1988, "Matrix Fractography of Fibre-Reinforced Thermoplastics, Part 2. Shear Failures," *Composites*, 19(2):115-126.
19. Bascom, W. D. and S. Y. Gweon, 1989, "Fractography and Failure Mechanisms of Carbon Fiber-Reinforced Composite Materials," *Fractography and Failure Mechanisms of Polymers and Composites*, A. C. Roulin-Moloney, ed., New York, NY: Elsevier Science Publishing Co., pp. 351-385.
20. Henaiff-Gardin, C. and M. C. Lafarie-Frenot, 1992, "Fatigue Behavior of Thermoset and Thermoplastic Cross-Ply Laminates," *Composites*, 23(2):109-116.
21. Chakachery, E. A. and W. L. Bradley, 1987, "A Comparison of the Crack Tip Damage Zone for Fracture of Hexcel F185 Neat Resin and T6T145/F185 Composite," *Polymer Engineering and Science*, 27(1):33-40.
22. Purslow, D, 1986, "Matrix Fractography of Fibre-Reinforced Epoxy Composites," *Composites*, 17(4):289-303.
23. Shihmanter, L., B. Cina and I. Eldror, 1991, "Fractography of Multidirectional CFRP Composites Tested Staticaly," *Composites*, 22(6):437-444.
24. Ladeveze, P, 1992, "A Damage Computational Method for Composite Structures," *Computers & Structures*, 44(1/2):79-87.
25. Kausch, H. H, 1987, *Polymer Fracture*. New York: Springer-Verlag.
26. Jones, R, 1992, "Micromechanical Analysis of Inelastic Composite Behavior Including the Effects of Matrix Viscoplasticity and Evolving Damage," Texas A&M University Master's Thesis.
27. Jackson, W. C. and C. C. Poe, Jr, 1993, "The Use of Impact Force as a Scale Parameter for the Impact Response of Composite Laminates," *Journal of Composites Technology & Research*, 15(4):282-289.
28. Sun, C. T. and M. G. Manoharan, 1989, "Growth of Delamination Cracks Due to Bending in a [90<sub>1</sub>/0<sub>1</sub>/90<sub>1</sub>] Laminate," *Composite Science and Technology*, 34:365-377.

29. Farley, G. L., B. T. Smith and J. Maiden, 1992, "Compression Response of Thick Layer Composite Laminates with Through-the-Thickness Reinforcement," *Journal of Reinforced Plastics and Composites*, 11:787-809.
30. O'Dowd, N. P. and W. G. Knauss, 1993, "Time Dependent Large Principle Deformation of Polymers," *Use of Plastics and Plastic Composites: Materials and Mechanics Issues*, ASME MD, 46:77-95.
31. Hasan, O. A. and M. C. Boyce, 1993, "A Constitutive Model for the Nonlinear Viscoelastic Viscoplastic Behavior of Glassy Polymers," *Use of Plastics and Plastic Composites: Materials and Mechanics Issues*, ASME MD, 46:97-120.
32. Hui, C. Y. and E. J. Kramer, 1993, "Molecular Weight Dependence of the Fracture Toughness of Glassy Polymers Arising from Crack Propagation through a Craze," *Use of Plastics and Plastic Composites: Materials and Mechanics Issues*, ASME MD, 46:309-325.

In the past ten years the use of cohesive zone models has been extended to study separation along material interfaces. A systematic study of the modeling of single craze formation and growth has been conducted by Unguruwarungsri and Knauss [7-8] and Hui, Lagoudas and Ruina [9]. In these works c.z. models are elevated to full status constitutive models for the interface, which is treated as a two-dimensional physical entity distinct from the material that surrounds it. Such a notion of interface naturally leads to the formulation of constitutive equations similar to that of other material systems. For example, Suo, Ortiz and Needleman [10], in the study of microcracking formation problems at the material interface of a composite system, have modeled the interface as a non-linear elastic cohesive zone and have derived its constitutive equations from a strain energy

of the evolving microstructure that determines the material toughness. In the past ten years the use of cohesive zone models has been extended to study separation along material interfaces. A systematic study of the modeling of single craze formation and growth has been conducted by Unguruwarungsri and Knauss [7-8] and Hui, Lagoudas and Ruina [9]. In these works c.z. models are elevated to full status constitutive models for the interface, which is treated as a two-dimensional physical entity distinct from the material that surrounds it. Such a notion of interface naturally leads to the formulation of constitutive equations similar to that of other material systems. For example, Suo, Ortiz and Needleman [10], in the study of microcracking formation problems at the material interface of a composite system, have modeled the interface as a non-linear elastic cohesive zone and have derived its constitutive equations from a strain energy

## 1. INTRODUCTION

A global thermodynamic analysis of the running crack problem is presented. The crack is modeled as an evolving partially cohesive interface endowed with a thermodynamic structure distinct from that of the surrounding body. Constitutive relationships for the cohesive part of the crack surface are formulated in a general way that allows one to account for various dissipative mechanisms and to recover most of the cohesive zone models available from the literature. Particular attention is focused on some of the fundamental and necessary requirements for formulating cohesive zone models. The relationship between such requirements and the interface evolution is discussed and analysed.

### Abstract

15 September 1994

Texas A&M University, College Station, TX 77843-3141, U.S.A.  
 †Center for Mechanics of Composites,  
 Texas A&M University, College Station, TX 77843-3368, U.S.A.  
 ‡Department of Mathematics,

F. COSTANZO<sup>†</sup> and D.H. ALLEN<sup>‡</sup>

# A CONTINUUM THERMODYNAMIC ANALYSIS OF COHESIVE ZONE MODELS

potential function. A c.z. model endowed with a strain energy function has been also employed by Li and Liang [11] in the study of fracture eigenvalue problems.

Clearly, the development of general interface constitutive theories requires the exercise of great care since such theories must explicitly account for the transition from a fully cohesive system to a partially cohesive one or, in other words, for the spontaneous formation of cracks on the interface surface. In the treatment of these problems continuum thermodynamics offers unique advantages. In fact, continuum thermodynamics provides a rigorous and consistent framework both for discussing the admissibility of the c.z. constitutive equations and for characterizing the energetics of crack growth (Gurtin [12-14]; Nguyen [15-16]; Costanzo and Allen [17]).

Gurtin [14] was the first to propose a thermodynamics of the cohesive zone in fracture. Gurtin treated the crack surface as a two-dimensional system endowed with thermodynamic potentials, namely an internal energy, entropy and free energy functions, dependent on the crack temperature and the crack opening displacement. The fundamental contribution in Gurtin's work is represented by convenient statements of the first and second laws of thermodynamics for the crack and in particular for the crack tip, where the latter is defined as a two-dimensional thermodynamic system of finite size with its own constitutive response. The second law is then used as the starting point for the analysis of the crack tip constitutive equations and for the derivation of the necessary conditions for crack advancement.

In the present paper Gurtin's thermodynamic analysis is further expanded to formulate a class of c.z. constitutive equations able to provide useful information about some specific issues which emerged in works such as those by Ungswarungsi and Knäuss [7-8], Hui, Lagoudas and Ruina [9] and Fager *et al.* [18]. There are three main issues that are selected and analyzed here. The first one regards the requirement, discussed in section 2 of Hui *et al.* [9], that the function expressing the cohesive force per unit (crack) surface  $\sigma$ , in terms of the crack opening displacement (COD)  $\delta$  be set-valued for  $\delta = 0$ , i.e.  $\delta = 0 \Rightarrow \sigma \in [0, \bar{\sigma}]$ , where  $\bar{\sigma}$  is a conveniently chosen maximum value for the cohesive force. Note that although for the moment the quantities  $\delta$  and  $\sigma$  are considered as scalar functions, later they will be more properly re-defined as interface vector fields. Such a formulation reflects the assumption that until a known threshold stress is reached, the interface deformation is negligible with respect to that of the bulk material. Under said circumstances it is therefore more convenient to treat the interface as perfectly cohesive, requiring that any load level below the threshold be transferred (across the interface) while the interface opening displacement remains null. Physically, such an assumption seems quite reasonable for almost all cases, especially those, such as crazing (the phenomenon studied by Hui *et al.* [9]), for which an actual material interface does not exist a priori, but is formed when a critical stress state nucleates a particular and localized microstructure. Other examples of this class of phenomena include microcracking in brittle materials (Ortiz [3]) and crack bridging in polycrystals and composites (Budiansky *et al.* [4]). The rigid part of the c.z. constitutive response can be mathematically modeled as indicated in Hui *et al.* [9], that is, either by an appropriate function  $\sigma = \sigma(\delta)$  whose domain is an open set  $(0, \delta_c)$ , where  $\delta_c$  is a conveniently chosen critical opening displacement, or by an implicit equation  $f(\delta, \sigma) = 0 \quad \forall \delta \mid \delta \geq 0$ . Although mathematically valid, from a thermodynamic viewpoint the above representation fails to provide a clear description of a particular interface formation and/or damage process and of its intrinsically dissipative nature. An alternative description has been provided by Li and Liang [11] via the use of an interface strain energy function  $f(\delta)$  such that  $\sigma = \partial f(\delta) / \partial \delta$ ,  $\sigma(0) \neq 0$ . This latter formulation, certainly useful in the study of interface bifurcation via the employment of classical elastic stability methods, cannot address the issue of dissipation. Moreover, it poses the problem, especially in homogeneous materials, of physically interpreting the origin of a strain energy function that yields a non-null cohesive force field with  $\delta = 0$  even when external loads are absent.

From a macroscopic viewpoint, a description of the interface behavior at  $\delta = 0$  that is typical of rigid plastic systems seems more appropriate. The idea is to assume that the cohesive force must belong to an admissible set of forces analogous to the interior of a yield surface in plasticity and that a  $\delta \neq 0$ , rather than a  $\delta \geq 0$ , can occur when the cohesive force takes on values on the given yield surface. This approach will be presented in a more precise manner later. The product  $\sigma \cdot \delta$ , representing the specific work of separation, will then provide a measure of energy dissipation at the interface. The difficulty of this latter approach consists in providing a convenient form and evolution equation for the c.z. yield surface. In general, this requires a rheological theory for the interface at hand. In this paper, the c.z. yield surface is assumed to be time independent and constant, leaving further generalizations to future works.

The second issue considered herein concerns the problem of formulating c.z. constitutive equations which allow for the prediction of the transition from an open but cohesive interface to an incoherent or cracked one. This problem is not solved completely by defining a specific interface fracture criterion. In fact, a simple fracture criterion would not allow one to predict, in general, the formation of patterns of microcracks separated by cohesive zones from a uniformly strained interface. In order to predict such phenomena, bifurcation of equilibrium solutions must be allowed to occur. Interface bifurcation has been studied by Hui *et al.* [9] and by Suo *et al.* [10]. In both cases bifurcation is treated as the limit stage of the global elastic stability. This approach, although quite useful, in reality does not reflect the fact that microcracking initiation and growth can occur under globally stable conditions. Physically, it seems more appropriate to endow the interface with constitutive equations that allow the interface bifurcation problem to be reformulated in such a way that it remains distinct from that of global stability for a portion of the interface life. Such a result can be achieved if the interface constitutive equations include some history dependent behavior. The idea presented earlier of describing the rigid part of the interface behavior through a rigid-plastic model certainly fulfills this requirement, although it is not always sufficient to ensure the possibility of bifurcation, as will be shown later. As already indicated by Suo *et al.* [10] and by Li and Liang [11], this requires the interface free energy to be a non-convex function of the opening displacement. Such a feature is included in the present formulation. The issue of bifurcation and stability will then be addressed using a variational formulation of the problem which represents an extension to interfaces of the stability and bifurcation theory proposed by Nguyen [19] for systems that conform to the maximum dissipation principle. In fact, one of the main objectives of the present work is precisely that of extending to interfaces the theory of generalized standard materials (GSM) (Halphen and Nguyen [20]), i.e. systems that conform to the principle of maximum dissipation, within the thermodynamic framework proposed by Gurtin [14]. The main difference between the present theory and the GSM theory is the assumption that the interface free energy is non-convex. Interestingly enough, this property does not affect the possibility of implementing Nguyen's procedure (Nguyen [19]) for the study of bifurcation and stability. It will be shown that the general constitutive theory presented herein is able to recover and generalize most of the cohesive zone models proposed in the open literature.

The third and last point addressed in the paper is a discussion of the relation between fracture studies with and without cohesive zone models. The purpose of this discussion is to show under what circumstances a crack with a cohesive zone behaves like a sharp crack. In this analysis an interesting result is derived showing that the formulation of the Griffith criterion according to Nguyen [15-16] is directly derivable from Dugdale's model viewed as a model for a rigid perfectly plastic and purely dissipative (no free energy) interface. Although such equivalence has been suggested by other authors a formal proof has been lacking.



## 2.1. Notation. Body and Crack Geometry.

Throughout the paper vectors and second order tensors will be distinguished from scalar quantities by using lower case boldface letters (latin or greek) (e.g.  $\mathbf{u}$  or  $\delta$ ) and upper case boldface latin letters (e.g.  $\mathbf{S}$ ), respectively. The notation  $\mathbf{A}\mathbf{v}$  will indicate a linear mapping that transforms a vector  $\mathbf{v}$  into another vector  $\mathbf{u}$ , that is,  $\mathbf{A}\mathbf{v} = \mathbf{u}$ . The inner product of two tensors will be indicated as a dot product, that is,  $\mathbf{A} \cdot \mathbf{B}$ . An upper case  $T$  superscript applied to a tensor will indicate the transposition operation (e.g.  $\mathbf{A}^T$  is the transpose of  $\mathbf{A}$ ).

With reference to Fig. 1, consider a two dimensional body  $B$  containing a crack  $C$ .

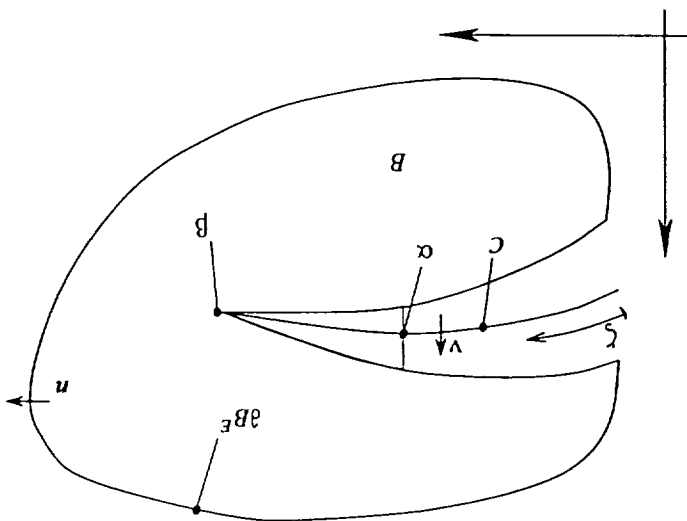


Figure 1: A Crack With a Cohesive Zone

An edge crack is considered for simplicity, so that attention can be focused on a single moving crack tip.  $B$  is assumed to be an open region of the two dimensional euclidian space  $E^2$ .  $C$  is assumed to be a simple, open and piecewise smooth line in  $E^2$  such that  $C \cap B = \emptyset$ ,  $C \subset \bar{B}$ , where  $\bar{B}$  is the closure of  $B$ . Following Gurtin [12-14], the crack  $C$  is represented by a continuous piece-wise smooth map  $(\zeta, t) \mapsto z(\zeta, t)$  where  $\zeta \in [0, \beta(t)]$  is the curvilinear abscissa along  $C$ ,  $\beta(t)$  is the crack length and  $t$  is time. The map  $(\zeta, t) \mapsto z(\zeta, t)$  is such that

$$(2.1) \quad (1)g' = g, \quad [g', 0] \in \zeta, \quad (5)z = z$$

with the additional requirement that

$$(2.7) \quad (g, 0] \in \mathfrak{S}_A, \quad 0 = \frac{ip}{zp} = z.$$

The crack tip velocity is the vector

$$(2.3) \quad 1 = |z|, \quad \frac{\partial p}{\partial z} = z, \quad \partial_z z = \bar{z}$$

The crack vector field  $\nu(\zeta)$  is the unit normal to  $C$ , positively oriented when forming an angle  $\frac{\pi}{2}$  measured counterclockwise with respect to the tangent vector  $z'$ . The vector field  $x = x(x^0, t)$ , represents the position of points in  $B$  with respect to a cartesian coordinate system such that

$$\mathbf{A}_k \in \partial\omega(\mathbf{B}_m) \quad k, m = 1, \dots, N \quad (2.9)$$

evolution of the internal state is given by  
 GSM theory, it is assumed that a convex dissipation potential  $\omega = \omega(\mathbf{B}_k)$  exists such that the  
 mented by a set of evolution equations for the internal variables. As mentioned above, within the  
 Constitutive theories with internal state variables require that the state equations be comple-  
 thermodynamics (cf. Halphen and Nguyen [20]).

to be always null. The two inequalities in eq. (2.8) express a strong form of the second law of  
 where  $dT_h$  is the dissipation due to heat conduction,  $d_{mic}$  is the dissipation due to microstruc-  
 tural rearrangements and  $q$  is the heat flux. The pointwise heat source field has been assumed

$$d = dT_h + d_{mic}, \quad dT_h = \mathbf{q} \cdot \nabla \left( \frac{T}{\rho} \right) \geq 0, \quad d_{mic} = \sum_{k=1}^N \mathbf{B}_k \cdot \dot{\mathbf{A}}_k \geq 0 \quad (2.8)$$

by  
 gate to the set of internal state variables, respectively. The total pointwise dissipation  $d$  is given  
 where  $S, \rho, \mathbf{B}_k$  are the Piola-Kirchhoff stress tensor, the density and the generalized forces conju-

$$S = \rho \frac{\partial E}{\partial h}, \quad s = -\frac{\partial h}{\partial T}, \quad \mathbf{B}_k = -\frac{\partial \mathbf{A}_k}{\partial h}, \quad k = 1, \dots, N \quad (2.7)$$

Partial derivatives of the Helmholtz free energy provide all the necessary equations of state:

convenience.  
 variables do not need to be second order tensors: the present choice is motivated only by notational  
 function  $h$  is assumed to be convex in the deformation tensor  $\mathbf{E}$ . Also, note that the internal state  
 where  $\nabla$  represents the gradient operator. Note that, in the context of the GSM theory, the

$$\mathbf{E} = \nabla \mathbf{u} \quad (2.6)$$

usual relationship  
 respectively, and the deformation tensor  $\mathbf{E}$  is defined in terms of the displacement field  $\mathbf{u}$  by the  
 where  $e = e(\mathbf{E}, T, \mathbf{A}_k)$  and  $s = s(\mathbf{E}, T, \mathbf{A}_k)$  are the internal energy and the total entropy functions,

$$h = e - sT, \quad h = h(\mathbf{E}, T, \mathbf{A}_k), \quad k = 1, \dots, N \quad (2.5)$$

that is  
 tensor  $\mathbf{E}$ , the absolute temperature  $T$  and a convenient set of  $N$  internal variables  $\mathbf{A}_k, k = 1, \dots, N$ ,  
 The pointwise thermodynamic state is assumed to be completely described by the deformation  
 potential that governs the material equations of state is the specific Helmholtz free energy,  $h$ .

internal state variables. In this paper a strain formulation is chosen. Therefore, the thermodynamic  
 state variables and a dissipation potential function of the generalized forces work conjugate of the  
 by two scalar convex functions: a thermodynamic potential function of the chosen independent  
 (Halphen and Nguyen [20]). This entails that the material behavior is completely characterized  
 The constitutive behavior of points in  $B$  is assumed to be that of a generalized standard material

## 2.2. Constitutive Behavior in $B$ . Equilibrium Equations.

$\partial B^E$  is oriented by a unit normal field  $\mathbf{n}$ , positive in the outward direction with respect to  $B$ .

$$\partial B = \partial B^E \cup C. \quad (2.4)$$

the external boundary of  $B$ , and the crack  $C$ :  
 $\mathbf{x} = \mathbf{x}^o$  at  $t = 0$ . The boundary  $\partial B$  of  $B$  is considered to be the union of a set  $\partial B^E$  referred to as

$$\sigma(\zeta, t) = S^+ v = S^- v, \quad S^\pm = \lim_{r \rightarrow 0^+} S(z(\zeta) \pm rv, t), \quad \zeta \in c.z., \quad r \in \mathbb{R}^+ \quad (2.16)$$

$\sigma(\zeta, t)$  is defined as and it will be referred to as a *cohesive zone*, abbreviated *c.z.*. The cohesive force (per unit surface) of such regions. For simplicity, in this particular study only one cohesive region is assumed to exist force system. As depicted in Fig. 1, the crack tip, consisting of all points  $z(\zeta, t)$ ,  $\zeta \in [\alpha, \beta]$  is one It is assumed that there are regions on the crack surface that can sustain the action of a cohesive gation, that is, when  $\alpha \neq 0$ .

Furthermore, the function  $\psi(\zeta, t)$  will be assumed to be continuous at  $\zeta = \alpha$  during crack propa-

$$\psi(\zeta, t) = 2\gamma \quad \forall \zeta \in [0, \alpha) \quad \gamma \geq 0. \quad (2.15)$$

Accordingly, the free energy  $\psi(\zeta, t)$  with  $\zeta \in [0, \alpha)$  is assumed to be at most a function of temperature. Such a function is usually referred to as the crack surface energy  $2\gamma$ :

$$\varepsilon(\beta, t) = 0, \quad \varphi(\beta, t) = 0; \quad \varepsilon(\zeta, t) = \varepsilon_0 = \text{const.}, \quad \varphi(\zeta, t) = \varphi_0 = \text{const.} \quad \forall \zeta \in [0, \alpha) \quad (2.14)$$

The functions  $\varepsilon(\zeta, t)$  and  $\varphi(\zeta, t)$  are assumed to vanish where  $C$  does not experience separation and are assumed to take on constant value where  $C$  experiences actual fracture:

$$\psi(\zeta, t) = \varepsilon(\zeta, t) - \varphi(\zeta, t)\theta(\zeta, t). \quad (2.13)$$

The crack  $C$  can be treated as a partially coherent interface endowed with thermodynamic structure. Following the description by Gurtin [14], let  $\psi(\zeta, t)$ ,  $\varepsilon(\zeta, t)$ ,  $\varphi(\zeta, t)$ , and  $\theta(\zeta, t)$  be the crack free energy, internal energy, total entropy and absolute temperature, respectively. The function  $\psi(\zeta, t)$  is defined in the following traditional way:

### 2.3. Crack Thermodynamics. Regularity Requirements.

where  $u^d$  and  $t^d$  represent the fields of prescribed boundary displacement and tractions, respectively.

$$u = u^d \text{ on } \partial B_F^I; \quad S n = t^d \text{ on } \partial B_F^I; \quad \partial B_F^I \cup \partial B_F^E = \partial B^E \quad (2.12)$$

Hence, we have

The boundary conditions on the external boundary of  $B$  are, in general, of the mixed type. The expression of the equilibrium equations for the crack will be discussed in the next section.

$$\text{div}(S) = 0. \quad (2.11)$$

material will take on the form

be quasi-static. Accordingly, in the absence of body forces, the equilibrium equations in the bulk For the sake of simplicity, the interface evolution problem addressed herein will be assumed to expression of the principle of maximum dissipation.

The internal state variable space that maximizes the function  $d_{m.c.}$ . Equation (2.9) is therefore the The formulation in eq. (2.9) ensures that the evolution of the internal state follows the path in

$$\dot{A}_k = \frac{\partial \omega(B_m)}{\partial B_k} \quad k, m = 1, \dots, N. \quad (2.10)$$

where the notation  $\partial \omega(B_m)$  identifies the subgradient of  $\omega$ . Such a notation has been chosen so as to include rate independent evolutionary phenomena such as perfect plasticity. When the function  $\omega$  is Frechet differentiable eq. (2.9) can be rewritten in the more conventional form

In this section a general framework for the construction of thermodynamically based c.z. constitutive equations is presented. As mentioned in the introduction, one of the main concerns of the present theory is the formulation of constitutive equations able to reflect both the c.z. nucleation and deformation processes. The theory is introduced in this section and subsequently completed in section 4. Some practical examples are postponed until section 5.

### 3. A GENERAL COHESIVE ZONE CONSTITUTIVE MODEL

It should be noted that in solving a specific boundary value problem most of the assumptions discussed in this section cannot be enforced a priori. Rather, they need to be verified once a solution is obtained. This circumstance is typical of thermodynamic theories of fracture (cf. Nguyen [16]).

As already mentioned, the fields  $u$  and  $q$  are allowed to undergo at most jump discontinuities across  $C$ . As far as other thermomechanical quantities are concerned, the fields  $E$  and  $S$  are assumed to be non-singular, and the temperature field  $T$  is assumed to be continuous on  $\bar{B}$ . This latter assumption implies that

$$T(z(\zeta), t) = \theta(\zeta, t) < \infty \quad \forall \zeta \in C. \quad (2.22)$$

On the crack surface the displacement field  $u$  is subject to the following unilateral condition expressing the requirement that the crack faces do not penetrate each other:

$$[u] \cdot \nu \geq 0 \quad \forall t \text{ and } \forall \zeta \in [0, \beta] \quad (2.21)$$

Inequality (2.20) will prove quite useful in discussing the c.z. constitutive equations. Using the relationships introduced in this preliminary section, a general c.z. constitutive theory of  $B$  and the use of the Reynold's transport theorem.

where  $[q]$  is the jump in the heat flux across the interface. As discussed by Gurtin [14], inequality (2.19) is a postulate, whereas Costanzo [21] and Costanzo and Allen [17] have shown that eq. (2.18) can be also obtained from a local statement of the conservation of energy principle for the interior of  $B$  and the use of the Reynold's transport theorem.

$$\phi \geq \frac{1}{\theta} [q] \cdot \nu \quad (2.19)$$

$$\dot{\epsilon} = \sigma \cdot \dot{\delta} + [q] \cdot \nu \quad (2.18)$$

Under the above assumptions the c.z. can be shown to be characterized by the following statements of the first and second laws of thermodynamics (Gurtin [14]):

The quantity  $\delta$  will be referred to as the c.z. opening displacement. The notation  $[\cdot]$  represents the jump across the crack surface of the quantity placed within the brackets. Note that although the quantity  $[u]$  is defined everywhere on  $C$ , the quantity  $\delta$  is defined only on the c.z..

$$\delta(\zeta, t) = [u(z(\zeta), t)] = u^+ - u^-, \quad u^\pm = \lim_{r \rightarrow 0^+} u(z(\zeta) \pm r\nu, t), \quad \zeta \in c.z., \quad r \in \mathbb{R}^+. \quad (2.17)$$

The displacement field  $u$  is allowed to undergo at most a jump discontinuity across the crack surface  $C$ . Such a jump in displacement represents an important kinematic quantity in the description of the c.z. energetics and is therefore given the following autonomous definition:

Using the GSM theory (Halphen and Nguyen [20]) it is assumed that the *c.z.* free energy  $\psi$  is a function of the opening displacement  $\delta$ , the temperature  $\theta$  and, possibly, a set of internal parameters representing the interface microstructure. For simplicity only one of such parameters will be included herein and will be indicated by the symbol  $\mu$ . The present formulation differs from the GSM theory in that the function  $\psi$  is not required to be convex in the kinematic variable  $\delta$ .

The total cohesive force  $\sigma$  is assumed to be expressed by the following additive decomposition:

$$\sigma = \sigma^{ir} + \sigma^e. \quad (3.1)$$

$\sigma^e$  is assumed to be the part of the total cohesive force that is mechanically conservative for all processes constrained on hypersurfaces with  $\theta = \text{const.}$  and  $\mu = \text{const.}$ . In other words, any transformation with  $\theta = \text{const.}$ ,  $\mu = \text{const.}$  and  $\sigma^{ir} = 0$  is an elastic process.

Under the above assumption the *c.z.* free energy is therefore a function of the following type:

$$\psi = \psi(\delta, \theta, \mu) \quad (3.2)$$

definable in the following manner (Edelen [22]):

$$\forall \delta, \theta, \mu \quad \psi(\delta, \theta, \mu) = \psi_o(\theta, \mu) + \int_0^1 \delta \cdot \sigma^e(\lambda \delta; \theta, \mu) d\lambda \quad \lambda \in [0, 1] \quad (3.3)$$

where it has been assumed that for any given pair  $\theta = \text{const.}$ ,  $\mu = \text{const.}$ , all admissible points  $\delta$  on the hyperplane  $\theta = \text{const.}$ ,  $\mu = \text{const.}$  are reachable from the origin of said hyperplane along a straight path. For the sake of simplicity and without loss of generality the function  $\psi_o(\theta, \mu)$  is assumed to vanish identically:

$$\psi_o(\theta, \mu) \equiv 0. \quad (3.4)$$

The above definition of free energy is clearly consistent with the classical one usually employed in constitutive theories with internal state variables (see e.g. Rice [23]).

Eq. (3.3) implies that the  $\sigma^{ir}$  component of the cohesive force does not contribute to any local energy storage mechanisms, whereas eq. (3.1) implies that  $\sigma^{ir}$  expresses the mechanics of some phenomena acting in parallel with the *c.z.* deformation process. Hence,  $\sigma^{ir}$  lends itself to the description of those dissipative phenomena, such as the *c.z.* nucleation process, that cannot be fully described in terms of the chosen set of *c.z.* state variables. Clearly, neither eq. (3.1) nor eq. (3.3) are sufficient to fully characterize the function  $\sigma^{ir}$ . In this regard it must be noted that if  $\sigma^{ir}$  is assumed to be a function of the chosen state variables and possibly of their rates, such a function cannot be totally arbitrary. In fact, in order for eqs. (3.1) and (3.3) to be compatible the relationship linking  $\delta$  and  $\sigma^{ir}$  cannot associate a unique  $\sigma^{ir}$  to a given  $\delta$  (for any fixed pair  $\theta = \text{const.}$ ,  $\mu = \text{const.}$ ) since, in this latter case,  $\sigma$  would have to replace  $\sigma^e$  in the integrand in eq. (3.3). In other words, eqs. (3.1) to (3.3) also imply that for any given  $\delta$  (and in particular for  $\delta = 0$ ) the mapping  $\delta \rightarrow \sigma^{ir}$ , and in turn the mapping  $\delta \rightarrow \sigma$ , is in general set valued. Thus, the constitutive assumptions reflected in eqs. (3.1) to (3.3) provide a possible solution to the problem discussed in the introduction regarding the necessity for the mapping  $\delta \rightarrow \sigma$  to be set-valued at  $\delta = 0$ .

For the proposed formulation to be completely acceptable we have yet to show that the force  $\sigma^{ir}$  can be physically related to a particular crack or interface nucleation mechanism. In order to achieve this result we will rely on considerations based on the second law of thermodynamics and on a global thermodynamic analysis. The latter, presented in the next section, will show that the field  $\sigma^{ir}$  and the field  $\delta$ , although seemingly unrelated at the local level, are conjugate with respect to the total free energy of the system  $B \cup C$ . This in turn suggests that the proper

characterization of the relationship between  $\sigma^{ir}$  and  $\delta$  is expressed by a kinetic equation, that is, an equation of evolution. In the present theory, the *c.z.* evolution will be required to conform to the maximum dissipation principle. Such a requirement will then be formalized by assuming that the *c.z.* evolution equation can be derived from a dissipation potential.

The decomposition in eq. (3.1), central to the present formulation, has been suggested explicitly in a number of works available in the materials science literature (Verheulpen-Heymans [24]; Leonov and Brown [25]). Gurtin [14], in his discussion of viscoelastic *c.z.* models, also concludes that a decomposition such as eq. (3.1) can be introduced, but the issue of giving  $\sigma^{ir}$  a consistent physical interpretation and a proper evolution equation is left unaddressed. Eq. (3.1) has also been less explicitly suggested by other authors such as Riedel [26] and Hui *et al.* [9].

Substituting eqs. (3.1) to (3.3) into eq. (2.20) we have

$$\left(\frac{\partial\psi}{\partial\delta} - \sigma^e\right) \cdot \dot{\delta} - \sigma^{ir} \cdot \dot{\delta} + \left(\varphi + \frac{\partial\psi}{\partial\theta}\right) \dot{\theta} + \frac{\partial\psi}{\partial\mu} \cdot \dot{\mu} \leq 0 \quad (3.5)$$

By the use of classical arguments of the GSM theory (Germain, Nguyen and Suquet [27]), we see that equation (3.3) and inequality (3.5) yield the following *c.z.* state equations:

$$\sigma^e = \frac{\partial\psi}{\partial\delta}, \quad \varphi = -\frac{\partial\psi}{\partial\theta}, \quad \kappa = -\frac{\partial\psi}{\partial\mu} \quad (3.6)$$

where  $\kappa$  is the local free energy conjugate of the state variable  $\mu$ .

From eqs. (3.6) and inequality (3.5) we see that the energy dissipation in the *c.z.* is given by

$$\sigma^{ir} \cdot \dot{\delta} + \kappa \cdot \dot{\mu} \geq 0. \quad (3.7)$$

Having assumed that the *c.z.* thermodynamic state depends also on some internal variable  $\mu$ , it is necessary to complement the set of *c.z.* constitutive relations with the appropriate equation of evolution for the variable  $\mu$ . In analogy to eq. (2.9) we assume that

$$\dot{\mu} \in \partial\omega_I(\kappa) \quad (3.8)$$

where the subscript *I* stands for *interface*.

#### 4. GLOBAL THERMODYNAMIC ANALYSIS

As discussed in section 3, the cohesive force decomposition in eq. (3.1) and the *c.z.* free energy definition in eq. (3.3) yield the desired result of a set valued relation between  $\sigma$  and  $\delta$ . However, eqs. (3.1) and (3.3) fail to provide a complete characterization of the *c.z.* constitutive behavior since the quantity  $\sigma^{ir}$  is left undetermined. The purpose of this section is that of completing the *c.z.* constitutive equations by providing a thermodynamically consistent characterization of the force  $\sigma^{ir}$ . In order to achieve this goal considerations based on global thermodynamics will be used. By global thermodynamics we mean a thermodynamic analysis of the system at hand as a whole (almost as if it were a single material point). A more precise definition is given in the excellent discussion by Germain *et al.* [27]. Thus, similarly to what is done at the local level, the main objective of the global analysis is the determination of thermodynamic potentials for the whole body. Such potentials will be functions of all those parameters that one has to specify to fully determine the amount of strain energy stored in the system at a given time. Said parameters will be referred to as global state variables and they include the system geometric descriptors, the boundary data and the internal microstructural configuration. Clearly, the global state variables in general belong

to an infinite dimensional space, contrary to what happens in the local theory. Apart from this important distinction, Germain *et al.* [27] have shown that under quite unrestrictive assumptions on the pointwise thermodynamic behavior there is an impressive formal similarity between the global thermodynamic potentials and the local ones. In particular, one can find quantities that, although loosely related at the local level, behave like thermodynamic conjugates pairs with respect to the global potentials. Moreover, those global variables that cannot be directly controlled through the boundary of the body can be shown to behave like internal state variables at the local level. In fact, it can be shown that the evolution of global internal variables can be characterized using a global dissipation potential. A remarkable example of the usefulness of these concepts has been provided by Nguyen [16, 19] in the field of fracture mechanics and plasticity. Generalizing an earlier analysis by Rice [28], Nguyen [16] has shown that the total potential energy of an elastic cracked body can be used to define a global thermodynamic potential that behaves at the global level like the Helmholtz free energy at the local one, and has extended this result to elasto-plastic systems. In such a context, the crack energy release rate, in both elastic and elasto-plastic systems, has been shown to be precisely the generalized thermodynamic force conjugate to the crack length with respect to the global free energy (cf. Rice [28]). Furthermore, Nguyen [16] has reformulated the Griffith criterion as a crack evolution law obtained from a global dissipation potential function of the energy release rate. Other important applications of global thermodynamics can be found in the field of homogenization theories for composite materials (cf. Germain *et al.* [27]).

In the present section the set of the global state variables (external and internal) for the system at hand will be determined. The crack fields  $\sigma^{ir}$  and  $\delta$  will be shown to be conjugate with respect to the global free energy of the system. The existence of a global dissipation potential governing the evolution of the (global) internal field  $\delta$  as a function of  $\sigma^{ir}$  will be postulated and a class of evolution equations for the field  $\delta$  will be obtained from said dissipation potential. In section 5 it will be shown that the formalisms developed in sections 3 and 4 can be given a clear physical meaning and can be used in a great variety of practical applications.

Germain [29] has shown that the concept of global free energy for dissipative systems can be derived by an extension of the concept of total potential energy. The total potential energy in the sense of Germain [29] for the system  $\bar{B}$  in Fig. 1 is the functional

$$\mathcal{E}[\mathbf{u}, \mathbf{u}^d, \mathbf{f}^d, \mathbf{A}, T, \alpha, \beta, \delta, \mu] = \int_B \rho h(\mathbf{E}(\mathbf{u}), \mathbf{A}, T) dA - \int_{\partial B_2^E} \mathbf{f}^d \cdot \mathbf{u} dl + \int_0^\beta \psi(\delta, T, \mu) d\zeta \quad (4.1)$$

where,  $\theta = T$  on *c.z.*, and  $\mathbf{u} = \mathbf{u}^d$  on  $\partial B_1^E$ . For the moment, all the parameters listed within brackets on the left hand side of (4.1) are assumed to be specifiable arbitrarily. This assumption will be verified a posteriori with the intent of showing that in general the parameters  $\alpha$  and  $\beta$  do not satisfy such a requirement and therefore must be eliminated from the list of independent global state variables. Furthermore, the field  $\delta$  will be shown to be a global independent field only when the *c.z.* constitutive equations conform to the assumptions in eqs. (3.1) to (3.3).

The functional  $\mathcal{E}$  can be thought of as a 9-parameter family of elastic total potential energy functionals, each of which is obtained by computing the right hand side of (4.1) for an arbitrarily given 9-tuple of said parameters. Since  $\mathcal{E}$  is well defined for any given 9-tuple of parameters, the latter are not required (at least at this stage) to satisfy the equilibrium equations or to be compatible with any actual evolution.

The satisfaction of the equilibrium equations, in a sense that will be made clear below, is now used as a criterion to select a subfamily of potential energy functionals that will be later defined to be the global Helmholtz free energy for the system at hand.

Among all possible displacement fields  $\mathbf{u}$  a particular one can be found by specifying all other

parameters on the left hand side of (4.1) and by solving the corresponding purely elastic boundary value problem. The latter is defined as follows:

*Given the fields  $\mathbf{u}^d$ ,  $\mathbf{f}^d$ ,  $\mathbf{A}$ ,  $T$ ,  $\delta$ , and  $\mu$  on the corresponding domains of definition  
find the field  $\mathbf{u} \in K$  such that the equilibrium equations (2.11) are satisfied,  
subject to the boundary conditions in eq. (2.12).*

where  $K$  is the set of all admissible displacement fields:

$$K = \left\{ \begin{array}{ll} \mathbf{u} & \in C^1(B) \\ \mathbf{u} = \mathbf{u}^d & \forall t, \forall \mathbf{x} \in \partial B_1^E \\ [\mathbf{u}(\zeta, t)] = \delta(\zeta, t) & \forall \zeta \in [\alpha, \beta] \\ [\mathbf{u}] \cdot \boldsymbol{\nu} \geq 0 & \forall \zeta \in [0, \beta] \end{array} \right. \quad (4.2)$$

Note that  $\alpha$  and  $\beta$  do not need to be explicitly specified since their position is implicitly assigned once the field  $\delta$  is given.

In essence, the problem just defined is a classical elastic boundary value problem (BVP) where together with the usual set of boundary data in eq. (2.12) some other (and less traditional) conditions are specified, equivalent to the assignment of some eigenstrain fields. Thus, under the assumption that the free energy  $h(\mathbf{E}(\mathbf{u}), \mathbf{A}, T)$  is a convex function of  $\mathbf{E}$ , the displacement field  $\mathbf{u}$  solution of the above BVP is unique and is such that

$$\mathcal{E}[\mathbf{u}; \mathbf{u}^d, \dots, \mu] = \min_{\mathbf{u}^* \in K} \mathcal{E}[\mathbf{u}^*; \mathbf{u}^d, \dots, \mu]. \quad (4.3)$$

Under these conditions, a unique global thermodynamic potential  $\mathcal{H}$  for the system  $\bar{B}$  can be defined as the value of  $\mathcal{E}$  corresponding to the field  $\mathbf{u}$  solution of eq. (4.3) (Germain [29]):

$$\mathcal{H}[\mathbf{u}^d, \mathbf{f}^d, \mathbf{A}_k, T, \alpha, \beta, \delta, \mu] = \min_{\mathbf{u}^* \in K} \mathcal{E}[\mathbf{u}^*; \mathbf{u}^d, \mathbf{f}^d, \mathbf{A}_k, T, \alpha, \beta, \delta, \mu]. \quad (4.4)$$

Globally, the functional  $\mathcal{H}$  corresponds to the Helmholtz free energy  $h$  at the local level. Note that since the field  $\mathbf{u}$  is no longer considered as an independent parameter, it has been eliminated from the list within brackets on the left hand side of eq. (4.4).

Once the potential  $\mathcal{H}$  is defined, it is possible to determine the thermodynamic conjugate pairs that characterize the crack energetics. In other words, it is possible to determine those thermodynamic forces, analogous to the energy release rate in fracture mechanics, that govern the c.z. evolution. In order to do this one needs to take derivatives of  $\mathcal{H}$  with respect to the chosen global independent state variables. Clearly, when referred to  $\mathcal{H}$  the term *derivative* must be intended in the sense of Gateaux (Sewell [30]). The notation  $\mathcal{H}_{,\phi}$  will indicate the Gateaux derivative of  $\mathcal{H}$  with respect to the quantity ' $\phi$ ', relative to a convenient topology.

The derivatives of  $\mathcal{H}$  with respect to the fields  $\mathbf{u}^d$  and  $\mathbf{f}^d$  on  $\partial B$  and of the fields  $\mathbf{A}$  and  $T$  in  $B$  can be considered a classical result in global thermodynamics (Germain *et al.* [27]):

$$\begin{aligned} \mathcal{H}_{,\mathbf{A}_k} &= -\mathbf{B}_k(\mathbf{x}, t) \quad \mathbf{x} \in B; \quad \mathcal{H}_{,T} = -s(\mathbf{x}, t) \quad \mathbf{x} \in B; \\ \mathcal{H}_{,\mathbf{u}^d} &= \mathbf{f}(\mathbf{x}, t) \quad \mathbf{x} \in \partial B_1^E; \quad \mathcal{H}_{,\mathbf{f}^d} = \mathbf{u}(\mathbf{x}, t) \quad \mathbf{x} \in \partial B_2^E. \end{aligned} \quad (4.5)$$

$\mathcal{H}_{,T}$  on  $\mathcal{C}$  will be derived below along with the other results concerning the crack.

Next, the derivatives of  $\mathcal{H}$  with respect to the crack state variables will be derived and discussed. One simple way to obtain such derivatives is to compute the first variation of the potential  $\mathcal{H}$  and



apply the Reynold's transport theorem. Thus, recalling that the function  $\psi(\delta(\zeta, t), \theta(\zeta, t), \mu(\zeta, t))$  has been assumed continuous at  $\zeta = \alpha$  whenever  $\delta\alpha \neq 0$  we have

$$\begin{aligned} \delta\mathcal{H} = & -\int_B (s\delta T + \mathbf{B}_k \cdot \delta \mathbf{A}_k) dA + \int_{\partial B_1^E} \mathbf{f} \cdot \delta \mathbf{u}^d dl - \int_{\partial B_2^E} \mathbf{u} \cdot \delta \mathbf{f}^d dl \\ & - \int_\alpha^\beta (\sigma - \frac{\partial \psi}{\partial \delta}) \cdot \delta \delta d\zeta - \int_\alpha^\beta (\varphi \delta T + \kappa \cdot \delta \mu) d\zeta + \psi|_\beta \delta \beta \end{aligned} \quad (4.6)$$

The top line of eq. (4.6) essentially represents the results already listed in eq. (4.5). Hence, recalling that  $\psi(\delta(\beta, t), \theta(\beta, t), \mu(\beta, t)) \equiv 0$  (where the symbol ' $\equiv$ ' signifies *identically equal to*), from eqs. (3.1) and (3.6) we have

$$\mathcal{H}_{,\delta} = -\sigma^{ir} \quad \mathcal{H}_{,T} = -\varphi \quad \mathcal{H}_{,\mu} = -\kappa \quad \text{on c.z..} \quad (4.7)$$

Furthermore, we have

$$\mathcal{H}_{,\beta} \equiv 0 \equiv \mathcal{H}_{,\alpha}. \quad (4.8)$$

Equations (4.8) show that the global thermodynamic potentials  $\mathcal{H}$  and, in turn,  $\mathcal{E}$  are independent of the variables  $\alpha$  and  $\beta$ . An important consequence of this result is that the variables  $\alpha$  and  $\beta$  cannot be assigned arbitrarily under any circumstance. This is in contrast with the usual outcome of standard fracture mechanics analyses. In fact, in fracture mechanics a quantity such as  $\mathcal{H}_{,\alpha}$  is in general non-null and represents the crack energy release rate according to the definition given by Griffith [31]. If  $\mathcal{H}_{,\alpha}$  ( $\mathcal{H}_{,\beta}$ ) had not been identically null, then  $\alpha$  ( $\beta$ ) could have been considered a global internal variable and its evolution could have been characterized via a dissipation potential function of the energy release rate  $\mathcal{H}_{,\alpha}$  ( $\mathcal{H}_{,\beta}$ ) as it can be done in a more traditional fracture mechanics context (cf. Nguyen [16]). In the present case neither  $\alpha$  nor  $\beta$  can be considered global internal variables. Their values during an actual evolution are therefore completely determined once the c.z. constitutive equations are accounted for in satisfying the equilibrium equations. The quantity that replaces the energy release rate in expressing the driving force for the c.z. evolution is the conjugate with respect to  $\mathcal{H}$  of the c.z. opening displacement, namely the field  $-\sigma^{ir} \forall \zeta \in [\alpha, \beta]$ . This latter point will be discussed in greater detail in section 6.

In view of the above result, it must be noted that if the c.z. constitutive equations were chosen so that  $\sigma$  could be derivable from the free energy potential  $\psi$ , i.e. if  $\sigma^{ir} \equiv 0$ , even the first of eqs. (4.7) would vanish identically. This does not only imply that the potential  $\mathcal{H}$  is independent of the field  $\delta$  but also, and more importantly, that in reality a unique  $\mathcal{H}$  cannot always be defined due to the third of (4.2) ( $\mathcal{H}_{,\delta} \equiv 0 \equiv \mathcal{E}_{,\delta}$  implies that  $\delta$  cannot be treated as a boundary data) and to the assumption that the c.z. free energy is non-convex and that the elastic bifurcation/stability problem associated to eq. (4.3) must always be addressed before anything can be said on the c.z. evolution. Moreover, the latter is essentially determined by the equilibrium equations (totally determined in the absence of c.z. internal variables such as  $\mu$ ).

As mentioned in the introduction, the issue of elastic bifurcation and stability of a purely linear elastic body with a non-linear elastic interface (i.e. non convex interfacial free energy with  $\sigma^{ir} \equiv 0$ ) has been studied by Suo *et al.* [10] by establishing the existence of certain interface stationary waves. In the present context, the same problem can be treated using standard variational calculus. The loss of solution uniqueness for the problem defined in eqs. (4.2) and (4.3) can be readily seen by studying the sign of the second variation of the potential  $\mathcal{E}$ . Under the hypotheses that  $\sigma^{ir} \equiv 0$ ,  $\delta^2 \mathcal{E}$  takes on the form

$$\delta^2 \mathcal{E} = \int_B \delta \mathbf{E} \cdot \frac{\partial^2 h(\mathbf{E})}{\partial \mathbf{E} \partial \mathbf{E}} \delta \mathbf{E} dA + \int_\alpha^\beta \delta \delta \cdot \frac{\partial^2 \psi}{\partial \delta \partial \delta} \delta \delta d\zeta > 0. \quad (4.9)$$

Since the function  $\psi$  is not convex, the integral on the right hand side of inequality (4.9) may become negative and overcome the positive contribution from the first integral thus leading to a

loss of uniqueness in the solution of the given boundary value problem. Note that if the system at hand is fully elastic (as in the case of Suo *et al.* [10]) then inequality (4.9) governs both the uniqueness and the stability properties of the problem.

When a non-null field  $\sigma^{ir}$  is included into the picture, bifurcation and stability become, at least in principle, two separate issues and can be treated by studying the properties of the second derivatives of the functional  $\mathcal{H}$  as shown by Nguyen [19] in the context of plasticity and by Nguyen *et al.* [32] in the context of brittle fracture. This topic will be considered separately in section 6.

Going back to the global thermodynamic analysis, we now need to provide an expression for the system global dissipation. In reality the part of the dissipation that is of interest here is that associated with the microstructural rearrangements occurring in the system  $\bar{B}$ . Such a dissipation, indicated by  $D_{mic}$ , can be determined by computing the difference between the time rate of change of  $\mathcal{H}$  under isothermal conditions and the power expended on the body:

$$D_{mic} = \int_B \mathbf{B}_k \cdot \dot{\mathbf{A}}_k dA + \int_\alpha^\beta (\sigma^{ir} \cdot \dot{\delta} + \kappa \cdot \dot{\mu}) d\zeta \geq 0. \quad (4.10)$$

The result here above is certainly consistent with the third of inequalities (2.8) and with inequality (3.7).

Relations (4.7) and (4.10) indicate that the field  $\sigma^{ir}$  is the global thermodynamic force conjugate to the field  $\delta$ , and that the latter can be regarded as an internal variable at the global level. Therefore, in the context of the GSM theory (Germain *et al.* [27]) the relationship between  $\sigma^{ir}$  and  $\delta$  must be given in the form of an equation of evolution. The latter, consistent with the principle of maximum dissipation, will be assumed to be derivable from a global dissipation potential convex in the conjugate force  $\sigma^{ir}$ :

$$\dot{\delta} \in \partial \Omega_I(\sigma^{ir}). \quad (4.11)$$

Eq. (4.11) is formally identical to eq. (3.8). Note though that the potential  $\omega_I(\kappa)$  is a local dissipation potential whereas  $\Omega_I(\sigma^{ir})$  is a global one. In other words, it is only through a global analysis that the evolution equation in (4.11) can be declared thermodynamically consistent (at least in the context of the GSM theory).

The existence of the potential  $\Omega_I$  is one of the most important assumptions in the present theory. The choice of expressing  $\dot{\delta}$  as the subgradient of  $\Omega_I$  is motivated by the intent to construct a theory applicable to rate independent models such as that by Dugdale [2], as well as to rate dependent ones.

With the introduction of eq. (4.11) the cohesive zone constitutive equations are complete. In fact, although the first of eqs. (4.7) can be used to evaluate the field  $\sigma^{ir}$  at a given state once everything else is known, it does not yield any information about the physically admissible  $\sigma^{ir}$  fields and their evolution. It is only through eq. (4.11) that the physics underlying the field  $\sigma^{ir}$  enters the problem and can be given a proper mathematical formulation.

## 5. A FEW COHESIVE ZONE MODELS RE-EXAMINED

Before moving to the analysis of the differences between the present formulation of the running crack problem and a more classical one (i.e. without a c.z.), a few c.z. models available from the literature are now reformulated using the present thermodynamic framework.

The model introduced in section 3 can be schematically represented by the rheological analog model depicted in Fig. 2. It essentially consists of two parts: a purely dissipative element, such as the friction element of the Coulomb type in Fig. 2, placed in parallel with a non-linear spring that in turn is placed in series with another dissipative element represented by the box with the symbol  $\mu$ .

The simplest model that can be described in terms of the general one introduced herein is the celebrated Dugdale model (Dugdale [2]). In its most elementary formulation, the Dugdale model is expressed by the following relationships

$$0 \leq \sigma_\nu < \sigma^Y \Rightarrow \delta = 0; \quad \sigma_\nu = \sigma^Y \Rightarrow 0 \leq \delta_\nu \leq \delta_{cr} \quad (5.1)$$

where  $\sigma_\nu = \sigma \cdot \nu$ ,  $\delta_\nu = \delta \cdot \nu$  and  $\sigma^Y$  and  $\delta_{cr}$  represent the critical values for the cohesive force and the c.z. opening displacement, respectively. The  $\sigma - \delta$  graph corresponding to the eqs. (5.1) is depicted in Fig. 3a.

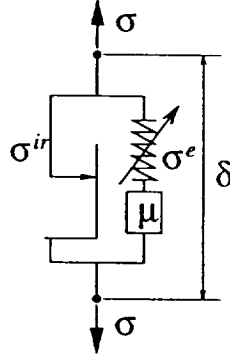


Figure 2: Mechanical Analog of the Cohesive Zone Constitutive Relations.

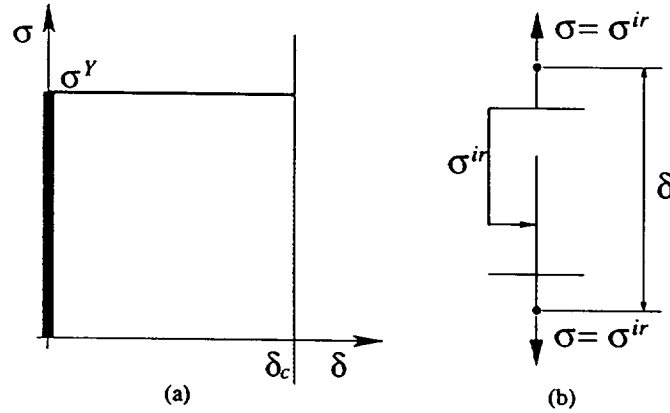


Figure 3: The Dugdale Model.

Dugdale [2] introduced this model to estimate the size of the plastic flow region ahead of a stationary crack. Thus, eqs. (5.1) are intended to describe a rigid perfectly plastic behavior, and, from a thermodynamic viewpoint, a purely dissipative one.

Under isothermal conditions and assuming that the opening displacement  $\delta$  is the only c.z. state variable, a purely dissipative interface can be readily modeled by setting  $\psi(\delta) \equiv 0$ . Moreover, using some elements of rate independent plasticity (Moreau [33]), eqs. (5.1) can be recast in the following variational form:

$$(\sigma - \sigma^*) \cdot \dot{\delta} \geq 0 \quad \forall \sigma^* \in C_D, \quad C_D \equiv [0, \sigma^Y], \quad \sigma^Y = |\sigma^Y| \frac{\delta}{|\delta|}, \quad |\sigma^Y| = \text{const.} \quad (5.2)$$

It can be shown (Moreau [34]) that constitutive relationships of the type given in eq. (5.2) essentially describe a friction law of the Coulomb type.

Eq. (5.2) can also be recast in a form identical to that indicated in eq. (4.11) as follows:

$$\dot{\delta} \in \partial I_{C_D}(\sigma) \quad (5.3)$$

where  $I_{C_D}(\sigma)$  is the indicator function of the convex domain  $C_D$ :

$$I_{C_D}(\sigma) = \begin{cases} 0 & \text{if } \sigma \in C_D \\ +\infty & \text{if } \sigma \notin C_D \end{cases} \quad (5.4)$$

Eq. (5.3) is therefore the kinetic equation that governs the evolution of the Dugdale model. Note that eq. (5.3) is more general than eq. (5.1) since it includes both the behavior for  $\dot{\delta} \cdot \nu \geq 0$  and that for  $\dot{\delta} \cdot \nu \leq 0$ .

Budiansky and Hutchinson [35] extended the original Dugdale model by including compressive behavior for the study of crack closure effects during cyclic loading. Such a model can be reformulated using eqs. (5.3) and (5.4) extending the domain  $C_D$  to include a compressive cohesive force:

$$C_D \equiv [-\sigma^Y, \sigma^Y]. \quad (5.5)$$

Both the Dugdale and the Budiansky-Hutchinson models are represented by the simple rheological model depicted in Fig. 3b. In section 6, eqs. (5.2) and (5.3) will be shown to be quite important in the derivation of the Griffith criterion for brittle fracture as formulated by Nguyen [15-16].

A further rate independent generalization of the Dugdale model can be obtained by taking into account some possible hardening or softening effects. One possible way to achieve this result is to allow the convex domain  $C_D$  to be history dependent. For instance,  $C_D$  can be defined in the following way:

$$C_D \equiv [0, \sigma^Y(\delta)]. \quad (5.6)$$

In this case the evolution law relating  $\sigma^{ir}$  and  $\dot{\delta}$  cannot be expressed by eq. (4.11) since the function  $\Omega_I(\sigma^{ir})$  would depend on other variables in addition to  $\sigma^{ir}$ . Furthermore, in the case of strain softening behavior the property of local stability in the sense of Drucker would be lost.

Another way of proceeding is that of endowing the c.z. model with a convenient free energy function schematically represented in Fig. 2 by the non-linear spring. Some examples of the possible relationships between  $\sigma^e$  and  $\delta$  are shown in Fig. 4.

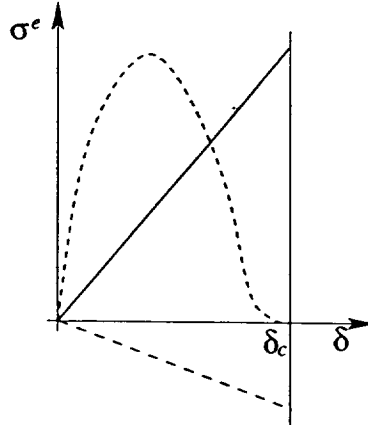


Figure 4: A Few Possible  $\sigma^e - \delta$  Relations.

Assuming that  $\psi = \psi(\delta)$ , i. e.  $\mu \equiv 0$ , the evolution law in eq. (4.11) remains valid and the strain hardening/softening effects are accounted for via the effect of  $\sigma^e$  on  $\sigma^{ir}$ . Consider, for example, the following model:

$$\begin{aligned}\psi(\delta) &= \psi_o - \frac{1}{2}\delta \cdot \mathbf{A}\delta, \quad \psi_o = \text{const.} > 0 \quad \mathbf{A} = \mathbf{A}^T, \det(\mathbf{A}) > 0 \\ \sigma &= \sigma^e + \sigma^{ir}, \quad \sigma^e = -\mathbf{A}\delta \\ \sigma^{ir} &\in C_D \equiv [-\sigma^Y, \sigma^Y], \quad \dot{\delta} \in \partial I_{C_D}\end{aligned}\tag{5.7}$$

For a one dimensional case with  $\dot{\delta} \cdot \nu > 0$ , the forces  $\sigma$ ,  $\sigma^e$  and  $\sigma^{ir}$  are shown in Fig. 5a.

The model described by eqs. (5.7) is in essence a rate independent version of that recently proposed by Xu, Hui, Kramer and Creton [36] for the description of crack growth along the interface between two homopolymers toughened by di-block copolymer chains. Xu *et al.* [36] described the loss of interface coherence using an idealized pull-out model. Indeed, force-displacement diagrams like those depicted in Fig. 5a are qualitatively similar to those obtained in fiber pull-out experiments. For such problems an interface free energy like the one proposed in the first of eqs. (5.7) can be justified with the following qualitative argument. Consider the pull-out problem depicted in Fig. 5b, in which a rigid whisker of diameter  $d + \epsilon$  ( $\epsilon > 0$ ) is extracted from a hole of initial diameter  $d$  within a purely elastic matrix. When the whisker is still entirely surrounded by the matrix a certain strain energy  $\psi(\delta)$  is stored in the residual stress fields caused by the difference in diameter between the whisker and the hole. Clearly,  $\psi(\delta)$  is a monotonically decreasing function of the displacement  $\delta$ , with a maximum  $\psi_o$  for  $\delta = 0$  and a minimum equal to zero for  $\delta = L$  where  $L$  is the depth of the hole in the matrix. As the whisker is pulled out of the matrix, such a strain energy is released at a rate  $\partial\psi/\partial\delta$  which is nothing but the elastic cohesive force  $\sigma^e$  and such that  $\sigma^e \cdot \dot{\delta} \leq 0$ .

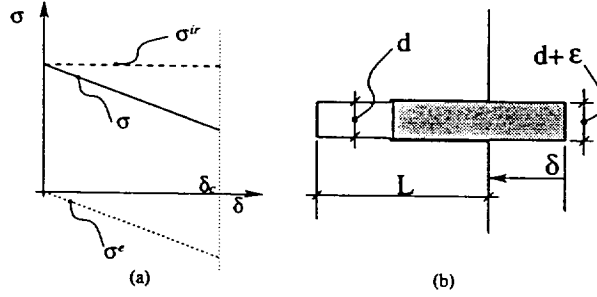


Figure 5: Interface Model Corresponding to Fiber Pull-Out.

From eq. (3.1) we then see that

$$|\sigma^{ir}| \geq |\sigma| \tag{5.8}$$

which can be interpreted by saying that the  $\sigma^e$  component of the cohesive force facilitates the pull-out action. The interesting element of this particular example is that the model in eqs. (5.7) does indeed predict a global strain softening effect in the  $\sigma - \delta$  curve, and that the energy dissipated during separation is greater than the net pull-out work since  $\sigma^{ir} \cdot d\delta \geq \sigma \cdot d\delta$ . This last observation may be significant in studies concerned with the determination of thermal effects at the interface.

In order to generalize the model in eqs. (5.7) to include rate effects such as those considered by Xu *et al.* [36], it is sufficient to modify the dissipation potential  $\Omega_I(\sigma^{ir})$  in the following way:

$$\begin{aligned}\Omega_I(\sigma^{ir}) &= \Omega_1(\sigma^{ir}) + \Omega_2(\sigma^{ir}) \\ \Omega_1(\sigma^{ir}) &= I_{C_D}, \quad \Omega_2(\sigma^{ir}) = \frac{1}{2\eta} \sigma^{ir} \cdot \sigma^{ir}, \quad \eta = \text{const.} \neq 0\end{aligned}\tag{5.9}$$

where  $\eta$  is a scalar viscosity coefficient. In essence, eqs. (5.9) describe the rigid-viscoplastic cohesive zone model, with instantaneous plasticity and linear viscosity whose analogical model is depicted in Fig. 6a.

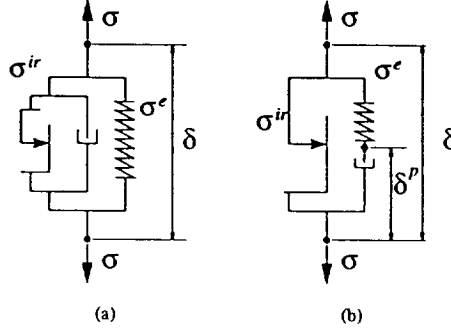


Figure 6: (a) Model by Xu *et al.* [36]; (b) Model by Riedel [26].

As an example of a model with internal state variables, consider that depicted in Fig. 6b. Using the formalism introduced in section 3, the equations describing the model are

$$\begin{aligned}\delta &= \delta^e + \delta^p & \mu &= \delta^p \\ \psi(\delta, \mu) &= \psi(\delta - \delta^p)\end{aligned}\tag{5.10}$$

Thus, the state equations are

$$\sigma^e = \frac{\partial \psi}{\partial \delta} \quad \kappa = -\frac{\partial \psi}{\partial \mu} = -\frac{\partial \psi}{\partial \delta^p} = \sigma^e.\tag{5.11}$$

The c.z. dissipation takes on the form

$$\sigma^{ir} \dot{\delta} + \sigma^e \dot{\delta}^p \geq 0.\tag{5.12}$$

Consistently with eq. (3.7) the variable  $\delta^p$  is assumed to evolve according to the following kinetic equation:

$$\dot{\delta}^p \in \partial \omega_I(\sigma^e)\tag{5.13}$$

In order to see that the equations here above can indeed be used to obtain a cohesive zone model of interest, consider a case in which the dominant interface deformation behavior is creep plastic flow. In this case then the following approximations are justified:

$$\begin{aligned}\dot{\delta}^p &\gg \dot{\delta}^e \Rightarrow \dot{\delta}^p \approx \dot{\delta} \\ \omega_I(\sigma^e) &= A(\sigma^e)^n.\end{aligned}\tag{5.14}$$

Thus,

$$\dot{\delta} = A(\sigma - \sigma^{ir})^n\tag{5.15}$$

where  $A$  and  $n$  are material parameters obtainable from experiments. In particular, if the viscosity coefficient  $A$  is allowed to be a function of  $\delta$ , e.g.  $A = B(\delta)^{pn}$  and  $B$ ,  $p$ , and  $n$  are constants, then eq. (5.15) describes exactly the c.z. model for creep fracture proposed by Riedel [26]. A similar model has been also proposed by Kramer and Hart [37].

## 6. COHESIVE ZONE MODELS AND FRACTURE MECHANICS

### 6.1. Introduction.

In the preceding sections a general c.z. constitutive theory has been presented. The proposed model has been shown to be both thermodynamically consistent and to satisfy the requirement that the relation  $\sigma \rightarrow \delta$  be set valued. As discussed in the introduction, in order for a c.z. model to be applicable to a wide range of phenomena it should also allow for the prediction of the transition from a fully cohesive interface to a cracked one, and, subsequently, for the analysis of the crack propagation stage of the interface life. The purpose of the present section is exactly that of confronting these last two issues. In particular, section 6.2 deals with the problem of crack nucleation where the latter is seen as the evolution from full cohesion to the appearance of microcracks whereas section 6.3 deals more properly with the running crack problem and analyzes the differences and similarities between cracks with and without cohesive zones.

### 6.2. Cohesive Zone Models and Crack Nucleation.

In spite of the fact that they were not originally intended to study crack nucleation, interface models in general carry an intrinsic capability of providing useful information about the crack initiation process or, more specifically, on the possibility of microcrack pattern formation. As mentioned in the introduction, this capability has been explored by Hui *et al.* [9] and more recently by Suo *et al.* [10] by studying a bifurcation problem in which both the interface and the bulk behaviors are elastic. In this case, the bifurcation problem coincides with that of elastic stability.

The present formulation of the interface constitutive equations, by including dissipative effects, allows one to confront the interface bifurcation problem using methods developed in the field of plasticity, in which the issue of bifurcation does not necessarily coincide with that of stability. From a physical viewpoint this distinction is very important since the development of microcracking and damage in most materials occurs, at least in its early stage, under global stability.

The purpose of this section is to show how techniques from the theory of plasticity can be applied without significant changes to the study of the interface bifurcation problem.

For simplicity, the bulk material behavior will be assumed to be elastic and the c.z. constitutive behavior will be assumed to be that described in eqs. (5.7) except for the assumption that the function  $\psi(\delta)$  is now assumed to be general. Furthermore, the system  $\bar{B}$  is assumed to evolve under isothermal conditions, the external boundary data to be of the Dirichlet type only and the interface is assumed to be initially fully cohesive. Given the above hypotheses, the potential  $\mathcal{H}$  reduces to

$$\mathcal{H}[\mathbf{u}^d, \delta] = \int_B W(\mathbf{E}(\mathbf{u}^d, \delta)) dA + \int_0^\beta \psi(\delta) d\zeta \quad (6.1)$$

where  $W(\mathbf{E}) = \rho h(\mathbf{E})$  is the strain energy function (under isothermal conditions).

By definition, the potential  $\mathcal{H}$  already includes all the information that can be obtained from the boundary value problem that characterizes the equilibrium of the system  $\bar{B}$ , which, under the given constitutive assumptions has been shown to yield a unique solution. Thus, if a loss of uniqueness is to occur, it would appear in the solution of the rate problem that governs the interface evolution. The rate problem for the particular case considered herein is constructed by noting that when the domain  $C_D(\sigma^{ir})$  of the admissible irreversible cohesive forces is time independent, the following relation, usually referred to as the consistency condition, must hold:

$$\dot{\sigma}^{ir} \dot{\delta} = 0 \quad \forall \zeta \in [0, \beta] \text{ and } \forall t \quad (6.2)$$

Once the rate of the applied boundary condition  $\dot{\mathbf{u}}^d$  is given, the rate of the field  $\sigma^{ir}$  is obtained by using the first of eqs. (4.7):

$$\dot{\sigma}^{ir} = \mathcal{H}_{,\delta\delta}\dot{\delta} + \mathcal{H}_{,\delta\mathbf{u}^d}\dot{\mathbf{u}}^d \quad (6.3)$$

Now recall that the last of eqs. (5.7) can be interpreted by saying that the unknown vector  $\dot{\delta}$  belongs to the set  $N_{C_D}$ , defined to be the tangent cone to the set  $C_D$ :

$$N_{C_D}(\sigma^{ir}) = \{\xi \mid \xi \cdot (\sigma^{ir} - \sigma^*) \geq 0 \ \forall \sigma^* \in C_D\} \quad (6.4)$$

so that we have

$$\dot{\sigma}^{ir} \cdot \xi \geq 0 \quad \forall \xi \in N_{C_D}(\sigma^{ir}). \quad (6.5)$$

Hence, the rate problem whose primary unknown is the field  $\dot{\delta}$  can be reformulated in the following variational form:

$$(\xi - \dot{\delta}) \cdot (\mathcal{H}_{,\delta\delta}\dot{\delta} + \mathcal{H}_{,\delta\mathbf{u}^d}\dot{\mathbf{u}}^d) \geq 0 \quad \forall \xi \in N_{C_D}(\sigma^{ir}). \quad (6.6)$$

Lions [38] showed that solutions to the variational inequality (6.6) exist if the tensor field  $\mathcal{H}_{,\delta\delta}$  satisfies the following positivity condition:

$$\xi \cdot \mathcal{H}_{,\delta\delta}\xi > 0 \quad \forall \xi \in N_{C_D}(\sigma^{ir}). \quad (6.7)$$

Nguyen [19] showed that a unique solution to (6.6) exists if  $\mathcal{H}_{,\delta\delta}$  satisfies a positivity condition stronger than (6.7), namely

$$\xi \cdot \mathcal{H}_{,\delta\delta}\xi > 0 \quad \forall \xi \in \overline{N_{C_D}(\sigma^{ir})} \quad (6.8)$$

where  $\overline{N_{C_D}(\sigma^{ir})}$  is the vector space generated by  $N_{C_D}(\sigma^{ir})$  (i.e. the totality of all possible linear combinations of the elements of  $N_{C_D}(\sigma^{ir})$ ). Condition (6.8) is more restrictive than (6.7) because it must hold on the space  $\overline{N_{C_D}(\sigma^{ir})}$  which clearly includes  $N_{C_D}(\sigma^{ir})$  as a proper subset.

Solutions to inequality (6.8), being subject to a more severe constraint than that imposed on solutions to (6.7), identify bifurcation modes under stable conditions. A complete discussion of inequalities (6.7) and (6.8) is certainly out of the scope of the present paper and therefore will not be given here. Nonetheless, a few qualitative results can be established with little effort by simply providing a more concrete form for the abstract expressions in both (6.7) and (6.8).

Consider the second variation of the functional  $\mathcal{H}$ , as required in inequalities (6.7) and (6.8), under the requirement that the externally controlled displacement data remain fixed:

$$\delta^2 \mathcal{H} = \int_B \delta \mathbf{E} \cdot \frac{\partial^2 W}{\partial \mathbf{E} \partial \mathbf{E}} \delta \mathbf{E} \, dA + \int_0^\beta \delta \delta \cdot \frac{\partial^2 \psi}{\partial \delta \partial \delta} \delta \delta \, d\zeta > 0 \quad (6.9)$$

where, by definition of  $\mathcal{H}$ , the field  $\delta \mathbf{E}$  is not arbitrary, but is a function of the variation  $\delta \delta$  such that

$$\begin{aligned} \operatorname{div}(\delta \mathbf{S}) &= \operatorname{div}\left(\frac{\partial^2 W}{\partial \mathbf{E} \partial \mathbf{E}} \delta \mathbf{E}\right) = 0 \\ \delta \mathbf{E} &= \nabla(\delta \mathbf{u}) \mid \delta \mathbf{u} = 0 \text{ on } \partial B_E \text{ and } [\delta \mathbf{u}] = \delta \delta \text{ on } \mathcal{C} \end{aligned} \quad (6.10)$$

Having assumed that the function  $W$  is convex, inequality (6.9) allows one to establish that the interface evolution problem formulated herein has a unique solution for all interface constitutive models with a convex or null free energy  $\psi$ . The most renowned of such models is perhaps that of Dugdale, which cannot therefore be used to predict crack formation from an otherwise sound material via the use of bifurcation arguments. The Dugdale model, like any non-bifurcating model, can only be used in fracture problems where a crack is present to begin with. Furthermore, in the



present formulation, in order for a bifurcation in the solution  $\delta$  to occur it is necessary to have a non-convex free energy  $\psi$ .

In order to extract more information from inequality (6.9) it is necessary to rewrite it in such a way that all integrals evaluated on the domain  $B$  are transformed into integrals evaluated on the domain  $[0, \beta]$ . In general, the accomplishment of this task is quite difficult in that knowledge of the functional dependence of the field  $\delta \mathbf{E}$  on the field  $\delta \delta$  is required. Thus, for the sake of conciseness, and with the intent of providing only a qualitative result, assume that an admissible variation  $\delta \mathbf{u}$  of the displacement field  $\mathbf{u}$  can be given the following form:

$$\delta \mathbf{u} = \sum_{i=0}^{\infty} \mathbf{a}_i \sin(\mathbf{k}_i \cdot \mathbf{x}) \quad (6.11)$$

where the wave vectors  $\mathbf{k}_i$  ( $i = 1, \dots, \infty$ ) are to be determined as functions of geometry and material properties and where

$$[\delta \mathbf{u}] = \boldsymbol{\xi} = \sum_{i=0}^{\infty} [\mathbf{a}_i] \sin(\mathbf{k}_i \cdot \mathbf{z}) \quad \mathbf{z} \in \mathcal{C}. \quad (6.12)$$

Substituting (6.11) and (6.12) into (6.9) and employing the Reynold's transport theorem we obtain

$$\delta^2 \mathcal{H} = \int_0^\beta \boldsymbol{\xi} \cdot \left\{ \delta \boldsymbol{\sigma} + \frac{\partial^2 \psi}{\partial \delta \partial \delta} \boldsymbol{\xi} \right\} d\zeta > 0 \quad (6.13)$$

where

$$\delta \boldsymbol{\sigma} = \left( \frac{\partial^2 W}{\partial \mathbf{E} \partial \mathbf{E}} \sum_{i=0}^{\infty} \mathbf{a}_i \otimes \mathbf{k}_i \cos(\mathbf{k}_i \cdot \mathbf{x}) \right)^+ \boldsymbol{\nu} = \left( \frac{\partial^2 W}{\partial \mathbf{E} \partial \mathbf{E}} \sum_{i=0}^{\infty} \mathbf{a}_i \otimes \mathbf{k}_i \cos(\mathbf{k}_i \cdot \mathbf{x}) \right)^- \boldsymbol{\nu} \quad (6.14)$$

Inequality (6.13) can be further manipulated and cast in the form indicated in inequalities (6.7) and (6.8) to define a classical eigenvalue problem. For the purpose of this discussion it is sufficient to note that, from eq. (6.14), the sign of the integrand in (6.13) essentially depends on the magnitude of the bulk tangent elastic moduli relative to the interface elastic tangent moduli and on a set of characteristic length scales associated with the wave vectors  $\mathbf{k}_i$ . Note that the strain energy  $W$  does not need to be continuous across the interface. The above result is qualitatively consistent with that obtained in a quite different context by Suo *et al.* [10], and therefore shows that the treatment of the bifurcation problem suggested herein is a valid one.

### 6.3. Cohesive Zone Models and Crack Propagation.

We now turn our attention from the crack initiation problem to that of crack propagation. In classical fracture mechanics, i.e. in analysis without cohesive zones, the expression *crack growth problem* indicates a moving boundary problem in which the primary unknown is usually the trajectory of a single (non material) point referred to as the crack tip. The global thermodynamic analysis in section 4 has shown that in fracture problems with a cohesive zone the primary unknown associated with the crack is neither the trajectory of the point at  $\zeta = \alpha$  nor that of the point at  $\zeta = \beta$  (cf. eq. (4.8)), but rather the time evolution of the field  $\delta$ . Thus, the problem with and that without a c.z. appear very different, at least from a mathematical viewpoint. In reality, since the two problems are intended to model the same phenomenon it is reasonable to expect some similarities between them. The purpose of this section is therefore that of providing some insight on the relationship between the classical running crack problem and that with a c.z..

In order to relate the two problems it is necessary to constrain the *c.z.* to behave as much as possible like a single geometrical point. Taking into account that the *c.z.* must have finite size by definition, one possible way to impose said constraint is to assume that the *c.z.* is small with respect to the rest of the crack surface, i.e.  $\beta - \alpha \ll \alpha$  and to *rigidify* the *c.z.*, i.e. to assume that during crack propagation the crack tip behaves like a rigid wedge moving ahead of the physical crack tip. This latter approach is not at all new. In fact, it concides with that followed by Barenblatt [1] who formalized it through the following two assumptions (p. 59 in Barenblatt [1]):

- A1. ... the area of the part of crack surface acted upon by the forces of cohesion can be considered as negligibly small compared to the entire area of the crack surface.
- A2. ... the form of the crack surface near the edges, at which forces of cohesion have the maximum intensity, does not depend on the applied load.

Under assumptions A1 and A2 the function  $\delta(\zeta, t)$ ,  $\zeta \in [\alpha, \beta]$  takes on the form

$$\delta = \hat{\delta}(\chi, \mathcal{L}) \quad (6.15)$$

where

$$\chi = \zeta - \alpha \quad \forall \zeta \in [\alpha, \beta], \quad \mathcal{L} = \beta - \alpha = \text{const.}, \quad \frac{\partial \hat{\delta}}{\partial \chi} \cdot \nu \leq 0 \quad \forall \chi \in [0, \mathcal{L}]. \quad (6.16)$$

From eqs. (6.15) and (6.16) we also have

$$\dot{\delta} = \dot{\alpha} \frac{\partial \hat{\delta}}{\partial \alpha} = -\dot{\alpha} \frac{\partial \hat{\delta}}{\partial \chi}. \quad (6.17)$$

From eqs. (6.17) and (4.10) we see that the dissipation rate  $D_c$  due to crack propagation alone becomes

$$D_c = \dot{\alpha} \int_{\mathcal{L}}^0 \sigma^{ir} \cdot \frac{\partial \hat{\delta}}{\partial \chi} d\chi. \quad (6.18)$$

Eq. (6.18) indicates that assumptions A1 and A2 are certainly sufficient to render the trajectory of the point at  $\zeta = \alpha$  the primary unknown of the problem as in the classical fracture mechanical formulation. Moreover, now that  $\alpha$  has replaced the field  $\delta$  as a global internal state variable for the system  $\bar{B}$  we have

$$-\mathcal{H}_{,\alpha} = J = \int_{\mathcal{L}}^0 \sigma^{ir} \cdot \frac{\partial \hat{\delta}}{\partial \chi} d\chi. \quad (6.19)$$

where  $J$  is therefore the generalized thermodynamic force conjugate to  $\alpha$ . The force  $J$  can also be expressed via the following decomposition:

$$J = G - R \quad (6.20)$$

where

$$G = \int_{\mathcal{L}}^0 \sigma \cdot \frac{\partial \hat{\delta}}{\partial \chi} d\chi \quad \text{and} \quad R = \int_{\mathcal{L}}^0 \sigma^e \cdot \frac{\partial \hat{\delta}}{\partial \chi} d\chi. \quad (6.21)$$

The quantities  $G$  and  $R$  are the energy release rate, as defined by Griffith [31], and the resistance to crack growth, respectively. The quantity  $R$  is usually referred to as intrinsic fracture energy and expressed by the notation  $2\gamma$ . In view of the discussion given in section 5,  $R$  may not always be a positive number. Eqs. (6.18) and (6.19) bring support to the claim made in section 4 that when a *c.z.* is introduced into the formulation of a fracture problem, the generalized force  $\sigma^{ir}$  takes

the place that the energy release rate occupies in the classical approach. The first of eqs. (6.21) represents a generalization of a well known result obtained in the context of linear and nonlinear elasticity by Rice [39].

Eqs. (6.18) and (6.19) suggest that a dissipation potential  $\Omega_c(J)$  can be found such that the crack evolution law takes on the form:

$$\dot{\alpha} \in \partial \Omega_c(J) \quad (6.22)$$

consistent with the principle of maximum dissipation. In fact,  $\Omega_c(J)$  can be computed explicitly under assumptions A1 and A2 once the dissipation potential  $\Omega(\sigma^{ir})$  is given. As an elementary example, consider the Dugdale model formulated in eqs. (5.2) to (5.4) with the additional assumption that there exists a constant value  $\delta_c$  of the crack opening displacement at which fracture occurs. Hence, due to assumption A2, during crack propagation, every point in the c.z. experiences an opening rate  $\dot{\delta} = -\dot{\alpha} \partial \hat{\delta} / \partial \chi$ . From eqs. (5.2) we then have

$$\dot{\delta} \neq 0 \Rightarrow \sigma^{ir} = \begin{cases} \sigma^Y & \text{if } \dot{\delta} \cdot \nu > 0 \\ 0 & \text{if } \dot{\delta} \cdot \nu < 0 \end{cases} \quad (6.23)$$

Having assumed that  $\hat{\delta}(\chi, \mathcal{L}) \cdot \nu$  is a monotone decreasing function of  $\chi$ , from eqs. (6.19) and (6.23) we have

$$J = \begin{cases} \int_{\mathcal{L}}^0 \sigma^Y \cdot \frac{\partial \hat{\delta}}{\partial \chi} d\chi & \text{if } \dot{\alpha} > 0 \\ 0 & \text{if } \dot{\alpha} < 0 \end{cases} \quad (6.24)$$

The integral on the top right hand side of eq. (6.24) has the evaluation (cf. Rice [39]):

$$\int_{\mathcal{L}}^0 \sigma^Y \cdot \frac{\partial \hat{\delta}}{\partial \chi} d\chi = \sigma^Y \cdot \delta_c = \text{const.} \quad (6.25)$$

Letting  $J_{cr} = \sigma^Y \cdot \delta_c$ , from the above equation we see that  $J \in (0, J_{cr}) \Rightarrow \dot{\alpha} = 0$  and that  $\dot{\alpha} \neq 0 \Rightarrow J = 0$  or  $J = J_{cr}$ . Thus, the kinetic equation that governs the evolution of the independent state variable  $\alpha$  can be given the following form:

$$\dot{\alpha} \in \partial I_C(J) \quad (6.26)$$

where  $I_C(J)$  is the indicator function of the closed convex domain  $C_J = [0, J_{cr}]$ . Eq. (6.26) can also be formulated in the following variational form:

$$(J - J^*)\dot{\alpha} \geq 0 \quad \forall J^* \in C_J \quad (6.27)$$

or

$$(G - G^*)\dot{\alpha} \geq 0 \quad \forall G^* \in C_G \quad C_G = [\hat{R}, J_{cr} + \hat{R}] \quad (6.28)$$

where

$$\hat{R} = \int_{\mathcal{L}}^0 \frac{\partial \psi}{\partial \delta} \cdot \frac{\partial \hat{\delta}}{\partial \chi} d\chi = \psi(\delta_c) \quad (6.29)$$

Note that in the specific case of the Dugdale model, at least according to the formulation given herein,  $\hat{R}$  is always identically null. In general though, based on physical observation it is customary to assume that  $\hat{R} \ll J_{cr}$  so that  $C_G = [0, G_{cr}]$  where  $G_{cr} = J_{cr}$ .

The evolution equation (6.28) has been proposed by Nguyen [15-16] as a re-statement of the Griffith criterion suitable for the formulation of rate independent brittle fracture problems. As mentioned in the introduction, the derivation presented in this section shows that such evolution

equations can be derived under suitable assumptions (namely A1 and A2) directly from the Dugdale model.

The procedure with which eq. (6.28) was derived is quite general in nature. In other words, given a certain evolution equation for the c.z. one can always construct, under assumptions A1 and A2, a corresponding evolution equation for the global internal variable  $\alpha$  that is derived from a dissipation potential, where the latter can be explicitly constructed as shown above in the case of the Dugdale model.

## 7. SUMMARY

The present work is in essence an extension of modern constitutive theories to include stationary partially coherent interfaces. As stated in the introduction, the theory is built so as to satisfy three fundamental physical requirements. First, the interface is required to be capable of strain energy storage. It is assumed that such storage capability depends on the jump discontinuity in the displacement field across the interface itself, the interface temperature and, possibly, its microstructure. Second, the interface is assumed to be capable, at least in the initial stage of its life, of transferring forces across itself even in the absence of interface deformation, where the latter corresponds to a displacement field jump discontinuity as mentioned before. Physically, the mechanism responsible for this type of behavior is assumed to be purely dissipative. Third, the interface constitutive equations should permit the prediction of crack pattern formation from an otherwise fully cohesive interface via bifurcation arguments. The rationale for these requirements has been discussed in the introduction.

The first requirement has been formalized by the assumption that there exists a function  $\psi$  of the interface opening displacement, temperature and microstructure that is a work potential for the interface. This idea has been originally explored by Gurtin [14] who provided a useful thermodynamic theory for the development of the interface constitutive equations. Within such a framework, requirement two has been formalized by a decomposition of the cohesive force  $\sigma$  into two parts:  $\sigma^e$ ,  $\sigma^{ir}$ .  $\sigma^e$  is assumed to originate from the interface free energy and, in this sense, to be the expression of mechanically reversible transformations, such as bond stretching in crystalline materials or fibril elastic stretching in polymer crazing.  $\sigma^{ir}$  is not assumed to have an explicit and one-to-one relationship with the interface opening displacement. This allows the interface to transfer forces of various intensity even under the assumption of perfect cohesion, i.e. a situation characterized by a null opening displacement. The physics behind the irreversible part of the cohesive force  $\sigma^{ir}$  depends on the particular system at hand. For example, in the case of single craze formation,  $\sigma^{ir}$  can represent the average effect of the forces responsible for the craze nucleation through secondary bond breakage. Such forces, which macroscopically appear to be acting on the interface surface, do not originate from fibril stretching and for this reason are not associated with a particular energy storage mechanism.

The global thermodynamic analysis presented in section 4 shows that the fields  $\sigma^{ir}$  and  $\delta$  are conjugate with respect to the global free energy of the system. This result leads naturally to the hypothesis that the relationship between the fields  $\sigma^{ir}$  and  $\delta$  is governed by an equation of evolution. It should be noted that global thermodynamics becomes an almost indispensable tool in the thermodynamic analysis of multi-phase systems like the one considered herein (i.e. body-plus-interface). In particular global thermodynamics is extremely useful in the analysis of composite materials with an evolving internal microstructure.

The present theory has been shown to encompass most of the cohesive zone models available from the literature and, as shown in section 6.2, to satisfy the third of the requirements listed above under the assumption that the interface free energy is non-convex.

In section 6.3 the proposed model has been shown to have another important characteristic, namely that of naturally recovering the classical results of fracture mechanics once a macroscopic crack propagates along the interface in a self-similar fashion. In particular, the relationship between the interface dissipative behavior and the crack evolution law has been established.

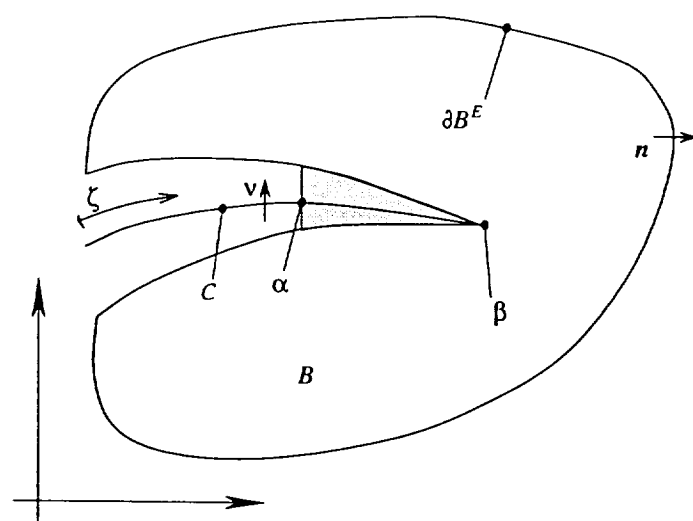
## ACKNOWLEDGEMENTS

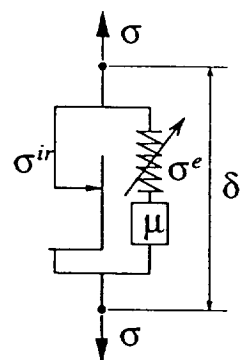
The authors wish to thank Dr. J. R. Walton (Department of Mathematics, Texas A&M University) for many valuable discussions, and gratefully acknowledge partial funding supplied by NASA Langley Research Center, under Grant NAG 1-1120.

## REFERENCES

- [1] G. I. BARENBLATT, *Adv. Appl. Mech.* **7**, 55 (1962).
- [2] D. S. DUGDALE, *J. Mech. Phys. Solids* **8**, 100 (1960).
- [3] M. ORTIZ, *Int. J. Solids Structures* **24**, 231 (1988).
- [4] B. BUDIANSKY, J. C. AMAZINGO and A. G. EVANS, *J. Mech. Phys. Solids* **36**, 167 (1988).
- [5] E. JOHNSON, *Int. J. Fracture* **55**, 47 (1992).
- [6] L. I. SLEPYAN, *J. Mech. Phys. Solids* **41**, 1019 (1993).
- [7] T. UNGSUWARUNGSRI and W. G. KNAUSS, *J. Appl. Mech.* **55**, 44 (1988).
- [8] T. UNGSUWARUNGSRI and W. G. KNAUSS, *J. Appl. Mech.* **55**, 52 (1988).
- [9] C. -Y. HUI, D. C. LAGOUDAS and A. RUINA, in *Constitutive Modelling for Nontraditional materials*, V. K. Stokes and D. Krajcinovic (eds.), ASME AMD-Vol. **85**, 87 (1987).
- [10] Z. SUO, M. ORTIZ and A. NEEDLEMAN, *J. Mech. Phys. Solids* **40**, 613 (1992).
- [11] Y. N. LI and R. Y. LIANG, *J. Mech. Phys. Solids* **8**, 100 (1993).
- [12] M. E. GURTIN, *J. Elasticity* **9**, 187 (1979).
- [13] M. E. GURTIN, *Int. J. Solids Structures* **15**, 553 (1979).
- [14] M. E. GURTIN, *ZAMP* **30**, 991 (1979).
- [15] Q. S. NGUYEN, *J. Mécanique* **19**, 363 (1980).
- [16] Q. S. NGUYEN, in *Three-Dimensional Constitutive Relations and Ductile Fracture*, IUTAM Symposium, Durdan, 315 (1980).
- [17] F. COSTANZO and D. H. ALLEN, *Int. J. Fracture* **63**, 27 (1993).
- [18] L. -O FAGER, J. BASSANI, C. -Y. HUI and B. -B. XU, *Int. J. Fracture* **52**, 119 (1991).
- [19] Q. S. NGUYEN, *J. Mécanique* **3**, 41 (1984).
- [20] B. HALPHEN and Q. S. NGUYEN, *J. Mécanique* **14**, 39 (1975).

- [21] F. COSTANZO, Ph.D. dissertation, Texas A&M University, College Station, Texas (1993).
- [22] D. G. B. EDELEN, *Applied Exterior Calculus*, John Wiley and Sons, New York (1985).
- [23] J. R. RICE, in *Constitutive Equations in Plasticity*, A. S. Argon (ed.), MIT Press, Cambridge (Mass.), 23 (1975).
- [24] N. VERHEULPEN-HEYMANS, *Polym. Eng. Sci.* **24**, 809 (1984).
- [25] A. I. LEONOV and H. R. BROWN, *H. R. J. Polym. Sci., /B Polym. Phys.* **29**, 197 (1991).
- [26] H. RIEDEL, (1977) *Mater. Sci. Eng.* **30**, 187 (1977).
- [27] P. GERMAIN, Q. S. NGUYEN and P. SUQUET, *J. Appl. Mech.* **50**, 1010 (1983).
- [28] J. R. RICE, *J. Mech. Phys. Solids* **16**, 61 (1978).
- [29] P. GERMAIN, (1982) *Int. J. Eng. Sci.* **20**, 245 (1982).
- [30] M. J. SEWELL, *Maximum and Minimum Principles*, Cambridge University Press, Cambridge (1987).
- [31] A. A. GRIFFITH, *Phil. Trans. R. Soc. A* **221**, 163 (1921).
- [32] Q. S. NGUYEN, C. STOLZ and G. DEBRUYNE, *Eur. J. Mech., A/Solids* **9**, 157 (1990).
- [33] J. J. MOREAU, in *New Variational Techniques in Mathematical Physics*, CIME, G. Capriz and G. Stampacchia (eds.), Edizioni Cremonese, Roma, 175 (1974).
- [34] J. J. MOREAU, in *Trends in Application of Pure Mathematics to Mechanics*, H. Zorski (ed.), Pitman Press, London, 263 (1979).
- [35] B. BUDIANSKY and J. W. HUTCHINSON, *J. Appl. Mech.* **45**, 267 (1978).
- [36] D. -B. XU, C. -Y. HUI, E. J. KRAMER and C. CRETON, *Mech. Mater.* **11**, 257 (1991).
- [37] E. J. KRAMER and E. W. HART, *Polymer* **25**, 1667 (1984).
- [38] J. L. LIONS, *Contrôle Optimal*, Dunod, Paris (1968).
- [39] J. R. RICE, *J. Appl. Mech.* **35**, 379 (1968).







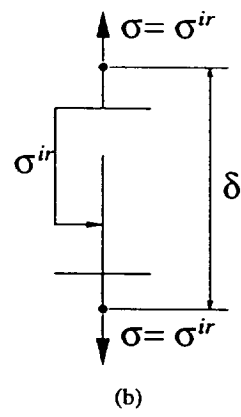
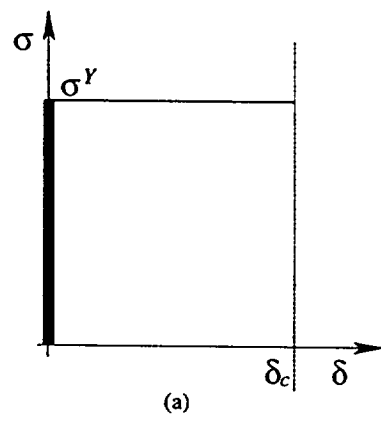


Fig. 3

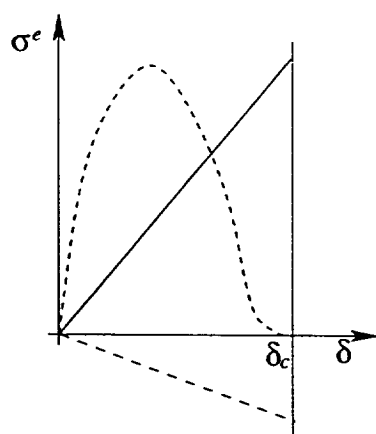


Fig. 1

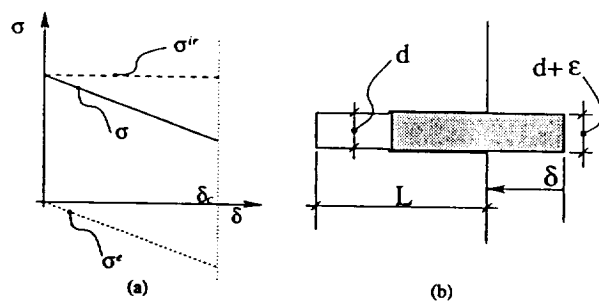
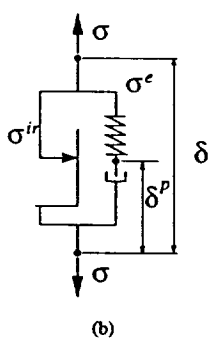
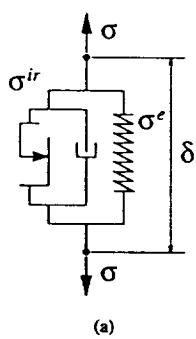


Fig. 5



# MECHANICS OF THICK COMPOSITES

PRESENTED AT  
THE 1st JOINT MECHANICS MEETING OF  
ASME • ASCE • SES — MEET'N'93  
CHARLOTTESVILLE, VIRGINIA  
JUNE 6-9, 1993

SPONSORED BY  
THE APPLIED MECHANICS DIVISION, ASME

EDITED BY  
YAPA D. S. RAJAPAKSE  
OFFICE OF NAVAL RESEARCH

THE AMERICAN SOCIETY OF MECHANICAL ENGINEERS  
345 East 47th Street ■ United Engineering Center ■ New York, N.Y. 10017

## MODELING OF DAMAGE EVOLUTION IN THICK LAMINATES SUBJECTED TO LOW VELOCITY IMPACT

D. C. Lo, F. Costanzo, M. A. Zocher, and D. H. Allen  
Center for Mechanics of Composites  
Texas A&M University  
College Station, Texas

### Abstract

The purpose of this paper is to construct models capable of predicting the growth of delaminations in thick laminates subjected to low-velocity impact. Experimental evidence contained herein suggests that these delaminations are initiated at the intersections of matrix cracks with the ply interfaces. Utilizing this observation, a nonlinear computational finite element scheme is developed to predict the delamination evolution in a test scenario using a [0,90,0] laminate composed of graphite/epoxy. Both the matrix cracks and delaminations are modelled using a nonlinear interface failure criterion previously proposed by Needleman (1987).

Based on the current interfacial constitutive model and failure criteria, the results suggest that there is a strong influence due to the ratio of normal to shear interface strength between plies. On the other hand, there appears to be a weaker influence of the interface failure energy on delamination propagation.

### Introduction

Thick laminates impacted at low velocity by blunt objects are susceptible to the development of subsurface damage. This damage can take the form of matrix cracks, delaminations, and fiber breakage. Often, more than one type of damage will be present. This is due to the damage induced stress redistribution creating favorable conditions for the initiation and propagation of other types of damage in the adjacent areas. While this subsurface damage is not readily visible at the surface, it is capable of substantially reducing the laminate's strength and stiffness. Therefore, it is essential to be able to predict the damage evolution occurring during the impact event so that the serviceability of the laminate can be determined.

A large sum of time, effort, and money has been directed in recent years toward gaining a better understanding of the damage that results when laminated composites are subjected to low velocity impact (LVI). This is evident from the numerous studies, both experimental and analytical, that have appeared in the literature. However, due to the complexity of the mechanisms involved in LVI damage, such as interactions between matrix cracks and delamination growth, the current understanding of the process is still incomplete. Only a small

sampling of the literature, with the emphasis being placed on analytical methods, will be noted here.

Greszczuk (1982) provides a textbook-type treatment of the fundamentals involved in the analysis of LVI. He has divided the problem into three logical steps: "(1) determination of impactor-induced surface pressure and its distribution," (the contact problem), "(2) determination of internal stresses in the composite target caused by the surface pressure, and (3) determination of failure modes in the target caused by the internal stresses."

Although most LVI events are three dimensional in nature, a great deal can be learned from a two dimensional simplification of the problem (as in the current work). Choi et al. (1991a, 1991b) have conducted an extensive experimental and analytical study of LVI that is truly two dimensional. In this study they have used a line-nosed impactor so as to produce a uniformly distributed transient dynamic load across the specimen width, thereby reducing the complexity of the problem from 3-D to 2-D. Tests were conducted on specimens of several different stacking sequences constructed from T300/976. Different values of mass and impact velocity were used as test parameters. A phenomenon observed to be common to all of the specimen types tested was that damage initiation took the form of what the authors called a critical matrix crack. These critical matrix cracks were located in the 90° plies, near the specimen midplane and were inclined at an angle of about 45°. Delaminations and concomitant secondary matrix cracks were observed to form and propagate after the formation of critical matrix cracks. The authors conducted a two-dimensional transient dynamic finite element analysis in an attempt to model the impact event. They assumed Hertzian contact and used plane strain constitutive relations. They were able to predict the location of damage initiation reasonably well using a matrix failure theory. Once the critical matrix crack had been predicted by the model, a "post-failure" analysis was conducted to predict damage growth. This analysis was executed by setting to zero certain members of the material modulus matrix for elements where the critical matrix crack occurred. Bogdanovich and Larve (1992) have conducted a two-dimensional analysis of the LVI problem. They investigated the impact of a rigid body of revolution on several different laminates; some of which possessed energy absorbing interleaves. The analysis used in this work employs some unique polynomial spline interpolation functions. A maximum stress failure criterion is used to predict failure initiation. Their results dramatically show the benefit that interleaves can provide. Sun and Rechak (1988, 1990) have also conducted a two dimensional analysis of the problem. They also report the presence of matrix cracks inclined at 45°. In addition, they address the optimal location of interleaf layers so as to reduce damage.

While few papers have appeared which attempt to address the three-dimensional problem of LVI, noteworthy are those of Wu and Springer (1988a, 1988b) and of Wu and Chang (1989). In these works a three dimensional transient dynamic finite element analysis is presented for the study of LVI.

Since the present work addresses delamination growth and the interface problem, it is appropriate to include reference to the body of work that has been conducted in this area. Rather than naming several papers, however, we shall refer to a survey recently conducted on the topic by Comninou (1990).

The present paper will examine the conditions conducive to the growth of delaminations in simply supported laminated beams subjected to low velocity impact loads. Of particular

interest is the delamination emanating from the tip of a transverse matrix crack. The impactor geometry and velocity are chosen to enable the simulation of the low velocity impact event as a monotonically increasing load applied under quasi-static loading conditions. The stress state in the individual plies and the damaged interfaces is determined by finite element analysis with the damaged interfaces being modeled by nonlinear interface elements. Delamination propagation is evaluated at each load step. If conditions are sufficient for propagation, the amount of growth is calculated and the corresponding reduction in the interface constitutive properties updated accordingly for the next load step. This procedure is repeated until the maximum impact load is reached.

### Advanced Interface Model

A development of interest in this research is the thermomechanical modeling of the damaged interface. The morphology of crack tips during delamination suggests that such tips can be modeled within the context of continuum mechanics, using a general cohesive model of the Dugdale-Barenblatt type (Dugdale, 1960; Barenblatt, 1962). A thermodynamic analysis of a generalized cohesive zone model has been presented by Gurtin (1979), and recently by Costanzo and Allen (1992). With reference to Fig. 1, a cohesive zone (c.z.) is defined as a portion of the

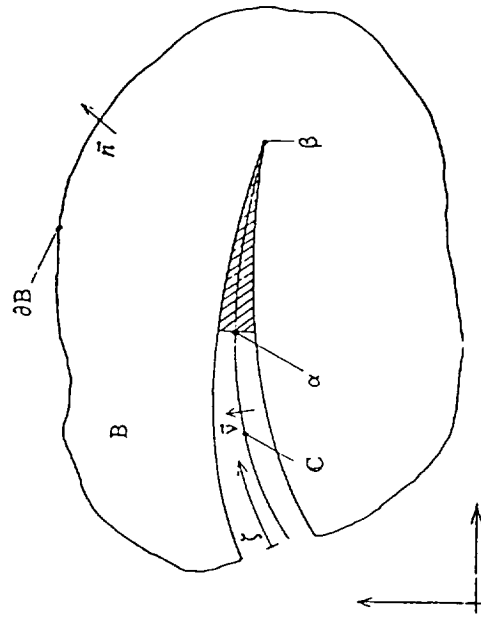


Fig. 1 Crack with a cohesive zone.

crack line such that along  $\sigma(t) \leq \tau \leq \beta(t)$  a system of cohesive forces per unit length  $\sigma_i(\tau, t)$  is acting. The cohesive zone is kinematically characterized by its opening displacement  $\delta_i(\tau, t)$ . We have

$$\delta_i(\zeta, t) = [u_i]; \delta_i(\beta(t), t) = 0 \quad (1)$$

and, by the conservation of linear momentum

$$\sigma_i(\zeta, t) = \sigma_{ji}^+ v_j = \sigma_{ji}^- v_j \quad (2)$$

where the brackets [ ] represent the jump across the crack line,  $v_i$  is the normal to the crack and  $\sigma_{ij}^+$  and  $\sigma_{ij}^-$  are the limits, from above and below respectively, of the stress tensor approaching the crack line.

The results of the thermodynamic analysis of the crack propagation process can be summarized as follows (Costanzo and Allen, 1992):

$$\int_0^R \left( \sigma_i \frac{\partial \delta_i}{\partial \tau} - \frac{\partial \epsilon}{\partial \tau} \right) d\zeta + (G - R) \dot{\alpha} = \int_0^R [q_i] v_i d\zeta \quad (3)$$

where  $G$  is the energy release rate and  $R$  is the resistance to crack propagation,  $\epsilon$  is the cohesive zone internal energy.

Through a global dissipation analysis it can be shown that in the presence of a c.z. we can have crack growth under a self-propagating regime when  $G \geq R$  or under a subcritical crack growth. The latter, under the assumption of quasi-isothermal evolution can be shown to be characterized by the following evolution equation:

$$\dot{\alpha} = \frac{\int_0^R \left( \sigma_i \frac{\partial \delta_i}{\partial \tau} - \frac{\partial \epsilon}{\partial \tau} \right) d\zeta}{(R - G)} \quad (4)$$

Naturally, other evolution equations can be considered. The thermodynamic analysis properly shows the relationship between the cohesive zone constitutive behavior and the crack driving force and the corresponding resistance, thus allowing for the construction of a well posed boundary value problem to study crack evolution. Several types of cohesive zone constitutive equations can be considered depending on the particular material system at hand. Efforts are in preparation to determine the constitutive relationships for polymeric fiber reinforced systems. In the meantime, we are utilizing the cohesive model previously proposed by Needleman (1987).

## Experimental Program

An experimental program has been initiated to identify and document the accumulation of damage caused by the transverse impact of laminated composites. In the current study, the low velocity transverse impact event is simulated by quasi-statically loading specimens in

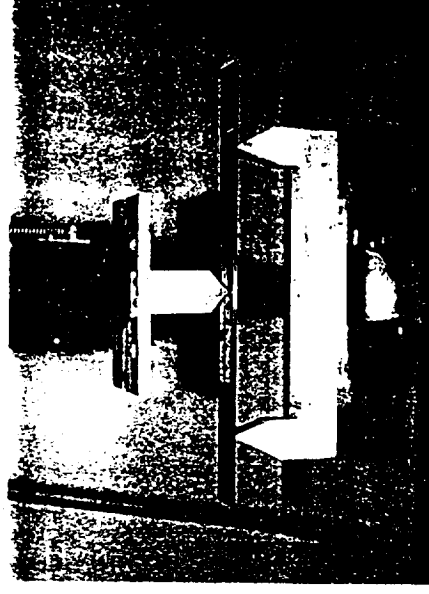


Fig. 2 Three-point bending apparatus.

three-point bending conditions. The three-point bending test apparatus, shown in Fig. 2, is attached to an Instron 1125 load frame. The distance between the supports in this particular fixture is 180mm and the loading pin diameter is 4.7mm. The impact load is simulated by applying a monotonically increasing load at a cross-head speed of 1.3 mm/min until the desired maximum load has been reached. The load is then removed at the same cross-head speed. The specimens are 254mm by 25.4mm in diameter and are machined from hot press cured AS4/976 graphite/epoxy composite panels.

The detection and tracking of damage along the edge of the specimen has been performed via an optical microscope as shown in Fig. 3. This microscope is mounted on a traversing platform that enables it to move along the length of the specimen as well as to follow the vertical displacement of the loading pin. A video camera is attached to the microscope eyepiece so that the damage can be viewed on a video monitor. Permanent records of the damage state have been made by replacing the video camera with a 35mm camera. In a typical test, the edge of the specimen is scanned during load application. The cross-head is stopped upon the detection of

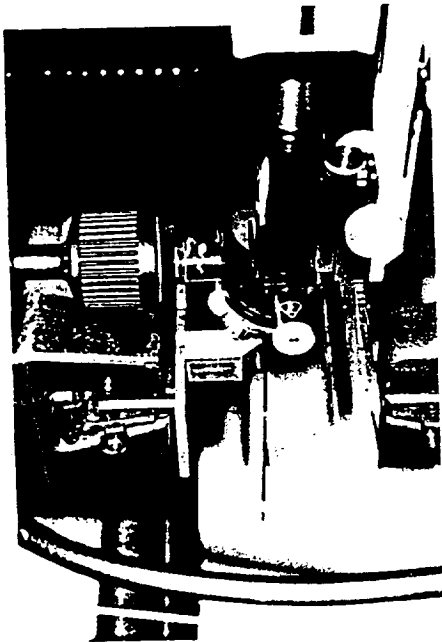


Fig. 3 Optical microscope setup for the detection of damage along the edge of the specimen.

damage and a photographic record made. Fig. 4 shows a matrix crack tip situated at the interface between the 0° and 90° plies of a crossply laminate. This crack was detected near the point of load application. Since subsequent damage will most likely propagate from this site, the scanning is now concentrated in this region. Photographic records are made at regular time intervals or when an appreciable amount of damage has grown. This record of the damage evolution should provide information about factors affecting the initiation and propagation of the various types of damage caused by low velocity impacts. The three-point bend test is halted before the catastrophic failure of the specimen. This permits the radiographic examination of the final impact damage state as well as the determination of the residual strength of the specimen.

#### Analytic Formulation

Due to the nonlinearity introduced by the interface failure criterion, the virtual work equation is solved in incremental form, resulting in:

$$\int_V C_{ijkl}^i \Delta \epsilon_k \Delta \epsilon_l dV = \int_{T_i} T_i^{*kl} \delta \Delta u_k dS - \int_V \sigma_{ij}^i \delta \Delta \epsilon_{ij} dV \quad (5)$$



Fig. 4 View of matrix crack with crack tip located at the interface between the 0° and 90° plies.

where

- $C_{ijkl}$  = material tangent modulus tensor
- $\epsilon_{ij}$  = infinitesimal strain tensor
- $T_i$  = traction vector
- $\Delta u_i$  = displacement increment vector
- $\sigma_{ij}$  = stress tensor

Also, the domain of interest has interior  $V$  and boundary  $\partial V$ , and superscripts  $i$  and  $i + \Delta t$  denote quantities at time  $t$  (which are assumed to be known), and quantities at time  $t + \Delta t$ , respectively. In the current paper the modulus tensor  $C_{ijkl}$  is everywhere constant except in the interface, which is modelled using bar elements.

The approximate nature of equation (1) is due to the fact that higher order terms in  $\Delta u_i$  are neglected in the incrementalization process. However, this approximation is accounted for in a rather standard way by incorporating a Newton-Raphson iteration scheme for each increment of boundary tractions. Thus, the displacement increment is successively updated as follows for the  $j^{\text{th}}$  iteration:



$$(\Delta u)_j = (\Delta u)_{j-1} + (\Delta \Delta u)_j \quad (2)$$

where  $(\Delta \Delta u)_j$  is obtained by solving the following on the  $j^{\text{th}}$  iteration:

$$[K](\Delta \Delta u)_j = \{F^{(j+1)}\} - \{R^{(j+1)}\} \quad (3)$$

where

- $[K]$  = global stiffness matrix
- $\{F\}$  = global force matrix
- $\{R\}$  = global reaction matrix

Equations (2) and (3) are solved recursively until the following convergence criterion is satisfied:

$$\frac{|\Delta u_j| - |\Delta u_{j-1}|}{|\Delta u_j|} \leq r_{\text{tol}} \quad (4)$$

where  $r_{\text{tol}}$  is a user specified convergence tolerance and  $|\cdot|$  signifies the Euclidean norm.

#### Computational Results

The algorithm discussed in the previous section has been implemented into an in-house FORTRAN computer program. The program currently utilizes constant strain triangles except at the interfaces, wherein both shearing and normal bar elements are incorporated at each node. At this time, the response of the interfacial region is modeled by a phenomenological relationship proposed by Needleman. This relationship assumes that the mechanical response is dependent on the displacement differences across the interface. The interfacial tractions for a 2-D case are (Needleman, 1987)

$$T_n = \frac{-27}{4} \sigma_{\text{max}} \left\{ \left( \frac{u_n}{\delta} \right) \left[ 1 - 2 \left( \frac{u_n}{\delta} \right) + \alpha \left( \frac{u_n}{\delta} \right)^2 \right] + \alpha \left( \frac{u_n}{\delta} \right)^2 \left[ \left( \frac{u_n}{\delta} \right) - 1 \right] \right\} \quad (7)$$

$$T_t = \frac{-27}{4} \sigma_{\text{max}} \left\{ \alpha \left( \frac{u_t}{\delta} \right) \left[ 1 - 2 \left( \frac{u_n}{\delta} \right) + \alpha \left( \frac{u_n}{\delta} \right)^2 \right] \right\} \quad (8)$$

where  $T_n$  and  $T_t$  are the normal and tangential interfacial tractions, respectively;  $u_n$  and  $u_t$  are the normal and tangential interfacial displacement differences;  $\sigma_{\text{max}}$  is the maximum normal interfacial stress,  $\delta$  is a characteristic interface length, and  $\alpha$  is the ratio of the shear modulus to the Young's modulus of the interface. These tractions are assumed to be equal to zero when  $u_n$  is greater than  $\delta$  (failure of the interface).

For modeling the resin rich region located in between the plies of a laminate,  $\sigma_{\text{max}}$  was approximated by the transverse lamina strength of the material system.  $\delta$  was assumed to be the thickness of this resin rich region. It is generally several fiber diameters in thickness.  $\alpha$  was determined from the material properties. The parameters for the interfaces thickening matrix cracks were determined in a similar manner. However, it has been found that  $\delta$  for the matrix crack interface should be several orders of magnitude less than the  $\delta$  for the resin rich region. The polynomial form of the constitutive relationship resulted in the tractions obtaining a maximum value before  $u_n$  reaches  $\delta$ . This has caused computational difficulties when the traction decrease with increasing interfacial separation. To lessen the impact of this problem, a stretch factor was incorporated into the program so that the rate of decrease in the tractions is reduced.

The damage evolution in a laminate with nonlinear interfacial response was modeled by the A simply supported 100mm long laminate loaded in three-point bending was modeled by the finite element mesh shown in Fig. 5. This mesh contained 272 constant strain triangular elements and 22 interface elements with a total of 368 degrees of freedom. It was assumed that the damage state will be symmetric along the axis of load application so that only half the laminate was modeled. The laminate consisted of one  $0^\circ$  ply on the top and bottom and four  $90^\circ$  plies in the center with a total laminate thickness of 0.77 mm. Based on elastic analysis and experimental observations, a row of interface elements spanning the height of the  $90^\circ$  ply group was placed at a location six ply thicknesses away from the axis of load application and was oriented at  $45^\circ$  toward this axis. This group of interfacial elements modeled the matrix crack that initiates the delaminations. At the top interface, a group of interfacial elements was located from the end where the load is applied to the tip of the matrix crack. For the bottom interface, a group of interfacial elements was placed from the intersection of the matrix crack and the bottom interface to the simply supported end. Isotropic material properties were assigned to the  $0^\circ$  and  $90^\circ$  plies. For the  $0^\circ$  plies,  $E=156.0$  GPa and  $\nu=0.23$  and for the  $90^\circ$  plies,  $E=9.1$  GPa and  $\nu=0.40$ . A concentrated force of 44.0 N was applied to the laminate in 100 load steps. Each load step increased the load by an equal amount. A limit of 100 iterations per load step was employed in the test cases.

Some of the properties for the interfacial elements were varied to examine its effect on the growth of the delamination along the interface. In the first case, the ratio of the shear stiffness to the Young's modulus,  $\alpha$ , for the delamination interface was varied from 0.10 to 0.30. For the delamination interface  $\sigma_{\text{max}} = 44.8$  MPa and  $\delta = 7.1\text{E-}4$  mm. The properties for the matrix crack interface were kept constant with  $\sigma_{\text{max}} = 20.7$  MPa,  $\delta = 7.1\text{E-}9$  mm, and

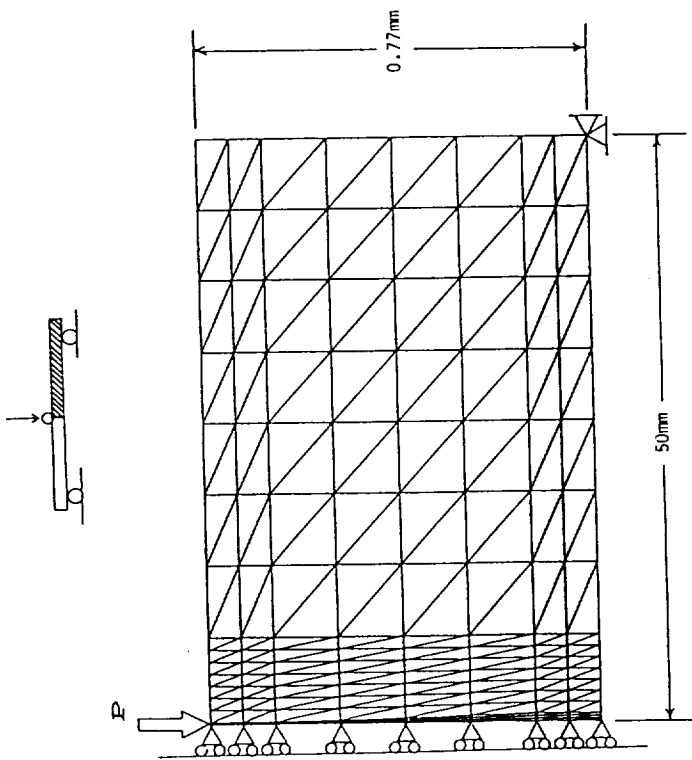


Fig. 5 Finite element model of laminate in three-point bending (thickness has been expanded to show detail.)

$\alpha = 0.10$ . Fig. 6 shows the number of failed delamination interfacial elements during the load steps. In all cases, failed delamination elements were first detected at step number three. Failure of all the matrix crack elements also occurred at this time. The data indicated that higher values of  $\alpha$  resulted in a lower number of failed elements at this step. This indicated that the interface failed in a shear dominated manner. As the load steps progressed, the number of failed elements appeared to approach a common value before an overflow error or nonconvergence flag was encountered. It should be noted, however, that this value did not correspond to the total number of delamination interface elements. Thus, it cannot be stated with certainty that a complete failure of the delamination interface resulted in the computational stoppages. Smaller load steps and a finite element mesh with more elements will have to be employed to clarify this trend as

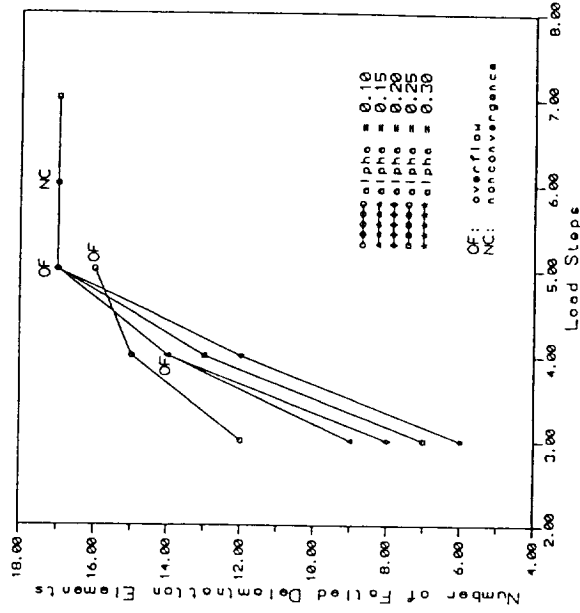


Fig. 6 The effect of the shear to Young's modulus ratio on the delamination damage state.

well as to capture the propagation of the matrix crack into the interface.

The next test case investigated the effect of the work required to fail an interface element on the overall delamination damage evolution. Needleman refers to this work as the work of separation. It is defined as the area under the interfacial traction/displacement curve (Needleman, 1987), and is analogous to the toughness value commonly used in fracture mechanics. From equations (7) and (8), it can be seen that the work of separation can be varied by changing  $\sigma_{max}$ ,  $\delta$ , and  $\alpha$ . In the current examples,  $\alpha$  is kept constant and  $\sigma_{max}$  and  $\delta$  are varied in a manner that maintains initial slope of the interfacial normal traction relationship with respect to the normal displacement. Once again the properties for the matrix crack interface were kept constant. The values employed were identical to those for the previous example. For the delamination interface,  $\alpha = 0.3$  and  $\sigma_{max}$  ranged from 38.0 MPa to 44.8 MPa while  $\delta$  ranged from 6.0E-4 mm to 7.1E-4 mm. The combination of  $\sigma_{max} = 44.8$  MPa and  $\delta = 7.1E-4$  mm with a work of separation of 3.2E-2 Nmm was chosen as the reference value. The other cases were identified by their work of separation normalized with the aforementioned reference value. Fig. 7 shows the amount of delamination damage accumulated during the load steps. The interface with the higher work of separation resulted in a lower number of failures when damage

insensitivity of the damage accumulation to the work of separation, it should be pointed out that in the work of separation the normal component of the interfacial displacement is the dominant term especially when  $\alpha$  is less than one. In the case where the shearing effects are the dominant factor, the assumed form of the interfacial constitutive relationship may not be adequate. A more sophisticated failure criteria, such as the strain energy rate criteria employed in the advanced interface model, may be able to capture the different modes of failure and thus aid in the examination of the sensitivity to the work of separation.

### Conclusion

The current paper reviews research underway by the authors to model the response of thick laminates to impact. Although we have as yet considered only  $[0,90_x,0]$  laminates under quasi-static conditions, the algorithm is being developed for the more general cases envisioned in the paper title.

Current results seem to indicate that the delamination propagates from the matrix crack tip, and this delamination growth is shear dominated. However, further research is warranted before substantive conclusions can be made. In particular, the interface model is being refined to better reflect the nature of the ply interfaces. The incorporation of this effect should produce further insight about the nature of damage evolution in graphite/epoxy laminates.

### Acknowledgement

The authors are grateful to NASA Langley Research Center for the support provided for this research under NASA Contract No. NAG 1-1120.

### References

- Barenblatt, G.I., 1962, "The Mathematical Theory of Equilibrium Cracks in Brittle Fracture," 1962, Advances in Applied Mechanics, Vol. 7, pp. 55-129.
- Bogdanovich, A.E., and Larve, E.V., 1992, "Numerical Analysis of Impact Deformation and Failure in Composite Plates," Journal of Composite Materials, Vol. 26, pp. 520-545.
- Choi, H.Y., Downs, R.J., and Chang, F.K., 1991a, "A New Approach toward Understanding Damage Mechanisms and Mechanics of Laminated Composites Due to Low Velocity Impact: Part I - Experiments," Journal of Composite Materials, Vol. 25, pp. 992-1011.
- Choi, H.Y., Wu, H.T., and Chang, F.K., 1991b, "A New Approach toward Understanding Damage Mechanisms and Mechanics of Laminated Composites Due to Low Velocity Impact: Part II - Analysis," Journal of Composite Materials, Vol. 25, pp. 1012-1038.

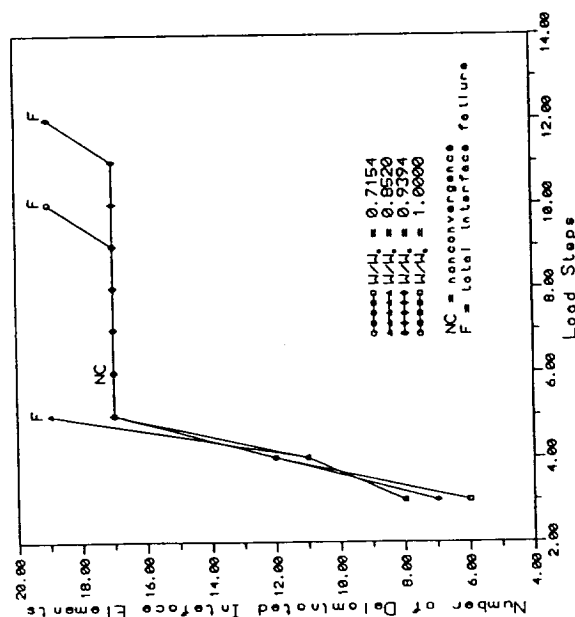


Fig. 7 The effect of the work of separation,  $W$ , on the delamination damage state ( $W_0 = 0.0318 \text{ Nmm}$ ).

was first detected. However, once damage occurred all four cases failed at a similar rate, which shows a relative insensitivity to the work of separation. With the exception of one case, the propagation of the delamination was halted at the same number of failed elements momentarily before complete failure of the interface occurred or a nonconvergence flag encountered. The case that did not follow this trend had a normalized work of separation of 0.85 and this was in between the extremes of the test cases. To check if this was due to a computational error, other cases with normalized work of separation close to 0.85 were examined and similar responses were obtained. Since there are interactions between the top and bottom interface, a normalized work of separation close to 0.85 may have caused damage states at the top and bottom interfaces to behave in a less stable manner. Further investigation is required. Returning now to the

- Comninou, M., 1990, "An Overview of Interface Cracks," *Engineering Fracture Mechanics*, Vol. 37, pp. 197-208.
- Costanzo, F., and Allen, D.H., 1992, "A Continuum Mechanics Approach to Some Problems In Subcritical Crack Propagation," submitted to the *International Journal of Fracture*, (also CMC Report No. 92-19, October 1992).
- Dugdale, D.S., 1960, "Yielding of Steel Sheets Containing Slits," *Journal of the Mechanics and Physics of Solids*, Vol. 8, pp. 100-104.
- Grzeszczuk, L.B., 1982, "Damage in Composite Materials Due to Low Velocity Impact," *Impact Dynamics*, John Wiley & Sons, New York, Chap. 3.
- Gurtin, M.E., 1979, "Thermodynamics and The Cohesive Zone in Fracture," *Zeitschrift für Angewandte Mathematik und Physik (ZAMP)*, Vol. 30, pp. 991-1003.
- Needleman, A., 1987, "A Continuum Model for Void Nucleation by Inclusion Debonding," *Journal of Applied Mechanics*, Vol. 54, pp. 525-531.
- Rechak, S., and Sun C.T., 1990, "Optimal Use of Adhesive Layers in Reducing Impact Damage in Composite Laminates," *Journal of Reinforced Plastics and Composites*, Vol. 9, pp. 569-582.
- Sun, C.T., and Rechak, S., 1988, "Effect of Adhesive Layers on Impact Damage in Composite Laminates," *Composite Materials Testing and Design (ASTM STP 972)*, pp. 97-123.
- Wu, H.T., and Chang, F.K., 1989, "Transient Dynamic Analysis of Laminated Composite Plates Subjected to Transverse Impact," *Computers and Structures*, Vol. 31, pp. 453-466.
- Wu, H.T., and Springer, G.S., 1988a, "Measurements of Matrix Cracking and Delamination Caused by Impact on Composite Plates," *Journal of Composite Materials*, Vol. 22, pp. 518-532.
- Wu, H.T., and Springer, G.S., 1988b, "Impact Induced Stresses, Strains, and Delaminations in Composite Plates," *Journal of Composite Materials*, Vol. 22, pp. 533-560.

# **DAMAGE MECHANICS IN COMPOSITES 1994**

**presented at**  
1994 International Mechanical Engineering Congress and Exposition  
Chicago, Illinois  
November 6–11, 1994

**sponsored by**  
The Applied Mechanics Division, ASME

**edited by**  
David H. Allen  
Texas A&M University

J. W. Ju  
University of California

THE AMERICAN SOCIETY OF MECHANICAL ENGINEERS  
UNITED ENGINEERING CENTER / 345 EAST 47TH STREET / NEW YORK, NEW YORK 10017

## **MODELING THE DAMAGE EVOLUTION IN LAMINATED COMPOSITES WITH DELAMINATIONS CONTAINING A DAMAGE ZONE**

**D. C. Lo and David H. Allen**  
Center for Mechanics of Composites  
Texas A&M University  
College Station, Texas

### **ABSTRACT**

Close examination of the delaminated surfaces of laminated polymeric composites will often reveal the presence of a damage zone ahead of the advancing delamination. In thermosetting polymeric matrices, the damage zone will most likely contain micro-shear cracks. Their presence can introduce nonlinearities to the response of the interface and thus affect the growth of the delamination. The evolution of delaminations containing this type of damage zone is examined. The formation of the damage zone is modeled via a non-linear interfacial constitutive relationship that is based on a micro-mechanics solution for distributed non-interacting cracks. The mechanical characteristics of the interface constitutive relationship are examined. In addition, the delamination behavior of a laminate possessing this type of interfacial response and subjected to simulated low velocity impact condition is investigated.

### **INTRODUCTION**

Laminated polymeric composites are prone to the formation of delaminations when subjected to low velocity impact loads. In addition to reducing the mechanical properties of the laminate, these delaminations can serve as initiators of other damage modes and can cause the failure of the laminate. Thus, the ability to model the low velocity impact damage process is crucial for the safe and efficient design of laminated composite structures.

It has been found from micrographic and fractographic examinations of delaminations that a damage zone develops ahead of the delamination front [1-9]. The mechanisms in this damage zone are dependent on the molecular structure of the resin rich interface. Micro-shear cracks are found in thermosetting resins and crazes are prevalent in thermoplastics. In general, the tendency to develop crazes or micro-shear cracks is dependent on the distance between chain entanglements or crosslinks in the molecule [10]. When

the molecular weight between side attachments is below a critical number, the crazing mechanism is suppressed and micro-cracking is activated. The presence of this process zone in the interface introduces nonlinearities to the interfacial response and thus affects the propagation of the delamination in the interface. Therefore, it should be included in the low velocity impact damage analysis. However, the interface region containing a process zone is not modeled in most low velocity impact damage analyses and of those analyses that do take this resin rich region into account most are for modeling linear elastic interleaves [11-13]. Some exceptions include Ladeveze's damage model in which the interface is explicitly modeled [14]. In his model, the mechanical properties of the interface are governed by internal damage variables. Since the internal state variables are volume averaged representations of the damage state, the stresses and strains obtained from this analysis are also averaged quantities. Lo et al. [15] accounted for the effects of the process zone by employing the interfacial constitutive relationships developed by Needleman [16] and Tvergaard [17]. These constitutive models assumed that the force normal to the interface behaves in a manner similar to the interatomic forces generated during the interatomic separation. While the aforementioned models introduce nonlinear response to the mechanical behavior of the interface, these models do not distinguish between the different mechanisms active in the process zone. The current paper will focus on the development of delaminations in thermosetting matrix composites and thus damage zones containing micro-shear cracks will be considered. An interface constitutive relationship adapted from a micro-mechanical solution for a micro-cracked solid will be employed in the analysis.

## INTERFACE MODELING

When the delaminated interfaces are examined optically under magnification, the presence of the micro-shear cracks is revealed by surface artifacts that appear as regularly stacked arrays of platelets. Their appearance is very much reminiscent of rows of dominoes that have been tipped over. This surface feature, commonly referred to as "hackles", is formed by microcracking perpendicular to the plane of principal stress in the resin rich interface [4]. Morris [9] has suggested that the hackles are formed in a peeling manner while Purslow [7] has proposed the coalescent of the micro shear cracks as the cause of the hackles as shown in Figure 1. Experimental evidence indicates that the spacing of the platelets appears to be related to the opening mode of the delaminated interface [18]. Under mode I opening condition, the hackle pattern may not be present, but as the contribution from mode II opening is increased, the spacing between the platelets becomes smaller. Therefore, it can be assumed that the micro-shear crack spacing also decreases with increasing mode II loading contribution. These experimental observations now serve as a guide in our development of an interface constitutive relationship.

In the current study, the response of the interface is assumed to behave isotropically when no micro-cracks are present. As the load is increased and the micro-cracks accumulate, the mechanical properties of the interface are degraded in accordance with the orientation and distribution of the microcracks. This then causes the mechanical response to behave orthotropically. For the case of non-interacting cracks with an arbitrary crack orientation distribution, the effective moduli for this type of material have been calculated by Kachanov. This method is based on the superposition of the solution for the averaged crack surface displacement of a single isolated crack subjected to remotely applied stresses. Since the mutual positions of the cracks do not enter into the analysis under the non-interaction assumption, the overall effect of the crack array is simply the sum of the contribution from each isolated crack. While the non-interaction assumption may not be suitable for some crack distributions, it does simplify the calculations and yields an approximation of the mechanical response for those distributions. The elastic

potential of the cracked body in a state of plane stress was expressed by Kachanov [19] as

$$f(\sigma, \alpha) = \frac{1 + \nu_o}{2E_o} \sigma_{ij} \sigma_{ij} - \frac{\nu_o}{2E_o} (\sigma_{kk})^2 + \frac{\pi}{E_o} \sigma_{ij} \sigma_{jk} \alpha_{ik} \quad (1)$$

where  $\nu$  is the Poisson ratio,  $E$  is the Young's modulus (The subscript "o" denotes the undamage isotropic properties and for a state of plane strain,  $E_o$  is replaced with  $\frac{E_o}{1-\nu_o}$  and  $\nu_o$  with  $\frac{\nu_o}{1-\nu_o}$ ),  $\sigma_{ij}$  are components of the stress tensor, and  $\alpha_{ik}$  is the crack density tensor, defined by

$$\alpha_{ik} = \frac{1}{A} \sum_{m=1}^M (l_m^2 n_{m_i} n_{m_k}) \quad (2)$$

where the summation is performed over the  $M$  number of cracks found in the representative area,  $A$ .  $l_m$  and  $n_m$ , are the length and components of the crack surface normal of the  $m^{th}$  crack, respectively. The compliance tensor,  $S_{ijkl}$ , of the cracked solid is obtained from

$$S_{ijkl} = \frac{\partial^2 f}{\partial \sigma_{ij} \partial \sigma_{kl}} \quad (3)$$

Since the crack density tensor is a real symmetric tensor, it can be expressed in terms of its principal values as follows:

$$\alpha_{ij} = \rho_1 e_{1i} e_{1j} + \rho_2 e_{2i} e_{2j} \quad (4)$$

where  $\rho_1$  and  $\rho_2$  are the principal values and  $e_1$  and  $e_2$  are the principal vectors. This is a convenient reference frame to work in as the material orthotropy axes are coincident with the principal axes of the damage density tensor. If all the cracks in the representative area are oriented normal to the  $e_2$  axis,  $\rho_1$  is equal to zero and the effective moduli have been found by Kachanov to be

$$E_1 = E_o \quad (5)$$

$$E_2 = \frac{E_o}{1 + 2\pi\rho_2} \quad (6)$$

$$\nu_{12} = \nu_o \quad (7)$$

$$\nu_{21} = \frac{\nu_o}{1 + 2\pi\rho_2} \quad (8)$$

$$G_{12} = \frac{G_o}{1 + \left(2\pi \frac{G_o}{E_o}\right) \rho_2} \quad (9)$$

where  $G_o$  is the undamage shear modulus. Note that these effective moduli are referenced to the principal crack density axes. To obtain the effective properties referenced to another set of coordinate axes, the stiffness tensor is first constructed using the quantities shown in Equations (5-9) and then transformed to the new coordinate axes.

The crack damage tensor as defined by Equation (2) requires the knowledge of the number of cracks in the representative area, the individual crack length and their spatial orientation. Since there could be many micro-cracks embedded in the resin rich interface, simplifying assumptions are taken to maintain tractability of the problem. Based on experimental observations that the micro-cracks form perpendicular to the plane of principal stress, the initial orientation can be determined from the stress state just prior to initiation. Although as the micro-crack grows, the stress state will change and cause



the micro-cracks to diverge from their initial orientation, it will be assumed that the micro-crack orientation remains constant. Furthermore, subsequent micro-cracks in the representative area will share the same orientation. Each micro-crack is assumed to grow instantaneously to a final crack length,  $l$ , as dictated by an interfacial thickness parameter,  $t_{int}$ , as given by

$$l = \beta t_{int} \quad (10)$$

where  $\beta$  is the micro-crack length scaling factor. The accumulation of the micro-cracks is related to the maximum interfacial separation experienced by the representative area during the loading history in the following manner

$$\eta = \lambda \text{Max} \left( \frac{u_t}{t_{int}} \right) \quad (11)$$

where  $\eta$  is the number of micro-cracks in the representative area,  $u_t$  is the tangential interfacial separation, and  $\lambda$  is the micro-crack accumulation parameter. Thus, when the interface is only opening in mode I, there will not be any accumulation of micro-cracks and as the mode II separation is introduced, the micro-cracks evolve accordingly. Finally, the failure of the interface is defined to occur when

$$\frac{u_n}{t_{int}} + \sqrt{\left( \frac{u_n}{t_{int}} \right)^2 + \left( \frac{u_t}{t_{int}} \right)^2} \geq \delta_{crit} \quad (12)$$

where  $u_n$  is the normal component of the interfacial separation and  $\delta_{crit}$  is a critical strain-like constant. The above description is similar to the phenomenological models previously proposed by Needleman [16] and Tvergaard [17].

## PROBLEM APPROACH

This interfacial constitutive model is incorporated into an in-house finite element code to facilitate the analysis. The damage zone is modeled in a manner similar to the Dugdale-Barenblatt cohesive model [20, 21]. In this code, the delamination propagates along the prescribed inter-element boundaries on which the tractions are specified by the interfacial constitutive relationship. Due to the nonlinearity introduced by the micro-cracked process zone, the virtual work equation is solved in incremental form, resulting in [22]:

$$\int_V C_{ijkl}^T \Delta \epsilon_{kl} \delta \Delta \epsilon_{ij} dV \cong \int_{\partial V} T_i^{\tau+\Delta\tau} \delta \Delta u_i dS - \int_V \sigma_{ij}^T \delta \Delta \epsilon_{ij} dV \quad (13)$$

where  $C_{ijkl}$  is the material tangent modulus tensor,  $\epsilon_{ij}$  is the infinitesimal strain tensor,  $T_i$  is the traction vector,  $\Delta u_i$  is the displacement increment vector, and  $\sigma_{ij}$  is the stress tensor. Also, the domain of interest has interior  $V$  and boundary  $\partial V$ . The superscript  $\tau$  and  $\tau + \Delta\tau$  denote quantities at time  $\tau$  (which are assumed to be known) and quantities at time  $\tau + \Delta\tau$ , respectively. In order to focus on the effects of the interface model, the modulus tensor,  $C_{ijkl}$ , is everywhere constant and linear elastic except at the interface. The approximate nature of Equation (13) is due to the deletion of the higher order terms in  $\Delta u_i$  during the incrementalization process. To account for this approximation, a Newton-Raphson iteration scheme is employed for each increment of boundary tractions. The displacement increment is thus successively updated as follows for the  $j^{th}$  iteration:

$$\{\Delta u\}_j = \{\Delta u\}_{j-1} + \{\Delta \Delta u\}_j \quad (14)$$

where  $\{\Delta\Delta u\}_j$  is obtained by solving the following on the  $j^{th}$  iteration:

$$[K]^T \{\Delta\Delta u\}_j = \{F^{r+\Delta r}\} - \{R^{r+\Delta r}\}_{j-1} \quad (15)$$

where  $[K]$  is the global stiffness matrix,  $\{F\}$  is the global force matrix, and  $\{R\}$  is the global reaction matrix.

Equations (14) and (15) are solved recursively until the following convergence criterion is satisfied:

$$\frac{\|\Delta u\|_j - \|\Delta u\|_{j-1}}{\|\Delta u\|_j} \leq r_{tol} \quad (16)$$

where  $r_{tol}$  is a user specified convergence tolerance and the quantities bracketed by the double vertical bars are the Euclidean norms.

## COMPUTATIONAL RESULTS

It was mentioned previously that the response of the interface is dependent on the number of micro-cracks, the individual crack lengths, and the spatial orientation of the micro-cracks. How these factors affect the mechanical response will be examined in this section. This is followed by an analysis of a laminate possessing this type of response at the interfaces.

In this section, all the micro-cracks are assumed to be oriented at  $45^\circ$  unless otherwise specified and the undamaged mechanical properties shown in Table 1 are used in the calculations. The first factor to be examined is the crack density. Since the number of micro-cracks, as shown in Equation (11), is related to the maximum shearing interfacial displacement via the parameter  $\lambda$ , this parameter serves as a convenient representation of the crack density when comparing the effective properties at a given interfacial displacement. Figures 2 and 3 show the effective values for two components of the stiffness tensor.  $C_{nn}$  represents the component normal to the plane of the interface and  $G_{nt}$ , the shearing component. For  $\lambda = 0.0$ , no micro-cracks are accumulated and thus the linear elastic response is obtained. At other values of  $\lambda$ , it is observed that the majority of the stiffness reduction occurs during the early part of the damage accumulation. The stiffness normal to the interface shows the greater percentage change of the two components to the accumulation micro-cracks. In both cases, the effective properties appear to approach "saturated" values as the micro-crack density increases. This is in accordance with the expressions for the effective moduli shown in Equations (5-9), but these "saturated" properties may not be reached in the analysis or in the actual material as the interface may suffer catastrophic failure at a lower crack density.

The effects of the micro-crack length on the normal and shearing components of the stiffness tensor are shown in Figures 4 and 5. In this set of data, the micro-crack lengths are normalized by the interfacial thickness parameter,  $t_{int}$ , to yield the scaling factor,  $\beta$ . The most distinct feature of this set of results is the manner in which the mechanical properties are reduced. For the shorter normalized lengths, the decrease in the effective stiffnesses is more gradual than for the longer micro-crack lengths. The results for  $\beta = 0.2$  appear to decrease linearly as compared to the results for the other micro-crack lengths. While the trends observed for the various micro-crack lengths are similar to those observed for the various crack densities, the effects of changing the micro-crack length are more pronounced as the crack density tensor defined in Equation (2) is dependent on the micro-crack length to the second power and the number of micro-cracks only to the first power.

The last parameter to be examined is the orientation of the micro-cracks. As shown in Figure 6, the normal stiffness component,  $C_{nn}$ , decreases with an increasing number

of micro-cracks. The majority of the decrease occurs at the early stages of damage accumulation with the smaller angles showing the most decrease in stiffness. For a given number of micro-cracks, the change in the effective stiffness for a change in the orientation angle is greatest in the vicinity of  $45^\circ$ . When the orientations are near  $0^\circ$  or  $90^\circ$ , variation in the orientation angles has only a relatively minor effect on the effective stiffness. On the other hand, the shearing stiffness exhibits the opposite trend, as shown in Figure 7. The effective shearing stiffnesses for angles between  $30^\circ$  and  $60^\circ$  are almost identical for a given number of micro-cracks. Furthermore, the effective shear stiffness response is identical for angle pairs that are oriented the same number of degrees above and below  $45^\circ$  (eg.  $15^\circ$  and  $75^\circ$ .) Finally, the results indicate that the effective shear stiffness curves intersect at a common point for a non-zero number of micro-cracks. The order of relative stiffnesses at a given damage state reverses at this point.

The results presented in this parametric study reflects the mathematical characteristics of the interfacial constitutive model. This should be correlated with experimental measurements to determine the range of response in which the model assumptions are valid. Consideration must be taken when evaluating the assumptions to the possibility that the interface may have failed before reaching some of these responses. In addition, experimental measurements of the energy required to separate the interface will assist in the selection of the model parameters.

Now that the characteristics of the interfacial constitutive model have been examined, some of its effects on a laminated composite is examined. Because of the interest in the development of low velocity impact induced delaminations, the analysis will be set up to approximate the low velocity impact damage event. At the present time, the analysis is model as a two dimensional end-clamped center-loaded bending problem. The impact induced mid-span displacement is simulated by monotonically increasing displacement applied under quasi-static conditions. The stresses in the individual layers and the resin rich interface are obtained from the finite element analysis. Delamination propagation is evaluated at each displacement increment and if the conditions are sufficient for propagation, the amount of growth is calculated and the corresponding changes in the interfacial properties are updated for the next displacement increment. This procedure is repeated until the maximum mid-span displacement is reached.

The end-clamped center loaded bending configuration shown in Figure 8 is utilized for the analysis. This laminate has a  $[0_4/90_4]$  stacking sequence and possess the ply level mechanical properties shown in Table 2. The interfacial parameters are listed in Table 3. Due to the low transverse strength of the lamina, a transverse matrix crack will often appear in the mid-span of the  $90^\circ$  layer upon the application of the displacement. This transverse matrix crack then serves as the initiation point for the delamination at the  $0^\circ/90^\circ$  interface. In order to focus on the evolution of this delamination, the transverse matrix crack is assumed to exist prior to the application of the mid-span displacement. Since the damage state is assumed to be symmetric about the mid-span, only the right half of the span has been modeled by the finite element analysis.

Figure 9 shows the evolution of the delamination with respect to the mid-span displacement for several values of the micro-crack accumulation parameter,  $\lambda$ . The results indicate that the case with the largest value of the  $\lambda$  ( $\lambda = 1.0E5$ ) has the highest rate of delamination growth while the lower values of  $\lambda$  ( $\lambda = 1.0E2, 1.0E1, 1.0$ ) have the slowest rates of delamination growth. There are only minor differences in the delamination evolution predicted by the lower values of  $\lambda$ . Since these values translate to a smaller number of micro-cracks, the delamination response may be close to that of a laminate with a linear elastic interface. Common to all the cases considered is the increase in the rate of delamination growth when the delamination reaches a normalized length of 0.1. As shown in Figure 10, this increase corresponds to a change in the mode of interfacial separation. The delamination starts out opening in a mode II dominant manner, then

changes to mode I dominance when the "critical" delamination length is reached. The switch to mode I dominance would indicate a reduction in the influence of the micro-crack damage zone as the delamination propagates. This is because the accumulation of the micro-cracks, in this model, is dependent only on the tangential component of the interfacial displacement. However, by changing the laminate stacking sequence it is possible to give the damage zone an increasing influence as the delamination grows.

The reaction force at the point of mid-span displacement application is shown in Figure 11. This result corresponds to  $\lambda = 1.0E5$ . As the mid-span displacement is increased and the delamination grows, the transverse stiffness of the laminate decreases. While the response appears to be relatively smooth, close up examination of the force-displacement response indicates instabilities in the form of sudden drops in the reaction force when the delamination grows. Figure 12 shows the drop in the reaction force caused by the delamination initiation. After this drop, the reaction force increases with increasing mid-span displacement. The next drop occurs when sufficient micro-cracks have accumulated in the damage zone for the delamination to advance. From Figure 11, it can be surmised that the transverse stiffness after the sudden force drop is less than the stiffness prior to the delamination propagation. Similar behavior has been observed experimentally by Jackson and Poe for quasi-isotropic laminates [23]. They noted that the ability to predict the damage dependent reaction force is important in the use of the impact force as a scaling parameter for the impact response of laminates.

## CONCLUDING REMARKS

The formation of a damage zone containing micro-shear cracks and located ahead of a delamination crack is accounted for in this analysis of delamination evolution in polymeric laminated composites. A sample of the results is presented in this paper. In the development of the interfacial constitutive relationship, consideration is given to the geometric characteristics of the micro-cracks. Since this interfacial relationship is based on a micro-mechanics solution that assumes the non-interaction of the micro-cracks, experimental verification must be performed to determine the range of responses in which this assumption is valid for the current application. The process in which the micro-cracks lead to the failure of the interface also requires further examination. Two possible sequences are mentioned in this paper. Both seem plausible and their occurrence is most likely dictated by the loading condition. The interfacial failure criterion should be updated to reflect this. These issues will be the subject of future investigations.

## ACKNOWLEDGMENT

The authors are grateful for the support provided by NASA Contract No. 32531-40960 to Texas A&M University.

## REFERENCES

- [1] Gilbert, D.G., Beaumont, P.W.R., and Nixon, W.C.; "Direct Observations of the Micromechanisms of Fracture in Polymeric Solids Using the Scanning Electron Microscope," *Mechanical Behaviors of Materials-IV, ICM4*, Vol. 2, pp. 705-710, 1983.
- [2] Purslow, D.; "Matrix Fractography of Fibre-Reinforced Thermoplastics, Part 1. Peel Failures," *Composites*, Vol. 18, No. 5, pp. 365-374, November, 1987.
- [3] Purslow, D.; "Matrix Fractography of Fibre-Reinforced Thermoplastics, Part 2. Shear Failures," *Composites*, Vol. 19, No. 2, pp. 115-126, March, 1988.

- [4] Bascom, W.D. and Gweon, S.Y.; "Fractography and Failure Mechanisms of Carbon Fiber-Reinforced Composite Materials," *Fractography and Failure Mechanisms of Polymers and Composites*, A.C. Roulin-Moloney, ed., Elsevier Science Publishing Co., New York, N.Y., pp. 351-385, 1989.
- [5] Henaff-Gardin, C. and Lafarie-Frenot, M.C.; "Fatigue Behavior of Thermoset and Thermoplastic Cross-Ply Laminates," *Composites*, Vol.23, No.2, pp.109-116, March, 1992.
- [6] Chakachery, E.A. and Bradley, W.L.; "A Comparison of the Crack Tip Damage Zone for Fracture of Hexcel F185 Neat Resin and T6T145/F185 Composite," *Polymer Engineering and Science*, Vol. 27, No. 1, pp. 33-40, Mid-January, 1987.
- [7] Purslow, D.; "Matrix Fractography of Fibre-Reinforced Epoxy Composites," *Composites*, Vol. 17, No. 4, pp. 289-303, October, 1986.
- [8] Shikhmanter, L., Cina, B., and Eldror, I.; "Fractography of Multidirectional CFRP Composites Tested Staticaly," *Composites*, Vol. 22, No. 6, pp. 437-444, November, 1991.
- [9] Morris, G.E.; "Determining Fracture Directions and Fracture Origins on Failed Graphite/Epoxy Surfaces," *Nondestructive Evaluation and Flaw Criticality for Composite Materials*, ASTM STP 696, R.B.Pipes, Ed., American Society for Testing and Materials, pp. 274-297, 1979.
- [10] Donald, A.M. and Kramer, E.J.; "Effect of Molecular Entanglements on Craze Microstructure in Glassy Polymers," *Journal of Polymer Science: Polymer Physics Edition*, Vol.20, pp. 899-909, 1982.
- [11] Bogdanovich, A.E., Iarve, E.V., and Joshi, S.P.; "Impact Deformation and Failure Analysis of Laminated Composite Plates," *Impact and Buckling of Structures*, ASME AMD-Vol. 114, pp. 1-5, 1990.
- [12] Bogdanovich, A.E., and Iarve, E.V.; "Numerical Analysis of Impact Deformation and Failure in Composite Plates," *Journal of Composite Materials*, Vol. 26, pp. 520-545, 1992.
- [13] Sun, C.T., and Rechak, S.; "Effect of Adhesive Layers on Impact Damage in Composite Laminates," *Composite Materials Testing and Design (Eighth Conference)*, ASTM STP 972, J.D.Whitcomb, Ed., American Society for Testing and Materials, pp. 97-123, 1988.
- [14] Ladeveze, P.; "A Damage Computational Method for Composite Structures," *Computers & Structures*, Vol. 44, No. 1/2, pp. 79-87, 1992.
- [15] Lo, D.C. and Allen, D.H.; "Modeling of Delamination Damage Evolution in Laminated Composites Subjected to Low Velocity Impact," submitted to the *International Journal of Damage Mechanics*.
- [16] Needleman, A.; "A Continuum Model for Void Nucleation by Inclusion Debonding," *Journal of Applied Mechanics*, Vol. 54, pp.525-531, 1987.
- [17] Tvergaard, V.; "Effects of Fibre Debonding in a Whisker-Reinforced Metal," *Materials Science & Engineering A: Structural Materials: Properties, Microstructure, and Processing*, Vol. A125, No.2, pp. 203-213, June 1 1990.
- [18] Reeder, J.R.; "An Evaluation of Mixed-Mode Delamination Failure Criteria," *NASA Technical Memorandum 104210*, National Aeronautics and Space Administration, Washington, D.C., February 1992.
- [19] Kachanov, M.; "Effective Elastic Properties of Cracked Solids: Critical Review of Some Basic Concepts," *Applied Mechanics Review*, Vol.45, No. 8, pp. 304-335, August 1992.

- [20] Dugdale, D.S.; "Yielding of Steel Sheets Containing Slits," *Journal of the Mechanics and Physics of Solids*, Vol. 8, pp. 100-104, 1960.
- [21] Barenblatt, G.I.; "The Mathematical Theory of Equilibrium Cracks in Brittle Fracture," *Advances in Applied Mechanics*, Vol. 7, pp.55-129, 1962.
- [22] Jones, R.; "Micromechanical Analysis of Inelastic Composite Behavior Including the Effects of Matrix Viscoplasticity and Evolving Damage," *Texas A&M University Master's Thesis*, 1992.
- [23] Jackson, W.C., and Poe, C.C. Jr.; "The Use of Impact Force as a Scale Parameter for the Impact Response of Composite Laminates," *Journal of Composites Technology & Research*, Vol. 15, No. 4, pp. 282-289, Winter 1993.

Table 1. Undamaged Isotropic Interfacial Constitutive Properties

$E_o$	1.4 <i>Msi</i> ( 9.65 <i>GPa</i> )
$\nu_o$	0.3
$G_o$	0.5 <i>Msi</i> ( 3.45 <i>GPa</i> )

Table 2. Ply Level Mechanical Properties for Laminates Tested

$E_x$	17.4 <i>Msi</i> (120.0 <i>GPa</i> )
$E_y$	1.4 <i>Msi</i> (9.8 <i>GPa</i> )
$E_z$	1.4 <i>Msi</i> (9.8 <i>GPa</i> )
$G_{xy}$	0.8 <i>Msi</i> (5.2 <i>GPa</i> )
$G_{yz}$	0.5 <i>Msi</i> (3.5 <i>GPa</i> )
$\nu_{xy}$	0.3
$\nu_{yz}$	0.3

Table 3. Interfacial Model Parameters for End-Clamped Center-Loaded Bending Test Case

$E_o$	1.4 <i>Msi</i> ( 9.65 <i>GPa</i> )
$\nu_o$	0.3
$G_o$	0.5 <i>Msi</i> ( 3.45 <i>GPa</i> )
$\delta_{crit}$	0.0058 <i>in.</i> ( 0.15 <i>mm</i> )
$\lambda$	100000.0
$t_{int}$	0.0002 <i>in.</i> ( 0.01 <i>mm</i> )
$\beta$	1.0

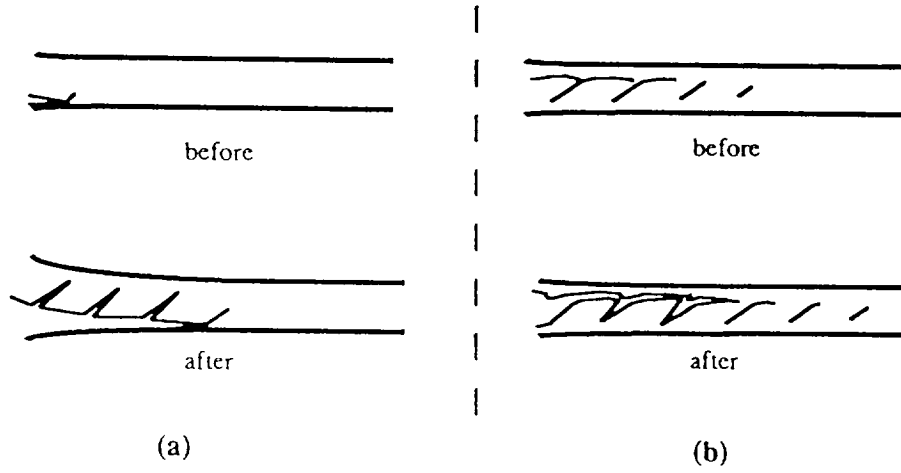


Figure 1. Possible modes of hackle formation: a) peeling [9] and b) micro-crack coalescent [7].

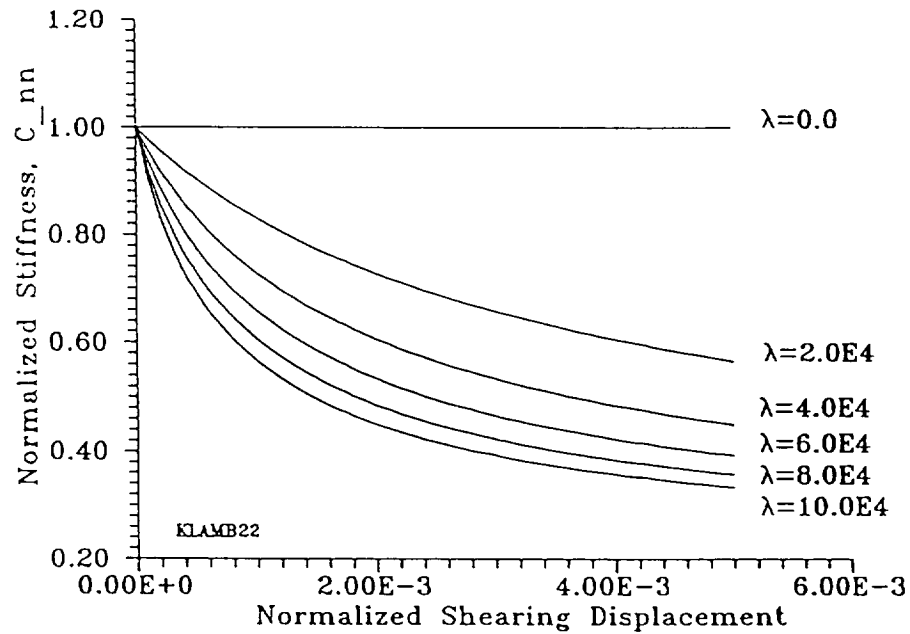


Figure 2. The effect of the micro-crack accumulation parameter,  $\lambda$ , on the normal stiffness component,  $C_{nn}$ .



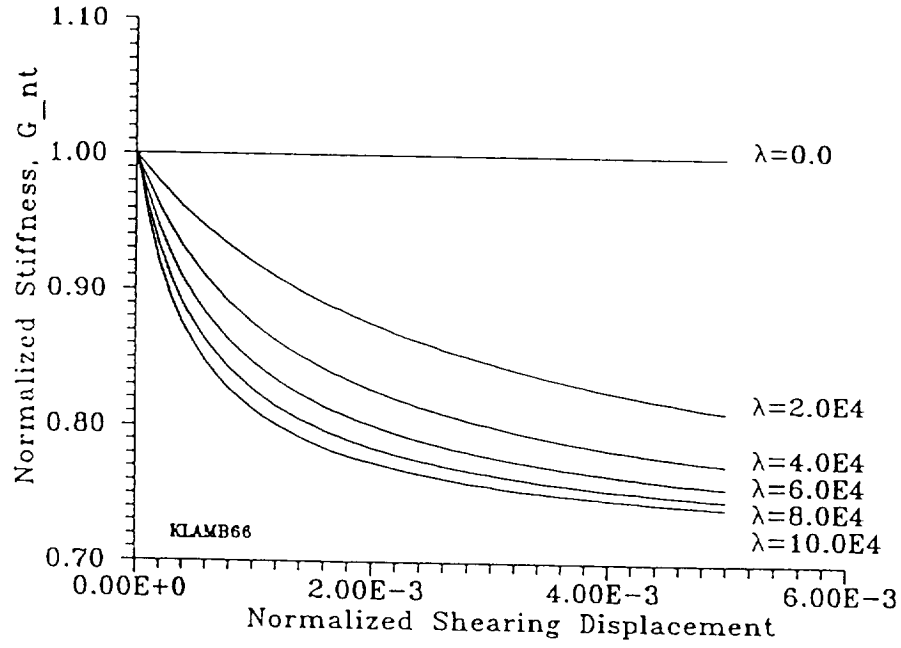


Figure 3. The effect of the micro-crack accumulation parameter,  $\lambda$ , on the shearing stiffness component,  $G_{nt}$ .

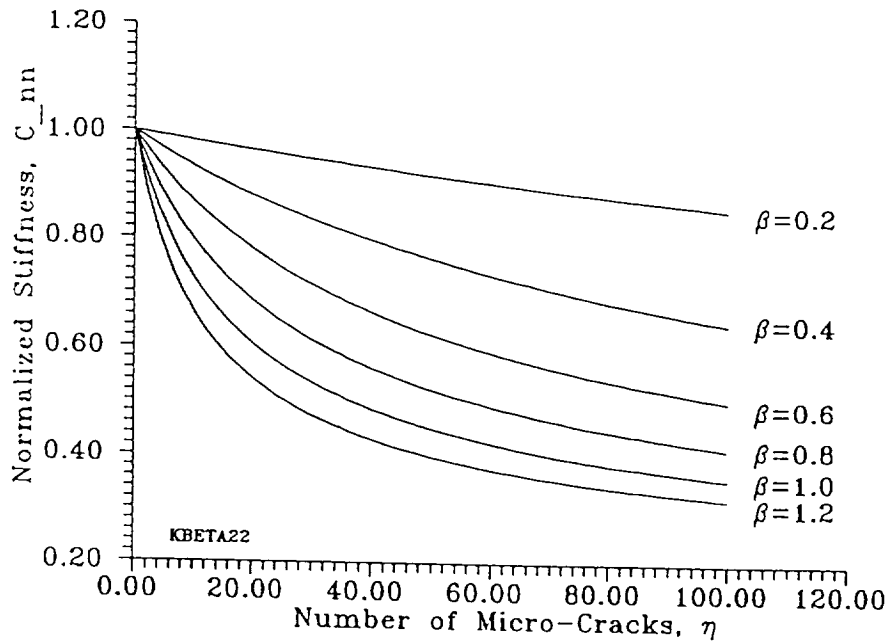


Figure 4. The effect of the normalized micro-crack length,  $\beta$ , on the normal stiffness component,  $C_{nn}$ .

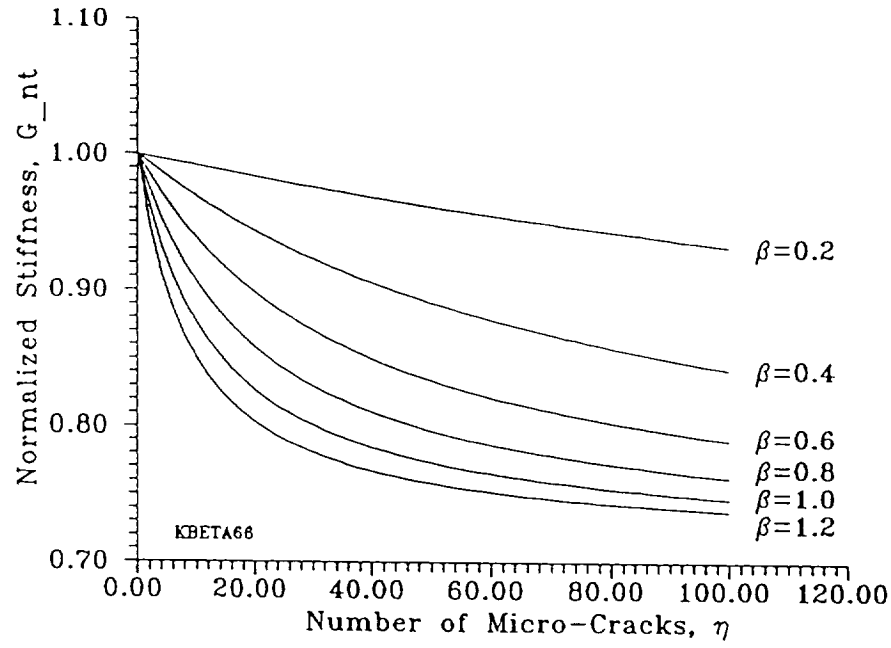


Figure 5. The effect of the normalized micro-crack length,  $\beta$ , on the shearing stiffness component,  $G_{nt}$ .

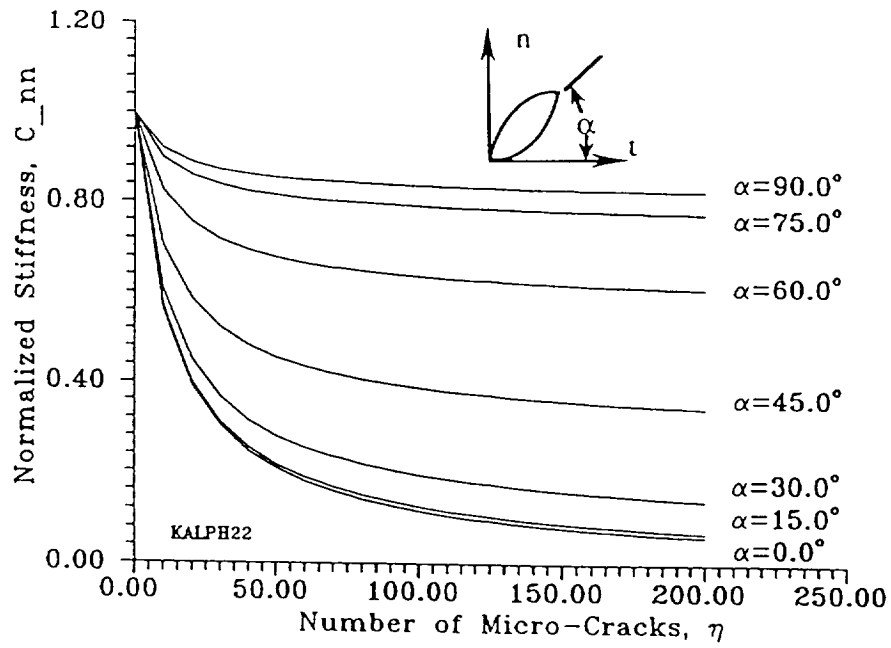


Figure 6. The effect of the micro-crack orientation angle,  $\alpha$ , on the normal stiffness component,  $C_{nn}$ .

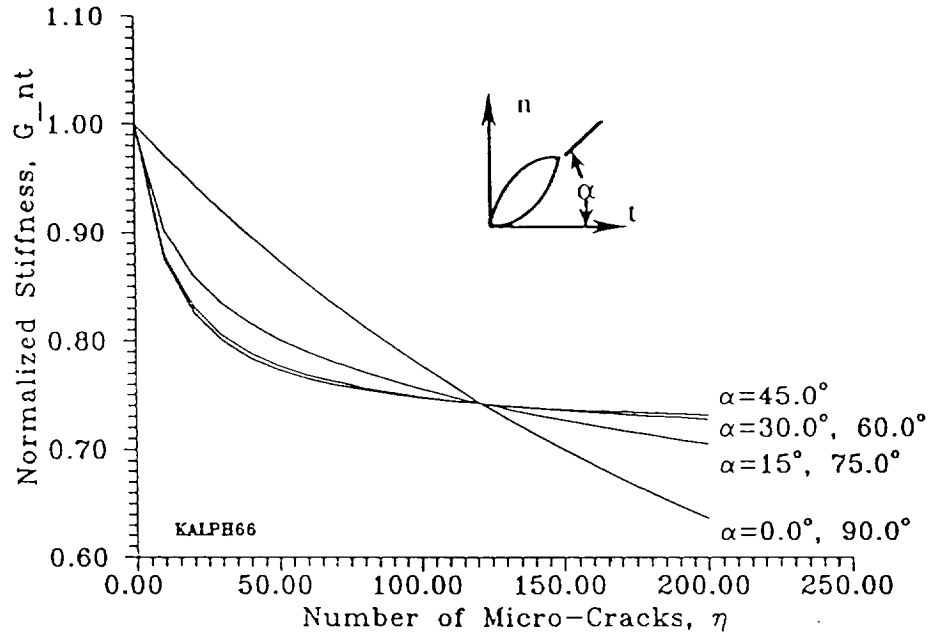


Figure 7. The effect of the micro-crack orientation angle,  $\alpha$ , on the shearing stiffness component,  $G_{nt}$ .

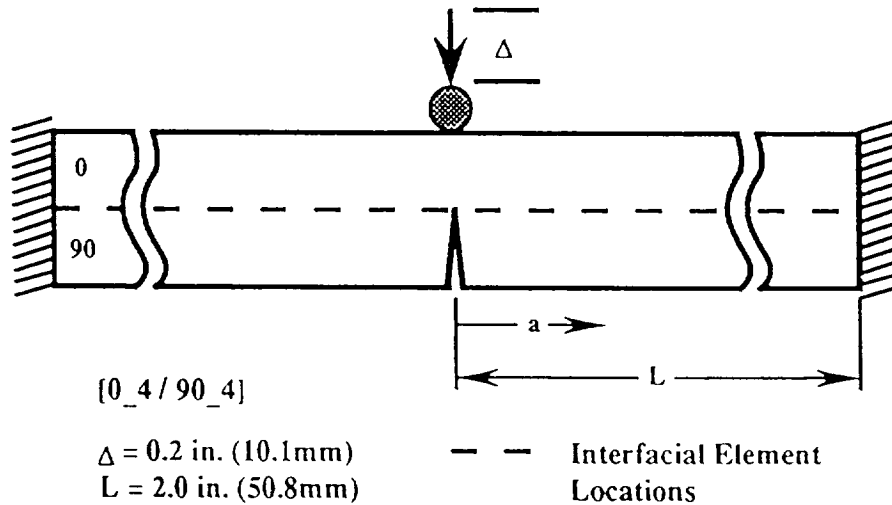


Figure 8. Schematic showing the geometry of the end-clamped center-loaded  $[0_4/90_4]$  laminate used in the analysis.

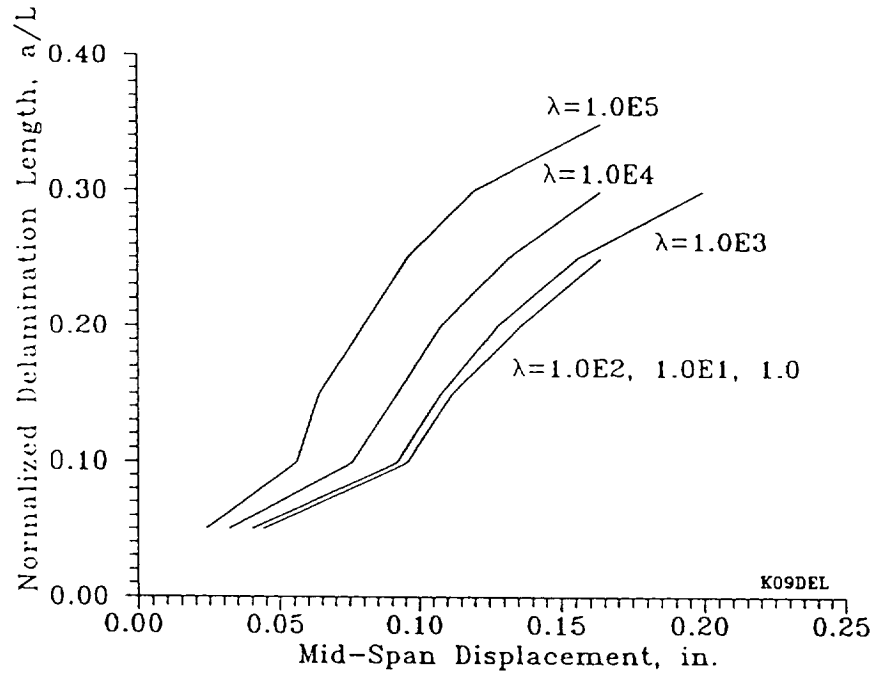


Figure 9. The accumulation of delamination damage in the end-clamped center-loaded  $[0_4/90_4]$  laminate for different values of the damage parameter,  $\lambda$ .

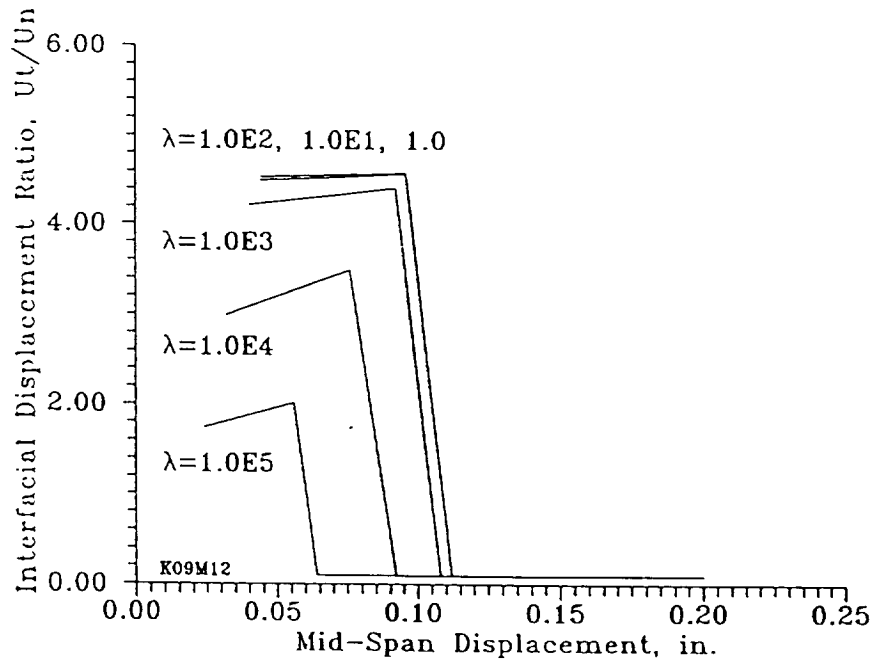


Figure 10. The interfacial displacement ratio,  $u_t/u_n$ , at the moment of delamination propagation for the end-clamped center-loaded  $[0_4/90_4]$  laminate.

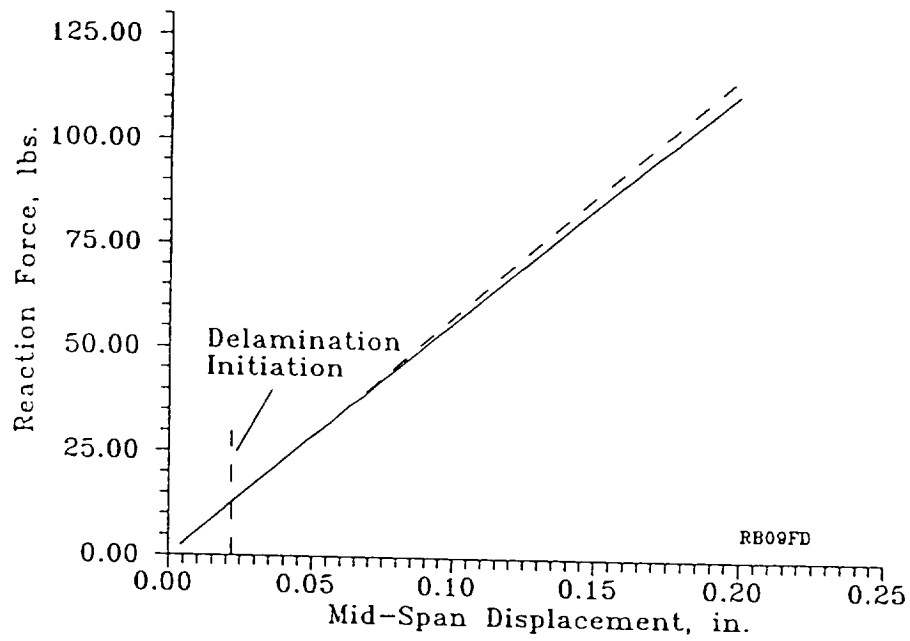


Figure 11. Force-displacement response for the  $[0_4/90_4]$  laminate ( $\lambda = 1.0E5$ ).

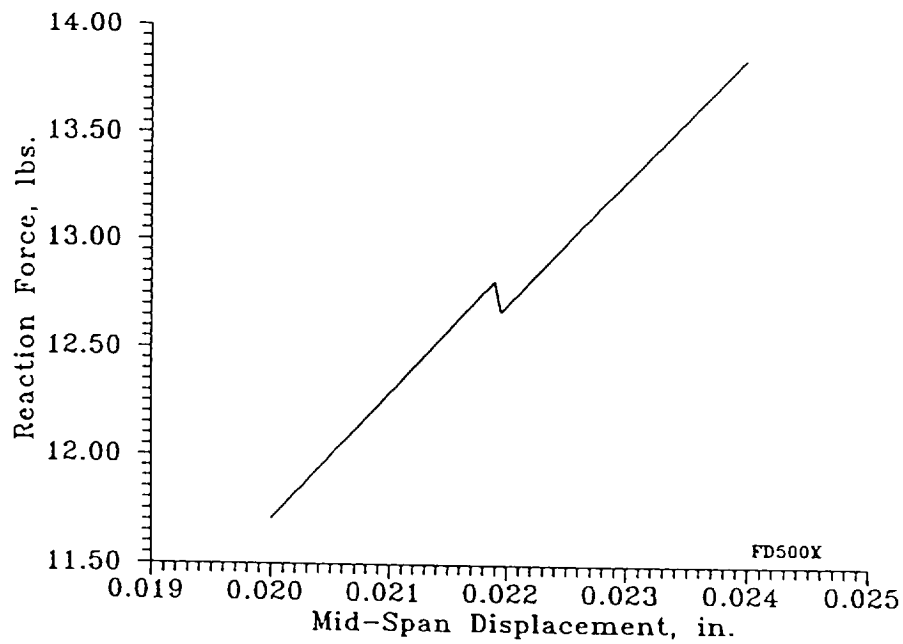


Figure 12. Close up view of the force-displacement response at delamination initiation for the  $[0_4/90_4]$  laminate.

# **Progressive Damage Analysis of Laminated Composites due to Tension Fatigue**

by

Dr. Charles E. Harris  
Mail Stop 188M  
NASA Langley Research Center  
Hampton, VA 23681

Timothy W. Coats  
Old Dominion University

Professor David H. Allen  
and  
David C. Lo  
Texas A&M University

## **ABSTRACT**

The durability and damage tolerance of laminated composites are critical design considerations for airframe composite structures. Therefore, the ability to model damage initiation and growth and predict the life of laminated composites is necessary to achieve efficient and economical structural designs. The purpose of the research presented in this paper is to experimentally verify the application of the damage model developed by the authors to predict progressive damage development in a toughened material system. Damage growth, stiffness degradation, and residual strength were experimentally determined for cross-ply and quasi-isotropic IM7/5260 graphite/bismaleimide laminates due to monotonic and tension-tension fatigue. The damage model, which has been implemented into a finite element code, was used to predict the stiffness loss and residual strength of unnotched and notched laminates. The model predictions were in good agreement to experimental results for several different fatigue loading histories and several different laminate stacking sequences.

## **KEY WORDS**

composites, graphite/epoxy, damage, matrix cracks, delamination, internal state variables.

## Introduction

Because of their light weight and high specific stiffness, laminated continuous fiber-reinforced composite materials are being used in some primary components in aircraft structures. However, when subjected to high service loads, environmental attack, impact, or a combination of any or all of the above, laminated composite materials may develop damage. As the service load or the time in service increases, damage develops and grows and could eventually reduce the residual strength of the structure.

There are four main types of damage. These are matrix cracking, fiber-matrix interface debonding, delamination, and fiber fracture. Usually, matrix cracking and fiber-matrix interface debonding are the first forms of damage to occur, followed by delamination, and finally fiber fracture resulting in catastrophic failure. While matrix cracking is usually arrested at the fibers or adjacent plies, it will result in a redistribution of load to the surrounding regions. As a result, these surrounding regions contain stress fields which are favorable to the initiation and propagation of additional damage. During the accumulation of subcritical damage, changes in material stiffness and strength results in the load redistribution until the principle load-carrying plies are unable to support the load, in which case, catastrophic failure occurs.

The initiation and propagation of damage is one of the problems in using laminated continuous fiber composite structures. To address durability and damage tolerance requirements, damage must be modelled and methods developed to predict the residual strength and life of composite structures. For example, one of the most complicated structural configurations is that of built-up laminated composite structures connected by mechanical fasteners such as rivets. These laminates with fastener holes develop local damage that cannot be easily treated using stress concentration factors. Another example is the non-visible damage that develops during foreign object impacts and ground handling accidents. Current methods for treating these local damage details are empirical and very conservative. Therefore, an accurate model of the damage initiation and propagation will

enhance current analysis and design capabilities thus leading to improvements in structural efficiency.

Many damage progression models are being developed to model damage and predict life. An example of the type of microcrack damage that is currently being studied by damage models is shown by the x-ray radiograph in Figure 1. This damage is both stacking sequence dependent and loading history dependent. An overview of damage resulting from fatigue loading in composites has been presented by Reifsnider [1,2]. Some researchers have tried to model this damage by considering each crack as an internal boundary and the stress or displacement fields are obtained either in closed form or numerically, such as in finite elements. This approach works well as long as there are a relatively small number of cracks. Talug and Reifsnider [3] have obtained finite difference approximate solutions to equilibrium equations to solve for interlaminar stresses in composite laminates. The "damage tolerance/fail safety methodology" developed by O'Brien [4] is an engineering approach to ensuring adequate durability and damage tolerance by treating only delamination onset and the subsequent delamination accumulation through the laminate thickness. Chang [5] developed a progressive damage model for notched composite laminates subjected to monotonic tensile loading. This particular model assesses the damage and predicts the ultimate tensile strength in laminates with arbitrary ply-orientations via an iterative combination of stress analysis and failure analysis. Chamis [6] studied structural characteristics such as natural frequencies and buckling loads and the corresponding mode shapes during progressive fracture of angle-ply polymer matrix composites. This study concluded that the individual nature of the structural change was dependent on laminate configuration, fiber orientation, and the boundary conditions. The model proposed by Talreja [7,8,9] incorporates internal state variables (ISV's) for matrix cracks and delaminations and exhibits ply stacking sequence dependence. The ISV's are strain-like quantities which represent the damage as volume averaged quantities, i.e., a continuous medium.



The treatment of a damaged volume of material as a continuous medium and the representation of the damage with averaged quantities was first proposed by Kachanov [10] in 1958 and is referred to as continuum damage mechanics. From this concept of averaging the effects of microcracking in a small local volume, the authors developed a damage model for laminated composites [11-16]. This damage model utilizes internal state variables (ISV's) and is phenomenological; however, it is formulated at the ply and sublaminar level and accounts for the influence of stacking sequence. The model has been recently implemented into a finite element analysis code and has the capability to predict damage growth and residual strength for monotonic and tension-tension fatigue loading histories. The model was originally developed for brittle graphite/epoxy composite systems but has been extended to also address toughened polymer matrix composites. This paper will present results for both unnotched and notched specimens subjected to several different monotonic and fatigue loading histories.

### **The Allen and Harris Model**

The damage model of Allen and Harris [11-16] was originally developed to model the behavior of microcrack damage in brittle epoxy systems and has recently been extended to toughened polymer systems. The model predicts the growth of intraply matrix cracks for monotonic tensile loadings and for tension-tension fatigue, the associated ply level damage-dependent stress and strain states, and the residual strength of laminates with geometric discontinuities. The model also accounts for the effects of delaminations but uses an empirical relationship that requires the user to supply an estimate of the delamination area. The empirical relationship must be used because the model currently does not calculate free edge interlaminar stresses. A summary of the model can be found in the literature [17]. The model uses internal state variables (ISV) to represent the local deformation effects of the various modes of damage. Loading history dependence is modelled by ISV damage

growth laws. The progression of damage is predicted by an iterative and incremental procedure outlined in the flowchart shown in Figure 2. This entire progressive failure analysis scheme has been implemented into the finite element formulation in the NASA Computational Mechanics Testbed (COMET) [18] computer code. The first block of Figure 2 is a description of the information needed as model input. A FORTRAN code consisting of the damage dependent constitutive model and a damage growth law for matrix cracking was incorporated into a classical lamination theory analysis to produce effective lamina and laminate properties for unnotched laminates. The program is called FLAMSTR (Fatigue LAMinate STress) [19] and makes up the first constitutive module. The fourth block is a damage dependent finite element analysis code [18] from which the second constitutive module performs a ply level elemental stress analysis and simulates damage growth via damage growth laws for each element. The damage growth calculations, block six, are used to update the damage state, block seven, for the notched laminates. For unnotched laminates, only the first constitutive module is needed to update the damage state.

The material property descriptions required for the model include standard ply stiffness and strength data determined in the usual manner. In addition, the tension-tension fatigue matrix crack growth law must be determined from test data obtained from the  $[0/90_2/0]_s$  laminate. Under tension-tension fatigue, matrix cracks accumulates in the 90 degree layers and, therefore, the effects of mode I matrix crack growth is isolated. The mode II matrix crack growth law can be obtained from fatigue tests of the  $[45/-45]_s$  laminate which isolates the 45 degree plies in pure shear. A procedure [19] has been developed for determining the ISV (damage parameters) from the test data obtained from these two laminates.

THE MODE II  
GROWTH LAW  
IS NOT  
CURRENTLY  
EMPLOYED IN  
THE FINITE  
ELEMENT CODE

REFERENCE 20 GIVES  
GREATER DETAIL ON THE  
PROCEDURE

## Experimental Procedures

The material chosen to experimentally verify the continuum damage model was IM7/5260 graphite/bismaleimide laminates. This material system was fabricated with a

toughened interlayer between the plies of the laminate. Cross-ply and quasi-isotropic laminates were tested with the following stacking sequences:  $[0/90_2/0]_s$ ,  $[0/90_3]_s$ ,  $[0/45/-45/90]_s$ , and  $[90/-45/45/0]_s$ . The laminates were cut into 2.54 cm x 25.4 cm (1"x10") coupons, both unnotched and notched. The notched laminates had a 6.35 mm (1/4 inch) hole drilled in the center.

Each laminate was subjected to tension-tension fatigue up to 100,000 cycles at a frequency of 5 Hz and a stress ratio of 0.1. Prior to the fatigue tests, several unnotched and notched specimens from each laminate were monotonically loaded to failure to measure the ultimate strength and the open-hole residual strength of each laminate. This data provided a baseline for assessing the effects of the fatigue loading history on residual strength. For each cross-ply laminate, three replicate specimens were subjected to a maximum tension fatigue stress of 30% of the ultimate failure strength of the laminate and an additional three replicate specimens were tested at 60% of ultimate. For the quasi-isotropic laminates, three replicate specimens were subjected to a maximum tension fatigue stress of 50% of the ultimate failure strength of the laminate and an additional three were tested at 60% of ultimate. In situ edge replicas and x-ray radiographs to characterize damage were taken throughout the testing and the specimen did not have to be removed from the load frame. The edge replicas and x-ray radiographs provided the means to measure matrix crack and delamination surface areas. A Direct Current Displacement Transducer (DCDT) with a 4" gage length was used to measure strain and remained secured to the specimen throughout the test. The fatigue test was stopped periodically to take edge replicas and x-rays, and to monotonically load the specimen to record the stress-strain behavior. At the end of 100,000 fatigue cycles, the specimens were monotonically loaded to failure to record the post-fatigue residual strength of each laminate.

The material damage parameters for the model were determined from the fatigue tests of the unnotched  $[0/90_2/0]_s$  laminate. The crack surface area as a function of fatigue cycles was measured from the edge replicas and the x-ray radiographs [20]. From this data, the

matrix crack internal state variables were calculated and used to determine the material parameters. The parameters are then used in the matrix crack growth law to compute the predicted damage evolution, stiffness loss, and residual strength for the other 3 laminate stacking sequences. For those laminates exhibiting significant delaminations, the delamination surface area and locations were determined from the x-ray radiographs and edge replicas and used in an empirical relationship contained in the damage model.

## Comparisons of Model Predictions to Experimental Results

### Stiffness Loss

The material damage parameters determined experimentally for the mode I matrix cracking growth law were used in a fatigue laminate stress program (FLAMSTR) [19] and a damage dependent finite element code installed in the COMET [18] to predict reductions in stiffness due matrix cracking. Predictions for the  $[0/90_3]_s$  laminate are illustrated in Figure 3. The predicted reductions in stiffness are in close agreement with the experimental stiffness loss which is due solely to matrix cracking in the 90 degree plies. The distinct trends for the two different constant amplitude maximum stress levels are accurately predicted.

The  $[0/45/-45/90]_s$  laminate exhibited edge delaminations primarily at the  $-45/90$  interface. The experimentally measured delamination surface areas were used to predict stiffness loss due to delaminations and the matrix crack growth law was used to analytically predict the growth of matrix cracks in the various plies of the laminate. The experimental results are compared to the model predictions for the two maximum fatigue stress levels in Figures 4. Once again, the model predictions are accurate. The stiffness loss in the quasi-isotropic laminate was more significantly effected by the delaminations than by the intraply matrix cracks.

THE RESULTS  
IN THE "STIFFNESS  
LOSS" SECTION  
WERE CALCULATED  
BY THE FLAMSTR  
PROGRAM USING  
THE STIFFNESS  
FINITE ELEMENT  
CODE "LFEMCR"

The effects of different delamination growth patterns was illustrated by the different behavior of the  $[90/-45/45/0]_s$  and  $[0/45/-45/90]_s$  quasi-isotropic laminates. The x-ray radiographs revealed that the delaminations in the  $[90/-45/45/0]_s$  laminate were localized whereas the  $[0/45/-45/90]_s$  laminate exhibited large prominent edge delaminations. The stiffness loss of a  $[90/-45/45/0]_s$  laminate is given in Figure 5. Again, the model correctly predicted the stiffness behavior as a function of the fatigue loading history. (Close attention should be paid to the differences between the effects of edge delaminations and local delaminations [21].)

The analysis of the notched laminates yielded good results as well. Figure 6 shows the damage state in the open-hole specimens for the two different stacking sequences. It would be expected that the matrix crack in the 0-degree ply adjacent to the hole (axial split) would have a significant effect in reducing the stress concentration at the notch. This would increase the global displacements of the laminate prior to failure. The damage dependent finite element code [18] implemented into the NASA COMET was used to calculate matrix crack damage growth, laminate stresses and strains, and far field displacements. The finite element mesh shown in Figure 7 is a quarter section of the notched laminate. The finite element code predicts the damage state in each element as a function of the local element stresses. An iterative procedure is used to calculate the element damage-dependent properties and associated load redistribution throughout the finite element model. The analytical far field displacements calculated over a 4" gage length are compared to the experimental stiffness loss in Figure 8. This figure illustrates the ability of the code to predict separate trends in stiffness reductions due to mode I matrix cracking for different constant amplitude stress levels and layups for a spatially varying damage state. Edge and local delaminations were included in the predictions and were found to have very little effect, especially compared to the mode I matrix cracking of the axial split for the  $[0/90]_s$  laminate. The comparison of the results for the two laminates given in Figures 6 and 8 confirms the ability of this model to predict damage growth as a function of the laminate

stacking sequence. The  $[0/90_3]_s$  laminate has more severe axial splitting, i.e. more mode I matrix cracking, thus the predicted loss in stiffness due to mode I matrix cracking is larger. The reductions in stiffness are greater for this laminate because more load is transferred away from the stress concentration at the hole.

### ***Residual Strength***

Residual strength predictions were also made for the two laminates and damage states shown in Figure 6. A more refined finite element mesh is required for residual strength predictions than for stiffness loss predictions. The mesh shown in Figure 9 was used to predict the residual strength. The mesh near the hole was refined in order to try to capture the local stress effects produced by the pronounced axial split in the 0-degree plies. The comparison of the model predictions to the experimental results are shown in Figure 10. The model uses a simple maximum strain failure criterion for the fibers as determined from the ultimate tensile strength of the 0-degree unidirectional laminate. When the fiber direction strain in the principal load-carrying ply reaches the fiber failure strain, the element will not sustain additional load, ie, the material is assumed to exhibit elastic-perfectly plastic behavior. Progressive failure is then predicted by an iterative process to account for the interelement load redistribution after an element has been determined to have fiber fracture. The loads applied to the model boundaries are then incrementally increased until complete failure occurs. The fiber failure criterion and the computational procedure are currently under investigation. The authors believe the accuracy of the model will be greatly improved by implementing a more sophisticated failure criterion.

CALCULATED  
USING COMET

## **Conclusions**

The damage model developed by Allen and Harris was used successfully to predict the stiffness degradation and residual strength of the IM7/5260 toughened matrix composite


material. Experimental verification of the model was established by comparing the stiffness loss of cross-ply and quasi-isotropic laminates with and without open holes for tension fatigue loadings. Residual strength predictions were also reasonably close to the experimental values. The model has predictive capability for intraply matrix cracks and correlative capability for delaminations. The model successfully predicted both the effects of laminate stacking sequence and loading history on damage growth and stiffness loss. The ability of the model to predict damage growth in the open hole specimens was particularly encouraging. These results suggest that the model is appropriate for spatially varying damage developing in strain gradient fields and not confined to uniform damage that develops in the gage length of an unnotched uniaxial test specimen. The spatial variation in damage is treated through the finite element discretization since the damage is assumed to be uniform within an element. The empirical relationship for delamination provided trends in stiffness loss that agreed with the experimental trends. It should be noted, however, that the predictive capability of this model would increase dramatically if delamination growth laws were available. Also, a more sophisticated fiber failure criterion and computational procedure needs to be developed to improve the accuracy of the residual strength predictions.

## R E F E R E N C E S

- [1] Reifsnider, K.L., "Fatigue Behavior of Composite Materials," *International Journal of Fracture*, Vol. 16, No. 6, December 1980, pp. 563-583.
- [2] Reifsnider, K.L., "The Mechanics of Fatigue in Composite Laminates," *Composite Materials*, K. Kawata and T. Adasada, Ed., Proc. Japan-U.S. Conference, Tokyo, 1981, pp. 131-144.
- [3] Talug, A. and Reifsnider, K.L., "Analysis of Stress Fields in Composite Laminates with Interior Cracks," *Fiber Science and Technology*, Vol. 12, 1979, pp. 201-215.
- [4] O'Brien, T.K., "Towards a Damage Tolerance Philosophy for Composite Materials and Structures," *Composite Materials: Testing and Design* (Ninth

- Volume), ASTM STP 1059, S.P. Garbo, Ed., American Society for Testing and Materials, Philadelphia, 1990, pp. 7-33.
- [5] Chang, Fu-Kuo and Chang, Kuo-Yen, "A Progressive Damage Model for Laminated Composites Containing Stress Concentrations," *J. of Composite Materials*, Vol. 21, Sept. 1987, pp. 834-855.
  - [6] Chamis, C.C., Murphy, P.L.N., and Minnetyan, L., "Structural Behavior of Composites with Progressive Fracture," *J. of Reinforced Plastics and Composites*, Vol. 11, April 1992, pp. 413-442.
  - [7] Talreja, R., "A Continuum Mechanics Characterization of Damage in Composite Materials," *Proc. R. Soc. London*, Vol. 399A, 1985, pp. 126-216.
  - [8] Talreja, R., "Residual Stiffness Properties of Cracked Composite Laminates," *Advances in Fracture Research, Proc. Sixth Int. Conf. De Fracture*, New Delhi, India, Vol. 4, 1985, pp. 3013-3019.
  - [9] Talreja, R., "Transverse Cracking and Stiffness Reduction in Composite Laminates," *J. of Composite Materials*, Vol 19, 1985, pp. 355-375.
  - [10] Vakulenko, A. A. and Kachanov, M. L., "Continuum Theory of Cracked Media," *Izv. AN SSR. Mekhaniha Tverdogo Tela*, Vol. 6, p. 159, 1971.
  - [11] Harris, C.E., Allen, D.H., O'Brien, T.K., "Progressive Failure Methodologies for Predicting Residual Strength and Life of Laminated Composites," *Proceedings of 1<sup>st</sup> NASA Advanced Composites Technology Conference*, Oct 30 - Nov 1, 1990.
  - [12] Allen, D.H., Groves, S.E., and Harris, C.E., "A Cumulative Damage Model for Continuous Fiber Composite Laminates with Matrix Cracking and Interply Delamination," *Composite Materials: Testing and Design (8<sup>th</sup> Conference)*, ASTM STP 972, J.D. Whitcomb, Ed., American Society for Testing and Materials, Philadelphia, 1988, pp. 57-80.
  - [13] Allen, D.H., Harris, C.E., Groves, S.E., "A Thermomechanical Constitutive Theory for Elastic Composites with Distributed Damage-I. Theoretical Development," *Int. J. Solids Structures*, Vol. 23, No. 9, 1987, pp. 1301-1318.
  - [14] Allen, D.H., Harris, C.E., Groves, S.E., "A Thermomechanical Constitutive Theory for Elastic Composites with Distributed Damage-II. Application to Matrix Cracking in Laminated Composites," *Int. J. Solids Structures*, Vol. 23, No. 9, 1987, pp. 1319-1338.
  - [15] Lee, J.W., Allen, D.H., Harris, C.E., "Internal State Variable Approach for Predicting Stiffness Reductions in Fibrous Laminated Composites with Matrix Cracks," *J. of Composite Materials*, Vol. 23, Dec. 1989, pp. 1273-1291.
  - [16] Lo, D.C., Allen, D.H., Harris, C.E., "A Continuum Model for Damage Evolution in Laminated Composites," *IUTAM Symposium on Inelastic Deformation of Composite Materials*, 1990.

pp. 549-561





- [17] Harris, C.E. and Allen, D.H., "A Continuum Damage Model of Fatigue-Induced Damage in Laminated Composites," *SAMPE Journal*, July/August 1988, pp. 43-51.
- [18] Lo, D.C., Allen, D.H., and Harris, C.E., "A Procedure for the Performance of Progressive Failure Analysis on the Computational Structural Mechanics Testbed," *NASA Technical Memorandum* , NASA LaRC,
- [19] Lo, D.C., Allen, D.H., and Harris, C.E., "A Procedure for Utilization of a Damage-Dependent Constitutive Model for Laminated Composites," *NASA Technical Memorandum 104219*, NASA LaRC, February 1992.
- [20] Coats, T.W., "Experimental Verification of a Progressive Damage Model for Composite Laminates Utilizing Continuum Damage Mechanics," Master's Thesis, Old Dominion University, December 1992, 200 pages.
- [21] O'Brien, T.K., "Analysis of Local Delamination and Their Influence on Composite Laminate Behavior," *Delamination and Debonding of Materials*, Philadelphia, 1985, pp. 282-297.

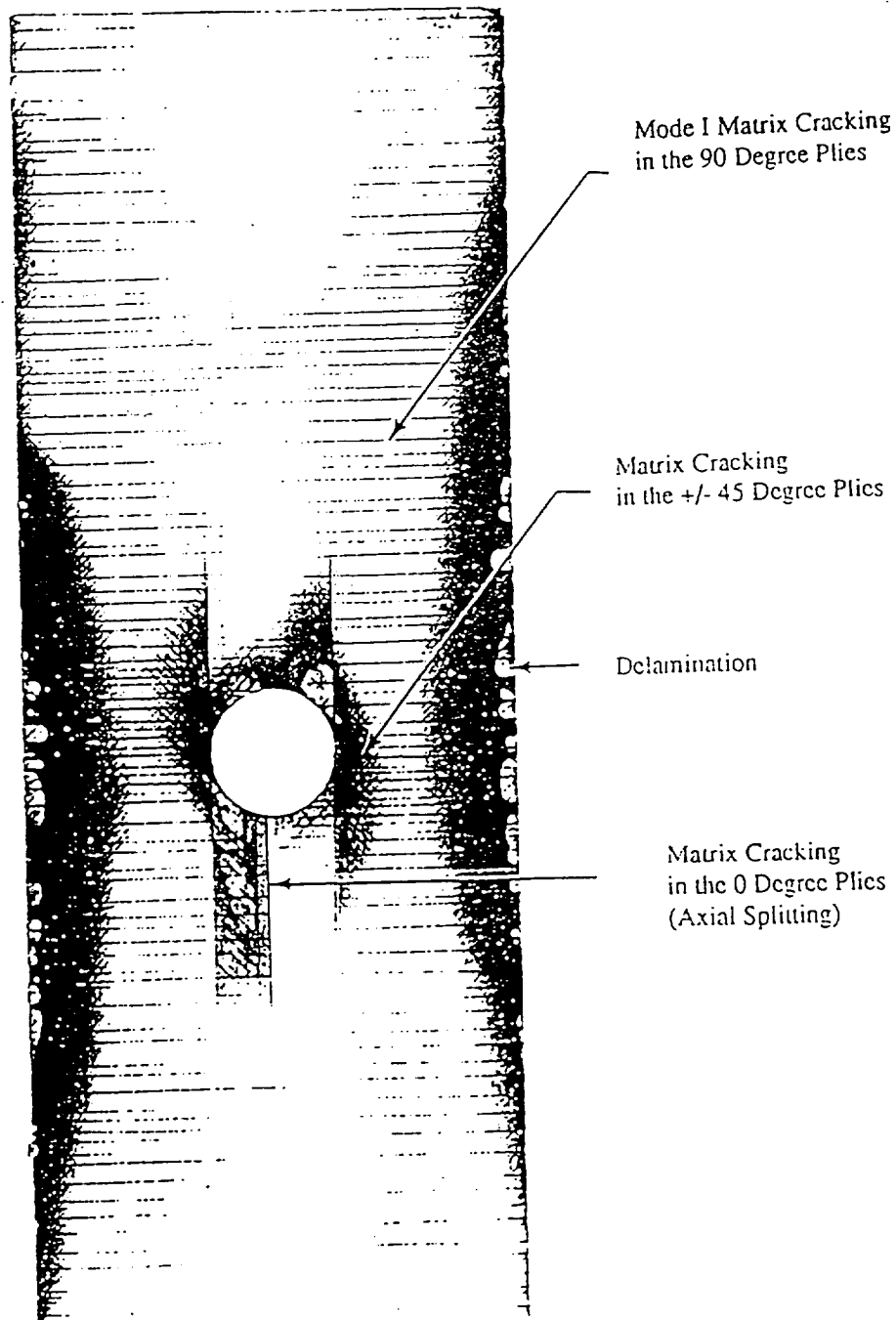


Figure 1 - Tension-Tension Fatigue Damage in a Notched  
[0/45/-45/90]<sub>s</sub> IM7/5260 Laminate

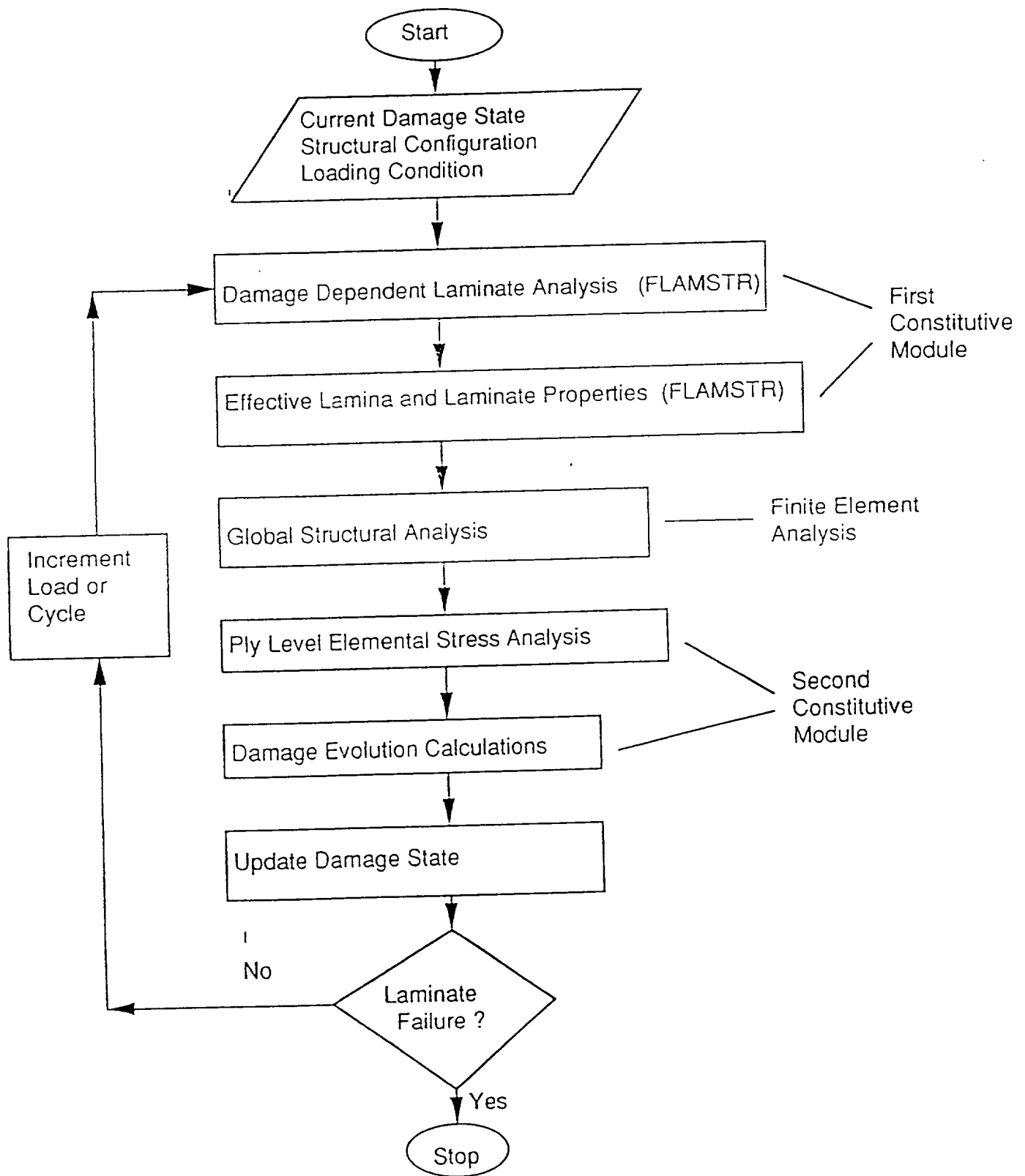
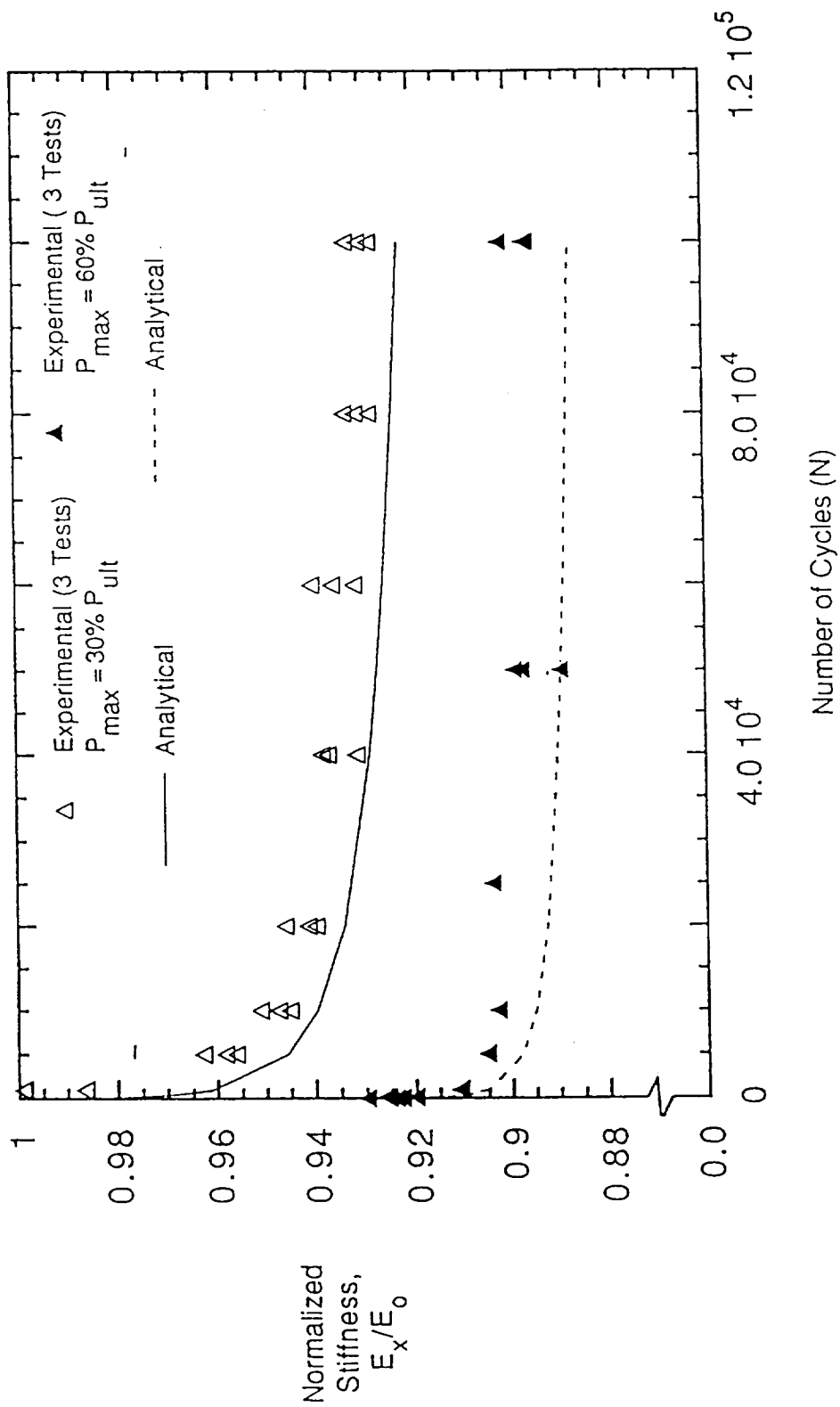
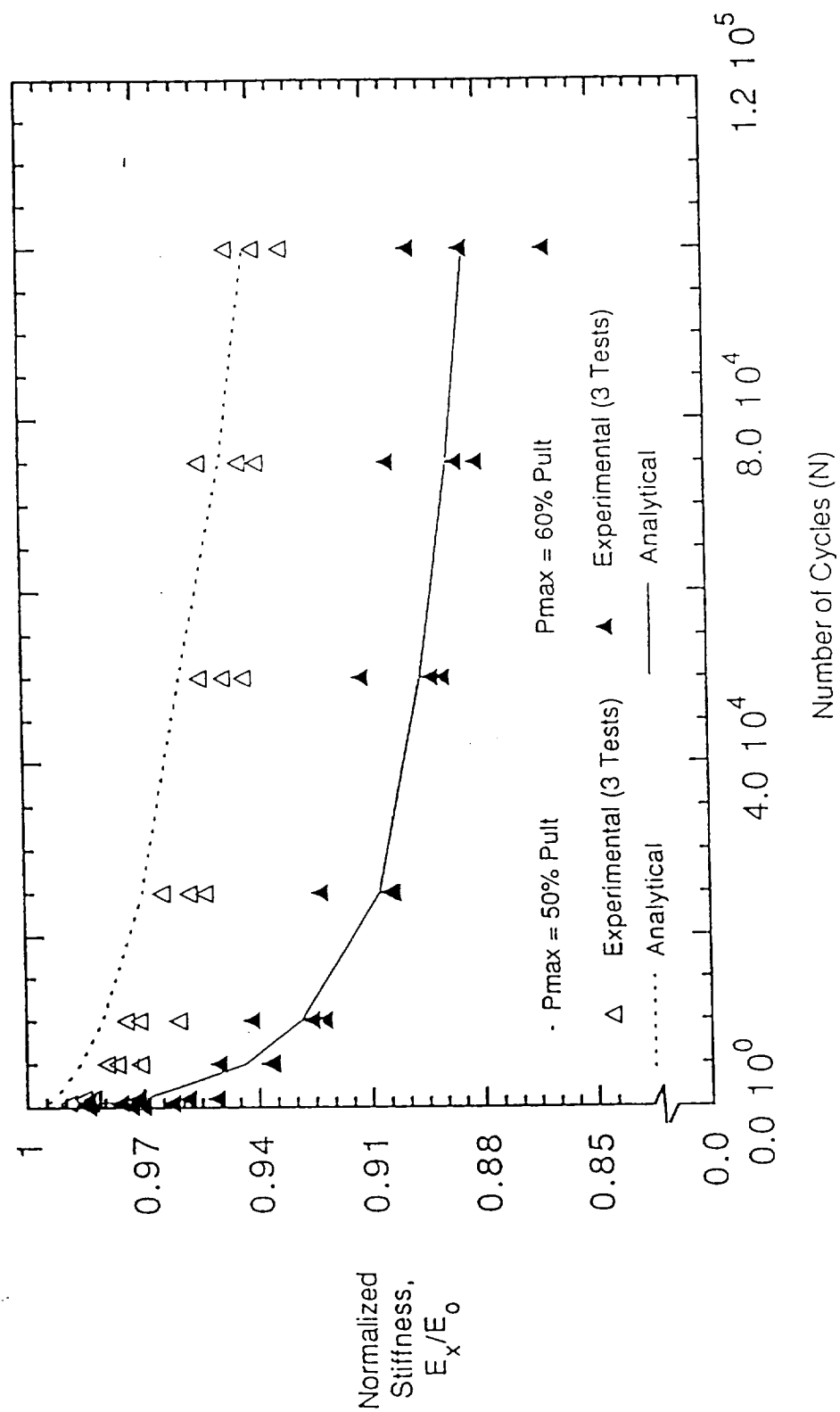
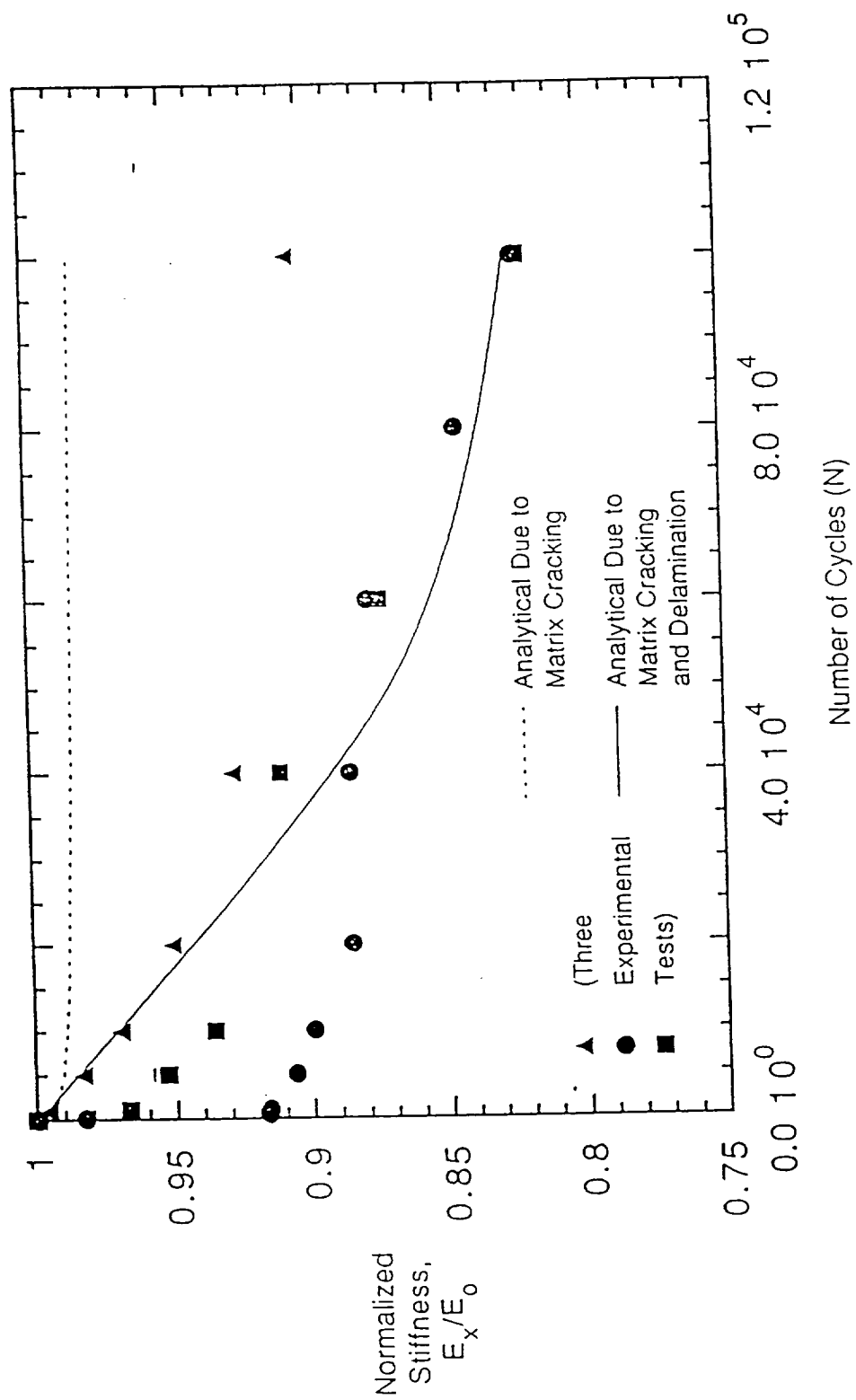


Figure 2 - Progressive Failure Analysis Scheme

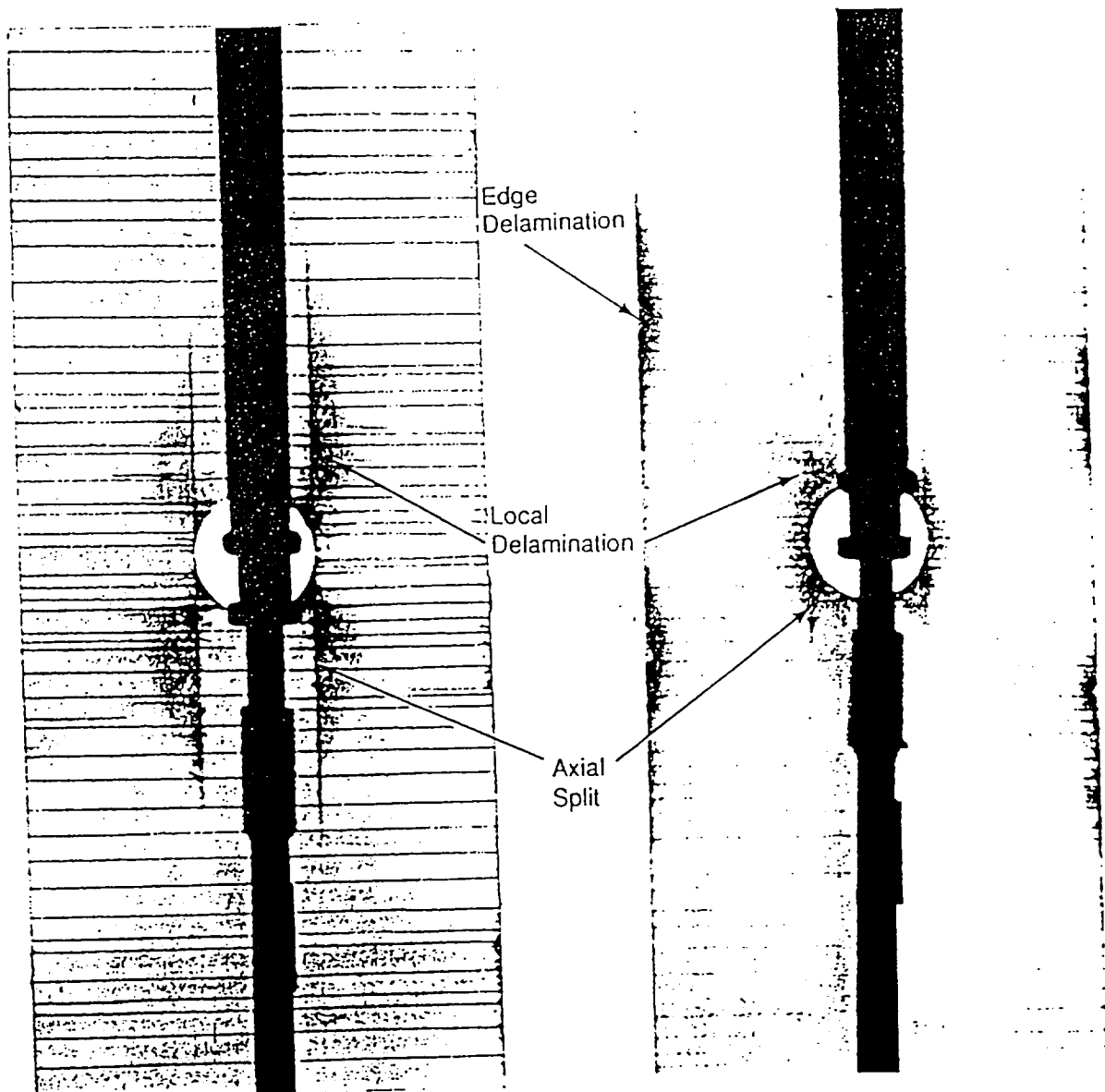


3  
Figure 3 - Experimental vs Analytical Stiffness Degradation of  $[0/90_3]_s$  IM7/5260 for Tension-Tension Fatigue





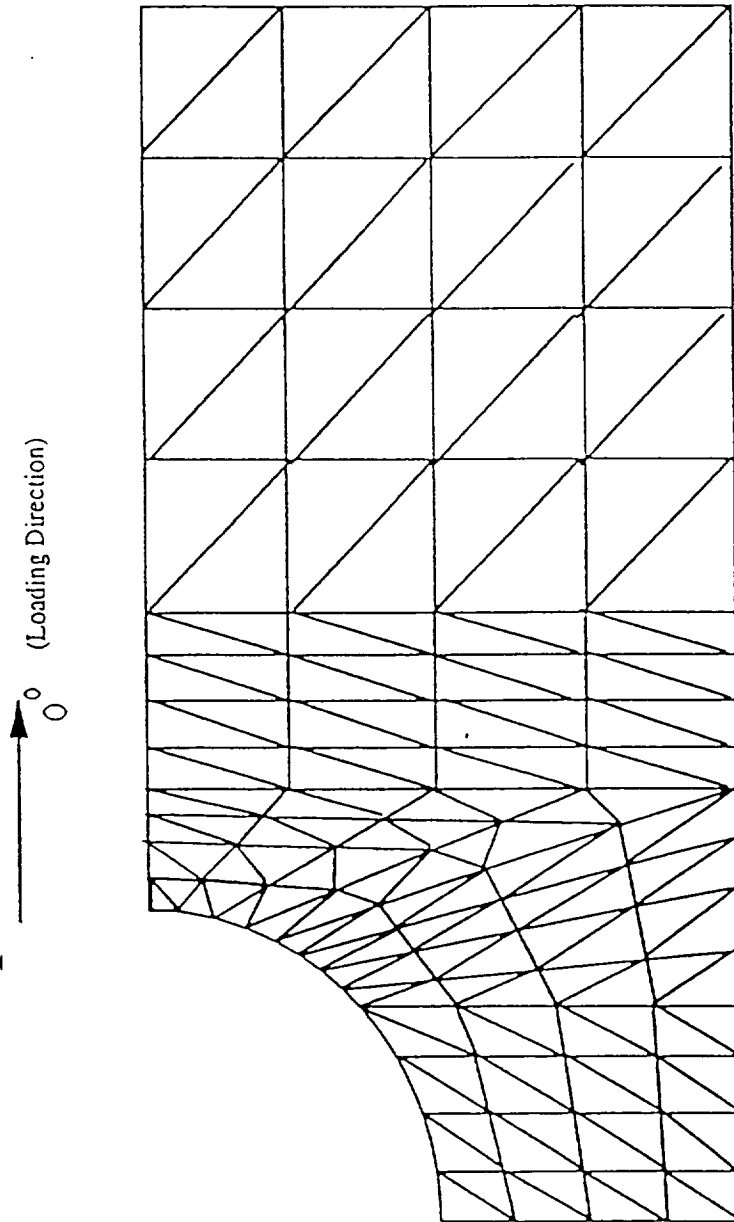
5  
Figure 11 - Stiffness Degradation of  $[90/-45/45/0]_s$  IM7/5260.



[0/90<sub>3</sub>]<sub>s</sub>  
 N = 100,000 Cycles  
 P<sub>max</sub> = 60% P<sub>ult</sub>  
 E<sub>x</sub>/E<sub>0</sub> = 10.83%

[0/45/-45/90]<sub>s</sub>  
 N = 100,000 Cycles  
 P<sub>max</sub> = 60% P<sub>ult</sub>  
 E<sub>x</sub>/E<sub>0</sub> = 2.65%

6  
 Figure 6 - X-Ray Radiograph of IM7/5260 Notched Laminates.



7  
 Figure ~~14~~ - Finite Element Mesh for Laminates with  
 a Central Circular Notch



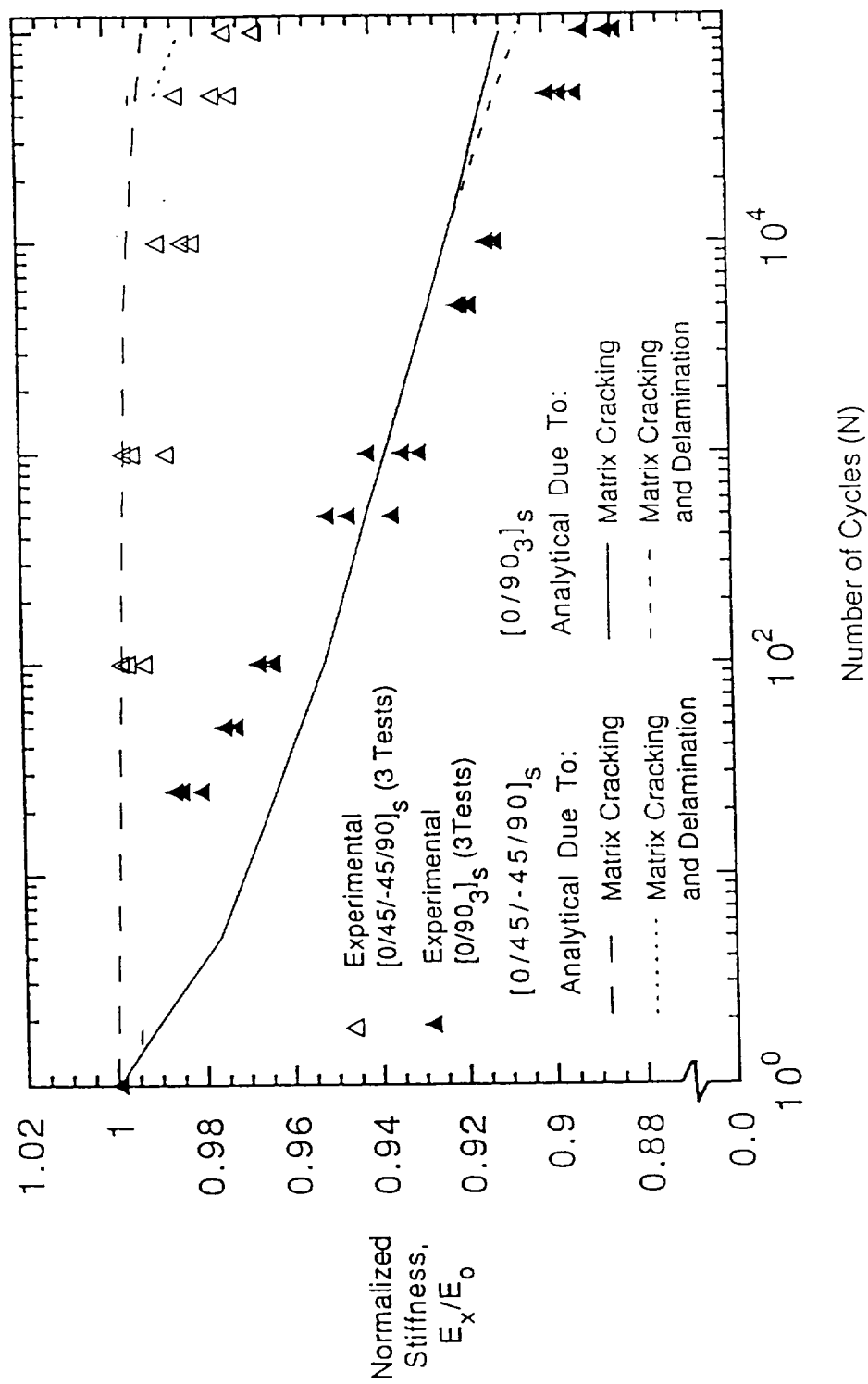
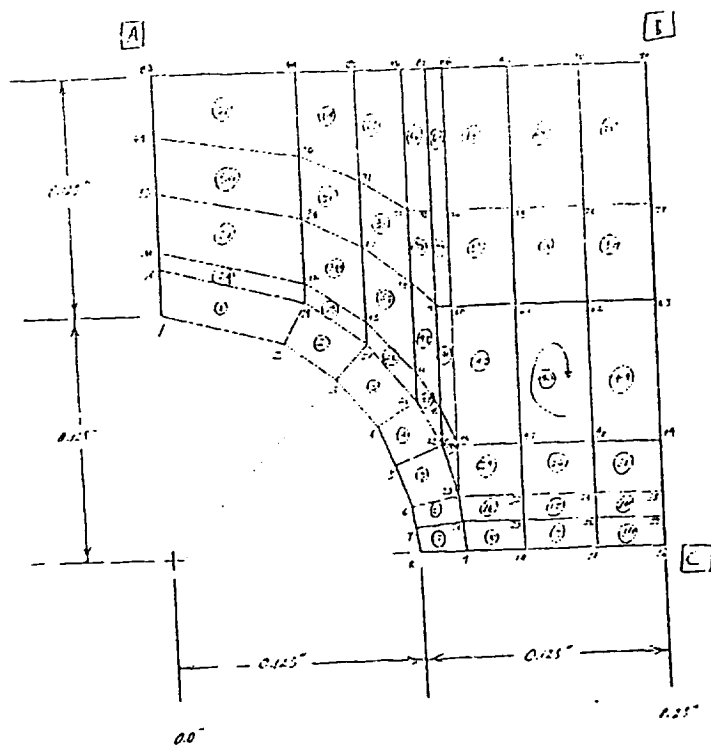
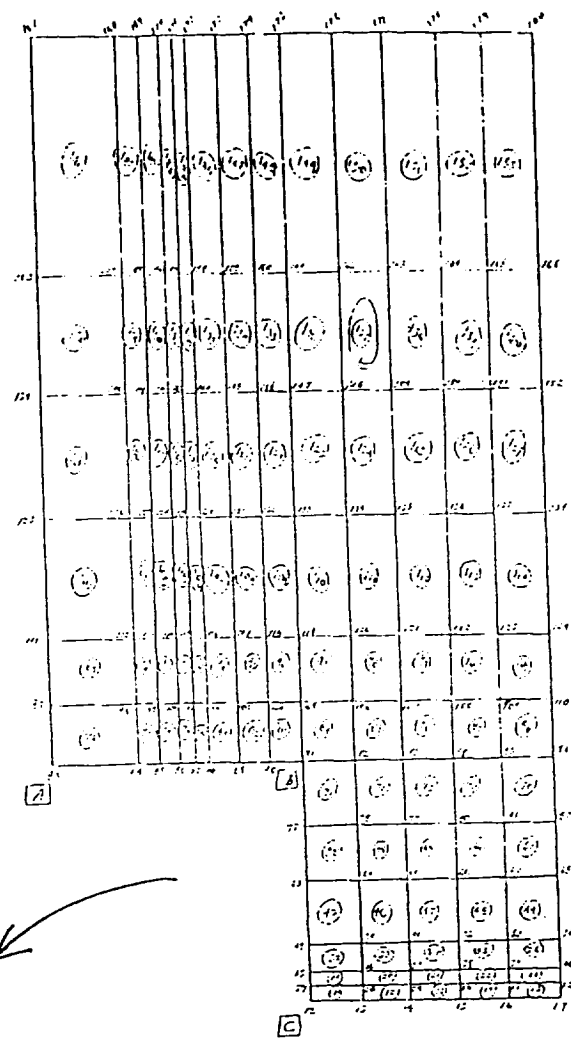


Figure 8 - Stiffness Loss of IM7/5260 Laminates with a Central Circular Notch.



a) notch region



b) Far Field

Figure 9 Finite element mesh used in the residual strength predictions

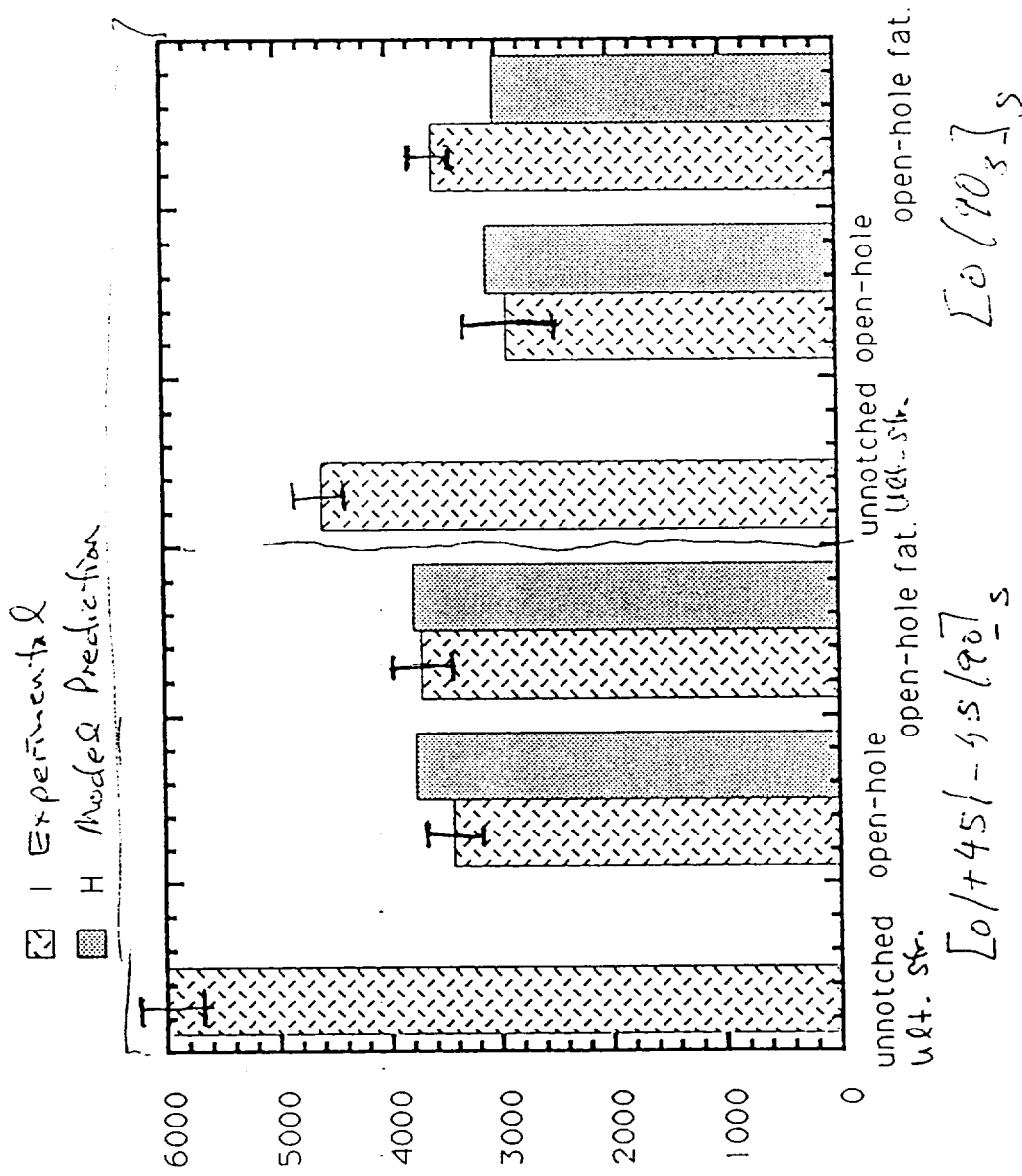


Fig. 10 Predictions of residual strength

## **Delamination Evolution in Composites Using a Cohesive Zone Model**

D. C. Lo, F. Costanzo, and D. H. Allen

Texas A&M University, Texas, U.S.A.

### **1. INTRODUCTION**

It has been found from micrographic and fractographic examinations of delaminations that a damage zone develops ahead of the delamination front in many polymeric composites [1-3]. The presence of this damage zone in the interface introduces nonlinearities to the interfacial response and thus affects the propagation of the delamination in the interface. Lo et al. [4-6] previously modeled the response of the damage zone by employing the interfacial constitutive relationships developed by Needleman [7] and Tvergaard [8]. While the aforementioned models introduce nonlinear response to the mechanical behavior of the interface, these models do not distinguish between the different mechanisms active in the damage zone. The current paper will focus on the development of delaminations with a damage zone containing micro cracks. This type of damage zone is usually found in thermosetting matrix composites. An interface constitutive relationship adapted from a micro-mechanical solution for a micro-cracked solid will be employed in the analysis.

### **2. INTERFACE MODELING**

In the current study, the response of the interface is assumed to behave isotropically when no micro-cracks are present. As the load is increased and the micro-cracks accumulate, the mechanical properties of the interface are degraded in accordance with the orientation and distribution of the microcracks. This then causes the mechanical response to behave orthotropically. For the case of non-interacting cracks with an arbitrary crack orientation distribution, the effective moduli for this type of material have been calculated by Kachanov [9]. This method is based on the superposition of the solution for the averaged crack surface displacement of a single isolated crack subjected to remotely applied stresses. Since the mutual positions of the cracks do not enter into the analysis under the non-interaction assumption, the overall effect of the crack array is simply the sum of the contribution

from each isolated crack. If it is assumed that all the cracks in the representative area are oriented in the same direction, the effective moduli are

$$E_1 = E_o \quad (1)$$

$$E_2 = \frac{E_o}{1 + 2\pi\rho} \quad (2)$$

$$\nu_{12} = \nu_o \quad (3)$$

$$\nu_{21} = \frac{\nu_o}{1 + 2\pi\rho} \quad (4)$$

$$G_{12} = \frac{G_o}{1 + \left(2\pi \frac{G_o}{E_o}\right) \rho} \quad (5)$$

where  $E_o$ ,  $\nu_o$ , and  $G_o$  are the undamage Young's modulus, Poisson's ratio, and shear modulus, respectively.  $\rho$  is the micro-crack damage variable and is defined as

$$\rho = \frac{1}{A} \sum_{m=1}^M l_m^2 \quad (6)$$

where the summation is performed over the  $M$  number of cracks found in the representative area,  $A$ .  $l_m$  is the length of the  $m^{th}$  crack. Note that these effective moduli are referenced to the physical crack axes. (The subscripts "1" and "2" denoting the axes parallel and perpendicular to the length of the crack, respectively.) Base on experimental observations that the micro-cracks form perpendicular to the plane of principal stress, the micro-crack orientation can be determined from the stress state in the interface.

The micro-crack damage variable as defined by Equation (6) requires the knowledge of the number of cracks in the representative area and the individual crack length. Since there could be many micro-cracks embedded in the resin rich interface, simplifying assumptions are taken to maintain tractability of the problem. Firstly, each micro-crack is assumed to grow instantaneously to a final crack length,  $l$ , as dictated by an interfacial thickness parameter,  $t_{int}$ , in the following manner

$$l = \beta t_{int} \quad (7)$$

where  $\beta$  is the micro-crack length scaling factor. Second, the accumulation of micro-cracks is related to the highest principal stress experienced by the representative area as shown

$$\eta = \lambda \text{Max}(\sigma_{P_{max}}) \quad (8)$$

where  $\eta$  is the number of micro-cracks in the representative area,  $\sigma_{P_{max}}$  is the maximum principal stress at a given stress state, and  $\lambda$  is the micro-crack

accumulation parameter. Finally, the failure of the interface is defined to occur when

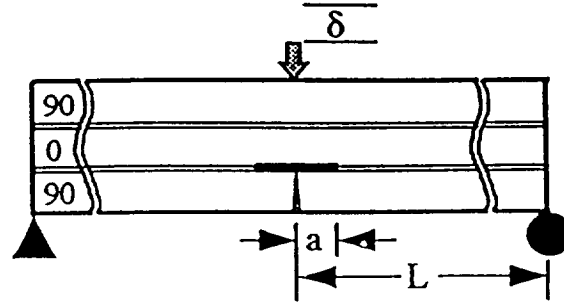
$$\frac{u_n}{t_{int}} + \sqrt{\left(\frac{u_n}{t_{int}}\right)^2 + \left(\frac{u_t}{t_{int}}\right)^2} \geq \delta_{crit} \quad (9)$$

where  $u_n$  and  $u_t$  are the normal and tangential components of the interfacial separation, respectively, and  $\delta_{crit}$  is a critical strain-like constant. The above description is similar to the phenomenological models previously proposed by Needleman [7] and Tvergaard [8]. This interfacial constitutive model is incorporated into an in-house two dimensional finite element code to facilitate the analysis [4-6]. The damage zone is modeled in a manner similar to the Dugdale-Barenblatt cohesive model [10,11]. In this code, the delamination propagates along the prescribed inter-element boundaries on which the tractions are specified by the interfacial constitutive relationship. Due to the nonlinearity introduced by the micro-cracked cohesive zone, incremental and iterative solution techniques are employed with the finite element algorithm. Delamination propagation is evaluated at each load step.

### 3. COMPUTATIONAL RESULTS

This model was applied to the analysis of low velocity impact induced delamination damage. The impact problem was modeled as a two dimensional three-point bending problem where the impact induced displacement was simulated by a monotonically increasing displacement applied at the mid-span under quasi-static conditions. The stresses in the individual layers of the laminate and the resin rich interfaces were obtained from the finite element analysis. To focus on the effects of the interface model, the mechanical properties of the individual layers were everywhere constant and linear elastic. The accumulation of micro-damage in the interface was evaluated at each displacement increment and the corresponding changes in the interfacial properties were updated for the next displacement increment. This procedure was repeated until the interface fails and the delamination advances.

The three point bending configuration shown in Fig.1 was utilized for the analysis. This laminate has a  $[90_4/0_8]_s$  stacking sequence and possess the ply level mechanical properties shown in Table 1. The interfacial parameters are listed in Table 2. Due to the low transverse strength of the lamina, a transverse matrix crack will often appear in the mid-span of the bottom  $90^\circ$  layer upon the application of the displacement. This transverse matrix crack then serves as the initiation point for the delamination at the bottom interface. In the current test case it was assumed to exist prior to any mid-span deflection. Furthermore, the damage state was assumed to be symmetric about the mid-span, thus only the right half of the span was modeled by the finite element analysis. In figure 2, the model predicted delamination evolution is shown along with the



$[90_4 / 0_8]_s$  AS4/3502

$\delta_{\max} = 0.3 \text{ in.}$      $L = 2.0 \text{ in.}$

$\lambda = 0.1e3$      $\epsilon_{\text{crit}} = 0.02$      $t_{\text{int}} = 0.85e-4$

Figure 1. Schematic of the 3-point bending test case.

Table 1. Ply Level Mechanical Properties

$E_x$	17.4 Msi	(120.0 GPa)
$E_y$	1.4 Msi	(9.8 GPa)
$E_z$	1.4 Msi	(9.8 GPa)
$G_{xy}$	0.8 Msi	(5.2 GPa)
$G_{yz}$	0.5 Msi	(3.5 GPa)
$\nu_{xy}$	0.3	
$\nu_{yz}$	0.3	

Table 2. Interfacial Model Parameters for 3-Point Bending Test Case

$E_o$	1.4 Msi	( 9.65 GPa )
$\nu_o$	0.3	
$G_o$	0.5 Msi	( 3.45 GPa )
$\delta_{\text{crit}}$	0.02 in.	( 0.51 mm )
$\lambda$	100.0	
$t_{\text{int}}$	$0.85 \times 10^{-4} \text{ in.}$	( $0.22 \times 10^{-2} \text{ mm}$ )
$\beta$	1.0	

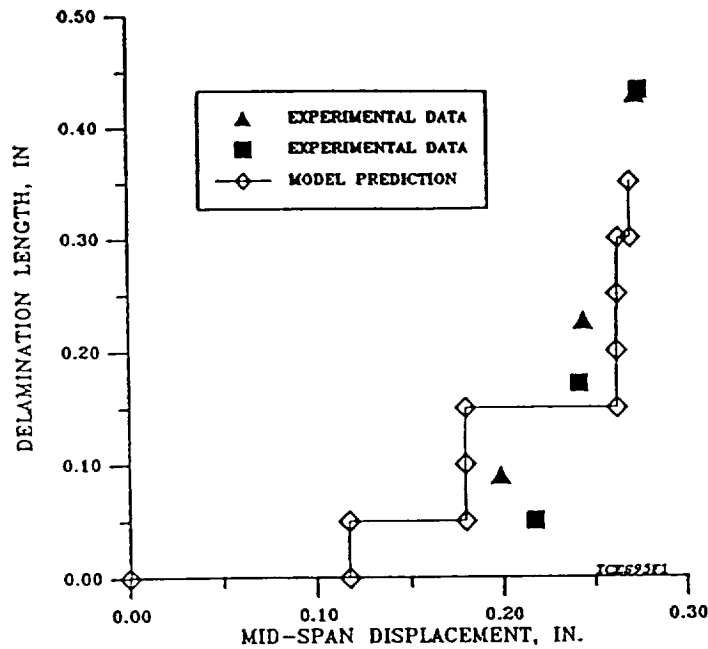


Figure 2. The accumulation of delamination damage in the  $[90_4/0_8]$  laminate.

experimental data obtained from displacement controlled three-point bend tests. Damage initiation occurred at a lower mid-span displacement than those observed experimentally. This was attributed to the prior existence of the matrix crack in the finite element model. However, the model predictions were in good agreement with the experimentally observed delamination evolution in the region of the interface away from the matrix crack. To remedy the early delamination initiation, the matrix crack can be modeled as an interface and allowed to evolve as the mid-span displacement is applied.

#### 4. CONCLUDING REMARKS

The formation of a damage zone containing micro-shear cracks and located ahead of a delamination crack is accounted for in this analysis of delamination evolution in polymeric laminated composites via a cohesive zone model. In the development of the interfacial constitutive relationship, consideration is given to the geometric characteristics of the micro-cracks. Since this interfacial relationship is based on a micro-mechanics solution that assumes the non-interaction of the micro-cracks, further investigation is required to determine the range of responses in which this assumption is valid.



## 5. ACKNOWLEDGMENT

The authors are grateful for the support provided by NASA Contract No. 32531-40960 to Texas A&M University.

## 6. REFERENCES

- [1] Bascom, W.D. and Gweon, S.Y.; "Fractography and Failure Mechanisms of Carbon Fiber-Reinforced Composite Materials," *Fractography and Failure Mechanisms of Polymers and Composites*, A.C. Roulin-Moloney, ed., Elsevier Science Publishing Co., New York, N.Y., pp. 351-385, 1989.
- [2] Chakachery, E.A. and Bradley, W.L.; "A Comparison of the Crack Tip Damage Zone for Fracture of Hexcel F185 Neat Resin and T6T145/F185 Composite," *Polymer Engineering and Science*, Vol. 27, No. 1, pp. 33-40, Mid-January, 1987.
- [3] Purslow, D.; "Matrix Fractography of Fibre-Reinforced Epoxy Composites," *Composites*, Vol. 17, No. 4, pp. 289-303, October, 1986.
- [4] Lo, D.C., Costanzo, F., Zocher, M.A., and Allen, D.H.; "Modeling of Damage Evolution in Thick Laminates Subjected to Low Velocity Impact," *Mechanics of Thick Composites*, AMD-Vol. 162, Y.D.S. Rajapakse, Ed., American Society of Mechanical Engineers, New York, 1993, pp.137-150.
- [5] Lo, D.C. and Allen, D.H.; "Modeling the Damage Evolution in Laminated Composites with Delaminations Containing a Damage Zone," *Damage Mechanics in Composites 1994*, AMD-Vol. 185, D.H. Allen and J.W. Ju, Eds., American Society of Mechanical Engineers, New York, 1994, pp.57-65.
- [6] Lo, D.C. and Allen, D.H.; "Modeling of Delamination Damage Evolution in Laminated Composites Subjected to Low Velocity Impact," submitted to the *International Journal of Damage Mechanics*.
- [7] Needleman, A.; "A Continuum Model for Void Nucleation by Inclusion Debonding," *Journal of Applied Mechanics*, Vol. 54, pp.525-531, 1987.
- [8] Tvergaard, V.; "Effects of Fibre Debonding in a Whisker-Reinforced Metal," *Materials Science & Engineering A: Structural Materials: Properties, Microstructure, and Processing*, Vol. A125, No.2, pp. 203-213, June 1 1990.
- [9] Kachanov, M.; "Effective Elastic Properties of Cracked Solids: Critical Review of Some Basic Concepts," *Applied Mechanics Review*, Vol.45, No. 8, pp. 304-335, August 1992.
- [10] Dugdale, D.S.; "Yielding of Steel Sheets Containing Slits," *Journal of the Mechanics and Physics of Solids*, Vol. 8, pp. 100-104, 1960.
- [11] Barenblatt, G.I.; "The Mathematical Theory of Equilibrium Cracks in Brittle Fracture," *Advances in Applied Mechanics*, Vol. 7, pp.55-129, 1962.

## DAMAGE EVOLUTION IN VISCOELASTIC COMPOSITES WITH DELAMINATIONS CONTAINING A PROCESS ZONE

D.C. Lo and David H. Allen  
Center for Mechanics of Composites  
Texas A&M University  
College Station, TX 77843-3141

### ABSTRACT

The development of delamination damage in a viscoelastic laminated composite is examined in this paper. Mechanical response at the ply level is obtained from micromechanics in which the matrix is assumed to possess viscoelastic behavior. This model accounts for the process zone that forms ahead of the delamination via nonlinear interfacial constitutive responses. The transformation of this process zone into a pair of delaminated surfaces is dictated by the interfacial opening displacement. Simulations of delamination evolution in cross-ply laminates subjected to displacement controlled three-point bending indicate a considerable amount of damage occurs while at constant mid-span displacement.

### INTRODUCTION

Laminated polymeric composites are susceptible to delamination damage when subjected to low velocity impact loads. This type of damage can be very detrimental to the structure as the mechanical properties can be greatly reduced. The delamination can further serve as initiators of other damage modes and can cause the catastrophic failure of the structure. In order to produce safe and efficient laminated composite structure, the capability to predict the effect of the delamination damage on the component and the subsequent response must be developed.

It has been observed that a process zone develops ahead of the delamination front. The presence of this process zone in the interface introduces nonlinearities to the interfacial response. This in turn affects the propagation of the delamination in the interface and thus the overall response of the laminate. It is therefore important to include the effects of the process zone into the delamination damage analysis. Lo and Allen [1] have accounted for the effects of the process zone in a manner similar to the Dugdale-Barenblatt cohesive model [2, 3]. The interfacial tractions ahead of the delamination followed the constitutive relationships developed by Needleman [4] and Tvergaard [5].

In these constitutive models the force normal to the interface behaves in a manner similar to the interatomic forces generated during the interatomic separation. Recently, a micromechanics based interfacial model have been employed by Lo and Allen [6]. Ladeveze approached this problem by modeling the interface explicitly in his finite element mesh. The interfacial constitutive equation employed internal damage variable to represent the damage ahead of the delamination [7]. These studies assumed that the nonlinearities reside solely in the constitutive response of the resin rich interface. In the present work, the delamination damage analysis performed by Lo and Allen [1] is extended to account for the viscoelastic responses in the surrounding plies. The motivation for including viscoelastic effects arises from the current interest in using polymer matrix composites in propulsion systems and high speed aerospace transports.

#### PROBLEM STATEMENT

The problem of a crack propagating through a linear viscoelastic body can be posed as an initial/boundary value problem by replacing the physical crack with a thin cohesive strip. This, of course, necessitates the apriori specification of the crack path. Since, it can be assumed for the current application that the crack propagates through the resin rich ply interfaces, the placement of the cohesive strips is known. With this in consideration, the initial/boundary value problem is expressed mathematically as,

$$\sigma_{ji,j} = 0 \quad (1)$$

$$\sigma_{ji} = \sigma_{ij} \quad (2)$$

$$\epsilon_{ij} = \frac{1}{2} \left( \frac{\partial u_i}{\partial x_j} + \frac{\partial u_j}{\partial x_i} \right) \quad (3)$$

$$\sigma_{ij} = \int_{-\infty}^{\tau} C_{ijkl} \frac{\partial \epsilon_{kl}}{\partial \tau} d\tau \quad (4)$$

with the following boundary conditions:

$$u_i = \hat{u}_i \quad \text{on } S_1 \quad (5)$$

$$T_i = \sigma_{ij} n_j = \hat{T}_i \quad \text{on } S_2 \quad (6)$$

$$\tilde{T}_i = \tilde{T}_i(\bar{u}) \quad \text{on } S_3 \quad (7)$$

and the following initial conditions ( $t < 0$ ):

$$u_i(x, t) = 0 \quad (8)$$

$$\sigma_{ij}(x, t) = 0 \quad (9)$$

where equations (1) and (2) are, respectively, the conservation of linear and angular momentum in which  $\sigma_{ij}$  are components of the stress tensor. The current form of these equations assumes that the body is in static equilibrium and is absent of body forces and moments. Equation (3) is the strain-displacement relation where  $\epsilon_{ij}$  are components of the infinitesimal strain tensor and  $u_i$  are the displacement components. Equation (4) is the constitutive equation for a linear viscoelastic material.  $C_{ijkl}$  are components of the relaxation modulus tensor. The tractions,  $\hat{T}_i$ , are prescribed along  $S_1$  and the

displacements,  $\hat{u}_i$ , are imposed over  $S_2$ . The cohesive strip is represented by the surface (or curve in two dimensions),  $S_3$ , where

$$S_3 = S_3^+ + S_3^- . \quad (10)$$

$S_3^+$  and  $S_3^-$  represent the upper and lower crack surfaces, respectively. Associated with these surfaces are their respective crack surface normals,  $n_{S_3}^+$  and  $n_{S_3}^-$ . In the undeformed state, these surfaces occupy the same space, but as the body deforms, these surfaces separate. The distance separating the formerly coincidental points on these surfaces is the crack opening displacement,  $\bar{u}$ . Acting on this surface,  $S_3$ , is a traction,  $\bar{T}$ , whose magnitude is a function of the crack opening displacement,  $\bar{u}$ . For time,  $t < 0$ , the body is undeformed and is free from residual stresses as indicated by the initial conditions shown in equations (8) and (9). The specific constitutive relationships for the viscoelastic body and the interfacial traction used in the current study are presented in the following sections.

#### VISCOELASTIC CONSTITUTIVE RELATIONSHIP

The relaxation moduli,  $C_{ijkl}$ , found in equation (4), represent the effective properties of a continuous fiber reinforced polymer matrix lamina. These effective viscoelastic properties were calculated by Zocher, et al. [8] using Hashin and Rosen's composite cylinders assemblage model [9]. In Zocher's approach, the fibers were assumed to be isotropic linear elastic and the matrix isotropic but linear viscoelastic. This enabled the estimation of the nine viscoelastic properties for an orthotropic material with the use of only a single constituent viscoelastic property, the matrix relaxation modulus. In this study, the matrix relaxation modulus is obtained from experimental data and is fitted with a Wiechert model for the numerical calculations. The expressions for these orthotropic viscoelastic properties can be found in reference 8.  $C_{ijkl}$  are then calculated from these nine orthotropic viscoelastic properties.

To facilitate the numerical solution of the initial/boundary value problem, the constitutive equation shown in equation (4) was rewritten in incremental form [10]. If each component of the relaxation tensor,  $C_{ijkl}$ , is fitted by a Wiechert model such that

$$C_{ijkl}(t) = C_{ijkl\infty} + \sum_{m=1}^M C_{ijklm} e^{-\frac{t}{\rho_{ijklm}}} \quad (11)$$

where

$$\rho_{ijklm} = \frac{\eta_{ijklm}}{C_{ijklm}} \quad (\text{no summation on } i,j,k,l) \quad (12)$$

in which  $\eta_{ijklm}$  is the dashpot coefficient,  $C_{ijklm}$  is the spring constant and  $M$  is the number of elements in the Wiechert model, then the incremental form of the constitutive equation is

$$\Delta\sigma_{ij} = C'_{ijkl}\Delta\epsilon_{kl} + \Delta\sigma_{ij}^R \quad (13)$$

where

$$C'_{ijkl} \equiv C_{ijkl\infty} + \frac{1}{\Delta t} \sum_{m=1}^M \eta_{ijklm} \left( 1 - e^{-\frac{\Delta t}{\rho_{ijklm}}} \right) \quad (14)$$

$$\Delta\epsilon_{kl} = \dot{\epsilon}_{kl}\Delta t \quad (15)$$

$$\Delta \sigma_{ij}^R = - \sum_{m=1}^M \left( 1 - e^{-\frac{\Delta t}{\rho_{ijklm}}} \right) S_{ijklm}(t) \quad (16)$$

in which

$$S_{ijklm}(t) = e^{-\frac{\Delta t}{\rho_{ijklm}}} S_{ijklm}(t - \Delta t). \quad (17)$$

Equation (4) is now replaced with its incremental form shown in equation (11) in the mathematical statement of the initial/boundary value problem. The derivation of equation (13) can be found in reference 10.

#### INTERFACE MODELING

The mechanical response of the resin rich interface is governed by the deformation mechanism occurring at the molecular level. These mechanisms include uncoiling and straightening of molecular chains, dislocation movement, reorientation of molecular chain segments, void formation, and chain breakage [11]. Some of these mechanisms result in the formation of micro-cracks and crazes ahead of the delamination [12-16]. Whether one or more of these dissipative mechanisms are activated will depend on such factors as molecular structure, loading rate, temperature, and processing history. Moreover, the mechanical response of the resin in the interface region may be different from that of the response measured in bulk resin specimens. The constraints imposed by the reinforcing fibers, especially when the resin is sandwiched between two plies with different fiber orientations, will alter the stress state in the resin rich region and thus suppressing some deformation mechanisms while enabling other deformation mechanisms to occur.

In the current analysis, a phenomenological constitutive model proposed by Tvergaard [5] is used to approximating the interfacial response. This interface model assumes that the normal traction exerted on the interface during purely normal separation behaves similarly to the interatomic forces during interatomic separation.

The interface surface tractions for the two dimensional case are described by

$$\bar{T}_n = \frac{27}{4} \sigma_{max} \frac{\bar{u}_n}{\delta_n} (1 - 2\lambda + \lambda^2) \quad (18)$$

$$\bar{T}_t = \alpha \frac{27}{4} \sigma_{max} \frac{\bar{u}_t}{\delta_t} (1 - 2\lambda + \lambda^2) \quad (19)$$

where

$$\lambda = \sqrt{\left( \frac{\bar{u}_n}{\delta_n} \right)^2 + \left( \frac{\bar{u}_t}{\delta_t} \right)^2} \quad (20)$$

for  $0 \leq \lambda \leq 1$ . Complete separation occurs when  $\lambda \geq 1$ .  $\bar{T}$  is the interfacial traction and  $\bar{u}$  is the interfacial displacement as mentioned previously. The subscripts  $n$  and  $t$  signify the normal and tangential components of the specific quantity, respectively.  $\sigma_{max}$  is the maximum traction acting on the interface during a purely normal separation.  $\delta$  is the characteristic length and  $\alpha$  is the ratio of the interfacial shear stiffness to the normal stiffness. When the interface is undergoing a pure normal separation, the normal component of traction increases to a value of  $\sigma_{max}$  at  $\frac{\bar{u}_n}{\delta_n} = \frac{1}{3}$  then decreases to zero at  $\frac{\bar{u}_n}{\delta_n} = 1$  as shown in Figure 1. The associated work done by this traction going from  $\frac{\bar{u}_n}{\delta_n} = 0$  to  $\frac{\bar{u}_n}{\delta_n} = 1$  is

$$W_{sep} = \frac{9}{16} \sigma_{max} \delta_n. \quad (21)$$

Needleman refers to this as the *work of separation*. Thus, a larger  $\sigma_{max}$  or  $\delta$  will result in a greater amount of energy required to fail an interface. These two parameters also control the initial stiffness of the interface as shown by the expression for the initial stiffness in the mode I opening case,

$$\left. \frac{\partial T_n}{\partial u_n} \right|_{u_n, u_t=0} = \frac{27}{7} \frac{\sigma_{max}}{\delta_n}. \quad (22)$$

If the initial stiffness and the work of separation can be determined analytically or experimentally, then the model parameters,  $\sigma_{max}$  and  $\delta$  can be calculated from equations (14) and (15). Although this data is not readily available, equations (14) and (15) are used to check whether the selected  $\sigma_{max}$  and  $\delta$  produce values for the work of separation and initial stiffness that are reasonable from the physical and computational stand point. An often encountered problem is the selection of  $\sigma_{max}$  and  $\delta$  combinations that produce high initial stiffnesses as to result in computational difficulties.

#### NUMERICAL SOLUTION PROCEDURE

The constitutive models are incorporated into an in-house finite element code to facilitate the analysis. In this code, the delamination propagates along the prescribed inter-element boundaries on which the tractions are specified by the interfacial constitutive relationship. Due to the nonlinearities introduced by the micro-cracked process zone and the viscoelastic response, the problem is solved incrementally with the virtual work equation expressed in the following form [17]:

$$\int_V C_{ijkl}^T \Delta \epsilon_{kl} \delta \Delta \epsilon_{ij} dV \cong \int_S T_i^{\tau+\Delta\tau} \delta \Delta u_i dS - \int_V \sigma_{ij}^T \delta \Delta \epsilon_{ij} dV \quad (23)$$

where  $C_{ijkl}$  is the material tangent modulus tensor calculated from equation (13) and  $\Delta u_i$  is the displacement increment vector. Also, the domain of interest has interior  $V$  and boundary  $S$ . The superscripts  $\tau$  and  $\tau + \Delta\tau$  denote quantities at time  $\tau$  (which are assumed to be known) and quantities at time  $\tau + \Delta\tau$ , respectively. The approximate nature of Equation (23) is due to the deletion of the higher order terms in  $\Delta u_i$  during the incrementalization process. To account for this approximation, a Newton-Raphson iteration scheme is employed for each increment of boundary tractions. The displacement increment is thus successively updated as follows for the  $j^{th}$  iteration:

$$\{\Delta u\}_j = \{\Delta u\}_{j-1} + \{\Delta \Delta u\}_j \quad (24)$$

where  $\{\Delta \Delta u\}_j$  is obtained by solving the following on the  $j^{th}$  iteration:

$$[K]^\tau \{\Delta \Delta u\}_j = \{F^{\tau+\Delta\tau}\} - \{R^{\tau+\Delta\tau}\}_{j-1} \quad (25)$$

where  $[K]$  is the global stiffness matrix,  $\{F\}$  is the global force matrix, and  $\{R\}$  is the global reaction matrix.

Equations (14) and (15) are solved recursively until the following convergence criterion is satisfied:

$$\frac{\|\Delta u\|_j - \|\Delta u\|_{j-1}}{\|\Delta u\|_j} \leq r_{tol} \quad (26)$$

where  $r_{tol}$  is a user specified convergence tolerance and the quantities bracketed by the double vertical bars are the Euclidean norms.

## ANALYSIS OF DELAMINATION DAMAGE

To gain a better understanding on how viscoelastic behavior affected the low velocity impact induced damage process, the computational simulation was set up to mimic conditions encountered by the laminate during the low velocity impact event. The three point bending problem, shown in Figure 2, was considered in the analysis of delamination evolution in a laminated composite. This laminate had a  $[0_6/90_3]$ , stacking sequence and possessed the fiber and matrix properties shown in Table 1. Listed in Table 2 are the interfacial parameters for Tvergaard's model. The viscoelastic results presented in this section corresponded to the mid-span displacement history shown in Figure 3. During the ramp up portion, the mid-span was displaced at 0.001 inches per second for the first 100 seconds to produce a maximum mid-span displacement of 0.1 inches. Following this ramp up, the mid-span displacement was held at 0.1 inches until the simulation ended at  $t=10000$  seconds. For comparative purposes, the delamination evolution responses were also generated for the same laminate but with linear elastic behavior at the ply level. The mid-span displacement in these cases was increased at a rate of 0.001 inches per second until a displacement of 0.1 inches was achieved. This was identical to the ramp-up portion of the mid-span displacement history used in the viscoelastic case. In the finite element mesh, a transverse matrix crack was positioned at the mid-span of the bottom  $90^\circ$  layer to serve as the initiation point at the bottom  $0/90$  interface. Since the damage state was assumed to be symmetric about the mid-span, only the right half of the span was modeled in the analysis. Finally, a state of plane strain was assumed in the calculations with the predicted interface opening displacements used in the determination of delamination propagation.

Shown in Figure 4 is the predicted delamination evolution in the bottom interface of the viscoelastic laminate. In this case, where the interfacial shear stiffness to normal stiffness ratio,  $\alpha$ , was 0.15, no delamination damage was predicted in the upper  $0/90$  interface. Furthermore, the results indicated that the majority of the delamination evolution occurred after the maximum displacement has been reached. Two third of the final delamination length was attributed to propagation during the constant mid-span displacement period. The small amount of damage development during the ramp-up displacement was in contrast to the linear elastic results shown in Figure 5. At the point when the maximum displacement was reached ( $t=100$  sec.), the delamination in the elastic laminate was twice the length of the delamination predicted in the viscoelastic laminate. However, the delamination for the viscoelastic case grew during the constant mid-span displacement period and eventually exceeded the length predicted for the elastic case. When the interfacial shear stiffness to normal stiffness ratio,  $\alpha$ , was reduced to 0.125, a comparable amount of delamination damage was predicted in the bottom interface at  $t=100$  seconds for both the viscoelastic and elastic cases. This is illustrated in Figures 6 and 7, respectively. Once again no damage was predicted in the upper interface. Subsequent delamination growth during the constant mid-span displacement period in the viscoelastic laminate resulted in the final delamination length being almost twice that of the elastic case.

## DISCUSSION

The results presented above illustrates the effects that stress redistribution can have on the damage evolution. For the viscoelastic cases, the mechanism for stress redistribution is due primarily to the relaxation of the viscoelastic matrix and the accumulation of damage. It is possible, for the example shown in Figure 4, that the stress relieve due to relaxation near the delamination front operating in conjunction with the nonlinear response of the interface hindered the advancement of the delamination during the displacement ramp-up period. On the structural scale, the shift of load due to relaxation

from the matrix dominated plies to the fiber dominated ones may have assisted damage evolution during the constant mid-span displacement time period. From the preliminary results presented here, it appears that under certain circumstances, the viscoelastic effects cannot be neglected in the analysis. This is exemplified by the case where the interfacial shear stiffness to normal stiffness ratio was equal to 0.15. In this case, the delamination predicted by assuming ply level viscoelastic response was initially less than the elastic results, but with time, the delamination in the viscoelastic laminate actually exceeded the elastic prediction.

In the performance of this analysis, several assumptions were taken concerning the constitutive response of the lamina and the resin rich interface. One assumption is the elastic response of the reinforcing fibers. While this may be a reasonable assumption in the axial direction of the fiber, there could be a noticeable amount of viscoelastic response in the radial direction [18]. The absence of time dependence in the interfacial constitutive model is another area that warrants further examination. These are some of the issues that will be addressed in the continue development of this model.

#### REFERENCES

- [1] Lo, D.C. and Allen, D.H.; "Modeling of Delamination Damage Evolution in Laminated Composites Subjected to Low Velocity Impact," *International Journal of Damage Mechanics*, Vol. 3, pp. 378-407, October, 1994.
- [2] Dugdale, D.S.; "Yielding of Steel Sheets Containing Slits," *Journal of the Mechanics and Physics of Solids*, Vol. 8, pp. 100-104, 1960.
- [3] Barenblatt, G.I.; "The Mathematical Theory of Equilibrium Cracks in Brittle Fracture," *Advances in Applied Mechanics*, Vol. 7, pp.55-129, 1962.
- [4] Needleman, A.; "A Continuum Model for Void Nucleation by Inclusion Debonding," *Journal of Applied Mechanics*, Vol. 54, pp.525-531, 1987.
- [5] Tvergaard, V.; "Effects of Fibre Debonding in a Whisker-Reinforced Metal," *Materials Science & Engineering A: Structural Materials: Properties, Microstructure, and Processing*, Vol. A125, No.2, pp. 203-213, June 1 1990.
- [6] Lo, D.C. and Allen, D.H.; "Modeling the Damage Evolution in Laminated Composites with Delaminations Containing a Damage Zone," *Damage Mechanics in Composites, 1994*, ASME, AD-Vol.185, pp. 57-72, 1994.
- [7] Ladeveze, P.; "A Damage Computational Method for Composite Structures," *Computers & Structures*, Vol. 44, No. 1/2, pp. 79-87, 1992.
- [8] Zocher, M.A., Allen, D.H., and Groves, S.E.; "Analysis of the Effects of Matrix Cracking in a Viscoelastic Composite at Elevated Temperature," to appear in the volume "1994 Proceedings of the 9<sup>th</sup> Conference of the American Society for Composites."
- [9] Hashin, Z. and Rosen, B.W.; "The Elastic Moduli of Fiber-Reinforced Materials," *Journal of Applied Mechanics*, Vol.31, No.2, 1964, pp. 223-232.
- [10] Zocher, M.A.; "A Three Dimensional Finite Element Evaluation of Linear Viscoelastic Composites With Particular Reference to Matrix Cracking," *Texas A&M University Dissertation*, 1995.
- [11] Kausch, H.H.; *Polymer Fracture*, Springer-Verlag, New York, 1987.
- [12] Gilbert, D.G., Beaumont, P.W.R., and Nixon, W.C.; "Direct Observations of the Micromechanisms of Fracture in Polymeric Solids Using the Scanning Electron Microscope," *Mechanical Behaviors of Materials-IV, ICM4*, Vol. 2, pp. 705-710, 1983.



- [13] Purslow, D.; "Matrix Fractography of Fibre-Reinforced Thermoplastics, Part 1. Peel Failures," *Composites*, Vol. 18, No. 5, pp. 365-374, November, 1987.
- [14] Purslow, D.; "Matrix Fractography of Fibre-Reinforced Thermoplastics, Part 2. Shear Failures," *Composites*, Vol. 19, No. 2, pp. 115-126, March, 1988.
- [15] Bascom, W.D. and Gweon, S.Y.; "Fractography and Failure Mechanisms of Carbon Fiber-Reinforced Composite Materials," *Fractography and Failure Mechanisms of Polymers and Composites*, A.C. Roulin-Moloney, ed., Elsevier Science Publishing Co., New York, N.Y., pp. 351-385, 1989.
- [16] Chakachery, E.A. and Bradley, W.L.; "A Comparison of the Crack Tip Damage Zone for Fracture of Hexcel F185 Neat Resin and T6T145/F185 Composite," *Polymer Engineering and Science*, Vol. 27, No. 1, pp. 33-40, Mid-January, 1987.
- [17] Jones, R.; "Micromechanical Analysis of Inelastic Composite Behavior Including the Effects of Matrix Viscoplasticity and Evolving Damage," *Texas A&M University Master's Thesis*, 1992.
- [18] Dillard, D.A.; "Viscoelastic Behavior of Laminated Composite Materials," in *Fatigue of Composite Materials*, K.L. Reifsnider, ed., Elsevier Science Publishers, pp. 339-384. 1990.

Table 1. Lamina Elastic and Viscoelastic Constituent Properties

Fiber:		
$E_f$		$0.40 \times 10^8 \text{ psi}$
$\nu_f$		0.3
$V_f$		0.6
Matrix (Elastic):		
$E_m$		$0.14 \times 10^7 \text{ psi}$
$\nu_m$		0.3
$V_m$		0.4

Matrix (Viscoelastic): Parameters for 11 element Wiechert model		
$E_\infty$	$0.48 \times 10^5 \text{ psi}$	
$i$	$E_{m_i}, \text{ psi}$	$\eta_{m_i}, \frac{\text{sec}}{\text{psi}}$
1	$0.44 \times 10^4$	$0.87 \times 10^2$
2	$0.90 \times 10^4$	$0.18 \times 10^4$
3	$0.19 \times 10^5$	$0.38 \times 10^5$
4	$0.39 \times 10^5$	$0.78 \times 10^6$
5	$0.78 \times 10^5$	$0.16 \times 10^8$
6	$0.14 \times 10^6$	$0.28 \times 10^9$
7	$0.20 \times 10^6$	$0.41 \times 10^{10}$
8	$0.22 \times 10^6$	$0.44 \times 10^{11}$
9	$0.18 \times 10^6$	$0.37 \times 10^{12}$
10	$0.11 \times 10^6$	$0.21 \times 10^{13}$
11	$0.81 \times 10^5$	$0.16 \times 10^{14}$

Table 2. Interfacial Model Parameters Used in Test Cases.

$\sigma_{maz}$	$0.50 \times 10^3 \text{ psi}$
$\delta_n, \delta_t$	$0.15 \times 10^{-4} \text{ in.}$
$\alpha$ (case A)	0.150
$\alpha$ (case B)	0.125

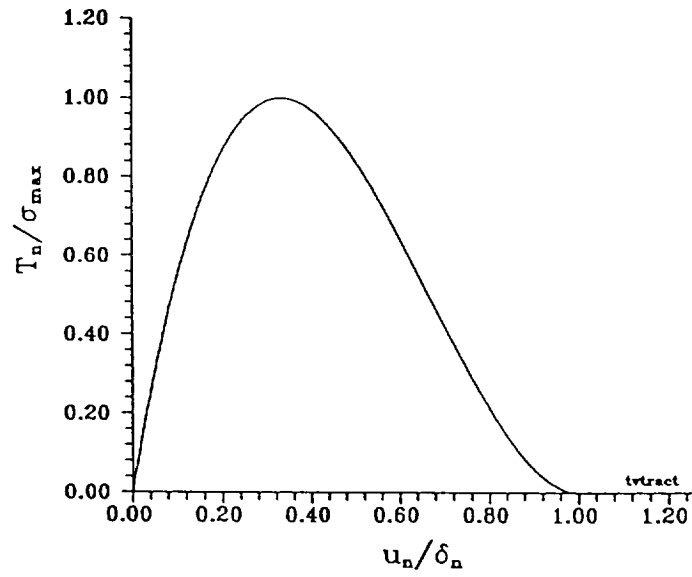
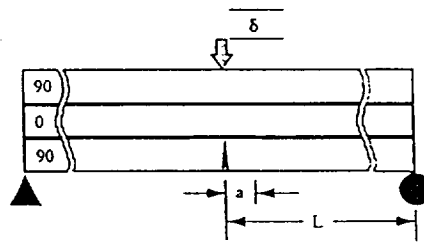


Figure 1. The response of the normal interfacial traction force to the normal separation of the interface as model by Tvergaard [5].

### DELAMINATION SPECIMEN GEOMETRY



$[90_6 / 0_3]_s$

$\delta = 0.10$  in.  $L = 2.0$  in.

$\sigma_{max} = 0.50e3$  psi.  $\alpha = 0.15$   $\delta = 1.50e-5$  in.

Figure 2. Schematic showing the geometry of the three point loaded  $[0_6/90_3]_s$  laminate used in the analysis.

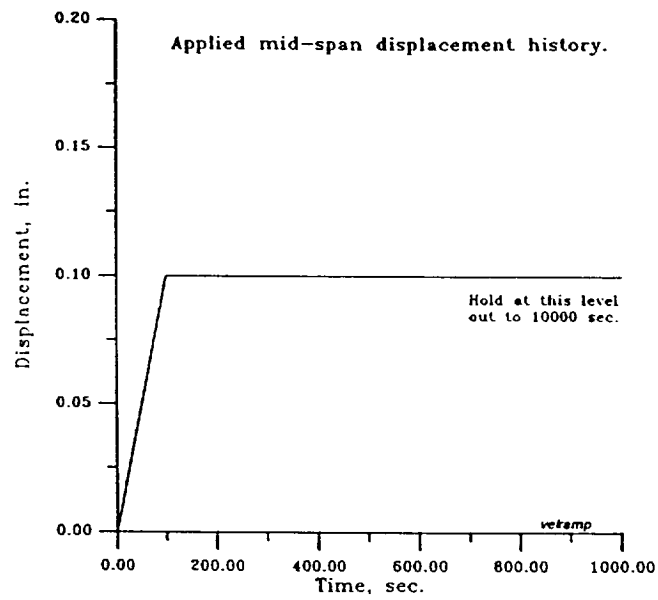


Figure 3. Mid-span displacement input used in the three point bending viscoelastic test cases.

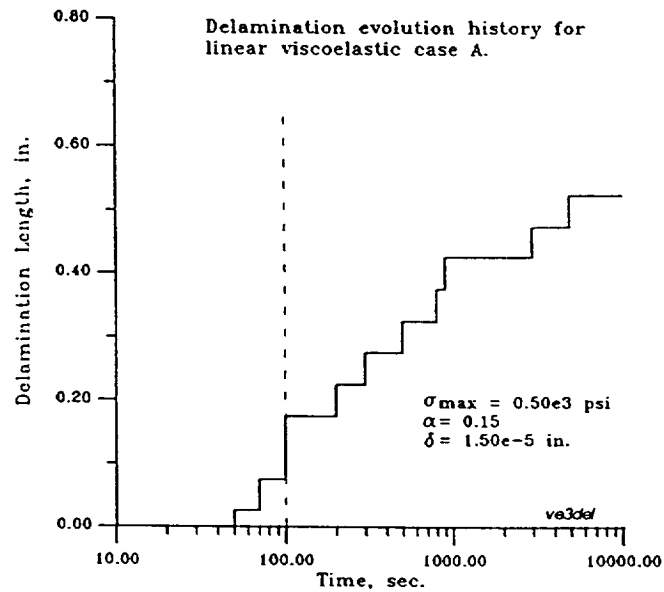


Figure 4. Accumulation of delamination damage in the bottom interface of the viscoelastic  $[90_6/0_3]$  laminate with an interfacial shear stiffness to normal stiffness ratio of 0.15.

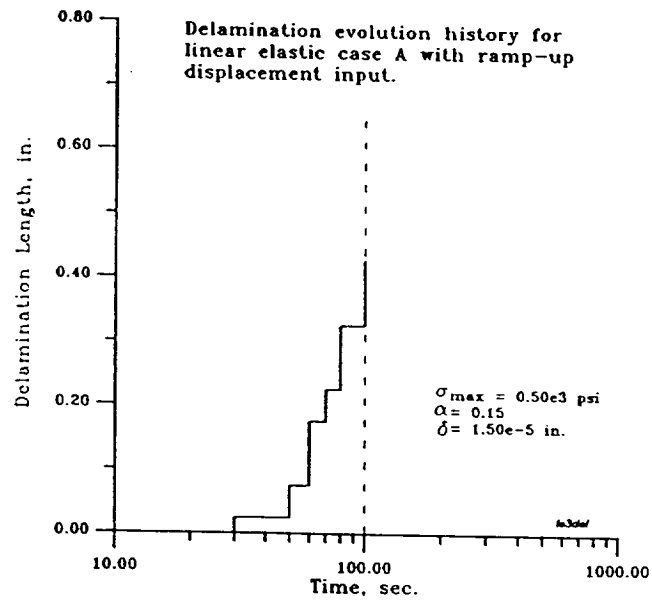


Figure 5. Delamination damage accumulation in the bottom interface of the elastic  $[90_6/0_3]$  laminate with an interfacial shear stiffness to normal stiffness ratio of 0.15 .

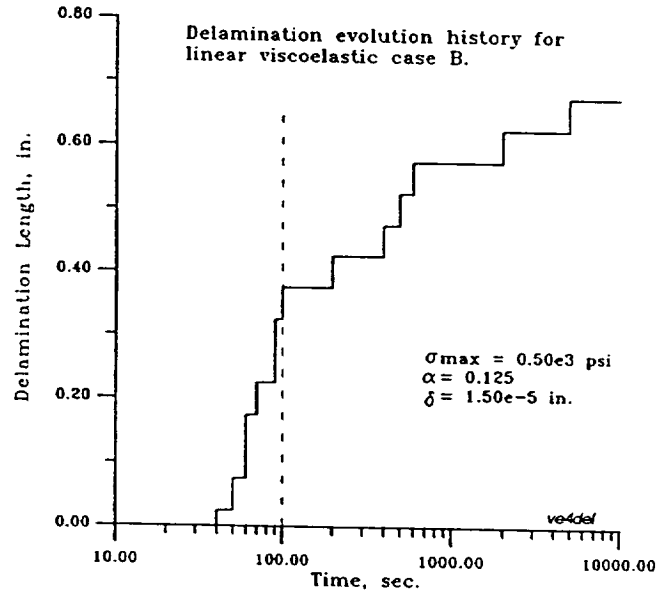


Figure 6. Accumulation of delamination damage in the bottom interface of the viscoelastic  $[90_6/0_3]$  laminate with an interfacial shear stiffness to normal stiffness ratio of 0.125 .

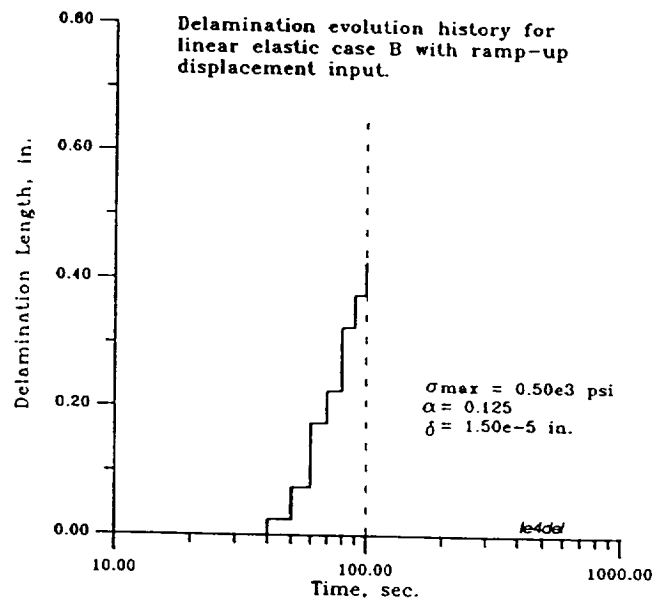


Figure 7. Delamination damage accumulation in the bottom interface of the elastic  $[90_6/0_3]$  laminate with an interfacial shear stiffness to normal stiffness ratio of 0.125 .

## **APPENDIX B**

```

*****
C
C
C      Delamination Analysis with Nonlinear COhesive Model
C      (DANCOM)
C
*****
C  MODIFIED TO INCLUDE DISPLACEMENT BOUNDARY CONDITIONS
C
C  ALSO MODIFIED TO PLANE STRAIN CONDITIONS
C
C  Routine to store force-displacement data added on March 9, 1994
C  by David Lo
C
C  Modified for non-zero displacement boundary conditions by
C  David Lo on April 18, 1994
C
C  Add modified Kachanov's model to interface constitutive module
C  by David Lo on June 9, 1994
C
*****
      REAL*8  FGL(2400),DS(1500,4),DE(1500,3),
1            Q(2400),DST(1500,4),DET(1500,3),KG(2400,600),
2            FG(2400),FORCE(2400),DN(500),DT(500)
      COMMON/ELAS1/S(1500,4),E(1500,3),EO(1500,3),DSTRAN(3),
1            DSTRES(4)
      COMMON/PLAS1/ALPHA(4,1500),EPBAR(1500),SIGBAR(1500),
1            IPLAS(1500),EPSP(1500,4),DEPSPT(1500,4),
2            DEPS(1500,4)
      INTEGER NODE(1500,3),NDOF(1500)
      COMMON/CHIST/RTOL,NN,NEL,NF,NDBC,IDUMP,IPRI,ISREF,
1            IEQUIT,ITEMAX,ITEMP,IINT
      COMMON/AREA2/NODE,NDOF
      COMMON/AREA4/Q
      COMMON/AREA7/NSTE,INCR,ITER
      COMMON/AREA10/DST,DET
      COMMON/LOAD/TIMV(1,1000),RV(1,1000),INODE(100),ICURVE(100),
1            DINC(1000),DPMINC(1000),DMULT(1,1000)
      COMMON/BANDED/MAXBW
      COMMON/HOMOG/SIG1AV,DEBAR11
CX      COMMON/INTFAC/NINT1,NINT2,SIGMAX,DELTA,ALPH,DBFAC,DN,DT,ETA
      COMMON/INTFAC/NIFEM,NIFGP,ITGPL(10,2),ITCON(500,2),
1            SIGMAX(10),DELTAN(10),DELTAT(10),ALPH(10),
2            ETA(10),DBFAC(10),DN,DT,INTDF(500),INTSP(500),
3            RMU(10),DISPN(500),DISPT(500),TNRATIO(500),
4            XRHO(500),SIGNN(500),TAUNT(500),FN(500),FT(500)
      COMMON/MODPARA/RMP1(10),RMP2(10),RMP3(10),RMP4(10),RMP5(10),
1            RMP6(10),RMP7(10),RMP8(10),RMP9(10),RMP10(10)
      COMMON/VPLAS1/DTIME,DEVPAI
      COMMON/DISPHIS/DELTAQ(2400),WORKN(500),WORKT(500),FSEPN(500),
1            FSEPT(500)
      COMMON/IPRISIG/ISELSIG,NUMSELSIG,MSELSIG(100)
C  INPUT DATA AND PRINT
      DTIME=1.0
      CALL INPUT(FGL,NSTE)
      CALL BANWD(2,NEL,NODE,2,MAXBW,1)
C  INITIALIZE DISPLACEMENTS
      NTOT=2*NN
      DO 100 I=1,NTOT
100 Q(I)=0.
C  INITIALIZE STRESS, STRAIN, AND INTERFACE TRACTIONS
      DO 44 I=1,NEL
      S(I,4)=0.
      EPSP(I,4)=0.
      DO 44 J=1,3
      S(I,J)=0.
      E(I,J)=0.
      EO(I,J)=0.0
      EPSP(I,J)=0.
44 CONTINUE
      DO 5500 I = 1, 500
      XRHO(I) = 0.0
      WORKN(I) = 0.0
      WORKT(I) = 0.0
      FSEPN(I) = 0.0
      FSEPT(I) = 0.0
      FN(I) = 0.0
      FT(I) = 0.0
5500 CONTINUE
C      SET GLOBAL FORCE MATRIX EQUAL TO A TEMPORARY VALUE USED TO

```



```

C     EVALUATE THE INCREMENTAL LOADS.....
DO 50 I=1,NTOT
50  FORCE(I)=FGL(I)
    IF(IDUMP.NE.1) GO TO 85
    WRITE(6,4400)
4400  FORMAT(/,10X,'STEP NO.',5X,'TIME',5X,
1'SIG11AV',5X,'EPS11AV',/)
85  CONTINUE
C THIS LOOP INCREMENTS THE LOAD
    TIME=0.
    EBAR11=0.
    DO 9999 INCR=1,NSTE
    EBAR11=EBAR11+DEBAR11
    TIME=TIME+DTIME
C DETERMINE GLOBAL LINEAR STIFFNESS MATRIX
DO 39 I=1,NEL
DST(I,4)=0.
DS(I,4)=0.
DEPSPT(I,4)=0.
DEPSP(I,4)=0.
DO 39 K=1,3
DST(I,K)=0.
DS(I,K)=0.
DEPSPT(I,K)=0.
DEPSP(I,K)=0.
39  DET(I,K)=0.
    CALL KGLOB(KG,NODE,NTOT,NDOF)
    ITER=1
C PERFORM NEWTON-RAPHSON ITERATION ON EACH LOAD INCREMENT IF
C SOLUTION IS NONLINEAR
C     INCREMENT THE LOADS HERE
    IF(NF.EQ.0) GO TO 240
    DO 239 I=1,NF
    K=ICURVE(I)
    L=INCR
    NN1=2*INODE(I)-1
    NN2=NN1+1
    FGL(NN1)=FORCE(NN1)*RV(K,L)
    FGL(NN2)=FORCE(NN2)*RV(K,L)
239  CONTINUE
240  CONTINUE
CX
    IF ( NDBC .EQ. 0 ) GO TO 243
    DO 242 I = 1, NDBC
CX
CX
CX
        K = ICURVE(I)
        K = 1
        L = INCR
        DPMINC(I) = DINC(I) * DMULT(K,L)
CX
CX 1234    WRITE(6,1234) L,I,DPMINC(I)
CX      +    FORMAT(/,'INCR = ',I5,5X,'NUMDBC = ',I5,5X,'DPMINC(I) = ',
        F14.5,/)
242  CONTINUE
243  CONTINUE
CX
9000  CONTINUE
DO 9010 J=1,NTOT
FG(J)=0.0
9010  CONTINUE
    IF(IDUMP.LT.2) GO TO 3004
CX
    WRITE(6,3010) INCR
3010  FORMAT(/,10X,'LOAD INCREMENT NUMBER ',I6,/)
CX
    WRITE(6,3002) ITER
3002  FORMAT(25X,'ITERATION NUMBER',I6,/)
3004  CONTINUE
C DETERMINE GLOBAL FORCE MATRIX
    CALL FGLOB(FGL,FG,NTOT,S)
C DETERMINE GLOBAL STIFFNESS MATRIX IF UPDATING
    IFLAG=1
    IF(ITER.EQ.1) GO TO 99
    ISQUIG=(ITER-1)/ISREF*ISREF
    IF(ISQUIG.NE.ITER-1) GO TO 98
    CALL KGLOB(KG,NODE,NTOT,NDOF)
98  CONTINUE
    IF(ITER.LT.ITEMAX) GO TO 99
    WRITE(6,3003)
3003  FORMAT(' ',3X,'SOLUTION HAS NOT CONVERGED',/)

```

```

      STOP
C SOLVE FOR DISPLACEMENT INCREMENTS USING GAUSS ELIMINATION
  99 CONTINUE
    CALL BANSOL(KG,FG,NTOT,MAXBW,2400,600,3)
    DO 87 I=1,NTOT
      87 DELTAQ(I)=FG(I)
C CHECK DISPLACEMENT INCREMENTS FOR CONVERGENCE
    VOLD=0.
    VNEW=0.
    DO 88 I=1,NTOT
      VOLD=VOLD+DELTAQ(I)**2
      Q(I)=Q(I)+DELTAQ(I)
    88 VNEW=VNEW+Q(I)**2
    VOLD=(VOLD)**0.5
    VNEW=(VNEW)**0.5
C CALCULATE STRESSES AND STRAINS
    CALL STRESS(NODE,DS,DE,DELTAQ)
    FRAC=VOLD/VNEW
    IF(FRAC.LT.0.) FRAC=-FRAC
    IF(FRAC.LT.RTOL) GO TO 887
    ITER=ITER+1
    IF(IDUMP.LT.2) GO TO 777
    WRITE(6,6001)
  6001 FORMAT(/,10X,'THE ESTIMATED DISPLACEMENTS ARE',/,5X,
1'NODE NO.',13X,'A1',13X,'A2',/)
    DO 739 I=1,NN
      I2M1=2*I-1
      I2=2*I
    739 WRITE(6,1004) I,Q(I2M1),Q(I2)
    ISIGP=1
CX   IF(ISIGP.NE.1) GO TO 777
CX   WRITE(6,740)
CX   740 FORMAT(' ',3X,'THE ESTIMATED STRESSES ARE',/,
CX   12X,'ELEMENT NO.',6X,'SIG-XX',6X,'SIG-YY',
CX   26X,'SIG-XY',6X,'SIG-ZZ',/)
CX   DO 741 I=1,NEL
CX   WRITE(6,742) I,S(I,1),S(I,2),S(I,3),S(I,4)
CX   742 FORMAT(' ',8X,I3,4(1X,E14.7),/)
CX   741 CONTINUE
    777 CONTINUE
    GO TO 9000
  887 CONTINUE
CY
CY   DO 772 I=1,NIFEM
CY   WRITE(6,771) INCR,I, XRH0(I)
CY   771 FORMAT(5X,'INCR= ',I5,5X,'INTF. ELEM. NUM.: ',I5,5X,'XRHO= ',E14.7)
CY   772 CONTINUE
CY
CY
CX
C STORE DATA FOR FORCE-DISPLACEMENT PLOT
C STRESSES FROM SELECTED ELEMENTS ARE RECORDED
C FOR LATER CONVERSION TO TRACTION FORCES
CX
CX   IF ( ISEL SIG .EQ. 0 ) GO TO 888
CX
CX   IF ( INCR .EQ. 1 ) THEN
    WRITE(8,8000)
  8000 FORMAT(/,5X,'LOAD STEP',2X,'ELEM',7X,'SXX',10X,'SYY',10X,'SXY',
1      10X,'SZZ',/)
    ENDIF
    SSUM1 = 0.0
    SSUM2 = 0.0
    SSUM3 = 0.0
    SSUM4 = 0.0
    DO 8005 IJ = 1, NUMSEL SIG
      IENUM = MSEL SIG(IJ)
      SSUM1 = SSUM1 + S(IENUM,1)
      SSUM2 = SSUM2 + S(IENUM,2)
      SSUM3 = SSUM3 + S(IENUM,3)
      SSUM4 = SSUM4 + S(IENUM,4)
CY   WRITE(8,8001) INCR, IENUM, S(IENUM,1), S(IENUM,2), S(IENUM,3),
CY   1      S(IENUM,4)
CY   8001 FORMAT(5X,I5,5X,I5,5X,4(2X,E12.5))
    8005 CONTINUE
    WRITE(8,8011) INCR, SSUM1, SSUM2, SSUM3, SSUM4
  8011 FORMAT(10X,I5,10X,4(2X,E12.5))
CX
  888 CONTINUE
CX

```

```

CXXXXXXXXXXXXXXXXXXXXXXXXXXXXXXXXXXXXXXXXXXXXXXXXXXXXXXXXXXXXXXXXXXXXX
CX
C      Routine to store damaged interface data
C
C      open and initialize data file "intf.out"
C
  IF ( INCR .EQ. 1 ) THEN
    OPEN (7,FILE='kintf.out',STATUS='UNKNOWN')
    WRITE(7,537) INCR
537    FORMAT(/,5X,'INCREMENT NUMBER ',I5,/)
    DO 540 I = 1, NIFGP
      DO 540 J = ITGPL(I,1), ITGPL(I,2)
        IA = 0
        IB = 0
        LN = 0
        SPN = 0.0
        SPT = 0.0
        TNRAT = 0.0
        WRITE(7,535) I, J, LN, IA, IB, SPN, SPT, TNRAT
540    CONTINUE
      REWIND 7
    ELSE
      REWIND 7
    ENDIF
C
C      check for failure and assign damage flags and load step
C
C      INTDF(I) = 1, tensile failure
C      INTDF(I) = 2, shear failure
C
    WRITE(7,537) INCR
    DO 530 J = 1, NIFGP
CX
C      ASSIGN VARIABLES FOR KACHANOV'S MODEL
C
      EO = SIGMAX(J)
      RNU = DELTAN(J)
      GO = DELTAT(J)
      ESPCRIT = ALPH(J)
      RLAMBDA = ETA(J)
      RL = DBFAC(J)
      RBETA = RMU(J)
C      CHANGE EO AND RNU TO PLANE STRAIN CONDITIONS
      EO = EO / ( 1.0 - (RNU**2) )
      RNU = RNU / ( 1.0 - RNU )
CX
      LN = 0
      DO 530 I = ITGPL(J,1), ITGPL(J,2)
        LN = LN + 1
        DISP = 0.0
        DISPT = 0.0
        TNRATIO = 0.0
        IF ( DN(I)/DELTAN(J) .LE. 1 ) GO TO 531
        IF ( INTDF(I) .EQ. 0 ) THEN
          INTDF(I) = 1
          INTSP(I) = INCR
          DISP = DN(I)
          DISPT = DT(I)
          TNRATIO = DT(I) / DN(I)
        ENDIF
CX 531      CONTINUE
        IF ( ALPH(J) .LT. 0.001 ) GO TO 532
        IF ( DABS(DT(I))/DELTAT(J) .LE. 1 ) GO TO 532
        IF ( INTDF(I) .EQ. 0 ) THEN
          INTDF(I) = 2
          INTSP(I) = INCR
          DISP = DN(I)
          DISPT = DT(I)
          TNRATIO = DT(I) / DN(I)
        ENDIF
CX 532      CONTINUE
      RLSQ = ( (DN(I)/RL) / 2.0 )**2 + ( (DT(I)/RL) / 2.0 )**2
      RLAM = SQRT( RLSQ )
      UM1 = (DN(I)/RL) / 2.0 + RLAM
      UM2 = (DN(I)/RL) / 2.0 - RLAM
      UMAX = DMAX1( UM1, UM2 )
      IF ( UMAX .GT. ESPCRIT ) THEN
        IF ( INTDF(I) .NE. 3 ) THEN
          INTDF(I) = 3
          INTSP(I) = INCR

```

```

        DISPN(I) = DN(I)
        DISPT(I) = DT(I)
        TNRATIO(I) = DT(I) / DN(I)
        TNRATIO(I) = ABS( TNRATIO(I) )
    ENDIF
ENDIF
C
C      STORE DATA: GROUP NUM., ELEMENT NUM., DAMAGE FLAG, FAILURE STEP
C
        WRITE(7,535) J, I, LN, INTDF(I), INTSP(I),
        DISPN(I), DISPT(I), TNRATIO(I)
535      FORMAT(5(2X,I5),3(2X,E14.7))
C
530 CONTINUE
CX
CXXXXXXXXXXXXXXXXXXXXXXXXXXXXXXXXXXXXXXXXXXXXXXXXXXXXXXXXXXXXXXXXXXXXXXXXXXXX
CX
CXXXXXXXXXXXXXXXXXXXXXXXXXXXXXXXXXXXXXXXXXXXXXXXXXXXXXXXXXXXXXXXXXXXXXXXXXXXX
CX
C      Routine to store work of separation data
C
C      open and initialize data file "kwork.out"
C
    IF ( INCR .EQ. 1 ) THEN
        OPEN (9,FILE='kwork.out',STATUS='UNKNOWN')
        WRITE(9,9537) INCR
9537      FORMAT(/,5X,'INCREMENT NUMBER ',I5,/)
        DO 9540 I = 1, NIFGP
            DO 9540 J = ITGPL(I,1), ITGPL(I,2)
                IA = 0
                IB = 0
                WOSN = 0.0
                WOST = 0.0
                WOSTOT = 0.0
                WRITE(9,9535) I, J, WOSN, WOST, WOSTOT
9540      CONTINUE
            REWIND 9
        ELSE
            REWIND 9
        ENDIF
C
        WRITE(9,9537) INCR
        DO 9530 J = 1, NIFGP
CX
            DO 9530 I = ITGPL(J,1), ITGPL(J,2)
C
C      STORE DATA: GROUP NUM., ELEMENT NUM., WORK OF SEPARATION
C
                WOSTOT = WORKN(I) + WORKT(I)
                WRITE(9,9535) J, I, WORKN(I), WORKT(I),
                WOSTOT
1          9535      FORMAT(2(2X,I5),3(2X,E14.7))
C
9530 CONTINUE
CX
CXXXXXXXXXXXXXXXXXXXXXXXXXXXXXXXXXXXXXXXXXXXXXXXXXXXXXXXXXXXXXXXXXXXXXXXXXXXX
CX
CX      IF(IDUMP.EQ.1) GO TO 84
CX      IF(INCR/IPRI*IPRI.NE.INCR) GO TO 9999
CX      WRITE(6,3001) INCR,ITER
3001      FORMAT(/,5X,'EQUILIBRIUM FOR LOAD STEP NUMBER ',I6,
1' OBTAINED AFTER ',I6,' ITERATIONS',/)
CX
CX      temporarily disabled
CX
CX      WRITE(6,1032) SIG1AV,EBAR11
CX 1032      FORMAT(/,10X,'SIG1AV=',E14.7,1X,'EBAR11 = ',E14.7,/)
CX      WRITE(6,1003)
1003      FORMAT(/,10X,'THE DISPLACEMENTS ARE ',/,5X,'NODE NO.',13X,
1'A1',13X,'A2',/)
        DO 93 I=1,NN
93      WRITE(6,1004) I,Q(2*I-1),Q(2*I)
1004      FORMAT(10X,I3,2(1X,E14.7))
CX      WRITE(6,1011)
CX 1011      FORMAT(/,2X,'ELE. NO.',3X,'SIGMA11',3X,'EPSILON11',3X,
CX      1'SIGMA22',3X,'EPSILON22',3X,'SIGMA12',3X,'EPSILON12',3X,
CX      2'SIGMA33',/)
CX      DO 1012 I=1,NEL
CX      WRITE(6,1013)I,S(I,1),E(I,1),S(I,2),E(I,2),S(I,3),E(I,3),
CX      1S(I,4)

```

```

CX 1012 CONTINUE
CX 1013 FORMAT(' ',5X,I3.7(E14.7,1X))
CX      IF(IDUMP.NE.O) GO TO 1041
CX      WRITE(6,4011)
CX 4011 FORMAT(/,2X,'ELEMENT NO.',3X,10X,'EPSP11',
CX      110X,'EPSP22',10X,'EPSP12',10X,'EPSP33',/)
CX      DO 4012 I=1,NEL
CX      WRITE(6,4013)I,EPSP(I,1),EPSP(I,2),EPSP(I,3),EPSP(I,4)
CX 4013 FORMAT(' ',6X,I3.7X,4(E13.6,2X))
CX 4012 CONTINUE
CX 1041 CONTINUE
CX
CX      end here
CX      IF(IINT.EQ.O) GO TO 9999
CX
CX      WRITE(6,4500)
CX 4500 FORMAT(/,10X,' THE INTERFACE DISPLACEMENTS ARE',/,
CX      15X,'NORMAL COMP.',5X,'TANGENTIAL COMP.',/)
CX      NUM=NINT2-NINT1+1
CX      DO 229 I=1,NUM
CX      WRITE(6,4501) DN(I),DT(I)
CX 4501 FORMAT(5X,E15.7,1X,E15.7)
CX 229 CONTINUE
CX      LLL=NINT1
CX      DO 230 I=1,NUM
CX      IF(DN(I)/DELTA.LE.1.) GO TO 231
CX      WRITE(6,4502) INCR,LLL
CX 4502 FORMAT(/,5X,'STEP NO. ',I5,1X,
CX      1'NODE NO.',I3,' DEBONDED IN TENSION',/)
CX 231 CONTINUE
CX      IF(ALPH.LT..001) GO TO 232
CX      IF(DABS(DT(I))/DELTA.LE.1) GO TO 232
CX      WRITE(6,4503) LLL,INCR
CX 4503 FORMAT(/,5X,'STEP NO. ',I5,1X,
CX      1'NODE NO.',I3,' DEBONDED IN SHEAR',/)
CX 232 CONTINUE
CX      LLL=LLL+1
CX 230 CONTINUE
CX
CX      DO 229 J = 1, NIFGP
CX      WRITE(6,5000) J
5000      FORMAT(/,,' INTERFACE ELEMENT GROUP NO. ',I5,/)
CX      WRITE(6,5050)
5050      FORMAT(10X,' THE INTERFACE DISPLACEMENTS ARE:',/,
CX      1      5X,'INTRF. ELEM. NO.',5X,'NORMAL COMP.',5X,
CX      2      'TANGENTIAL COMP.',/)
CX      DO 229 I = ITGPL(J,1), ITGPL(J,2)
CX      WRITE(6,5100) I, DN(I), DT(I)
5100      FORMAT(15X,I5,10X,E15.4,5X,E15.4)
229 CONTINUE
CX      DO 230 J = 1, NIFGP
CX      WRITE(6,5000) J
CX      DO 230 I = ITGPL(J,1), ITGPL(J,2)
CX      IF ( DN(I)/DELTAN(J) .LE. 1 ) GO TO 231
CX      WRITE(6,4502) INCR, I
4502      FORMAT(/,5X,'STEP NO. ',I5,1X,
CX      1      'NODE NO.',I6,' DEBONDED IN TENSION',/)
231 CONTINUE
CX      IF ( ALPH(J) .LT. 0.001 ) GO TO 232
CX      IF ( DABS(DT(I))/DELTAT(J) .LE. 1 ) GO TO 232
CX      WRITE(6,4503) INCR, I
4503      FORMAT(/,5X,'STEP NO. ',I6,1X,
CX      1      'NODE NO.',I6,' DEBONDED IN SHEAR',/)
232 CONTINUE
230 CONTINUE
CX
CX      GO TO 9999
84 CONTINUE
CX      WRITE(6,4404) INCR,TIME,SIG1AV,EBAR11
4404 FORMAT(10X,I5,F10.7,1X,E14.7,1X,E14.7)
9999 CONTINUE
CX      CLOSE(5)
CX      CLOSE(6)
CX      CLOSE(7)
CX      CLOSE(8)
CX      CLOSE(9)
CX      CLOSE(19)
CX      STOP
CX      END

```

```

C*****
C
C          SUBROUTINE INPUT
C
C          THIS SUBROUTINE READS IN AND PRINTS INPUT DATA
C*****
C
C          SUBROUTINE INPUT(FGL,NSTE)
C          IMPLICIT REAL*8(A-H,O-Z)
C          REAL*8 A1(1200),A2(1200),FGL(2400),T(1500),DN(500),DT(500)
C          INTEGER NODE(1500,3),NDOF(1500),MATSET(1500),MTYPE(1500)
C          CHARACTER*75 TITLE, INFILE, OUTFILE
C          COMMON/CHIST/RTOL,NN,NEL,NF,NDBC,IDUMP,IPRI,ISREF,
1          IEQUIT,ITEMAX,ITEMP,IINT
C          COMMON/ELAS1/S(1500,4),E(1500,3),EO(1500,3),DSTRAN(3),
1          DSTRES(4)
C          COMMON/ELAS2/EM1(4),EM2(4),VNU(4),G12(4),Y1(4),Y2(4),Y(4),
1          EM(4)
C          COMMON/PLAS1/ALPHA(4,1500),EPBAR(1500),SIGBAR(1500),
1          IPLAS(1500),EPSP(1500,4),DEPSPT(1500,4),
2          DEPS(1500,4)
C          COMMON/PLAS2/SX(10,4),EX(10,4),EPX(10,4),
1          SP(10,4),DEPSAL,BETA
C          COMMON/VPLAS1/DTIME,DEVPAI
C          COMMON/VPLAS2/RN,H1,H2,AA1,AA2,C2,DO,B1,TEMP,TMELT,QS
C          COMMON/AREA2/NODE,NDOF
C          COMMON/AREA5/T,MATSET,MTYPE
C          COMMON/AREA6/A1,A2
C          COMMON/BB/NUNIAx(4),IDUMP2,ISUB
C          COMMON/LOAD/TIMV(1,1000),RV(1,1000),INODE(100),ICURVE(100),
1          DINC(1000),DPMINC(1000),DMULT(1,1000)
CX          COMMON/INTFAC/NINT1,NINT2,SIGMAX,DELTA,ALPH,DBFAC,DN,DT,ETA
C          COMMON/INTFAC/NIFEM,NIFGP,ITGPL(10,2),ITCON(500,2),
1          SIGMAX(10),DELTAN(10),DELTAT(10),ALPH(10),
2          ETA(10),DBFAC(10),DN,DT,INTDF(500),INTSP(500)
3          ,RMU(10),DISPN(500),DISPT(500),TNRATIO(500),
4          XRHQ(500),SIGNN(500),TAUNT(500),FN(500),FT(500)
C          COMMON/MODPARA/RMP1(10),RMP2(10),RMP3(10),RMP4(10),RMP5(10),
1          RMP6(10),RMP7(10),RMP8(10),RMP9(10),RMP10(10)
C          COMMON/HOMOG/SIGIAV,DEBAR11
C          COMMON/IPRISIG/ISELSIG,NUMSELSIG,MSELSIG(100)
C
C          READ INPUT DATA
C          NN - NUMBER OF NODES
C          NEL - NUMBER OF ELEMENTS
C          NF - NUMBER OF NODES WITH EXTERNALLY APPLIED LOADS
C          NDBC - NUMBER OF DISPLACEMENT BOUNDARY CONDITIONS
C          DINC - DISPLACEMENT INCREMENTS
C          IDUMP - DUMPING CODE (1 TO DUMP)
C          ITEMP - TEMPERATURE EFFECTS FLAG (1 FOR TEMPERATURE EFFECTS)
C          RTOL - TOLERANCE USED TO MEASURE EQUILIBRIUM CONVERGENCE
C          IPRI - OUTPUT PRINTING INTERVAL
C          ISREF - NUMBER OF ITERATIONS BETWEEN REFORMATION OF STIFFNESS
C          MATRIX
C          IEQUIT - NUMBER OF STEPS BETWEEN EQUILIBRIUM ITERATIONS (NOT USED)
C          ITEMAX - MAXIMUM NUMBER OF EQUILIBRIUM ITERATIONS PERMITTED
C          BEFORE REFORMATION OF STIFFNESS MATRIX
C          IINT - EQ. ZERO UNLESS USING INTERFACE ELEMENTS
C          A1 - GLOBAL A1 COORDINATE OF ITH NODE
C          A2 - GLOBAL A2 COORDINATE OF ITH NODE
C          IEL - ELEMENT NUMBER ASSOCIATED WITH CONNECTIVITY MATRIX
C          NODE - NODAL CONNECTIVITY PARAMETER - GIVES GLOBAL NODE NO'S OF
C          ITH ELEMENT
C          MATSET - MATERIAL NUMBER FOR ITH ELEMENT
C          MTYPE - MATERIAL MODEL FOR ITH ELEMENT
C          - 1 = ISOTROPIC LINEAR ELASTIC
C          - 2 = ELASTIC PLASTIC
C          - 3 = VISCOPLASTIC
C          - 4 = VISCOELASTIC
C          T - THICKNESS OF ITH ELEMENT
C          NDOF - DEGREE OF FREEDOM OF ITH BOUNDARY CONDITION
C          INODE - NODE OF ITH FORCE VECTOR
C          FA1 - EXTERNAL LOAD IN A1 DIRECTION APPLIED TO ITH NODE
C          FA2 - EXTERNAL LOAD IN A2 DIRECTION APPLIED TO ITH NODE
C          NUNIAx - NUMBER OF UNIAXIAL STRESS-STRAIN POINTS
C          ISUB - SUBINCREMENTATION FLAG(.NE.O) NO SUBINCS
C          IDUMP2 - DUMPING CODE(EQ.O) NO PRINTS
C          EM - YOUNG'S MODULUS
C          VNU - POISSON'S RATIO

```

```

C Y - UNIAXIAL YIELD POINT
C BETA - HARDING RATIO
C DEPSAL - ALLOWABLE STRAIN SUBINCREMENT
C SX(J) - VALUE OF STRESS ON SIGMA-X VS EPSILON-X CURVE
C EX(J) - VALUE OF STRAIN ON SIGMA-X VS EPSILON-X CURVE
C FGL - GLOBAL FORCE MATRIX
C NLCUR - NUMBER OF LOAD CURVES
C TIMV - TIME VALUE OF LOAD MULTIPLIER
C RV - LOAD MULTIPLIER
C ICURVE - LOAD CURVE NUMBER
C FORCE - SET EQUAL TO INITIAL UNIT GLOBAL FORCE MATRIX
C
      OPEN(19,FILE='kdata.dat',READONLY,STATUS='OLD')
      READ(19,107) INFILE
107  FORMAT(A)
      OPEN(5,FILE=INFILE,STATUS='OLD')
      READ(19,107) OUTFILE
      OPEN(6,FILE=OUTFILE,STATUS='UNKNOWN')
      OPEN(8,FILE='kfordist.out',STATUS='UNKNOWN')
      WRITE(6,4956)
      WRITE(8,4956)
4956  FORMAT(//,5X,'DANCOM: MODIFIED KACHANOV MODEL',/)
      READ(5,5002) TITLE
5002  FORMAT(A75)
      WRITE(6,5001) TITLE
      WRITE(8,5001) TITLE
5001  FORMAT(//,A75//)
      READ(5,*) NN,NEL,NF,NDBC,IDUMP,ITEMP,NLCUR,NSTE,
1      IINT
CX   READ(5,1001) NN,NEL,NF,NDBC,IDUMP,ITEMP,NLCUR,NSTE,
CX   IINT
CX 1001 FORMAT(9I5)
      READ(5,*) RTOL,IPRI,ISREF,IEQUIT,ITEMAX,NOMAT
CX   READ(5,1002) RTOL,IPRI,ISREF,IEQUIT,ITEMAX,NOMAT
CX 1002 FORMAT(F10.6,5I5)
37  WRITE(6,2001) NN,NEL,NF,NDBC,NSTE,NOMAT
2001 FORMAT(5X,'THE INPUT DATA ARE AS FOLLOWS',//,10X,
1      'NUMBER OF NODES = ',I6,/,10X,'NUMBER OF ELEMENTS = ',
2      I6,/,10X,'NUMBER OF EXTERNAL FORCE COMPONENTS = ',
3      I3,/,10X,'NUMBER OF DISP. BOUNDARY CONDITIONS = ',I3,/,
4      10X,'NUMBER OF SOLUTION STEPS = ',I6,/,
5      10X,'NUMBER OF MATERIAL MODELS USED = ',I3,/)
      WRITE(6,2002) RTOL,IPRI,IDUMP,ISREF,IEQUIT,ITEMAX
2002 FORMAT(5X,'THE SOLUTION IS NONLINEAR',//,10X,
1      'TOLERANCE FOR EQUILIBRIUM CONVERGENCE IS = ',F10.6,/,10X,
2      'OUTPUT PRINTING INTERVAL = ',I6,/,10X,
3      'OUTPUT FORMAT OPTION = ',I3,/,10X,
4      'NO. OF ITER. BEFORE REFORMING STIFFNESS MATRIX = ',
5      I3,/,10X,
6      'NUMBER OF STEPS BETWEEN EQUILIBRIUM ITERATIONS = ',
7      I3,/,10X,
8      'MAX NO. ITERATIONS BEFORE REFORMATION OF K MATRIX = ',
9      I3,/)
      READ(5,*) (A1(I),A2(I),I=1,NN)
CX   READ(5,1003) (A1(I),A2(I),I=1,NN)
CX 1003 FORMAT(2F10.7)
      WRITE(6,2003)
2003 FORMAT(//,10X,'NODAL COORDINATES ARE',//,10X,
1      'NODE NO. '18X,'A1',18X,'A2',//)
      DO 17 II=1,NN
17  WRITE(6,2004) II,A1(II),A2(II)
2004 FORMAT(10X,I3,15X,F10.4,10X,F10.4)
      DO 100 I=1,NEL
100 READ(5,*) IEL,(NODE(IEL,J),J=1,3),MATSET(IEL),
1      MTYPE(IEL)
CX 100 READ(5,1004) IEL,(NODE(IEL,J),J=1,3),MATSET(IEL),
CX 1MTYPE(IEL)
CX 1004 FORMAT(6I5)
      WRITE(6,2005)
2005 FORMAT(//,10X,'GLOBAL NUMBERING OF ELEMENTS IS',
1      //,4X,'ELEMENT NO.',4X,'NODE 1',4X,'NODE 2',
2      4X,'NODE 3',4X,'MATSET',5X,'MTYPE',//)
      DO 101 I=1,NEL
101  WRITE(6,2006) I,(NODE(I,J),J=1,3),MATSET(I),MTYPE(I)
2006 FORMAT(5X,I5,2X,5(5X,I5))
      DO 20 I=1,NEL
20  T(I)=1.0
22  CONTINUE
      READ(5,*) (NDOF(I),I=1,NDBC)
CX   READ(5,1005) (NDOF(I),I=1,NDBC)

```

```

CX 1005 FORMAT(12I5)
      WRITE(6,2023)
2023 FORMAT(//,10X,
1      'THE DISP. BOUNDARY CONDITIONS ARE APPLIED AT',/,
2      10X,'DEGREES OF FREEDOM',//)
      WRITE(6,2024)(NDOF(I),I=1,NDBC)
2024 FORMAT(10X,10I5)
      READ(5,*) DEBAR11
CX      READ(5,7004) DEBAR11
CX 7004 FORMAT(F10.6)
      WRITE(6,7003) DEBAR11
7003 FORMAT(/,10X,'DEBAR11 = ',F10.6,/)
      READ(5,*) (DINC(J),J=1,NDBC)
CX      READ(5,7005) (DINC(J),J=1,NDBC)
CX 7005 FORMAT(6F10.4)
      WRITE(6,7006)
7006 FORMAT(10X,'THE DISPLACEMENT INCREMENTS ARE',//)
      WRITE(6,7007) (DINC(J),J=1,NDBC)
7007 FORMAT(5(2X,F10.8) )
      NTOT=2*NN
C
C ZERO GLOBAL FORCE MATRIX
C
      DO 102 I=1,NTOT
102 FGL(I)=0.
CX
CX      IF(NF.EQ.0) GO TO 504
CX
CX      IF ( NF .EQ. 0 ) GO TO 6666
CX
      WRITE(6,2007)
2007 FORMAT(//,5X,'FORCES ARE APPLIED AS FOLLOWS',//,5X,
1      'NODE NO.',2X,'LOAD CURVE NO.',5X,'A1 FORCE',5X,
2      'A2 FORCE',//)
      DO 103 I=1,NF
      READ(5,*) INODE(I),ICURVE(I),FA1,FA2
CX      READ(5,1006) INODE(I),ICURVE(I),FA1,FA2
CX 1006 FORMAT(2I5,2F10.0)
      WRITE(6,2008) INODE(I),ICURVE(I),FA1,FA2
2008 FORMAT(5X,I3,10X,I3,2(5X,F10.0))
C
C ASSEMBLE GLOBAL LINEAR FORCE MATRIX
C
      NN1=2*INODE(I)-1
      NN2=NN1+1
      FGL(NN1)=FGL(NN1)+FA1
103 FGL(NN2)=FGL(NN2)+FA2
      IF(IDUMP.LT.3) GO TO 6666
      WRITE(6,2014)
2014 FORMAT(//,20X,'GLOBAL LINEAR FORCE MATRIX',//)
      WRITE(6,2015) (FGL(I),I=1,NTOT)
2015 FORMAT(30X,E15.7)
6666 CONTINUE
C
C LOAD CURVE MULTIPLIERS
C
      DO 109 K=1,NLCUR
      DO 110 L=1,NSTE
CX      READ(5,*) TIMV(K,L),RV(K,L),DMULT(K,L)
CX
CX      READ(5,111) TIMV(K,L),RV(K,L)
CX 111 FORMAT(2F10.2)
110 CONTINUE
109 CONTINUE
      WRITE(6,112)
112 FORMAT(' ',//,10X,'LOAD CURVE AND DISPLACEMENT MULTIPLIERS',//)
      DO 113 K=1,NLCUR
      WRITE(6,114)K
CX
114 FORMAT(' ',5X,'LOAD CURVE NO.',
1      2X,I3,//,10X,'TIMV',13X,'RV',13X,'DMULT',/)
CX
      DO 115 L=1,NSTE
CX      WRITE(6,116) TIMV(K,L),RV(K,L),DMULT(K,L)
116 FORMAT(' ',3X,F10.4,8X,F10.4,8X,F10.4)
CX
115 CONTINUE

```



```

113 CONTINUE
504 CONTINUE
C
C READ IN MATERIAL PROPERTIES
C
      READ(5,*) MODNUM1,MODNUM2,MODNUM3,MODNUM4
CX      READ(5,2507) MODNUM1,MODNUM2,MODNUM3,MODNUM4
CX 2507 FORMAT(4I5)
      IF(MODNUM1.EQ.0) GO TO 451
C
C READ IN MATERIAL PROPERTIES FOR ELASTIC ELEMENTS
C
      WRITE(6,6707) MODNUM1
6707 FORMAT(/,5X,'THERE ARE ',I3,' ELASTIC MATERIAL SETS',
1      /,'SET NO.',6X,'E1',13X,'E2',13X,'NU12',
2      13X,'G12',10X,'Y1',14X,'Y2',/)
      DO 559 I=1,MODNUM1
        READ(5,*) MATNO,EM1(MATNO),EM2(MATNO),VNU(MATNO),
1        G12(MATNO),Y1(MATNO),Y2(MATNO)
CX      READ(5,6700) MATNO,EM(MATNO),VNU(MATNO),Y(MATNO)
CX 6700 FORMAT(4X,I5,3E15.7)
        WRITE(6,6702) MATNO,EM1(MATNO),EM2(MATNO),VNU(MATNO),
1        G12(MATNO),Y1(MATNO),Y2(MATNO)
6702 FORMAT(2X,I3,3X,6(1X,E14.7))
559 CONTINUE
451 CONTINUE
      IF(MODNUM2.EQ.0) GO TO 452
C
C READ IN MATERIAL PROPERTIES FOR ELASTIC-PLASTIC ELEMENTS
C
      WRITE(6,6701) MODNUM2
6701 FORMAT(/,5X,'THERE ARE ',I3,
1      ' ELASTIC-PLASTIC MATERIAL SETS',/)
      READ(5,*) ISUB,IDUMP2,BETA,DEPSAL
CX      READ(5,2050) ISUB,IDUMP2,BETA,DEPSAL
CX 2050 FORMAT(2I5,F10.0,F10.2)
      WRITE(6,2060) ISUB,IDUMP2,BETA,DEPSAL
2060 FORMAT(10X,'SUBINCREMENTATION FLAG = ',I5,/,
1      10X,'DUMPING CODE = ',I5,/,10X,'BETA = ',
2      F10.4,/,10X,'ALLOWABLE STRAIN SUBINCREMENT = ',
3      F10.5,/)
      DO 363 I=1,MODNUM2
        READ(5,*) MATNO,NUNIAX(MATNO),EM(MATNO),
1        VNU(MATNO),Y(MATNO)
CX      READ(5,2390) MATNO,NUNIAX(MATNO),EM(MATNO),
CX      1VNU(MATNO),Y(MATNO)
CX 2390 FORMAT(2I5,F10.0,F10.4,F10.0)
        READ(5,2070) (SX(J,MATNO),EX(J,MATNO),J=1,NUNIAX(MATNO))
2070 FORMAT(6F10.0)
        WRITE(6,2040) MATNO
2040 FORMAT(10X,'MATERIAL SET NUMBER = ',I5,/)
        WRITE(6,2043) EM(MATNO),VNU(MATNO),Y(MATNO)
2043 FORMAT(10X,'MODULUS OF ELASTICITY = ',E14.7,/,
1      10X,'POISSONS RATIO = ',E14.7,/,
2      10X,'YEILD POINT = ',E14.7,/)
        WRITE(6,2080)
2080 FORMAT(10X,'THE INPUT UNIAXIAL STRESS-STRAIN DATA ARE',/,
1      14X,'STRESS',14X,'STRAIN',/)
        DO 10 J=1,NUNIAX(MATNO)
          WRITE(6,2090) SX(J,MATNO),EX(J,MATNO)
2090 FORMAT(10X,F10.2,10X,F10.5)
10      CONTINUE
        WRITE(6,3000)
3000 FORMAT(/,10X,'THE UNIAXIAL K VS EPBAR DATA ARE',/,
1      19X,'K',15X,'EPBAR',/)
        DO 11 J=1,NUNIAX(MATNO)
          EPX(J,MATNO)=EX(J,MATNO)-SX(J,MATNO)/EM(MATNO)
          SP(J,MATNO)=Y(MATNO)+(SX(J,MATNO)-Y(MATNO))*BETA
          WRITE(6,2090) SP(J,MATNO),EPX(J,MATNO)
11      CONTINUE
363 CONTINUE
        DO 1007 J=1,NEL
          IF(MTYPE(J).NE.2) GO TO 1040
          EPBAR(J)=0.0
          IPLAS(J)=0
          SIGBAR(J)=Y(MATSET(J))
          DO 1008 I=1,4
            ALPHA(I,J)=0.0
1008 CONTINUE
1040 CONTINUE

```

```

1007 CONTINUE
452 IF(MODNUM3.EQ.O) GO TO 453
WRITE(6,2200) MODNUM3
2200 FORMAT(/,5X,'THERE IS ',I3,' VISCOPLASTICITY MODEL',/)
DO 222 I=1,MODNUM3
WRITE(6,2201) I
2201 FORMAT(10X,'VISCOPLASTICITY MODEL NO. ',I2)
READ(5,*) DTIME,DEVPAL
CX READ(5,2100) DTIME,DEVPAL
CX 2100 FORMAT(2E15.7)
WRITE(6,2101) DTIME,DEVPAL
2101 FORMAT(10X,'TIME STEP = ',E14.7,/,
1 10X,'ALLOWABLE STRAIN SUBINCREMENT = ',E14.7,/)
READ(5,*) MATNO,EM(MATNO),VNU(MATNO),Y(MATNO)
CX READ(5,2398) MATNO,EM(MATNO),VNU(MATNO),Y(MATNO)
CX 2398 FORMAT(I5,F10.0,F10.4,F10.0)
WRITE(6,2040) MATNO
WRITE(6,2043) EM(MATNO),VNU(MATNO),Y(MATNO)
READ(5,2202) RN,H1,H2,AA1,AA2,C2,DO,B1,TEMP,TMELT,QS
2202 FORMAT(4E15.7)
WRITE(6,2203) RN,H1,H2,AA1,AA2,C2,DO,B1,TEMP,TMELT,QS
2203 FORMAT(10X,'RN = ',E15.7,1X,'H1 = ',E15.7,/,
1 10X,'H2 = ',E15.7,1X,'AA1 = ',E15.7,/,
2 10X,'AA2 = ',E15.7,1X,'C2 = ',E15.7,/,
3 10X,'DO = ',E15.7,1X,'B1 = ',E15.7,/,
4 10X,'TEMP = ',E15.7,1X,'TMELT = ',E15.7,/,
5 10X,'QSTAR = ',E15.7,/)
222 CONTINUE
DO 5007 J=1,NEL
IF(MTYPE(J).NE.3) GO TO 5004
EPBAR(J)=O.O
IPLAS(J)=O
SIGBAR(J)=DO
DO 5008 I=1,4
ALPHA(I,J)=O.O
5008 CONTINUE
5004 CONTINUE
5007 CONTINUE
453 IF(MODNUM4.EQ.O) GO TO 455
GO TO 450
450 WRITE(6,5095)
5095 FORMAT(10X,'MATERIAL MODEL NOT IN CODE',/)
STOP
455 CONTINUE
IF(INT.EQ.O) GO TO 9999
CX READ(5,*) NINT1,NINT2,ETA
CXCX READ(5,4001) NINT1,NINT2,ETA
CXCX 4001 FORMAT(2I5,E15.7)
CX READ(5,*) SIGMAX,DELTA,ALPH,DBFAC
CXCX READ(5,4002) SIGMAX,DELTA,ALPH,DBFAC
CXCX 4002 FORMAT(4E15.7)
CX WRITE(6,4003)
CX 4003 FORMAT(/,5X,'INTERFACE ELEMENTS IN EFFECT',/)
CX WRITE(6,4004) NINT1,NINT2,SIGMAX,DELTA,ALPH
CX 4004 FORMAT(10X,'INTERFACE ELEMENTS START AT NODE NO.',
CX 1 I5,/,10X,
CX 2 'AND END AT NODE NUMBER',I5,/,
CX 3 10X,'MAX NORMAL INTERFACE STRESS = ',E15.7,/,
CX 4 10X,'LENGTH PARAMETER = ',E15.7,/,
CX 5 10X,'RATIO SHEAR/NORMAL INTERF. STIFFNESS = ',
CX 6 E15.7,/)
CX WRITE(6,4008) DBFAC,ETA
CX 4008 FORMAT(10X,'DEBOND COMPRESSIVE FACTOR = ',E15.7,/,
CX 1 10X,'UNLOADING STRETCH FACTOR = ',E15.7,/)
CX
C
C READ IN NO. OF INTRF ELEMS AND GROUPS
C
C READ(5,*) NIFEM, NIFGP
C
C READ IN FIRST AND LAST ELEMENT
C
DO 5000 J = 1, NIFGP
READ(5,*) ITGPL(J,1), ITGPL(J,2)
5000 CONTINUE
C
C READ IN INTRF CONNECTIVITY MATRIX
C
DO 5050 J = 1, NIFEM
READ(5,*) ITCON(J,1), ITCON(J,2)

```

```

5050 CONTINUE
C
C      READ IN INTERFACE CONSTITUTIVE CONSTANTS
C
      DO 5400 J = 1, NIFGP
        READ(5,*) SIGMAX(J), DELTAN(J), DELTAT(J), ALPH(J), ETA(J),
1         DBFAC(J), RMU(J), RMP1(J), RMP2(J), RMP3(J)
C
C      COMMON BLOCK SET FOR RMP1(10) TO RMP10(10)
C      USE ONLY RMP1(J) TO RMP3(J) FOR NOW
C
5400 CONTINUE
C
C      READ IN SELECTED ELEMENT NUMBERS FOR STRESS OUTPUT
C
      READ(5,*) ISELSIG
      IF ( ISELSIG .NE. 0 ) THEN
        READ(5,*) NUMSELSIG
        READ(5,*) (MSELSIG(J), J = 1, NUMSELSIG)
        WRITE(6,5475) NUMSELSIG
5475      FORMAT(/,10X,I5,' ELEMENTS SELECTED FOR STRESS OUTPUT:',/)
        WRITE(6,5485) (MSELSIG(J), J=1,NUMSELSIG)
5485      FORMAT(5I5)
      ENDIF
C
C      OUTPUT INTERFACE ELEMENT INFORMATION
C
      WRITE(6,5100)
5100      FORMAT(/,10X,'INTERFACE ELEMENTS IN EFFECT',/)
      IF ( NIFGP .GT. 1 ) THEN
        WRITE(6,5150) NIFEM, NIFGP
5150      FORMAT(10X,'THERE ARE ',I5,' INTERFACE ELEMENTS.',/
1         10X,'THEY ARE DIVIDED INTO ',I5,' GROUPS.',/)
      ELSE
        WRITE(6,5152) NIFEM, NIFGP
5152      FORMAT(10X,'THERE ARE ',I5,' INTERFACE ELEMENTS.',/
1         10X,'THEY ARE ASSIGNED TO ',I5,' GROUP.',/)
      ENDIF
      WRITE(6,5160)
5160      FORMAT(/,10X,'GROUP NO.',10X,'FIRST INTRF. ELEM.',
1         10X,'LAST INTRF. ELEM.',/)
      WRITE(6,5170) ( J,ITGPL(J,1),ITGPL(J,2) ,J=1,NIFGP)
5170      FORMAT(10X,I5,18X,I5,22X,I5)
      WRITE(6,5200)
5200      FORMAT(/,10X,'INTERFACE ELEMENT NO.',5X,'NODE 1',10X,
1         'NODE 2',/)
      WRITE(6,5250) ( J,ITCON(J,1),ITCON(J,2) , J=1,NIFEM)
5250      FORMAT(16X,I5,12X,I5,10X,I5)
      DO 5275 J = 1, NIFGP
        WRITE(6,5300) J, SIGMAX(J), DELTAN(J), DELTAT(J), ALPH(J),
1         ETA(J), DBFAC(J), RMU(J), RMP1(J), RMP2(J), RMP3(J)
5275      CONTINUE
CX
CX5300      FORMAT(/,10X,'GROUP NO.',I5,/
CX      1      10X,'MAX NORMAL INTERFACE STRESS= ',E15.7,/,
CX      2      10X,'NORMAL LENGTH PARAMETER= ',E15.7,/,
CX      3      10X,'TANGENTIAL LENGTH PARAMETER= ',E15.7,/,
CX      4      10X,'SHEAR/NORMAL INTERFACE STIFFNESS RATIO= ',E15.7,/,
CX      5      10X,'UNLOADING STRETCH FACTOR= ',E15.7,/,
CX      6      10X,'DEBOND COMPRESSIVE FACTOR= ',E15.7,/,
CX      7      10X,'INTERFACIAL COEFFICIENT OF FRICTION= ',E15.7,/)
CX
C      KACHANOV'S MODEL
5300      FORMAT(/,10X,'GROUP NO.',I5,/
1      10X,'YOUNGS MODULUS= ',E15.7,/,
2      10X,'POISSONS RATIO= ',E15.7,/,
3      10X,'SHEAR MODULUS= ',E15.7,/,
4      10X,'CRITICAL TENSILE STRAIN= ',E15.7,/,
5      10X,'RLAMDA= ',E15.7,/,
6      10X,'RL= ',E15.7,/,
7      10X,'RBETA= ',E15.7,/,
8      10X,'RMP1= ',E15.7,/,10X,'RMP2= ',E15.7,/,10X,'RMP3= ',E15.7,/)
CX
9999 CONTINUE
      RETURN
      END
C
C*****
C
C      SUBROUTINE KGLOB

```

```

C
C   THIS SUBROUTINE CALCULATES THE LINEAR OR NONLINEAR GLOBAL
C   STIFFNESS MATRIX
C*****
C
      SUBROUTINE KGLOBAL(KGL,NODE,NTOT,NDOF)
      IMPLICIT REAL*8(A-H,O-Z)
      REAL*8 KGL(2400,600),KEL(6,6),B(3,6),BC(6,3),C(3,3),T(1500),
1      DS(1500,4),KGS(2400,600),RKINT(4,4),DN(500),DT(500)
      INTEGER NODE(1500,3),NDOF(1500),NICON(2),MATSET(1500),MTYPE(1500)
      COMMON/CHIST/RTOL,NN,NEL,NF,NDBC,IDUMP,IPRI,ISREF,
1      IEQUIT,ITEMAX,ITEMP,IINT
CX      COMMON/INTFAC/NINT1,NINT2,SIGMAX,DELTA,ALPH,DBFAC,DN,DT,ETA
      COMMON/INTFAC/NIFEM,NIFGP,ITGPL(10,2),ITCON(500,2),
1      SIGMAX(10),DELTAN(10),DELTAT(10),ALPH(10),
2      ETA(10),DBFAC(10),DN,DT,INTDF(500),INTSP(500)
3      RMU(10),DISPN(500),DISPT(500),TNRATIO(500),
4      XRH0(500),SIGNN(500),TAUNT(500),FN(500),FT(500)
      COMMON/MODPARA/RMP1(10),RMP2(10),RMP3(10),RMP4(10),RMP5(10),
1      RMP6(10),RMP7(10),RMP8(10),RMP9(10),RMP10(10)
      COMMON/AREA1/B
      COMMON/AREA5/T,MATSET,MTYPE
      COMMON/AREA7/NSTE,INCR,ITER
      COMMON/BANDED/MAXBW
      COMMON/STIF/KGS
      DO 44 I=1,NTOT
      DO 44 J=1,MAXBW
44      KGL(I,J)=0.
      DO 99 I=1,NEL
C DETERMINE ELEMENT STIFFNESS MATRIX
      CALL SHAPE(I,IDUMP,AREA)
      IF(MTYPE(I).EQ.1) GO TO 451
      IF(MTYPE(I).EQ.2) GO TO 452
      IF(MTYPE(I).EQ.3) GO TO 453
      IF(MTYPE(I).EQ.4) GO TO 454
450      WRITE(6,6003)
6003      FORMAT(10X,'MATERIAL TYPE NOT IN CURRENT LIBRARY',/)
      STOP
451      CALL ELAS2D(I,C,DS,MATSET(I))
      GO TO 455
452      CALL PLAS2D(I,C,DS,1,MATSET(I))
      GO TO 455
453      CONTINUE
      CALL VPLAS2D(I,C,DS,1,MATSET(I))
      GO TO 455
454      GO TO 450
455      CONTINUE
      DO 66 L=1,6
      DO 66 J=1,3
      BC(L,J)=0.
      DO 66 K=1,3
66      BC(L,J)=BC(L,J)+B(K,L)*C(K,J)
      DO 67 L=1,6
      DO 67 J=1,6
      KEL(L,J)=0.
      DO 67 K=1,3
67      KEL(L,J)=KEL(L,J)+BC(L,K)*B(K,J)
      DO 68 L=1,6
      DO 68 J=1,6
68      KEL(L,J)=AREA*KEL(L,J)*T(I)
      IF(IDUMP.LT.4) GO TO 7777
      WRITE(6,2011) I
2011      FORMAT(//,20X,'ELEMENT STIFFNESS MATRIX FOR ELEMENT NO.',
1      I3,/)
      DO 54 L=1,6
54      WRITE(6,2012) (KEL(L,J),J=1,6)
2012      FORMAT(4(5X,E15.7) )
7777      CONTINUE
C ASSEMBLE ELEMENT STIFFNESS MATRIX INTO GLOBAL LINEAR STIFFNESS
C MATRIX
      CALL ASEMBL(KGL,KEL,3,NODE,2,I)
89      CONTINUE
      IF(IINT.EQ.0) GO TO 98
CX      NINEL=NINT2-NINT1+1
CX      I1=NINT1
CX      I2=I1+NINEL
CX      DO 97 I=1,NINEL
CX      CALL INTRFACE(I,I1,I2,RKINT)
CX      NICON(1)=I1

```

```

CX      NICON(2)=I2
CX      CALL ASEMINT(KGL,RKINT,2,NICON,2)
CX      I1=I1+1
CX      I2=I2+1
CX      97 CONTINUE
CX
      DO 500 I = 1, NIFGP
      DO 550 J = ITGPL(I,1), ITGPL(I,2)
      IF ( J .EQ. ITGPL(I,1) ) THEN
      ITFLAG = 1
      ELSE IF ( J .EQ. ITGPL(I,2) ) THEN
      ITFLAG = 2
CX
CX      SPECIAL TRUSS ELEMENT FOR FORCE CALCULATIONS
      ELSE IF ( ITGPL(I,1) .EQ. ITGPL(I,2) ) THEN
      ITFLAG = 3
CX
CX      ELSE
      ITFLAG = 0
      ENDIF
      I1 = ITCON(J,1)
      I2 = ITCON(J,2)
      CALL INTRFACE(J,I1,I2,RKINT,ITFLAG,I)
      NICON(1) = I1
      NICON(2) = I2
      CALL ASEMINT(KGL,RKINT,2,NICON,2)
550 CONTINUE
500 CONTINUE
CX
      98 CONTINUE
      IF(IDUMP.LT.4) GO TO 6666
      WRITE(6,2013)
2013 FORMAT(//,20X,'GLOBAL LINEAR STIFFNESS MATRIX',//)
      WRITE(6,2040) ((KGL(II,JJ),JJ=1,MAXBW),II=1,NTOT)
2040 FORMAT(4(5X,E15.7) )
6666 CONTINUE
      DO 988 I=1,NTOT
      DO 988 J=1,MAXBW
      988 KGS(I,J)=KGL(I,J)
C
C      APPLY DISPLACEMENT BOUNDARY CONDITIONS
C      ZERO-ONE TREATMENT TO STIFFNESS MATRIX
C
      DO 999 I=1,NDBC
      JJ=NDOF(I)
      KGL(JJ,1)=1.0
      DO 50 J=2,MAXBW
50 KGL(JJ,J)=0.0
      JJ=JJ-1
      M=2
      51 IF(M.GT.MAXBW.OR.JJ.LT.1) GO TO 52
      KGL(JJ,M)=0.0
      JJ=JJ-1
      M=M+1
      GO TO 51
      52 CONTINUE
999 CONTINUE
C
C      RETURN
C      END
C
C*****
C
C      SUBROUTINE SHAPE
C
C      THIS SUBROUTINE CALCULATES THE P AND D MATRICES
C*****
C
      SUBROUTINE SHAPE(I,IDUMP,AREA)
      IMPLICIT REAL*8(A-H,O-Z)
      REAL*8 B(3,6),A1(1200),A2(1200),T(1500)
      INTEGER NODE(1500,3),NDOF(1500),MATSET(1500),MTYPE(1500)
      COMMON/AREA1/B
      COMMON/AREA2/NODE,NDOF
      COMMON/AREA5/T,MATSET,MTYPE
      COMMON/AREA6/A1,A2
      COMMON/AREA7/NSTE,INCR,ITER

```

```

X1=A1(NODE(I,1))
X2=A1(NODE(I,2))
X3=A1(NODE(I,3))
Z1=A2(NODE(I,1))
Z2=A2(NODE(I,2))
Z3=A2(NODE(I,3))
AREA=(X2*Z3+X1*Z2+X3*Z1-X2*Z1-X3*Z2-X1*Z3)/2.
B(1,1)=(Z2-Z3)/2./AREA
B(2,2)=(X3-X2)/2./AREA
B(1,3)=(Z3-Z1)/2./AREA
B(2,4)=(X1-X3)/2./AREA
B(1,5)=(Z1-Z2)/2./AREA
B(2,6)=(X2-X1)/2./AREA
B(1,2)=0.
B(1,4)=0.
B(1,6)=0.
B(2,1)=0.
B(2,3)=0.
B(2,5)=0.
B(3,1)=B(2,2)
B(3,2)=B(1,1)
B(3,3)=B(2,4)
B(3,4)=B(1,3)
B(3,5)=B(2,6)
B(3,6)=B(1,5)
IF(IDUMP.LT.4) GO TO 4637
ISHAPE=0
IF(ISHAPE.NE.1) GO TO 4637
DO 4635 J=1,3
WRITE(6,4639)(B(J,K),K=1,6)
4639 FORMAT(' ',2X,6(E13.6,2X))
4635 CONTINUE
WRITE(6,4638) AREA,T(I)
4638 FORMAT(' ',3X,'AREA=',E14.7,3X,'THICKNESS=',E14.7,/)
4637 CONTINUE
RETURN
END

C
C*****
C
C          SUBROUTINE INTRFACE
C
C*****
C
SUBROUTINE INTRFACE(II,I1,I2,RKINT,ITFLAG,IG)
IMPLICIT REAL*8(A-H,O-Z)
REAL*8 RKINT(4,4),Q(2400),T(1500),A1(1200),A2(1200),
1 DN(500),DT(500)
DIMENSION MATSET(1500),MTYPE(1500)
COMMON/CHIST/RTOL,NN,NEL,NF,NDBC,IDUMP,IPRI,ISREF,
1 IEQUIT,ITEMAX,ITEMP,IINT
COMMON/DISPHIS/DELTAQ(2400),WORKN(500),WORKT(500),FSEPN(500),
1 FSEPT(500)
COMMON/AREA4/Q
COMMON/AREA5/T,MATSET,MTYPE
COMMON/AREA6/A1,A2
COMMON/AREA7/NSTE,INCR,ITER
CX COMMON/INTFAC/NINT1,NINT2,SIGMAX,DELTA,ALPH,DBFAC,DN,DT,ETA
COMMON/INTFAC/NIFEM,NIFGP,ITGPL(10,2),ITCON(500,2),
1 SIGMAX(10),DELTAN(10),DELTAT(10),ALPH(10),
2 ETA(10),DBFAC(10),DN,DT,INTDF(500),INTSP(500)
3 ,RMU(10),DISPN(500),DISPT(500),TNRATIO(500),
4 XRH0(500),SIGNN(500),TAUNT(500),FN(500),FT(500)
COMMON/MODPARA/RMP1(10),RMP2(10),RMP3(10),RMP4(10),RMP5(10),
1 RMP6(10),RMP7(10),RMP8(10),RMP9(10),RMP10(10)
PI=3.141592654
IF ( ITFLAG .EQ. 3 ) GO TO 711
CX NINEL=NINT2-NINT1+1
C
C CALCULATE INTERFACE (NORMAL) ANGLE PHI AND WIDTH W
C
CX
I1M1X = II - 1
I1P1X = II + 1
I1M1 = ITCON(I1M1X,1)
I1P1 = ITCON(I1P1X,1)
CX WRITE(6,100) I1M1, A1(I1M1), A2(I1M1)
CX WRITE(6,100) I1, A1(I1), A2(I1)
CX WRITE(6,100) I1P1, A1(I1P1), A2(I1P1)
CX100 FORMAT(/,5X,I5,10X,E15.4,10X,E15.4,/)

```

```

CX      IF ( A2(I1M1) .EQ. A2(I1) ) THEN          ! MODIFIED FOR 90 DEG.
          PHI1 = PI / 2.0
        ELSE
          PHI1=DATAN((A1(I1)-A1(I1M1))/(A2(I1M1)-A2(I1)))
        ENDIF
        IF ( A2(I1) .EQ. A2(I1P1) ) THEN          ! MODIFIED FOR 90 DEG.
          PHI2 = PI / 2.0
        ELSE
          PHI2=DATAN((A1(I1P1)-A1(I1))/(A2(I1)-A2(I1P1)))
        ENDIF
        W1W1 = ( A1(I1) - A1(I1M1) )**2 +
1      ( A2(I1M1) - A2(I1) )**2
        W2W2=( A1(I1P1) - A1(I1) )**2 +
1      ( A2(I1) - A2(I1P1) )**2
        W1 = SQRT(W1W1)
        W2 = SQRT(W2W2)

C
C ACCOUNT FOR FIRST AND LAST ELEMENT
C
CX      IF(II.GT.1) GO TO 334
CX      IF(PHI2.LT..001) GO TO 443
CX      PHI1=3.14159265-PHI2
CX      GO TO 3314
CX 443 PHI1=PHI2
CX 3314 W1=0.
CX 334 CONTINUE
CX      IF(II.LT.NINEL) GO TO 335
CX      IF(PHI1.LT..001) GO TO 444
CXCX    PHI2=-PHI1
CX      PHI2 = PHI1
CX      GO TO 3334
CX 444 PHI2=PHI1
CX 3334 W2=0.
CX 335 CONTINUE
CX
711 CONTINUE
      IF ( ITFLAG .EQ. 1 ) THEN
        PHI1 = PHI2
        W1 = 0.0
      ELSE IF ( ITFLAG .EQ. 2 ) THEN
        PHI2 = PHI1
        W2 = 0.0
CX      FORCE CALCULATION TRUSS ELEMENT
CX
      ELSE IF ( ITFLAG .EQ. 3 ) THEN
        W1 = 1.0
        W2 = 1.0
        PHI1 = PI / 2.0
        PHI2 = PI / 2.0
CX
CX      ENDIF
CX
C
C INITIALIZE INTERFACE ELEMENT STIFFNESS RKINT
C
      DO 9 I=1,4
      DO 9 J=1,4
      9 RKINT(I,J)=0.
C
C CALCULATE INTERFACE DISPLACEMENTS UN1,UN2,UT1,UT2
C
      N1X=2*I1-1
      N1Y=N1X+1
      N2X=2*I2-1
      N2Y=N2X+1
      PHIAB=(PHI1+PHI2)/2.
      UX=Q(N2X)-Q(N1X)
      UY=Q(N2Y)-Q(N1Y)
CY      UN=UX*DCOS(PHIAB)+UY*DSIN(PHIAB)
CY      UT=-UX*DSIN(PHIAB)+UY*DCOS(PHIAB)
      THETA1 = PHIAB - ( PI / 2.0 )
      UN = -UX * DSIN(THETA1) + UY * DCOS(THETA1)
      UT = UX * DCOS(THETA1) + UY * DSIN(THETA1)
CY
      DN(II)=UN
      DT(II)=UT
C
      DUX = DELTAQ(N2X) - DELTAQ(N1X)

```

```

      DUY = DELTAQ(N2Y) - DELTAQ(N1Y)
      DUN = -DUX * DSIN(THETA1) + DUY * DCOS(THETA1)
      DUT = DUX * DCOS(THETA1) + DUY * DSIN(THETA1)
C
C
C CALCULATE NORMAL AND SHEAR STIFFNESS COMPONENTS
C   RKN1,RKN2,RTN1,RTN2
C
C
C   ASSIGN VARIABLES FOR KACHANOV'S MODEL
C
      EO = SIGMAX(IG)
      RNU = DELTAN(IG)
      GO = DELTAT(IG)
      ESPCRIT = ALPH(IG)
      RLAMBDA = ETA(IG)
      RL = DBFAC(IG)
      RBETA = RMU(IG)
C   CHANGE EO AND RNU TO PLANE STRAIN CONDITIONS
      EO = EO / ( 1.0 - (RNU**2) )
      RNU = RNU / ( 1.0 - RNU )
C
C   IF ( ITFLAG .EQ. 3 ) GO TO 713
C
C NOTE: THESE ARE TANGENT STIFFNESSES
C
C*****
C   NEEDLEMAN OR TVERGAARD
CX   UND = UN / DELTAN(IG)
CX   UTD = UT / DELTAT(IG)
C
C-----
C   KACHANOV
C
      UND = UN / RL
      UTD = UT / RL
      DUND = DUN / RL
      DUTD = DUT / RL
C
C*****
C   KACHANOV'S MODEL
C
C   STIFFNESS CALCULATIONS
C
C*****
C   AREA.....TRUSS ELEMENT CROSS SECTIONAL AREA
C   RL.....THICKNESS OF INTERFACE (INP.)
C   EO.....YOUNG'S MODULUS OF INTERFACE (INP.)
C   GO.....SHEAR MODULUS OF INTERFACE (INP.)
C   RNU.....POISSON'S RATIO OF INTERFACE (INP.)
C   ESPCRIT.....CRITICAL TENSILE STRAIN (INP.)
C   RLAMBDA.....DAMAGE GROWTH PROPORTIONAL CONST. (INP.)
C   RAREA.....AREA OF DAMAGED ZONE
C   RLENGTH.....CRACK LENGTH
C   RBETA.....RLENGTH / RL (INP.)
C
C*****
CX   CALCULATE PRINCIPLE NORMALIZED DISPLACEMENTS
C
      RLSQ = ( UND / 2.0 )**2 + ( UTD / 2.0 )**2
      RLAM = SQRT( RLSQ )
      UM1 = UND / 2.0 + RLAM
      UM2 = UND / 2.0 - RLAM
      UMAX = DMAX1( UM1 , UM2 )
      AREA = ( W1 + W2 ) / 2.0 * T(1)
      RAREA = AREA / T(1) * RL
C
C   IF ( UMAX .LE. ESPCRIT ) THEN           ! INTERFACE INTACT
C
      IF ( UND .EQ. 0.0 .AND. UTD .EQ. 0.0 ) THEN
          Q22 = EO / ( 1.0 - RNU*RNU )
          Q66 = GO
          RKN = Q22 * AREA / RL
          RKT = Q66 * AREA / RL
      ELSE
          IF ( UND .LT. 0.0 ) THEN           ! MODIFY DISPLACEMENTS
              UNDC = 0.0                     ! FOR COMPRESSIVE LOADS

```



```

      UTDC = UTD
    ELSE
      UNDC = UND
      UTDC = UTD
    ENDIF

C
C
C TRANSFORM NORMALIZED DISPLACEMENTS TO PRINCIPLE DAMAGE
C COORDINATES (1,2)
C (CURRENTLY ASSUME ALL MATRIX CRACKS TO BE ORIENTED
C AT AN 45 DEGREES ANGLE)
C

      P4 = PI / 4.0
      P42 = P4 * 2.0
      DC2 = DCOS(P4) * DCOS(P4)
CX      UNDPD = -UTD*DSIN(P4) + UND*DCOS(P4)
CX      UTDPD = UTD*DCOS(P4) + UND*DSIN(P4)
      UNDPD = UNDC * DC2 - ( 0.5 * UTDC ) * DSIN(P42)
      UTDPD = 0.5 * UNDC * DSIN(P42) + ( 0.5 * UTDC ) * DCOS(P42)
      DUNDP = DUND * DC2 - ( 0.5 * DUTD ) * DSIN(P42)
      DUTDP = 0.5 * DUND * DSIN(P42) + ( 0.5 * DUTD ) * DCOS(P42)

C
C
C DETERMINE EFFECTIVE PROPERTIES

C
C
CXX MODIFICATION FOR STRESS DEPENDENT DAMAGE GROWTH
CXX
CXX      RI = RLAMBDA * DABS(UNDPD)      ! RLAMBDA * UNDPD
CXX      RI = RLAMBDA * DABS(UTDC)      ! RLAMBDA * UTDC
CXX      RLENGTH = RBETA * RL          ! RBETA * RL
CXX      RHO = RI * RLENGTH**2 / RAREA
CXX      RHO = DMAX1( RHO, XRHO(II) )
CXX      XRHO(II) = RHO
CXX      RHO = XRHO(II)

      RHO = XRHO(II)
      E1 = EO
      E2 = EO / ( 1.0 + 2.0*PI*RHO ) ! EO DEPENDS ON PLANE STRESS
      RNU12 = RNU
      RNU21 = RNU / ( 1.0 + 2.0*PI*RHO )
      G12 = GO / ( 1.0 + 2.0*PI*RHO*(GO/EO) )

C
C
C FORM REDUCED STIFFNESS MATRIX

      Q11 = E1 / ( 1.0 - RNU12*RNU21 )
      Q12 = RNU21 * Q11
      Q22 = E2 / ( 1.0 - RNU12*RNU21 )
      Q66 = G12

CXX
CXX
CXX BEGIN CXX MODIFICATIONS HERE
CXX
CXX CALCULATE PRINCIPAL STRESSES
CXX
CXX      SIGNN(II) = SIGNN(II) + Q22 * DUNDP
CXX      TAUNT(II) = TAUNT(II) + Q66 * DUTDP
CXX      SIGSIG = ( SIGNN(II) / 2.0 )**2 + ( TAUNT(II) / 2.0 )**2
CXX      RSIG = SQRT(SIGSIG)
CXX      SIGM1 = SIGNN(II)/2.0 + RSIG
CXX      SIGM2 = SIGNN(II)/2.0 - RSIG
CXX      SIGPRIN = DMAX1(SIGM1,SIGM2)
CXX      TAUMAX = RSIG

C
C
C CALCULATE THE VALUE OF RHO (MICRO CRACK DAMAGE)

CXX      RI = RLAMBDA * DABS(SIGPRIN)
CXX      RLENGTH = RBETS * RL
CXX      RHO = RI * RLENGTH**2 / RAREA
CXX      XRHO(II) = DMAX1( RHO, XRHO(II) )

C
C
C CALCULATE EFFECTIVE PROPERTIES WITH UPDATED VALUE OF RHO

CXX      E1 = EO
CXX      E2 = EO / ( 1.0 + 2.0*PI*RHO ) ! EO DEPENDS ON PLANE STRESS
CXX      RNU12 = RNU
CXX      RNU21 = RNU / ( 1.0 + 2.0*PI*RHO )
CXX      G12 = GO / ( 1.0 + 2.0*PI*RHO*(GO/EO) )

C
C
C FORM REDUCED STIFFNESS MATRIX

CXX      Q11 = E1 / ( 1.0 - RNU12*RNU21 )
CXX      Q12 = RNU21 * Q11

```

```

CXY          Q22 = E2 / ( 1.0 - RNU12*RNU21 )
CXY          Q66 = G12
CXX
CXX          END CXX MODIFICATION
CXX
C
C          TRANSFORM SELECTED STIFFNESS COMPONENTS TO INTERFACIAL COORD.
C          (-45 DEG)
          PN4 = -PI / 4.0
          QBAR11 = Q11*DCOS(PN4)**4
1          + 2.0*( Q12 + 2.0*Q66 )*DSIN(PN4)**2*DCOS(PN4)**2
2          + Q22*DSIN(PN4)**4
          QBAR12 = ( Q11 + Q22 - 4.0*Q66 )*DSIN(PN4)**2
1          *DCOS(PN4)**2
2          + Q12*( DSIN(PN4)**4 + DCOS(PN4)**4 )
          QBAR22 = Q11*DSIN(PN4)**4
1          + 2.0*( Q12 + 2.0*Q66 )*DSIN(PN4)**2*DCOS(PN4)**2
2          + Q22*DCOS(PN4)**4
          QBAR16 = ( Q11 - Q12 - 2.0*Q66 )*DSIN(PN4)*DCOS(PN4)**3
1          + ( Q12 - Q22 + 2.0*Q66 )*DSIN(PN4)**3*DCOS(PN4)
          QBAR26 = ( Q11 - Q12 - 2.0*Q66 )*DSIN(PN4)**3*DCOS(PN4)
1          + ( Q12 - Q22 + 2.0*Q66 )*DSIN(PN4)*DCOS(PN4)**3
          QBAR66 = ( Q11 + Q22
1          - 2.0*(Q12+Q66))*DSIN(PN4)**2*DCOS(PN4)**2
2          + Q66*( DSIN(PN4)**4 + DCOS(PN4)**4 )
C
C          INVERT TRANSFORMED REDUCED STIFFNESS MATRIX TO DETERMINE
C          S22 AND S66 OF MATERIAL, THEN TAKE RECIPROCAL TO GET
C          ED22 AND GD12
C
CX          S22 = ( QBAR11 * QBAR66 - QBAR16**2 ) /
CX          1      ( QBAR11 * QBAR22 * QBAR66 - QBAR12**2 * QBAR66 -
CX          2      QBAR11 * QBAR26**2 + 2.0 * QBAR12 * QBAR16 * QBAR26 -
CX          3      QBAR16**2 * QBAR22 )
CX          S66 = ( QBAR11 * QBAR22 - QBAR12**2 ) /
CX          1      ( QBAR11 * QBAR22 * QBAR66 - QBAR12**2 * QBAR66 -
CX          2      QBAR11 * QBAR26**2 + 2.0 * QBAR12 * QBAR16 * QBAR26 -
CX          3      QBAR16**2 * QBAR22 )
CX          ED22 = 1.0 / S22
CX          GD66 = 1.0 / S66
CYX
CX          WRITE(6,8899) ED22,GD66
CX          8899 FORMAT(5X,'ED22= ',E15.5,5X,'GD66= ',E15.5)
CYX
CX          RKN = ED22 * AREA / RL
CX          RKT = GD66 * AREA / RL
CX          RKN = QBAR22 * AREA / RL
CX          RKT = QBAR66 * AREA / RL
C
C          IF ( UND .LT. 0.0 ) THEN                ! MODIFY NORMAL STIFFNESS
CY          RKN = 10.OE2 * QBAR22 * AREA / RL ! FOR COMPRESSIVE LOADS
CY          RKN = QBAR22 * AREA / RL
C
C          ENDIF
CX          CHECK FOR PRIOR INTERFACIAL FAILURE
CX          IF ( INTDF(II) .GT. 0 ) THEN
CX          RKT = 0.0
CX          IF ( UND .GT. 0.0 ) THEN
CX          RKN = 0.0
CX          ENDIF
CX          ENDIF
CX          ENDIF
C
C          ELSE
C          ! INTERFACE SEPARATED
C
C          IF ( UND .LT. 0.0 ) THEN
CX          Q22 = E0 / ( 1.0 - RNU*RNU )
CX          RKN = 10.OE2 * Q22 * AREA / RL
CX          RKN = Q22 * AREA / RL
C
CX          RKT = 0.0
C          ELSE
CX          RKN = 0.0
CX          RKT = 0.0
CX          ENDIF
CX          ENDIF
C
C***** END KACHANOV'S MODEL *****
C

```

```

713 CONTINUE
CX      FORCE CALCULATION ELEMENT
CX
      IF ( ITFLAG .EQ. 3 ) THEN
          AREA = ( W1 + W2 ) / 2.0 * T(1)
          Q22 = EO / ( 1.0 - RNU*RNU )
          Q66 = GO
          RKN = Q22 * AREA / RL
          RKT = Q66 * AREA /RL
      ENDIF
CX
CX
C
C CALCULATE RKINT MATRIX
C
      C1=DCOS( PHIAV )
      S1=DSIN( PHIAV )
      C2=DCOS( PHIAV - PI/2. )
      S2=DSIN( PHIAV - PI/2. )
      IF(IDUMP.LT.3) GO TO 666
      WRITE(6,1001) C1,C2,S1,S2
1001  FORMAT(10X,'C1 = ',E15.7,5X,'C2 = ',E15.7,/,
1      10X,'S1 = ',E15.7,5X,'S2 = ',E15.7,/)
666 CONTINUE
CY      NEW
      RKINT(1,1)= RKN*C1**2 + RKT*C2**2
      RKINT(1,2)= RKN*C1*S1 + RKT*C2*S2
      RKINT(1,3)= -RKN*C1**2 - RKT*C2**2
      RKINT(1,4)= -RKN*C1*S1 - RKT*C2*S2
      RKINT(2,2)= RKN*S1**2 + RKT*S2**2
      RKINT(2,3)= -RKN*C1*S1 - RKT*C2*S2
      RKINT(2,4)= -RKN*S1**2 - RKT*S2**2
      RKINT(3,3)= RKN*C1**2 + RKT*C2**2
      RKINT(3,4)= RKN*C1*S1 + RKT*C2*S2
      RKINT(4,4)= RKN*S1**2 + RKT*S2**2
CY      OLD
CY      RKINT(1,1) = RKN*C1**2 + RKT*S1**2
CY      RKINT(1,2) = -RKN*C1*S1 + RKT*C1*S1
CY      RKINT(1,3) = -RKN*C1**2 - RKT*S1**2
CY      RKINT(1,4) = RKN*C1*S1 - RKT*C1*S1
CY      RKINT(2,2) = RKN*S1**2 + RKT*C1**2
CY      RKINT(2,3) = RKN*C1*S1 - RKT*C1*S1
CY      RKINT(2,4) = -RKN*S1**2 - RKT*C1**2
CY      RKINT(3,3) = RKN*C1**2 + RKT*S1**2
CY      RKINT(3,4) = -RKN*C1*S1 + RKT*C1*S1
CY      RKINT(4,4) = RKN*S1**2 + RKT*C1**2
CY
      DO 99 J=1,4
          J1=J+1
          DO 99 I=J1,4
79      RKINT(I,J)=RKINT(J,I)
          IF(IDUMP.LT.3) GO TO 667
          WRITE(6,1002)
1002  FORMAT(10X,'THE RKINT MATRIX IS',/)
          DO 44 I=1,4
              WRITE(6,1003) (RKINT(I,J),J=1,4)
1003  FORMAT(4(5X,E15.7))
          44 CONTINUE
          667 CONTINUE
          RETURN
          END
C
C*****
C
C      SUBROUTINE ASEINT
C
C      THIS ROUTINE ASSEMBLES THE INTERFACE ELEMENTS
C
C*****
C
      SUBROUTINE ASEINT(AK,RKINT,NPE,NICON,NDOFPN)
      IMPLICIT REAL*8(A-H,O-Z)
      REAL*8 AK(2400,600),RKINT(4,4)
      DIMENSION NICON(2)
C-----> FIRST THE ROWS
      DO 10 JJ = 1, NPE
          NROW = ( NICON(JJ) - 1 )*NDOFPN
          DO 10 J = 1, NDOFPN
              NROW = NROW + 1
              I = ( JJ-1 )*NDOFPN + J

```

```

C-----> THEN THE COLUMNS
      DO 10 KK = 1, NPE
      NCOLB = ( NICON(KK) - 1 ) * NDOFNP
      DO 10 K = 1, NDOFNP
      L = ( KK - 1 ) * NDOFNP + K
      NCOL = NCOLB + K + 1 - NROW
C-----> DO NOT STORE BELOW DIAGONAL
      IF ( NCOL .LE. 0 ) GO TO 10
      AK(NROW,NCOL)=AK(NROW,NCOL)+RKINT(I,L)
10 CONTINUE
      RETURN
      END

C
C*****
C
C      SUBROUTINE FGLOB
C
C      THIS SUBROUTINE CALCULATES THE GLOBAL FORCE MATRIX
C
C*****
C
      SUBROUTINE FGLOB(FGL,FG,NTOT,S)
      IMPLICIT REAL*8(A-H,O-Z)
      REAL*8 FEL(6),T(1500),FGL(2400),S(1500,4),A1(1200),A2(1200),
1      B(3,6),FG(2400),KGS(2400,600),Q(2400),FINT(4),DN(500),
2      DT(500)
      INTEGER NODE(1500,3),NDOF(1500),MATSET(1500),MTYPE(1500)
      COMMON/CHIST/RTOL,NN,NEL,NF,NDBC,IDUMP,IPRI,ISREF,
1      IEQUIT,ITEMAX,ITEMP,IINT
      COMMON/DISPHIS/DELTAQ(2400),WORKN(500),WORKT(500),FSEPN(500),
1      FSEPT(500)
      COMMON/AREA1/B
      COMMON/AREA2/NODE,NDOF
      COMMON/AREA4/Q
      COMMON/AREA5/T,MATSET,MTYPE
      COMMON/AREA6/A1,A2
      COMMON/AREA7/NSTE,INCR,ITER
      COMMON/LOAD/TIMV(1,1000),RV(1,1000),INODE(100),ICURVE(100),
1      DINC(1000),DPMINC(1000),DMULT(1,1000)
      COMMON/STIF/KGS
      COMMON/BANDED/MAXBW
CX      COMMON/INTFAC/NINT1,NINT2,SIGMAX,DELTA,ALPH,DBFAC,DN,DT,ETA
      COMMON/INTFAC/NIFEM,NIFGP,ITGPL(10,2),ITCON(500,2),
1      SIGMAX(10),DELTAN(10),DELTAT(10),ALPH(10),
2      ETA(10),DBFAC(10),DN,DT,INTDF(500),INTSP(500)
3      ,RMU(10),DISPN(500),DISPT(500),TNRATIO(500),
4      XRH0(500),SIGNN(500),TAUNT(500),FN(500),FT(500)
      COMMON/MODPARA/RMP1(10),RMP2(10),RMP3(10),RMP4(10),RMP5(10),
1      RMP6(10),RMP7(10),RMP8(10),RMP9(10),RMP10(10)
      NTOT=2*NN
      DO 8888 I=1,NEL
      CALL SHAPE(I,IDUMP,AREA)
      DO 33 L=1,6
      FEL(L)=0.
      DO 33 K=1,3
33 FEL(L)=FEL(L)+S(I,K)*B(K,L)
      DO 34 L=1,6
34 FEL(L)=FEL(L)*AREA*T(I)
      DO 55 K=1,3
      N2=NODE(I,K)*2-1
      II=2*(K-1)+1
      FG(N2)=FG(N2)-FEL(II)
55 FG(N2+1)=FG(N2+1)-FEL(II+1)
8888 CONTINUE
      IF(IDUMP.LT.3) GO TO 4935
      WRITE(6,6009)
6009 FORMAT(/25X,'FG IS',/)
      DO 999 I=1,NTOT
      WRITE(6,6010) FG(I)
6010 FORMAT(15X,E16.7)
999 CONTINUE
4935 CONTINUE
      IF(IINT.EQ.0) GO TO 9199

C
C INCLUDE FORCES CAUSED BY INTERFACE ELEMENTS
C
      PI = 3.141592654
CX      NINEL=NINT2-NINT1+1
CX      I1=NINT1
CX      I2=I1+NINEL

```

```

CX      DO 4544 I=1,NINEL
CX
      DO 4600 J = 1, NIFGP                ! LOOP OVER GROUPS
      DO 4544 I = ITGPL(J,1), ITGPL(J,2)  ! LOOP OVER ELEMENTS
C
      IF ( I .EQ. ITGPL(J,1) ) THEN
        ITFLAG = 1
      ELSE IF ( I .EQ. ITGPL(J,2) ) THEN
        ITFLAG = 2
CX      FORCE CALCULATION ELEMENT
CX
      ELSE IF ( ITGPL(J,1) .EQ. ITGPL(J,2) ) THEN
        ITFLAG = 3
CX
CX
      ELSE
        ITFLAG = 0
      ENDIF
C
      I1 = ITCON(I,1)
      I2 = ITCON(I,2)
CX
      IF ( ITFLAG .EQ. 3 ) GO TO 711
      I1M1X = I - 1
      I1P1X = I + 1
      I1M1 = ITCON(I1M1X,1)
      I1P1 = ITCON(I1P1X,1)
C
C      CALCULATE INTERFACIAL NORMAL ANGLE, PHI
C
      IF ( A2(I1M1) .EQ. A2(I1) ) THEN    ! MODIFIED FOR 90 DEG.
        PHI1 = PI / 2.0
      ELSE
        PHI1=DATAN((A1(I1)-A1(I1M1))/(A2(I1M1)-A2(I1)))
      ENDIF
      IF ( A2(I1) .EQ. A2(I1P1) ) THEN    ! MODIFIED FOR 90 DEG.
        PHI2 = PI / 2.0
      ELSE
        PHI2=DATAN((A1(I1P1)-A1(I1))/(A2(I1)-A2(I1P1)))
      ENDIF
      W1W1=(A1(I1)-A1(I1M1))**2 +
1      (A2(I1M1)-A2(I1))**2
      W2W2=(A1(I1P1)-A1(I1))**2 +
1      (A2(I1)-A2(I1P1))**2
      W1 = SQRT(W1W1)
      W2 = SQRT(W2W2)
C
C ACCOUNT FOR FIRST AND LAST ELEMENT
C
CX      IF(I.GT.1) GO TO 334
CX      IF(PHI2.LT..001) GO TO 443
CX      PHI1=3.14159265-PHI2
CX      GO TO 3314
CX 443 PHI1=PHI2
CX 3314 W1=0.
CX 334 CONTINUE
CX      IF(I.LT.NINEL) GO TO 335
CX      IF(PHI1.LT..001) GO TO 444
CXCX      PHI2=-PHI1
CX      PHI2 = PHI1
CX      GO TO 3334
CX 444 PHI2=PHI1
CX 3334 W2=0.
CX 335 CONTINUE
CX
711      CONTINUE
      IF ( ITFLAG .EQ. 1 ) THEN
        PHI1 = PHI2
        W1 = 0.0
      ELSE IF ( ITFLAG .EQ. 2 ) THEN
        PHI2 = PHI1
        W2 = 0.0
CX      FORCE CALCULATION ELEMENT
CX
      ELSE IF ( ITFLAG .EQ. 3 ) THEN
        W1 = 1.0
        W2 = 1.0
        PHI1 = PI / 2.0
        PHI2 = PI / 2.0
CX

```

```

CX      ENDIF
CX
      N1X=2*I1-1
      N1Y=N1X+1
      N2X=2*I2-1
      N2Y=N2X+1
      PHI1=(PHI1+PHI2)/2.
CY      UN=(Q(N2X)-Q(N1X))*DCOS(PHI1)+(Q(N2Y)-Q(N1Y))*DSIN(PHI1)
CY      UT=-(Q(N2X)-Q(N1X))*DSIN(PHI1)+(Q(N2Y)-Q(N1Y))*DCOS(PHI1)
      THETA1 = PHI1 - ( PI / 2.0 )
      UN = -(Q(N2X)-Q(N1X))*DSIN(THETA1) +
1          (Q(N2Y)-Q(N1Y))*DCOS(THETA1)
      UT = (Q(N2X)-Q(N1X))*DCOS(THETA1) +
1          (Q(N2Y)-Q(N1Y))*DSIN(THETA1)
CY
CX
C      ASSIGN VARIABLES FOR KACHANOV'S MODEL
C
      EO = SIGMAX(J)
      RNU = DELTAN(J)
      GO = DELTAT(J)
      ESPCRIT = ALPH(J)
      RLAMBDA = ETA(J)
      RL = DBFAC(J)
      RBETA = RMU(J)
C      CHANGE EO AND RNU TO PLANE STRAIN CONDITIONS
      EO = EO / ( 1.0 - (RNU**2) )
      RNU = RNU / ( 1.0 - RNU )
CX
C*****
C      NEEDLEMAN OR TVERGAARD
CX      UND = UN / DELTAN(J)
CX      UTD = UT / DELTAT(J)
C
C-----
C      KACHANOV
C
      UND = UN / RL
      UTD = UT / RL
C
C*****
C
CX      IF ( ITFLAG .EQ. 3 ) GO TO 713
C
C      DUX = DELTAQ(N2X) - DELTAQ(N1X)
      DUY = DELTAQ(N2Y) - DELTAQ(N1Y)
CY
CY      DUN = DUX * DCOS(PHI1) + DUY * DSIN(PHI1)
CY      DUT = -DUX * DSIN(PHI1) + DUY * DCOS(PHI1)
CY
      DUN = -DUX * DSIN(THETA1) + DUY * DCOS(THETA1)
      DUT = DUX * DCOS(THETA1) + DUY * DSIN(THETA1)
CY
      DUND = DUN / RL
      DUTD = DUT / RL
C
      IF(IDUMP.LT.3) GO TO 6034
      WRITE(6,1000) I1,PHI1,PHI2,W1,W2,UN,UT,UND,UTD
1000  FORMAT(10X,'IN FGL0B - I1 = ',I3,/,10X,'PHI1 = ',E15.7,
1      1X,'PHI2 = ',E15.7,/,10X,'W1 = ',E15.7,
2      1X,'W2 = ',E15.7,/,10X,'UN = ',E15.7,
3      1X,'UT = ',E15.7,/,10X,'UND = ',E15.7,
4      1X,'UTD = ',E15.7,/)
6034  CONTINUE
CX
CX      WRITE(6,3000) I1,UND,UTD
CX 3000  FORMAT(10X,'IN FGL0B - I1 = ',I3,/,15X,'UND = ',E15.7,5X,
CX      1      'UTD = ',E15.7,/)
CX
C
C      CALCULATE NORMAL AND TANGENTIAL FORCE COMPONENTS
C      FN,FT
C
C***** KACHANOV'S MODEL *****
CX
C      FORCE CALCULATIONS
C

```

```

C*****
C
C AREA.....TRUSS ELEMENT CROSS SECTIONAL AREA
C RL.....THICKNESS OF INTERFACE (INP.)
C EO.....YOUNG'S MODULUS OF INTERFACE (INP.)
C GO.....SHEAR MODULUS OF INTERFACE (INP.)
C RNU.....POISSON'S RATIO OF INTERFACE (INP.)
C ESPCRIT.....CRITICAL TENSILE STRAIN (INP.)
C RLAMBDA.....DAMAGE GROWTH PROPORTIONAL CONST. (INP.)
C RAREA.....AREA OF DAMAGED ZONE
C RLENGTH.....CRACK LENGTH
C RBETA.....RLENGTH / RL (INP.)
C
C*****
C
CX      CALCULATE PRINCIPLE NORMALIZED DISPLACEMENTS
C
      RLSQ = ( UND / 2.0)**2 + ( UTD / 2.0)**2
      RLAM = SQRT( RLSQ )
      UM1 = UND / 2.0 + RLAM
      UM2 = UND / 2.0 - RLAM
      UMAX = DMAX1( UM1 , UM2 )
      AREA = ( W1 + W2 ) / 2.0 * T(1)
      RAREA = AREA / T(1) * RL
C
      IF ( UMAX .LE. ESPCRIT ) THEN          ! INTERFACE INTACT
C
          IF ( UND .EQ. 0.0 .AND. UTD .EQ. 0.0 ) THEN
              Q22 = EO / ( 1.0 - RNU*RNU )
              Q66 = GO
              FN(I) = 0.0
              FT(I) = 0.0
          ELSE
              IF ( UND .LT. 0.0 ) THEN        ! MODIFY NORMALIZED
                  UNDC = 0.0                  ! DISPLACEMENTS FOR
                  UTDC = UTD                  ! COMPRESSIVE LOADS
              ELSE
                  UNDC = UND
                  UTDC = UTD
              ENDIF
          ENDIF
C
C      TRANSFORM NORMALIZED DISPLACEMENTS TO PRINCIPLE DAMAGE
C      COORDINATES (1,2)
C
      P4 = PI / 4.0
      P42 = P4 * 2.0
      DC2 = DCOS(P4) * DCOS(P4)
CX      UNDPD = -UTD*DSIN(P4) + UND*DCOS(P4)
CX      UTPD = UTD*DCOS(P4) + UND*DSIN(P4)
      UNDPD = UNDC * DC2 - ( 0.5 * UTDC ) * DSIN(P42)
      UTPD = 0.5 * UNDC * DSIN(P42) + ( 0.5 * UTDC ) * DCOS(P42)
      DUNDP = DUND * DC2 - ( 0.5 * DUTD ) * DSIN(P42)
      DUTDP = 0.5 * DUND * DSIN(P42) + ( 0.5 * DUTD ) * DCOS(P42)
C
C      DETERMINE EFFECTIVE PROPERTIES
C
C      CXX MODIFICATION TO USE STRESS DEPENDENT DAMAGE
C      GROWTH LAW
C
CX      RI = RLAMBDA * DABS(UNDPD)          ! RLAMBDA * UNDPD
CX      RI = RLAMBDA * DABS(UTDC)          ! RLAMBDA * UTDC
CX      RLENGTH = RBETA * RL              ! RBETA * RL
CX      RHO = RI * RLENGTH**2 / RAREA
CX      RHO = DMAX1( RHO, XRH0(I) )
CX      XRH0(I) = RHO
CX      RHO = XRH0(I)
C
CX      E1 = EO                          ! EO DEPENDS ON PLANE STRESS
CX      E2 = EO / ( 1.0 + 2.0*PI*RHO )    ! OR PLANE STRAIN CONDITIONS
CX      RNU12 = RNU
CX      RNU21 = RNU / ( 1.0 + 2.0*PI*RHO )
CX      G12 = GO / ( 1.0 + 2.0*PI*RHO*(GO/EO) )
C
C      FORM REDUCED STIFFNESS MATRIX
C
      Q11 = E1 / ( 1.0 - RNU12*RNU21 )
      Q12 = RNU21 * Q11
      Q22 = E2 / ( 1.0 - RNU12*RNU21 )
      Q66 = G12

```

```

CXX
CXX BEGIN CXX MODIFICATIONS
CXX
C
C CALCULATE PRINCIPAL STRESSES FOR DAMAGE GROWTH LAW
C
      SIGNN(I) = SIGNN(I) + Q22 * DUNDP
      TAUNT(I) = TAUNT(I) + Q66 * DUTDP
      SIGSIG = (SIGNN(I) / 2.0)**2 + (TAUNT(I) / 2.0)**2
      RSIG = SQRT(SIGSIG)
      SIGM1 = SIGNN(I)/2.0 + RSIG
      SIGM2 = SIGNN(I)/2.0 - RSIG
      SIGPRIN = DMAX1(SIGM1,SIGM2)
      TAUMAX = RSIG
C
C CALCULATE THE VALUE OF RHO (MICRO CRACK DAMAGE)
C
      RI = RLAMBDA * DABS(SIGPRIN)
      RLENGTH = RBETA * RL
      RHO = RI * RLENGTH**2 / RAREA
      XRH0(I) = DMAX1( RHO, XRH0(I) )
C
C RECALCULATE EFFECTIVE PROPERTIES WITH UPDATED RHO
C
      E1 = EO
      E2 = EO / ( 1.0 + 2.0*PI*RHO ) ! EO DEPENDS ON PLANE STRESS
      RNU12 = RNU
      RNU21 = RNU / ( 1.0 + 2.0*PI*RHO )
      G12 = GO / ( 1.0 + 2.0*PI*RHO*(GO/EO) )
C
C FORM REDUCED STIFFNESS MATRIX
C
      Q11 = E1 / ( 1.0 - RNU12*RNU21 )
      Q12 = RNU21 * Q11
      Q22 = E2 / ( 1.0 - RNU12*RNU21 )
      Q66 = G12
CXX
CXX END MODIFICATION FOR STRESS DEPENDENT DAMAGE GROWTH
CXX
C
C TRANSFORM SELECTED STIFFNESS COMPONENTS TO INTERFACIAL COORD.
C      (-45 DEG)
      PN4 = -PI / 4.0
      QBAR11 = Q11*DCOS(PN4)**4
      + 2.0*( Q12 + 2.0*Q66 )*DSIN(PN4)**2*DCOS(PN4)**2
      + Q22*DSIN(PN4)**4
      QBAR12 = ( Q11 + Q22 - 4.0*Q66 )*DSIN(PN4)**2
      *DCOS(PN4)**2
      + Q12*( DSIN(PN4)**4 + DCOS(PN4)**4 )
      QBAR22 = Q11*DSIN(PN4)**4
      + 2.0*( Q12 + 2.0*Q66 )*DSIN(PN4)**2*DCOS(PN4)**2
      + Q22*DCOS(PN4)**4
      QBAR16 = ( Q11 - Q12 - 2.0*Q66 )*DSIN(PN4)*DCOS(PN4)**3
      + ( Q12 - Q22 + 2.0*Q66 )*DSIN(PN4)**3*DCOS(PN4)
      QBAR26 = ( Q11 - Q12 - 2.0*Q66 )*DSIN(PN4)**3*DCOS(PN4)
      + ( Q12 - Q22 + 2.0*Q66 )*DSIN(PN4)*DCOS(PN4)**3
      QBAR66 = ( Q11 + Q22
      - 2.0*(Q12+Q66))*DSIN(PN4)**2*DCOS(PN4)**2
      + Q66*( DSIN(PN4)**4 + DCOS(PN4)**4 )
C
C INVERT TRANSFORMED REDUCED STIFFNESS MATRIX TO DETERMINE
C S22 AND S66 OF MATERIAL, THEN TAKE RECIPROCAL TO GET
C ED22 AND GD12
C
      S22 = ( QBAR11 * QBAR66 - QBAR16**2 ) /
      ( QBAR11 * QBAR22 * QBAR66 - QBAR12**2 * QBAR66 -
      QBAR11 * QBAR26**2 + 2.0 * QBAR12 * QBAR16 * QBAR26 -
      QBAR16**2 * QBAR22 )
      S66 = ( QBAR11 * QBAR22 - QBAR12**2 ) /
      ( QBAR11 * QBAR22 * QBAR66 - QBAR12**2 * QBAR66 -
      QBAR11 * QBAR26**2 + 2.0 * QBAR12 * QBAR16 * QBAR26 -
      QBAR16**2 * QBAR22 )
      ED22 = 1.0 / S22
      GD66 = 1.0 / S66
      FN(I) = FN(I) - QBAR22 * AREA * ( DUND )
      FT(I) = FT(I) - 2.0 * QBAR66 * AREA * ( 0.5 * DUTD )
      ADJUST NORMAL FORCE FOR COMPRESSIVE LOADS
      IF ( UND .LT. 0.0 ) THEN
      FN(I) = FN(I) -10.0E2 * QBAR22 * ( UND )
      FN(I) = FN(I) - QBAR22 * AREA * ( DUND )

```



```

CY
      ENDIF
CY      CHECK FOR PRIOR FAILURE
      IF ( INTDF(I) .GT. 0 ) THEN
        FT(I) = 0.0
        IF ( UND .GT. 0.0 ) THEN
          FN(I) = 0.0
        ENDIF
      ENDIF
CX
CX
CYX      WRITE(6,4567) ED22,GD66
CYX 4567 FORMAT(10X,'ED22= ',E15.6,5X,'GD66= ',E15.6)
CX
CX
C
      ENDIF
C
CCCCCCCCCCCCCCCCCCCCCCCCCCCCCCCCCCCCCCCCCCCCCCCCCCCCCCCCCCCC
C
C      CALCULATE INCREMENT OF WORK OF SEPARATION
C
      IF ( UND .LT. 0.0 ) THEN
        DWORKN = 0.0
      ELSE
        DWORKN = DABS(FN(I)) * DABS(DUN)
      ENDIF
      DWORKT = DABS(FT(I)) * DABS(DUT)
      IF ( INTDF(I) .GT. 0 ) THEN
        DWORKN = 0.0
        DWORKT = 0.0
      ENDIF
      WORKN(I) = WORKN(I) + DWORKN
      WORKT(I) = WORKT(I) + DWORKT
C
      ELSE
        ! INTERFACE SEPARATED
C
        IF ( UND .LT. 0.0 ) THEN
          Q22 = EO / ( 1.0 - RNU*RNU )
          FN(I) = FN(I) - 10.0E2 * Q22 * AREA * ( DUND )
          FN(I) = FN(I) - Q22 * AREA * ( DUND )
CY
          FT(I) = 0.0
        ELSE
          FN(I) = 0.0
          FT(I) = 0.0
        ENDIF
        DWORKN = 0.0
        DWORKT = 0.0
        WORKN(I) = WORKN(I) + DWORKN
        WORKT(I) = WORKT(I) + DWORKT
      ENDIF
CX
CX
C***** END KACHANOV'S MODEL *****
CX
713 CONTINUE
CX      FORCE CALCULATION ELEMENT
CX
      IF ( ITFLAG .EQ. 3 ) THEN
        Q22 = EO / ( 1.0 - RNU*RNU )
        Q66 = GO
        FN(I) = -Q22 * AREA * ( UND )
        FT(I) = -2.0 * Q66 * AREA * ( 0.5 * UTD )
      ENDIF
CX
CX
CY      OLD
CY      FINT(1)=FN(I)*DCOS(PHIAV)-FT(I)*DSIN(PHIAV)
CY      FINT(2)=FN(I)*DSIN(PHIAV)+FT(I)*DCOS(PHIAV)
CY      FINT(3)=-FN(I)*DCOS(PHIAV)+FT(I)*DSIN(PHIAV)
CY      FINT(4)=-FN(I)*DSIN(PHIAV)-FT(I)*DCOS(PHIAV)
CY      NEW
      RTHETAI = -1.0 * THETAI
      FINT(1) = -FN(I)*DSIN(RTHETAI) + FT(I)*DCOS(RTHETAI)
      FINT(2) = FN(I)*DCOS(RTHETAI) + FT(I)*DSIN(RTHETAI)
      FINT(3) = -FINT(1)
      FINT(4) = -FINT(2)
CY
CY

```

```

      IF(IDUMP.LT.3) GO TO 3398
      WRITE(6,2007) (FINT(K),K=1,4)
2007 FORMAT(10X,'FINT = ',4E15.7,/)
3398 CONTINUE
      FG(N1X)=FG(N1X)-FINT(1)
      FG(N1Y)=FG(N1Y)-FINT(2)
      FG(N2X)=FG(N2X)-FINT(3)
      FG(N2Y)=FG(N2Y)-FINT(4)
CX      I1=I1+1
CX      I2=I2+1
      4544 CONTINUE
      4600 CONTINUE
      9199 CONTINUE
      DO 7777 J=1,NTOT
      7777 FG(J)=FG(J)+FGL(J)
C
C APPLY DISPLACEMENT BOUNDARY CONDITIONS
C
      IF(IDUMP.LT.4) GO TO 521
      WRITE(6,5003) ITER,NDBC,MAXBW
5003 FORMAT(5X,'ITER=',I3,' NDBC=',I3,' MAXBW=',I3,/)
      WRITE(6,5004) (DINC(I),I=1,NDBC)
5004 FORMAT(5X,'DINC = ',3E15.7)
      WRITE(6,5005) (NDOF(I),I=1,NDBC)
5005 FORMAT(5X,'NDOF = ',10I5)
      WRITE(6,7013)
7013 FORMAT(//,20X,'GLOBAL LINEAR STIFFNESS MATRIX',/)
      WRITE(6,7040) ((KGS(II,JJ),JJ=1,MAXBW),II=1,NTOT)
7040 FORMAT(4(5X,E15.7) )
      521 CONTINUE
      IF(NDBC.EQ.0) GO TO 44
      IF(ITER.GT.1) GO TO 43
      DO 9999 K=1,NDBC
C
C SUBTRACT DISPLACEMENTS ABOVE DIAGONAL
C
      JJ=NDOF(K)
      II=1
      97 IF(JJ.GT.MAXBW) GO TO 95
CX      IF ( IDUMP .LT. 3 ) GO TO 2345
CX      WRITE(6,2344) FG(II),KGS(II,JJ),DPMINC(K)
CX 2344 FORMAT(/,'A-BEFORE: FG(II)= ',E14.7,5X,'KGS(II,JJ)= ',E14.7,
CX      1      5X,'DPMINC(K)= ',E14.7,/)
CX 2345 CONTINUE
      FG(II) = FG(II) - KGS(II,JJ) * DPMINC(K)
CX      IF ( IDUMP .LT. 3 ) GO TO 2347
CX      WRITE(6,2346) FG(II),KGS(II,JJ),DPMINC(K)
CX 2346 FORMAT(/,'A-AFTER: FG(II)= ',E14.7,5X,'KGS(II,JJ)= ',E14.7,
CX      1      5X,'DPMINC(K)= ',E14.7,/)
CX 2347 CONTINUE
      95 II=II+1
      98 JJ=JJ-1
      IF(JJ.GT.1) GO TO 97
C
C SUBTRACT DISPLACEMENTS BELOW DIAGONAL
C
      JJ=NDOF(K)
      II=NDOF(K)+1
      LL=2
CX      IF ( IDUMP .LT. 3 ) GO TO 3345
CX      WRITE(6,3344) FG(II),KGS(JJ,LL),DPMINC(K)
CX 3344 FORMAT(/,'B-BEFORE: FG(II)= ',E14.7,5X,'KGS(II,JJ)= ',E14.7,
CX      1      5X,'DPMINC(K)= ',E14.7,/)
CX 3345 CONTINUE
      96 FG(II) = FG(II) - KGS(JJ,LL) * DPMINC(K)
CX      IF ( IDUMP .LT. 3 ) GO TO 3347
CX      WRITE(6,3346) FG(II),KGS(JJ,LL),DPMINC(K)
CX 3346 FORMAT(/,'B-AFTER: FG(II)= ',E14.7,5X,'KGS(II,JJ)= ',E14.7,
CX      1      5X,'DPMINC(K)= ',E14.7,/)
CX 3347 CONTINUE
      II=II+1
      LL=LL+1
      IF(II.GT.NTOT) GO TO 9999
      IF(LL.LE.MAXBW) GO TO 96
      9999 CONTINUE
      DO 9994 K=1,NDBC
      JJ=NDOF(K)
      9994 FG(JJ)=DPMINC(K)
      GO TO 44
      43 DO 9998 K=1,NDBC

```

```

9998 FG(NDOF(K))=0.
44 CONTINUE
   IF(IDUMP.LT.3) GO TO 6666
   IRIGHT=1
   IF(IRIGHT.NE.1) GO TO 6666
   WRITE(6,2014)
2014 FORMAT(//,20X,'RIGHT HAND SIDE MATRIX',//)
   WRITE(6,2015) (FG(I),I=1,NTOT)
2015 FORMAT(30X,E15.7)
6666 CONTINUE
   RETURN
   END

C
C*****
C
C           SUBROUTINE BANDWD
C
C           THIS ROUTINE DETERMINES THE BAND WIDTH OF THE STIFFNESS
C           MATRIX
C*****
C
SUBROUTINE BANWD(MODEL,NELEMS,NCON,NDOFPN,MAXBW,IDUMP)
DIMENSION NCON(1500,3)
MAXBW=0
DO 10 J=1,NELEMS
  KA=NCON(J,1)
  KB=NCON(J,2)
  KC=NCON(J,3)
  IF(MODEL.LE.3) GOTO 2
  KAA=NCON(J,4)
  KBB=NCON(J,5)
  KCC=NCON(J,6)
2  KAMB=IABS(KA-KB)
  KAMC=IABS(KA-KC)
  KBMC=IABS(KB-KC)
  IF(MODEL.LE.3) GOTO 3
  KAMAA=IABS(KA-KAA)
  KAMBB=IABS(KA-KBB)
  KAMCC=IABS(KA-KCC)
  KBMAA=IABS(KB-KAA)
  KBMBB=IABS(KB-KBB)
  KBMCC=IABS(KB-KCC)
  KCMAA=IABS(KC-KAA)
  KCMBB=IABS(KC-KBB)
  KCMCC=IABS(KC-KCC)
3  ICK=(MAXO(KAMB,KAMC,KBMC)+1)*NDOFPN
  IF(MODEL.LT.4) GO TO 1430
  ICK=(MAXO(KAMB,KAMC,KBMC,KAMAA,KAMBB,KAMCC,KBMAA,
*      KBMBB,KBMCC,KCMAA,KCMBB,KCMCC)+1)*NDOFPN
1430 CONTINUE
  IF(MAXBW.LT.ICK) MAXBW=ICK
10 CONTINUE
  IF(IDUMP.LT.2) GOTO 15
  WRITE(6,20) MAXBW
20 FORMAT(/10X,'THE MAXIMUM SEMI-BANDWIDTH IS',I3)
15 CONTINUE
  RETURN
  END

C
C*****
C
C           SUBROUTINE BANDSOL
C*****
C
C           SYMMETRIC BAND MATRIX EQUATION SOLVER.  GAUSS-DOOLITTLE
C           METHOD SOLVES EQUATIONS (AK)(X)=R
C           AK = SYMMETRIC BANDED COEFFICIENT MATRIX STORED IN
C               COMPACTED FORM
C           R  = RIGHT HAND SIDE MATRIX
C           NEQ = NUMBER OF EQUATIONS BEING SOLVED
C           IBAND = SEMI-BANDWIDTH OF EQUATIONS BEING SOLVED
C           MAXEQ = NO. OF ROWS FOR WHICH AK AND R ARE DIMENSIONED
C                 (MAX EQUATIONS)
C           MAXBND = NO. OF COLUMNS FOR WHICH AK IS DIMENSIONED
C                 (MAX BANDWIDTH)
C           KKK = 1 TRIANGULARIZES THE SYMMETRIC, BANDED MATRIX AK
C                   AND OVERWRITES IT INTO AK (HENCE, AK IS
C                   DESTROYED AND IS REPLACED BY ITS TRIANGULARIZED

```

```

C          FORM).  NOTE THAT R IS NOT NEEDED.
C          KKK = 2  OBTAINS SOLUTION TO (AK)(X)=R FOR A PARTICULAR
C                   RIGHT-HAND-SIDE R (ASSUMES THAT TRIANGULARIZED
C                   FORM OF AK IS STORED IN AK).  SOLUTION IS
C                   RETURNED IN R.
C          KKK = 3  PERFORMS BOTH FORWARD ELIMINATION AND BACK
C                   SUBSTITUTION AT THE SAME TIME
C          NOTE---FOR SOLUTION OF SEVERAL SETS OF EQUATIONS WITH SAME
C                   LEFT SIDE (AK) BUT DIFFERENT RIGHT SIDES (R), THE
C                   FIRST SOLUTION SHOULD BE OBTAINED WITH KKK=3 (OR
C                   KKK=1 AND KKK=2).  SUBSEQUENT SOLUTIONS WITH NEW
C                   RIGHT-HAND-SIDES REQUIRES ONLY CALLING BANSOL WITH
C                   KKK=2 (TRIANGULARIZED AK AND NEW R NEEDED).
C          WARNING--THIS PROGRAMS ASSUMES THAT AK IS POSITIVE
C                   DEFINITE AND DIAGONALLY DOMINANT.  NO PIVOTING OR
C                   CHECKING FOR ZERO DIAGONAL ELEMENTS IS PERFORMED.
C          SEE W.E. HAISLER IF YOU HAVE PROBLEMS
C

```

```

C          SUBROUTINE BANSOL(AK,R,NEQ,IBAND,MAXEQ,MAXBND,KKK)
C          IMPLICIT REAL*8 (A-H,O-Z)
C          DIMENSION AK(MAXEQ,MAXBND),R(MAXEQ)
C          NRS = NEQ - 1
C          NR = NEQ
C          GO TO (100,200,100), KKK
C          PERFORM TRIANGULARIZATION OF AK
C100 DO 120 N=1,NRS
C      M = N - 1
C      MR = MINO(IBAND,NR-M)
C      PIVOT = AK(N,1)
C      DO 120 L=2,MR
C      CP = AK(N,L)/PIVOT
C      I = M + L
C      J = 0
C      DO 110 K=L,MR
C      J = J + 1
C110 AK(I,J) = AK(I,J) - CP*AK(N,K)
C120 AK(N,L) = CP
C      IF (KKK.EQ.1) RETURN
C          FORWARD ELIMINATION OF R
C200 DO 220 N=1,NRS
C      M = N - 1
C      MR = MINO(IBAND,NR-M)
C      CP = R(N)
C      R(N) = CP/AK(N,1)
C      DO 220 L=2,MR
C      I = M + L
C220 R(I) = R(I) - AK(N,L)*CP
C          BACKWARD SUBSTITUTION TO OBTAIN SOLUTION
C      R(NR) = R(NR)/AK(NR,1)
C      DO 320 I=1,NRS
C      N = NR - I
C      M = N - 1
C      MR = MINO(IBAND,NR-M)
C      DO 320 K=2,MR
C      L = M + K
C320 R(N) = R(N) - AK(N,K)*R(L)
C400 RETURN
C      END
C

```

```

C*****
C
C          SUBROUTINE ASEMBL
C*****
C

```

```

C          SUBROUTINE ASEMBL(AK,BK,NPE,NNCON,NDOFPN,II)
C          IMPLICIT REAL*8(A-H,O-Z)
C          REAL*8 AK(2400,600),BK(6,6)
C          DIMENSION NNCON(1500,3)
C-----> FIRST THE ROWS
C      DO 10 JJ = 1, NPE
C      NROW = ( NNCON(II,JJ) - 1 )*NDOFPN
C      DO 10 J = 1, NDOFPN
C      NROW = NROW + 1
C      I = ( JJ-1 )*NDOFPN + J
C-----> THEN THE COLUMNS
C      DO 10 KK = 1, NPE
C      NCOLB = ( NNCON(II,KK) - 1 )*NDOFPN
C      DO 10 K = 1, NDOFPN
C      L = ( KK-1 )*NDOFPN + K

```

```

      NCOL = NCOLB + K + 1 - NROW
C-----> DO NOT STORE BELOW DIAGONAL
      IF ( NCOL .LE. 0 ) GO TO 10
      AK(NROW,NCOL)=AK(NROW,NCOL)+BK(I,L)
10 CONTINUE
      RETURN
      END

C
C*****
C
C          SUBROUTINE STRESS
C
C          THIS SUBROUTINE CALCULATES STRESSES AND STRAINS
C*****
C
      SUBROUTINE STRESS(NODE,DS,DE,DELTAQ)
      IMPLICIT REAL*8(A-H,O-Z)
      REAL*8 B(3,6),DET(1500,3),DST(1500,4),DELTAQ(2400)
      REAL*8 DE(1500,3),DS(1500,4),C(3,3),T(1500),A1(1200),A2(1200)
      COMMON/ELAS1/S(1500,4),E(1500,3),EO(1500,3),DSTRAN(3),
1      DSTRES(4)
      COMMON/AREA7/NSTE,INCR,ITER
      COMMON/PLAS1/ALPHA(4,1500),EPBAR(1500),SIGBAR(1500),
1      IPLAS(1500),EPSP(1500,4),DEPSPT(1500,4),
2      DEPS(1500,4)
      INTEGER NODE(1500,3),MATSET(1500),MTYPE(1500)
      COMMON/CHIST/RTOL,NN,NEL,NF,NDBC,IDUMP,IPRI,ISREF,
1      IEQUIT,ITEMAX,ITEMP,IINT
      COMMON/AREA1/B
      COMMON/AREA5/T,MATSET,MTYPE
      COMMON/AREA6/A1,A2
      COMMON/AREA10/DST,DET
      COMMON/HOMOG/SIG1AV,DEBAR11
      VOLUME=0.
      SIG1AV=0.
      DO 9999 I=1,NEL
C CALCULATE STRAINS
      CALL SHAPE(I,IDUMP,AREA)
      N1=NODE(I,1)
      N2=NODE(I,2)
      N3=NODE(I,3)
      Q1=DELTAQ(2*N1-1)
      Q2=DELTAQ(2*N1)
      Q3=DELTAQ(2*N2-1)
      Q4=DELTAQ(2*N2)
      Q5=DELTAQ(2*N3-1)
      Q6=DELTAQ(2*N3)
      DE(I,1)=B(1,1)*Q1+B(1,3)*Q3+B(1,5)*Q5
      DE(I,2)=B(2,2)*Q2+B(2,4)*Q4+B(2,6)*Q6
      DE(I,3)=B(3,1)*Q1+B(3,2)*Q2+B(3,3)*Q3+B(3,4)*Q4+B(3,5)*
1      Q5+B(3,6)*Q6
      DO 93 J=1,3
      E(I,J)=E(I,J) + DE(I,J)
93 DET(I,J)=DET(I,J)+DE(I,J)
      IF(MTYPE(I).EQ.1) GO TO 451
      IF(MTYPE(I).EQ.2) GO TO 452
      IF(MTYPE(I).EQ.3) GO TO 453
      IF(MTYPE(I).EQ.4) GO TO 454
450 WRITE(6,6003)
6003 FORMAT(10X,'MATERIAL TYPE NOT IN CURRENT LIBRARY',/)
      STOP
451 CALL ELAS2D(I,C,DS,MATSET(I))
      GO TO 455
452 CALL PLAS2D(I,C,DS,O,MATSET(I))
      GO TO 455
453 CALL VPLAS2D(I,C,DS,O,MATSET(I))
      GO TO 455
454 GO TO 450
455 CONTINUE
      DO 94 J=1,4
      EPSP(I,J)=EPSP(I,J)+DEPSPT(I,J)
      S(I,J)=S(I,J)+DS(I,J)
      DEPSPT(I,J)=DEPSPT(I,J)+DEPSPT(I,J)
94 DST(I,J)=DST(I,J)+DS(I,J)
      VOLUME=VOLUME+AREA*T(I)
      SIG1AV=SIG1AV+S(I,1)*AREA*T(I)
9999 CONTINUE
      SIG1AV=SIG1AV/VOLUME
      RETURN

```

```

END
C
C*****
C
C      SUBROUTINE PLAS2D
C
C*****
C THIS IS A CONSTITUTIVE PACKAGE FOR RATE INDEPENDENT
C CLASSICAL PLASTICITY...
C THIS PROGRAM DRIVES AN INCREMENTAL CONSTITUTIVE ROUTINE
C IN THE FORM DS=(C)DEC THIS ROUTINE USES RATE INDEPENDENT
C INCREMENTAL PLASTICITY THEORY
C TO DETERMINE THE STRESS INCREMENT FOR A GIVEN STRAIN INCREMENT
C OF A 2-D MATERIAL POINT UNDER PLANE STRAIN CONDITIONS
C
C
      SUBROUTINE PLAS2D(J,C,DS,IPC,MATNO)
      IMPLICIT REAL*8 (A-H,O-Z)
      DIMENSION STRESS(4),STRAIN(3),SG(4),DDEPSP(4),
1      DFDS(6),DDFDS(6),DEPSE(3),DSG(4),SOLD(4),
2      EOLD(3)
      DIMENSION C(3,3),DST(1500,4),DS(1500,4),DET(1500,3)
      COMMON/ELAS1/S(1500,4),E(1500,3),EO(1500,3),DSTRAN(3),
1      DSTRES(4)
      COMMON/ELAS2/EM1(4),EM2(4),VNU(4),G12(4),Y1(4),Y2(4),Y(4),
1      EM(4)
      COMMON/PLAS1/ALPHA(4,1500),EPBAR(1500),SIGBAR(1500),
1      IPLAS(1500),EPSP(1500,4),DEPSPT(1500,4),
2      DEPSP(1500,4)
      COMMON/PLAS2/SX(10,4),EX(10,4),EPX(10,4),
1      SP(10,4),DEPSAL,BETA
      COMMON/BB/NUNIAX(4),IDUMP2,ISUB
      COMMON/AREA10/DST,DET
      COMMON/AREA7/NSTE,INCR,ITER
CX      EMI1=EM1(MATNO)
CX      EMI2=EM2(MATNO)
CX      VNUI12=VNU(MATNO)
CX      VNUI21=VNUI12*EMI2/EMI1
CX      RG12=G12(MATNO)
CX      YI1=Y1(MATNO)
CX      YI2=Y2(MATNO)
      EMI=EM(MATNO)
      VNUI=VNU(MATNO)
      YI=Y(MATNO)
      DO 11 I=1,3
      DEPSP(J,I)=0.
      STRESS(I)=S(J,I)
      STRAIN(I)=EO(J,I)
      DSTRAN(I)=E(J,I)-EO(J,I)
11      CONTINUE
      DEPSP(J,4)=0.
      STRESS(4)=S(J,4)
      C1=EMI/(1.+VNUI)
      C2=C1/(1.-2.*VNUI)
      D11=C2*(1.-VNUI)
      D12=VNUI*C2
      D44=C1/2.
      DSG(1)=D11*DSTRAN(1)+D12*DSTRAN(2)
      DSG(2)=D12*DSTRAN(1)+D11*DSTRAN(2)
      DSG(3)=D44*DSTRAN(3)
      DSG(4)=D12*(DSTRAN(1)+DSTRAN(2))
      DO 10 I=1,4
10      SG(I)=STRESS(I)+DSG(I)
      F=.5*((SG(1)-ALPHA(1,J)-SG(2)+ALPHA(2,J))**2+(SG(2)-
1      ALPHA(2,J)-SG(4)+ALPHA(4,J))**2
2      +(SG(4)-ALPHA(4,J)-SG(1)+ALPHA(1,J))**2+6.*(SG(3)-
3      ALPHA(3,J))**2)-SIGBAR(J)**2
      IF(DABS(F).LT.10.0) F=0.0
      IDUMP3=0
      IF(IDUMP3.EQ.0) GO TO 6004
      WRITE(6,6000)
6000      FORMAT(' ',/,3X,'STRESSES TO PLAS2D ARE',3X,'STRAINS',3X,
1      'STRAIN INCREMENTS',/)
      DO 6001 I=1,3
      WRITE(6,6002)S(J,I),E(J,I),DSTRAN(I)
6002      FORMAT(' ',3X,3(E13.6,3X))
6001      CONTINUE
6004      CONTINUE
      IDUMP4=0

```

```

      IF(IDUMP4.EQ.0) GO TO 6005
      WRITE(6,6003) SIGBAR(J),F
6003  FORMAT(' ',/,3X,'SIGBAR=',E13.6,3X,'F=',E13.6,/)
6005  CONTINUE
      IF(F) 20,30,40
      20  IPLAS(J)=1
          GO TO 2000
      30  IPLAS(J)=2
2000  DO 3000 I=1,4
      DSTRES(I)=DSG(I)
      DS(J,I)=DSTRES(I)
3000  STRESS(I)=STRESS(I)+DSTRES(I)
      DO 3001 I=1,3
      STRAIN(I)=STRAIN(I)+DSTRAN(I)
3001  EO(J,I)=E(J,I)
      12  CONTINUE
          C(1,1)=D11
          C(1,2)=D12
          C(1,3)=0.0
          C(2,1)=C(1,2)
          C(2,2)=C(1,1)
          C(2,3)=0.0
          C(3,1)=0.0
          C(3,2)=0.0
          C(3,3)=D44
          RETURN
      40  CONTINUE
          DO 4020 I=1,3
          SOLD(I)=STRESS(I)
4020  EOLD(I)=STRAIN(I)
          SOLD(4)=STRESS(4)
          IF(IPLAS(J).GT.1) GO TO 1000
          SMA1=STRESS(1)-ALPHA(1,J)
          SMA2=STRESS(2)-ALPHA(2,J)
          SMA3=STRESS(3)-ALPHA(3,J)
          SMA4=STRESS(4)-ALPHA(4,J)
          A=2.*DSG(1)**2+2.*DSG(2)**2-2.*DSG(1)*DSG(2)
          1  +6.*DSG(3)**2+2.*DSG(4)**2
          2  -2.*DSG(2)*DSG(4)-2.*DSG(1)*DSG(4)
          B=4.*SMA1*DSG(1)+4.*SMA2*DSG(2)+4.*SMA4*DSG(4)
          1  -2.*SMA2*DSG(1)-2.*SMA4*DSG(1)
          2  -2.*SMA1*DSG(2)-2.*SMA4*DSG(2)
          3  -2.*SMA1*DSG(4)-2.*SMA2*DSG(4)
          4  +12.*SMA3*DSG(3)
          CC=2.*SMA1**2+2.*SMA2**2+2.*SMA4**2
          1  -2.*SMA1*SMA2-2.*SMA1*SMA4
          2  -2.*SMA2*SMA4+6.*SMA3**2
          3  -2.*SIGBAR(J)**2
          ROOT=B**2-4.*A*CC
          IF(ROOT.LE.0.0) ROOT=0.0
          ZETA=(-B+DSQRT(ROOT))/2./A
          DO 500 I=1,3
          STRESS(I)=STRESS(I)+ZETA*DSG(I)
500  STRAIN(I)=STRAIN(I)+ZETA*DSTRAN(I)
          STRESS(4)=STRESS(4)+ZETA*DSG(4)
          DO 50 I=1,3
          50 DSTRAN(I)=(1.-ZETA)*DSTRAN(I)
          GO TO 1001
1000  ZETA=0.
1001  CONTINUE
          IF(ISUB.NE.0) GO TO 3030
          DE=(4./3.*(DSTRAN(1)**2+DSTRAN(2)**2+DSTRAN(1)*DSTRAN(2)
          1  +DSTRAN(3)**2))**.5
          M=DE/DEPSAL+.1
          IF(M.EQ.0) M=1
          DO 400 I=1,3
          400 DSTRAN(I)=DSTRAN(I)/M
          GO TO 3090
3030  M=1
3090  CONTINUE
          NPSUB=1
          IF(NPSUB.EQ.1) GO TO 3032
          WRITE (6,3031) M
3031  FORMAT(' ',/,3X,'NO. OF SUBINCREMENTS = ',I3,/)
3032  CONTINUE
          DO 5000 NSUB=1,M
          IJ=1
1002  IF(EPBAR(J).LE.(EPX(IJ,MATNO)-.0000002)) GO TO 1010
          IF(IJ.GT.NUNIAX(MATNO)) GO TO 1003
          IJ=IJ+1

```

```

GO TO 1002
1003 WRITE(6,7001)
7001 FORMAT(10X,'STOP - EPBAR IS TOO BIG')
      WRITE(6,7019) MATNO,J,EPBAR(J)
7019 FORMAT(10X,'MATERIAL NO. ',I3,
1         2X,'ELEMENT NO. ',I3,/,10X,
2         'EPBAR = ',E15.7,/)
      STOP
1010 IF(IJ.EQ.1) IJ=2
      HPRIME=2./3.*(SP(IJ,MATNO)-SP(IJ-1,MATNO))
1      /((EPX(IJ,MATNO)-EPX(IJ-1,MATNO))
      DFDS(1)=2.*(STRESS(1)-ALPHA(1,J))-STRESS(2)+ALPHA(2,J)
1      -STRESS(4)+ALPHA(4,J)
      DFDS(2)=2.*(STRESS(2)-ALPHA(2,J))-STRESS(1)+ALPHA(1,J)
1      -STRESS(4)+ALPHA(4,J)
      DFDS(3)=2.*(STRESS(4)-ALPHA(4,J))-STRESS(1)+ALPHA(1,J)
1      -STRESS(2)+ALPHA(2,J)
      DFDS(4)=0.
      DFDS(5)=0.
      DFDS(6)=6.*(STRESS(3)-ALPHA(3,J))
      DDFDS(1)=D11*DFDS(1)+D12*DFDS(2)+D12*DFDS(3)
      DDFDS(2)=D12*DFDS(1)+D11*DFDS(2)+D12*DFDS(3)
      DDFDS(3)=D12*DFDS(1)+D12*DFDS(2)+D11*DFDS(3)
      DDFDS(4)=D44*DFDS(4)
      DDFDS(5)=D44*DFDS(5)
      DDFDS(6)=D44*DFDS(6)
      SDFDS=DFDS(1)**2+DFDS(2)**2+DFDS(3)**2+DFDS(4)**2+DFDS(5)**2
1      +DFDS(6)**2
      DFDDF=DDFDS(1)*DFDS(1)+DDFDS(2)*DFDS(2)+DDFDS(3)*DFDS(3)
1      +DDFDS(4)*DFDS(4)+DDFDS(5)*DFDS(5)+DDFDS(6)*DFDS(6)
      DENOM=HPRIME*SDFDS+DFDDF
      C11=D11-DDFDS(1)*DDFDS(1)/DENOM
      C12=D12-DDFDS(1)*DDFDS(2)/DENOM
      C13=D12-DDFDS(1)*DDFDS(3)/DENOM
      C14=-DDFDS(1)*DDFDS(4)/DENOM
      C15=-DDFDS(1)*DDFDS(5)/DENOM
      C16=-DDFDS(1)*DDFDS(6)/DENOM
      C22=D11-DDFDS(2)*DDFDS(2)/DENOM
      C23=D12-DDFDS(2)*DDFDS(3)/DENOM
      C24=-DDFDS(2)*DDFDS(4)/DENOM
      C25=-DDFDS(2)*DDFDS(5)/DENOM
      C26=-DDFDS(2)*DDFDS(6)/DENOM
      C33=D11-DDFDS(3)*DDFDS(3)/DENOM
      C34=-DDFDS(3)*DDFDS(4)/DENOM
      C35=-DDFDS(3)*DDFDS(5)/DENOM
      C36=-DDFDS(3)*DDFDS(6)/DENOM
      C44=D44-DDFDS(4)*DDFDS(4)/DENOM
      C45=-DDFDS(4)*DDFDS(5)/DENOM
      C46=-DDFDS(4)*DDFDS(6)/DENOM
      C55=D44-DDFDS(5)*DDFDS(5)/DENOM
      C56=-DDFDS(5)*DDFDS(6)/DENOM
      C66=D44-DDFDS(6)*DDFDS(6)/DENOM
      C(1,1)=C11
      C(1,2)=C12
      C(1,3)=C16
      C(2,1)=C(1,2)
      C(2,2)=C22
      C(2,3)=C26
      C(3,1)=C(1,3)
      C(3,2)=C(2,3)
      C(3,3)=C66
      IF(IPC.EQ.1) RETURN
      DSTRES(1)=C11*DSTRAN(1)+C12*DSTRAN(2)+C16*DSTRAN(3)
      DSTRES(2)=C12*DSTRAN(1)+C22*DSTRAN(2)+C26*DSTRAN(3)
      DSTRES(3)=C16*DSTRAN(1)+C26*DSTRAN(2)+C66*DSTRAN(3)
      DSTRES(4)=C13*DSTRAN(1)+C23*DSTRAN(2)+C36*DSTRAN(3)
      DDEPSP(1)=DSTRAN(1)-DSTRES(1)/EMI+VNUI*DSTRES(2)/EMI
1      +VNUI*DSTRES(4)/EMI
      DDEPSP(2)=DSTRAN(2)+VNUI*DSTRES(1)/EMI-DSTRES(2)/EMI
1      +VNUI*DSTRES(4)/EMI
      DDEPSP(3)=DSTRAN(3)-2.*(1.+VNUI)*DSTRES(3)/EMI
      DDEPSP(4)=0.+VNUI*(DSTRES(1)+DSTRES(2))/EMI
1      -DSTRES(4)/EMI
      DO 1050 I=1,4
      DEPSP(J,I)=DEPSP(J,I)+DDEPSP(I)
1050 DEPSE(I)=DSTRAN(I)-DEPSP(J,I)
      DEPBAR=(2./9.*((DDEPSP(1)-DDEPSP(2))**2
1      +(DDEPSP(2)-DDEPSP(4))**2+(DDEPSP(4)-DDEPSP(1))**2
2      +6.*(DDEPSP(3)/2.)**2))**0.5
      EPBAR(J)=EPBAR(J)+DEPBAR

```



```

      IEP=0
      IF(IEP.NE.1) GO TO 1051
      WRITE(6,1052)EPBAR(J),DEPBAR,DEPSP(J,1),DEPSP(J,2)
1      ,DEPSP(J,3),DEPSP(J,4)
1052 FORMAT(' ',3X,'EPBAR=',E13.6,3X,'DEPBAR=',E13.6,3X,
1      'DEPSP(1)=' ,E13.6,3X,'DEPSP(2)=' ,E13.6,3X,
2      'DEPSP(3)=' ,E13.6,/)
1051 CONTINUE
      SMA1=STRESS(1)-ALPHA(1,J)
      SMA2=STRESS(2)-ALPHA(2,J)
      SMA3=STRESS(3)-ALPHA(3,J)
      SMA4=STRESS(4)-ALPHA(4,J)
      DEN=DFDS(1)*SMA1+DFDS(2)*SMA2+DFDS(3)*SMA4
1      +DFDS(6)*SMA3
      SIGOLD=SIGBAR(J)
      DO 1060 I=1,3
      STRESS(I)=STRESS(I)+DSTRES(I)
1060 STRAIN(I)=DSTRAN(I)+STRAIN(I)
      STRESS(4)=STRESS(4)+DSTRES(4)
      I=1
2002 IF(EPBAR(J).LE.EPX(I,MATNO)) GO TO 2010
      IF(I.GT.NUNIAX(MATNO)) GO TO 2003
      I=I+1
      GO TO 2002
2003 WRITE(6,7002)
7002 FORMAT(10X,'STOP - EPBAR EXCEEDS LAST POINT ON CURVE')
      WRITE(6,7020) MATNO,J,EPBAR(J)
7020 FORMAT(10X,'MATERIAL NO. ',I3,
1      2X,'ELEMENT NO. ',I3,/,10X,
2      'EPBAR = ',E15.7,/)
      STOP
2010 SIGBAR(J)=SP(I-1,MATNO)+(EPBAR(J)-EPX(I-1,MATNO))
1      *(SP(I,MATNO)-SP(I-1,MATNO))/(EPX(I,MATNO)
2      -EPX(I-1,MATNO))
      DSIGB=SIGBAR(J)-SIGOLD
      DMU=(DFDS(1)*DSTRES(1)+DFDS(2)*DSTRES(2)+DFDS(3)*DSTRES(4)
1      +DFDS(6)*DSTRES(3)
2      -2.*SIGOLD*DSIGB)/DEN
      ALPHA(1,J)=ALPHA(1,J)+DMU*SMA1
      ALPHA(2,J)=ALPHA(2,J)+DMU*SMA2
      ALPHA(3,J)=ALPHA(3,J)+DMU*SMA3
      ALPHA(4,J)=ALPHA(4,J)+DMU*SMA4
5000 CONTINUE
      DO 5001 I=1,4
      DSTRES(I)=STRESS(I)-SOLD(I)
5001 DS(J,I)=DSTRES(I)
      DO 5002 I=1,3
      E0(J,I)=E(J,I)
5002 DSTRAN(I)=STRAIN(I)-EOLD(I)
      IPLAS(J)=2
      RETURN
      END
C
C*****
C
C      SUBROUTINE ELAS2D
C
C*****
C
C THIS IS A CONSTITUTIVE PACKAGE FOR ISOTROPIC
C LINEAR ELASTICITY...
C TO DETERMINE THE STRESS INCREMENT FOR A GIVEN STRAIN INCREMENT
C OF A 2-D MATERIAL POINT
C PLANE STRAIN OR
C ORTHOTROPIC PLANE STRESS
C
      SUBROUTINE ELAS2D(J,C,DS,MATNO)
      IMPLICIT REAL*8 (A-H,O-Z)
      DIMENSION STRESS(4),STRAIN(3),SG(4),
1      DSG(4),C(3,3),DS(1500,4)
      COMMON/CHIST/RTOL,NN,NEL,NF,NDBC,IDUMP,IPRI,ISREF,
1      IEQUIT,ITEMAX,ITEMP,IINT
      COMMON/ELAS1/S(1500,4),E(1500,3),EO(1500,3),DSTRAN(3),
1      DSTRES(4)
      COMMON/ELAS2/EM1(4),EM2(4),VNU(4),G12(4),Y1(4),Y2(4),Y(4),
1      EM(4)
      COMMON/AREA7/NSTE,INCR,ITER
      E1=EM1(MATNO)
      E2=EM2(MATNO)
      VNU12=VNU(MATNO)

```

```

VNU21=VNU12*E2/E1
RG12=G12(MATNO)
YI=Y(MATNO)
YL=Y1(MATNO)
YT=Y2(MATNO)
DO 11 I=1,3
STRESS(I)=S(J,I)
STRAIN(I)=EO(J,I)
DSTRAN(I)=E(J,I)-EO(J,I)
11 CONTINUE
STRESS(4)=S(J,4)
CX C1=EMI/(1.+VNU1)
CX C2=C1/(1.-2.*VNU1)
CX D11=C2*(1.-VNU1)
CX D12=VNU1*C2
CX D44=C1/2.
c
c Plane Strain
c
C1=E1/(1.+VNU12)
C2=C1/(1.-2.*VNU12)
D11=C2*(1.-VNU12)
D12=VNU12*C2
D21=D12
D22=D11
D44=C1/2.
cy
c Plane Stress
cx
CX D11=E1/(1.0-VNU12*VNU21)
CX D12=VNU21*D11
CX D22=E2/(1.0-VNU12*VNU21)
CX D21=D12
CX D44=RG12
C
CX DSG(1)=D11*DSTRAN(1)+D12*DSTRAN(2)
DSG(2)=D21*DSTRAN(1)+D22*DSTRAN(2)
DSG(3)=D44*DSTRAN(3)
DSG(4)=D12*(DSTRAN(1)+DSTRAN(2))
CX DSG(4) = 0.0
DO 10 I=1,4
10 SG(I)=STRESS(I)+DSG(I)
C
C REDUCE TRANSVERSE STIFFNESS UPON MATRIX CRACK INITIATION
C
S1 = ( ( SG(1) - SG(2) ) / 2.0 )**2
S2 = SG(3)**2
S3S3 = S1 + S2
S3 = SQRT(S3S3)
SP1 = ( SG(1) + SG(2) ) / 2.0 + S3
SP2 = ( SG(1) + SG(2) ) / 2.0 - S3
SPMAX = DMAX1( SP1, SP2 )
IF ( SPMAX .GT. YL ) THEN
CX IF ( SG(1) .GT. YL ) THEN
MATNO = 3
WRITE (6,7000) J, INCR
7000 FORMAT(/,'MATRIX CRACK AT ELEMENT ',I5,' DURING STEP ',I5,/)
C
C WRITE(6,6100)
c 6100 FORMAT(' ',/,3X,'STRESSES TO ELAS2D ARE',3X,'STRAINS',3X,
c 1 'STRAIN INCREMENTS',/)
c DO 6101 I=1,3
c WRITE(6,6102)SG(I),E(J,I),DSTRAN(I)
c 6102 FORMAT(' ',3X,3(E13.6,3X))
c 6101 CONTINUE
C
C ENDIF
C
C
CX DISABLE YIELD FUNCTION
CX F=.5*((SG(1)-SG(2))**2+(SG(2)-SG(4))**2
CX 1 +(SG(4)-SG(1))**2+6.*SG(3)**2)-YI**2
CX
CX WRITE(6,6495) J
CX6495 FORMAT(/,'SG(1) - SG(4), F,YI FOR ELEMENT: ',I5,/)
CX WRITE(6,6500) SG(1), SG(2), SG(3), SG(4), F,YI
CX6500 FORMAT(3X,E15.4,3X,E15.4,3X,E15.4,3X,E15.4,/,
CX 1 3X,E15.5,3X,E15.5/)
CX

```

```

CX      IF(DABS(F).LT.10.0) F=0.0
CX
      IF(IDUMP.LT.4) GO TO 6004
      WRITE(6,6000)
6000 FORMAT(' ',/,3X,'STRESSES TO ELAS2D ARE',3X,'STRAINS',3X,
1        'STRAIN INCREMENTS',/)
      DO 6001 I=1,3
      WRITE(6,6002)S(J,I),E(J,I),DSTRAN(I)
6002 FORMAT(' ',3X,3(E13.6,3X))
6001 CONTINUE
6004 CONTINUE
CX      IF(IDUMP.LT.3) GO TO 6005
CX      WRITE(6,6003) YI,F
CX 6003 FORMAT(' ',/,3X,'Y = ',E13.6,3X,'F = ',E13.6,/)
6005 CONTINUE
CX      IF(F) 2000,30,30
CX 30 WRITE(6,7009) J
CX 7009 FORMAT(10X,'ELASTIC ELEMENT NO. ',I3,1X,'HAS YIELDED',/)
CX      STOP
2000 DO 3000 I=1,4
      DSTRES(I)=DSG(I)
      DS(J,I)=DSTRES(I)
3000 STRESS(I)=STRESS(I)+DSTRES(I)
      DO 3001 I=1,3
      STRAIN(I)=STRAIN(I)+DSTRAN(I)
3001 EO(J,I)=E(J,I)
12 CONTINUE
      C(1,1)=D11
      C(1,2)=D12
      C(1,3)=0.0
      C(2,1)=C(1,2)
      C(2,2)=D22
      C(2,3)=0.0
      C(3,1)=0.0
      C(3,2)=0.0
      C(3,3)=D44
      RETURN
      END

```

```

C
C*****
C
C      SUBROUTINE VPLAS2D
C
C*****

```

```

C
C THIS IS A CONSTITUTIVE PACKAGE FOR RATE DEPENDENT
C VISCOPLASTICITY USING MILLER'S MODEL
C TO DETERMINE THE STRESS INCREMENT FOR A GIVEN STRAIN INCREMENT
C OF A 2-D MATERIAL POINT
C

```

```

      SUBROUTINE VPLAS2D(J,C,DS,IPC,MATNO)
      IMPLICIT REAL*8 (A-H,O-Z)
      DIMENSION STRESS(4),STRAIN(3),DFDS(6),DDFDS(6),
1        SOLD(4),EOLD(3)
      DIMENSION C(3,3),DST(1500,4),DS(1500,4),DET(1500,3)
      COMMON/CHIST/RTOL,NN,NEL,NF,NDBC,IDUMP,IPRI,ISREF,
1        IEQUIT,ITEMAX,ITEMP,IINT
      COMMON/ELAS1/S(1500,4),E(1500,3),EO(1500,3),DSTRAN(3),
1        DSTRES(4)
      COMMON/ELAS2/EM1(4),EM2(4),VNU(4),G12(4),Y1(4),Y2(4),Y(4),
1        EM(4)
      COMMON/PLAS1/ALPHA(4,1500),EPBAR(1500),SIGBAR(1500),
1        IPLAS(1500),EPSP(1500,4),DEPSPT(1500,4),
2        DEPS(1500,4)
      COMMON/VPLAS1/DTIME,DEVPAL
      COMMON/VPLAS2/RN,H1,H2,AA1,AA2,C2,DO,B1,TEMP,TMELT,QS
      COMMON/BB/NUNIAX(4),IDUMP2,ISUB
      COMMON/AREA10/DST,DET
      COMMON/AREA7/NSTE,INCR,ITER

```

```

C
C RECALL DRAG STRESS D FROM SIGBAR ARRAY
C
      D=SIGBAR(J)

```

```

C
C INITIALIZE PLASTIC STRAIN RATE AND STRESS RATE
C FOR CALCULATION OF HPRIME FIRST TIME THROUGH
C SUBINCREMENTATION LOOP
C

```

```

      EPSPDOT1=DEPSP(J,1)/DTIME
      EPSPDOT2=DEPSP(J,2)/DTIME

```

```

      EPSPDOT3=DEPSP(J,3)/DTIME
      EPSPDOT4=DEPSP(J,4)/DTIME
      SIGDOT1=DS(J,1)/DTIME
      SIGDOT2=DS(J,2)/DTIME
      SIGDOT3=DS(J,3)/DTIME
      SIGDOT4=DS(J,4)/DTIME
C
C INITIALIZE SUBROUTINE STRESSES AND STRAINS
C
      DO 11 I=1,3
      DEPSP(J,I)=0.
      STRESS(I)=S(J,I)
      STRAIN(I)=EO(J,I)
      DSTRAN(I)=E(J,I)-EO(J,I)
11    CONTINUE
      STRESS(4)=S(J,4)
      DEPSP(J,4)=0.
      DO 4020 I=1,3
      SOLD(I)=STRESS(I)
4020  EOLD(I)=STRAIN(I)
      SOLD(4)=STRESS(4)
C
C CALCULATE ELASTIC MODULUS MATRIX
C
      EMI=EM(MATNO)
      VNUI=VNU(MATNO)
      YI=Y(MATNO)
      CC1=EMI/(1.+VNUI)
      CC2=CC1/(1.-2.*VNUI)
      D11=CC2*(1.-VNUI)
      D12=VNUI*CC2
      D44=CC1/2.
C
C SUBINCREMENTATION LOOP
C
      DE=(4./3.*(DSTRAN(1)**2+DSTRAN(2)**2+DSTRAN(1)*DSTRAN(2)
1      +DSTRAN(3)**2))*5
      M=DE/DEVPAL+.1
      IF(M.EQ.0) M=1
      DO 400 I=1,3
400   DSTRAN(I)=DSTRAN(I)/M
      DTSUB=DTIME/M
      GO TO 3090
3090  CONTINUE
      IF(IDUMP.LT.2) GO TO 3032
      WRITE (6,3031) M
3031  FORMAT(' ',//,3X,'NO. OF SUBINCREMENTS = ',I3,/)
      WRITE(6,3033) DE,DEVPAL
3033  FORMAT(5X,'DE = ',E15.7,1X,'DEVPAL = ',E15.7,/)
3032  CONTINUE
      DO 5000 NSUB=1,M
C
C CONSTRUCT C MATRIX
C
      DNUM1=SIGDOT1*EPSPDOT1+SIGDOT2*EPSPDOT2+
1      SIGDOT3*EPSPDOT3+SIGDOT4*EPSPDOT4
      DENOM1=EPSPDOT1**2+EPSPDOT2**2+EPSPDOT3**2+EPSPDOT4**2
      IF(INCR.EQ.1) GO TO 334
      GO TO 335
C
C ELASTIC CASE
C
334  CONTINUE
      C(1,1)=D11
      C(1,2)=D12
      C(1,3)=0.0
      C(2,1)=C(1,2)
      C(2,2)=C(1,1)
      C(2,3)=0.0
      C(3,1)=0.0
      C(3,2)=0.0
      C(3,3)=D44
      IF(IPC.EQ.1) GO TO 9999
      DSTRES(1)=D11*DSTRAN(1)+D12*DSTRAN(2)
      DSTRES(2)=D12*DSTRAN(1)+D11*DSTRAN(2)
      DSTRES(3)=D44*DSTRAN(3)
      DSTRES(4)=D12*(DSTRAN(1)+DSTRAN(2))
      SIGDOT1=DSTRES(1)/DTSUB
      SIGDOT2=DSTRES(2)/DTSUB
      SIGDOT3=DSTRES(3)/DTSUB

```

```

      SIGDOT4=DSTRES(4)/DTSUB
C
C UPDATE TOTAL STRESS AND STRAIN
C
      DO 1050 I=1,3
      STRESS(I)=STRESS(I)+DSTRES(I)
1050  STRAIN(I)=DSTRAN(I)+STRAIN(I)
      STRESS(4)=STRESS(4)+DSTRES(4)
      GO TO 5000
335  CONTINUE
C
C ELASTIC-PLASTIC CASE
C
      DFDS(1)=2.*(STRESS(1)-ALPHA(1,J))-STRESS(2)+ALPHA(2,J)
1      -STRESS(4)+ALPHA(4,J)
      DFDS(2)=2.*(STRESS(2)-ALPHA(2,J))-STRESS(1)+ALPHA(1,J)
1      -STRESS(4)+ALPHA(4,J)
      DFDS(3)=2.*(STRESS(4)-ALPHA(4,J))-STRESS(1)+ALPHA(1,J)
1      -STRESS(2)+ALPHA(2,J)
      DFDS(4)=0.
      DFDS(5)=0.
      DFDS(6)=6.*(STRESS(3)-ALPHA(3,J))
      DDFDS(1)=D11*DFDS(1)+D12*DFDS(2)+D12*DFDS(3)
      DDFDS(2)=D12*DFDS(1)+D11*DFDS(2)+D12*DFDS(3)
      DDFDS(3)=D12*DFDS(1)+D12*DFDS(2)+D11*DFDS(3)
      DDFDS(4)=D44*DFDS(4)
      DDFDS(5)=D44*DFDS(5)
      DDFDS(6)=D44*DFDS(6)
      SDFDS=DFDS(1)**2+DFDS(2)**2+DFDS(3)**2+DFDS(4)**2+DFDS(5)**2
1      +DFDS(6)**2
      DFDDF=DDFDS(1)*DFDS(1)+DDFDS(2)*DFDS(2)+DDFDS(3)*DFDS(3)
1      +DDFDS(4)*DFDS(4)+DDFDS(5)*DFDS(5)+DDFDS(6)*DFDS(6)
      IF(DABS(DENOM1).LT.1.D-20) GO TO 332
      HPRIME=DNUM1/DENOM1
      GO TO 333
332  HPRIME=1.0D25
333  CONTINUE
      DENOM=HPRIME*SDFDS+DFDDF
      C11=D11-DDFDS(1)*DDFDS(1)/DENOM
      C12=D12-DDFDS(1)*DDFDS(2)/DENOM
      C13=D12-DDFDS(1)*DDFDS(3)/DENOM
      C14=-DDFDS(1)*DDFDS(4)/DENOM
      C15=-DDFDS(1)*DDFDS(5)/DENOM
      C16=-DDFDS(1)*DDFDS(6)/DENOM
      C22=D11-DDFDS(2)**2/DENOM
      C23=D12-DDFDS(2)*DDFDS(3)/DENOM
      C24=-DDFDS(2)*DDFDS(4)/DENOM
      C25=-DDFDS(2)*DDFDS(5)/DENOM
      C26=-DDFDS(2)*DDFDS(6)/DENOM
      C33=D11-DDFDS(3)**2/DENOM
      C34=-DDFDS(3)*DDFDS(4)/DENOM
      C35=-DDFDS(3)*DDFDS(5)/DENOM
      C36=-DDFDS(3)*DDFDS(6)/DENOM
      C44=D44-DDFDS(4)**2/DENOM
      C45=-DDFDS(4)*DDFDS(5)/DENOM
      C46=-DDFDS(4)*DDFDS(6)/DENOM
      C55=D44-DDFDS(5)**2/DENOM
      C56=-DDFDS(5)*DDFDS(6)/DENOM
      C66=D44-DDFDS(6)**2/DENOM
      C(1,1)=C11
      C(1,2)=C12
      C(1,3)=C16
      C(2,1)=C(1,2)
      C(2,2)=C22
      C(2,3)=C26
      C(3,1)=C(1,3)
      C(3,2)=C(2,3)
      C(3,3)=C66
      IF(IPC.EQ.1) GO TO 9999
      IF(IDUMP.LT.2) GO TO 557
      WRITE(6,4228) (DSTRAN(I),I=1,4)
4228  FORMAT(5X,'DSTRAN = ',4E12.4)
      557  CONTINUE
C
C CALCULATE STRESS SUBINCREMENT
C
      DSTRES(1)=C11*DSTRAN(1)+C12*DSTRAN(2)+C16*DSTRAN(3)
      DSTRES(2)=C12*DSTRAN(1)+C22*DSTRAN(2)+C26*DSTRAN(3)
      DSTRES(3)=C16*DSTRAN(1)+C26*DSTRAN(2)+C66*DSTRAN(3)
      DSTRES(4)=C13*DSTRAN(1)+C23*DSTRAN(2)+C36*DSTRAN(3)

```

```

SIGDOT1=DSTRES(1)/DTSUB
SIGDOT2=DSTRES(2)/DTSUB
SIGDOT3=DSTRES(3)/DTSUB
SIGDOT4=DSTRES(4)/DTSUB
C
C CALCULATE DEVIATORIC STRESS TENSOR
C
  SKK=STRESS(1)+STRESS(2)+STRESS(4)
  SD1=STRESS(1)-SKK/3.
  SD2=STRESS(2)-SKK/3.
  SD3=STRESS(3)
  SD4=STRESS(4)-SKK/3.
  SMA1=SD1-ALPHA(1,J)
  SMA2=SD2-ALPHA(2,J)
  SMA3=SD3-ALPHA(3,J)
  SMA4=SD4-ALPHA(4,J)
  SIGEFF=(1.5*(SMA1**2+SMA2**2+SMA3**2+SMA4**2))*0.5
C
C UPDATE INTERNAL VARIABLES
C USING EULER INTEGRATION
C
C FIRST CALCULATE PLASTIC STRAIN RATE
C
  IF(DABS(SIGEFF).LE.1.0D-8) GO TO 301
  IF(DABS(SIGBAR(J)).LE.1.0D-8) GO TO 301
  FAC4=-QS*4.184/O.6/8.314/TMELT
  THETA=DEXP(FAC4*(DLOG(O.6*TMELT/TEMP)+1.))

  BTHETA=B1*THETA
  EPSBDOT=BTHETA*(DSINH((SIGEFF/D)**1.5))**RN
  FAC=1.5*(EPSBDOT/SIGEFF)
  EPSDOT1=FAC*SMA1
  EPSDOT2=FAC*SMA2
  EPSDOT3=FAC*SMA3
  EPSDOT4=FAC*SMA4
  GO TO 305
301 EPSBDOT=0.
  EPSDOT1=0.
  EPSDOT2=0.
  EPSDOT3=0.
  EPSDOT4=0.
305 CONTINUE
C
C NEXT CALCULATE BACK STRESS RATE
C
  BSIGDOT1=(2./3.)*H1*EPSDOT1
  BSIGDOT2=(2./3.)*H1*EPSDOT2
  BSIGDOT3=(2./3.)*H1*EPSDOT3
  BSIGDOT4=(2./3.)*H1*EPSDOT4
  BSIGBAR=((3./2.)*(ALPHA(1,J)**2+ALPHA(2,J)**2+
1    ALPHA(3,J)**2+ALPHA(4,J)**2))*0.5
  IF(BSIGBAR.LT.1.0D-7) GO TO 306
  FAC1=H1*BTHETA*(DSINH(AA1*BSIGBAR))**RN/BSIGBAR
  BSIGDOT1=BSIGDOT1-FAC1*ALPHA(1,J)
  BSIGDOT2=BSIGDOT2-FAC1*ALPHA(2,J)
  BSIGDOT3=BSIGDOT3-FAC1*ALPHA(3,J)
  BSIGDOT4=BSIGDOT4-FAC1*ALPHA(4,J)
306 CONTINUE
C
C FIND DRAG STRESS RATE
C
  DDOT=H2*EPSBDOT*(C2+BSIGBAR-(AA2/AA1*D**3))
  FAC2=DSINH(AA2*D**3)
  IF(DABS(FAC2).LT.1.0D-4) GO TO 307
  DDOT=DDOT-H2*C2*BTHETA*FAC2**RN
307 CONTINUE
C
C FINALLY, UPDATE ALL INTERNAL VARIABLES
C
  DEPSP(J,1)=DEPSP(J,1)+EPSDOT1*DTSUB
  DEPSP(J,2)=DEPSP(J,2)+EPSDOT2*DTSUB
  DEPSP(J,3)=DEPSP(J,3)+EPSDOT3*DTSUB
  DEPSP(J,4)=DEPSP(J,4)+EPSDOT4*DTSUB
  ALPHA(J,1)=ALPHA(J,1)+BSIGDOT1*DTSUB
  ALPHA(J,2)=ALPHA(J,2)+BSIGDOT2*DTSUB
  ALPHA(J,3)=ALPHA(J,3)+BSIGDOT3*DTSUB
  ALPHA(J,4)=ALPHA(J,4)+BSIGDOT4*DTSUB
  D=D+DDOT*DTSUB
  SIGBAR(J)=D

```

```

C
C UPDATE TOTAL STRESS AND STRAIN
C
      DO 1060 I=1,3
        STRESS(I)=STRESS(I)+DSTRES(I)
1060   STRAIN(I)=DSTRAN(I)+STRAIN(I)
        STRESS(4)=STRESS(4)+DSTRES(4)
5000   CONTINUE
C
C COMPLETE SUBINCREMENTATION LOOP -
C CALCULATE TOTAL STRESS INCREMENT
C
      DO 5001 I=1,4
        DSTRES(I)=STRESS(I)-SOLD(I)
5001   DS(J,I)=DSTRES(I)
C
C CALCULATE TOTAL STRAIN INCREMENT
C
      DO 5002 I=1,3
        EO(J,I)=E(J,I)
5002   DSTRAN(I)=STRAIN(I)-EOLD(I)
9999   CONTINUE
        RETURN
      END

```